

NAVAL POSTGRADUATE SCHOOL

Monterey, California



DISSERTATION

**TROPICAL CYCLONE AND MID-LATITUDE
CHARACTERISTICS AND PHYSICAL MECHANISMS
CONTRIBUTING TO EXTRATROPICAL TRANSITION IN
THE WESTERN NORTH PACIFIC**

by

Peter M. Klein

December 2000

Dissertation Supervisor:

Russell L. Elsberry

Approved for public release; distribution is unlimited.

20010320 033

REPORT DOCUMENTATION PAGE

Form Approved
OMB No. 0704-0188

Public reporting burden for this collection of information is estimated to average 1 hour per response, including the time for reviewing instruction, searching existing data sources, gathering and maintaining the data needed, and completing and reviewing the collection of information. Send comments regarding this burden estimate or any other aspect of this collection of information, including suggestions for reducing this burden, to Washington headquarters Services, Directorate for Information Operations and Reports, 1215 Jefferson Davis Highway, Suite 1204, Arlington, VA 22202-4302, and to the Office of Management and Budget, Paperwork Reduction Project (0704-0188) Washington DC 20503.

1. AGENCY USE ONLY (Leave blank)		2. REPORT DATE December 2000		3. REPORT TYPE AND DATES COVERED Dissertation	
4. TITLE AND SUBTITLE TROPICAL CYCLONE AND MID-LATITUDE CHARACTERISTICS AND PHYSICAL MECHANISMS CONTRIBUTING TO EXTRATROPICAL TRANSITION IN THE WESTERN NORTH PACIFIC				5. FUNDING NUMBERS	
6. AUTHOR(S) Peter M. Klein					
7. PERFORMING ORGANIZATION NAME(S) AND ADDRESS(ES) Naval Postgraduate School Monterey, CA 93943-5000				8. PERFORMING ORGANIZATION REPORT NUMBER	
9. SPONSORING / MONITORING AGENCY NAME(S) AND ADDRESS(ES)				10. SPONSORING / MONITORING AGENCY REPORT NUMBER	
11. SUPPLEMENTARY NOTES <i>The views expressed in this thesis are those of the author and do not reflect the official policy or position of the Department of Defense or the U.S. Government.</i>					
12a. DISTRIBUTION / AVAILABILITY STATEMENT <i>Approved for public release; distribution is unlimited.</i>				12b. DISTRIBUTION CODE	
13. ABSTRACT This study of extratropical transition (ET) of tropical cyclones (TCs) in the western North Pacific examines 30 cases during 1 June through 31 October 1994-98 using Navy analyses, plus geostationary satellite visible, infrared, water vapor, and microwave imagery. Based on the similarity of all 30 ET cases in satellite imagery, a three-dimensional conceptual model of the <i>transformation</i> stage of ET is proposed to describe how these ET cases evolve into an incipient, baroclinic cyclone. A climatology of ET during the period studied is presented, and three levels of re-intensification (<i>little</i> , <i>moderate</i> , and <i>deep</i>) are defined based on storm intensity at the end of ET. The re-intensification stage in nine cases is studied via Navy Coupled Ocean-Atmosphere Mesoscale Prediction System (COAMPS) control forecasts, simulations with the initial TC vortex removed, and simulations in which the initial TC vortex is displaced. These COAMPS simulations demonstrate that deep or moderate re-intensification depends on <i>phasing</i> of the poleward translating TC remnants with a <i>critical region</i> in which cyclogenesis is favored in the mid-latitude circulation. The mid-latitude circulation and TC contributions to the re-intensification stage are identified via superposition with the critical region and modification of its location and diagnostic values, respectively, and the combination of these contributions determines the final storm intensity at the end of ET.					
14. SUBJECT TERMS Extratropical Transition of Tropical Cyclones, Transformation Stage, Re-intensification Stage, Critical Region, Petterssen Type-B Extratropical Cyclogenesis, Mid-latitude Circulation Contributions to Re-Intensification, Tropical Cyclone Contributions to Re-Intensification				15. NUMBER OF PAGES 261	
				16. PRICE CODE	
17. SECURITY CLASSIFICATION OF REPORT Unclassified	18. SECURITY CLASSIFICATION OF THIS PAGE Unclassified		19. SECURITY CLASSIFI- CATION OF ABSTRACT Unclassified		20. LIMITATION OF ABSTRACT UL

NSN 7540-01-280-5500

Standard Form 298 (Rev. 2-89)
Prescribed by ANSI Std. Z39-18 298-102

Approved for public release; distribution is unlimited

**TROPICAL CYCLONE AND MID-LATITUDE CHARACTERISTICS AND
PHYSICAL MECHANISMS CONTRIBUTING TO EXTRATROPICAL
TRANSITION IN THE WESTERN NORTH PACIFIC**

Peter M. Klein
Lieutenant Commander, United States Navy
B.S., Cornell University, 1988
M.S., Naval Postgraduate School, 1997

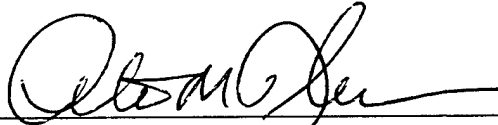
Submitted in partial fulfillment of the requirements for the degree of

DOCTOR OF PHILOSOPHY IN METEOROLOGY

from the

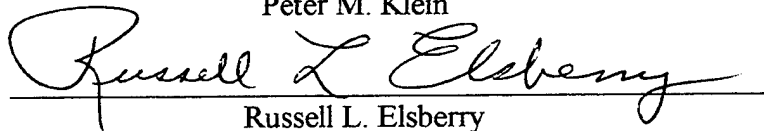
**NAVAL POSTGRADUATE SCHOOL
December 2000**

Author:



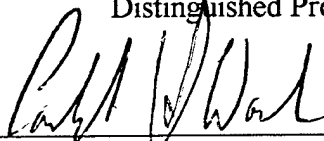
Peter M. Klein

Approved by:

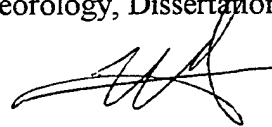


Russell L. Elsberry

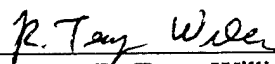
Distinguished Professor of Meteorology, Dissertation Supervisor



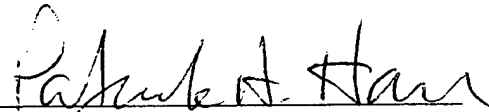
Carlyle H. Wash
Professor of Meteorology



Roland W. Garwood
Professor of Oceanography

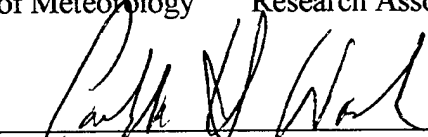


R. Terry Williams
Professor of Meteorology



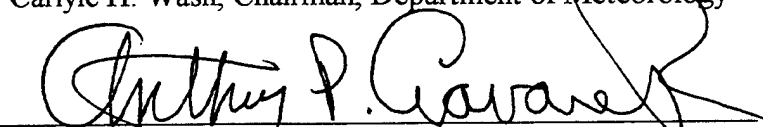
Patrick A. Harr
Research Associate Professor of Meteorology

Approved by:



Carlyle H. Wash, Chairman, Department of Meteorology

Approved by:



Anthony P. Ciavarella, Associate Provost for Instruction

ABSTRACT

This study of extratropical transition (ET) of tropical cyclones (TCs) in the western North Pacific examines 30 cases during 1 June through 31 October 1994-98 using Navy analyses, plus geostationary satellite visible, infrared, water vapor, and microwave imagery. Based on the similarity of all 30 ET cases in satellite imagery, a three-dimensional conceptual model of the *transformation* stage of ET is proposed to describe how these ET cases evolve into an incipient, baroclinic cyclone. A climatology of ET during the period studied is presented, and three levels of re-intensification (*little*, *moderate*, and *deep*) are defined based on storm intensity at the end of ET. The re-intensification stage in nine cases is studied via Navy Coupled Ocean-Atmosphere Mesoscale Prediction System (COAMPS) control forecasts, simulations with the initial TC vortex removed, and simulations in which the initial TC vortex is displaced. These COAMPS simulations demonstrate that deep or moderate re-intensification depends on *phasing* of the poleward translating TC remnants with a *critical region* in which cyclogenesis is favored in the mid-latitude circulation. The mid-latitude circulation and TC contributions to the re-intensification stage are identified via superposition with the critical region and modification of its location and diagnostic values, respectively, and the combination of these contributions determines the final storm intensity at the end of ET.

TABLE OF CONTENTS

I. INTRODUCTION.....	1
A. REVIEW OF PREVIOUS RESEARCH.....	1
B. REVIEW OF CHARACTERISTICS OF TROPICAL CYCLONES AND MID-LATITUDE CYCLONES.....	6
C. RESEARCH GOALS AND HYPOTHESES.....	14
II. DATA AND ANALYSIS PROCEDURES.....	19
A. DATA SOURCES.....	19
B. DEFINITIONS.....	19
C. METHOD.....	26
III. TRANSFORMATION STAGE OF EXTRATROPICAL TRANSITION.....	29
A. TYPICAL SATELLITE IMAGERY.....	29
B. TRANSFORMATION OF TY DAVID (SEPTEMBER 1997).....	35
C. A CONCEPTUAL MODEL OF THE TRANSFORMATION STAGE OF EXTRATROPICAL TRANSITION.....	65
D. THE DECAY OF SUPERTYPHOON IVAN (OCTOBER 1997).....	75
IV. CLIMATOLOGY OF EXTRATROPICAL TRANSITION.....	85
A. STATISTICS.....	85
B. MERGERS.....	94
V. RE-INTENSIFICATION STAGE OF EXTRATROPICAL TRANSITION.....	99
A. BACKGROUND.....	99
B. HYPOTHESES.....	114

1.	Phasing of the TC and the Critical Region	114
2.	Contributions of the Mid-Latitude Circulation Pattern and the TC during the Re-Intensification Stage.	117
3.	Combinations of Mid-Latitude and TC Contributions and Their Impact on the Outcome of the Re-Intensification Stage	119
C.	METHOD	120
1.	Experimental Framework	120
2.	Vortex Removal and Displacement	122
3.	Perturbed Fields in the no-TC and "displaced-TC" Simulations ...	127
D.	CHARACTERIZATION OF THE MID-LATITUDE CONTRIBUTION TO THE RE-INTENSIFICATION STAGE: THE CONTROL FORECASTS AND NO-TC SIMULATIONS.	131
1.	Favorable Mid-Latitude Circulation Contributions	132
2.	Neutral Mid-Latitude Circulation Contributions	141
3.	Unfavorable Mid-Latitude Circulation Contribution	148
E.	THE "DISPLACED-TC" SIMULATIONS.	154
1.	STY Bart, Mid-Latitude "Favorable" Contribution.	155
2.	STY Ginger, Mid-Latitude "Neutral" Contribution.	170
3.	STY Bing, Mid-Latitude "Unfavorable" Contribution.	182
4.	Discussion of Other Displaced-TC Simulations.	193
5.	Discussion of TC Contributions to the Re-Intensification Stage of ET.	199
6.	Summary of Displaced-TC Simulations and Characterization of the TC Contribution in Each.	206

VI. SUMMARY AND CONCLUSIONS.....	219
A. SUMMARY OF THE STAGES OF ET.....	219
B. CONCLUSIONS	224
1. The Transformation Stage of ET: New Findings	225
2. Climatology of ET in the Western North Pacific	225
3. The Re-intensification Stage of ET: New Findings.....	226
C. RECOMMENDATIONS.....	228
1. Guidance to Operational Forecasters.....	228
2. Future Research.....	231
APPENDIX A.....	233
APPENDIX B.....	239
LIST OF REFERENCES	245
INITIAL DISTRIBUTION LIST	249

ACKNOWLEDGMENT

This research was funded by the Office of Naval Research, Marine Meteorology Program. The author would like to thank Profs. Elsberry and Harr for their guidance and assistance during this research. In particular, Professor Elsberry made available the opportunity to present this research at conferences, and submit manuscripts for publication in AMS journals. His patience, wisdom, and tutelage were essential to the completion of this effort, and more importantly, ensured that much was learned from the effort itself. Professor Harr modified the Kurihara tropical cyclone vortex-removal technique so that it could be used effectively in this study.

In addition, Mr. Bill Thompson and Mr. Robert Creasy made available the satellite imagery and NOGAPS analyses studied herein, and Profs. Douglas Miller and Elizabeth Ritchie provided invaluable assistance in using the COAMPS numerical weather prediction model as a research tool.

Lastly, the author would like to thank his wife Christine for her sacrifices, interest, patience, and support, without which this doctoral research would never have been completed.

I. INTRODUCTION

A. REVIEW OF PREVIOUS RESEARCH

Tropical cyclones in the western North Pacific that complete extratropical transition (ET) can become powerful, mid-latitude storms capable of causing significant damage to coastal and maritime interests. Extratropical transition is a complex, four-dimensional evolution in which meteorological features on various horizontal and vertical scales interact over a range of temporal scales. The thermodynamic and dynamic characteristics of a mature tropical cyclone (TC) are well researched, as are the physical processes responsible for extratropical cyclogenesis. By contrast, the transition from TC to extratropical cyclone is poorly understood and incompletely researched. Furthermore, numerical weather prediction (NWP) models often fail to forecast accurately the onset of ET and the subsequent evolution of the resulting mid-latitude cyclone, and thus may have significant motion and intensity errors. Any effort that improves the description, understanding, and definition of ET would provide forecasters with better tools for diagnosing and forecasting ET, and lead to dissemination of more effective advisories and warnings.

The first comprehensive study of ET in the western North Pacific was completed by Matano and Sekioka (1971), who defined two characteristic types of ET (Fig. I-1) based only on surface pressure analyses. A *complex* transition occurs when a pre-existing mid-latitude front or trough interacts with a TC to produce a new extratropical cyclone on the front. A *compound* transition results when a mid-latitude cyclone approaches and

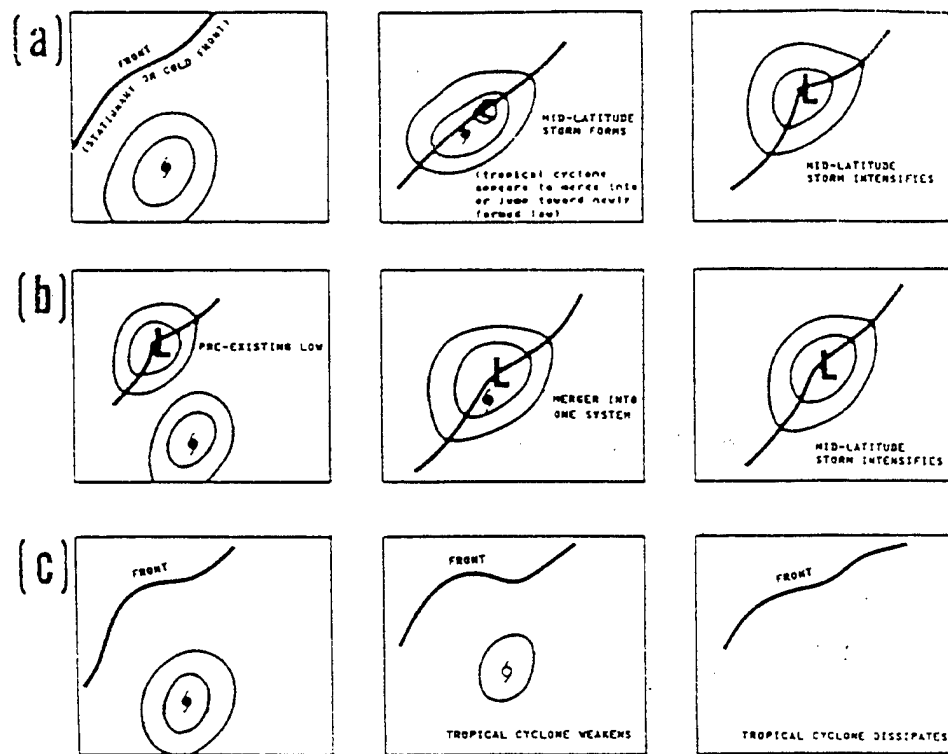


Fig. I-1. The conceptual model of Matano and Sekioka (1971), depicting (a) complex and (b) compound transitions, and (c) dissipators (Brand and Guard 1978).

appears to merge with a TC such that the TC is transformed into an extratropical cyclone. Brand and Guard (1978) added a third type of transition in which the TC dissipates after recurvature. Like Matano and Sekioka (1971), Foley and Hanstrum (1994) classified based on characteristic sea-level pressure (SLP) patterns two types of ET that occur along the west coast of Australia. Those TCs caught in pre-cold frontal poleward (southward) flow were said to be "captured" (a classification analogous to the complex transition), while those transiting poleward in a synoptic pattern featuring easterly flow to the poleward side were said to be "cradled."

The critical role of upper-tropospheric divergence and positive vorticity advection (PVA) in the extratropical re-intensification of tropical cyclones was identified and discussed in several papers (DiMego and Bosart 1982, Sinclair 1993, Foley and Hanstrum

1994, Klein 1997, Harr et al. 2000). Instead of only the sea-level pressure characteristics, these studies illustrate the three-dimensional character of ET. DiMego and Bosart (1982) described the ET of Hurricane Agnes as occurring in three stages: predevelopment, in which Agnes begins to lose its tropical characteristics; re-intensification and transformation, in which Agnes briefly redeepens as a tropical storm, and then is transformed into an extratropical cyclone; and dissipation. They demonstrated that lower-tropospheric diabatic heating and cyclonic vorticity associated with the transforming TC, together with upper-tropospheric divergence and positive vorticity advection (PVA) superposed above a pre-existing baroclinic zone, played a significant role in the ET of Agnes. Sinclair (1993) suggested that the coupling of TC Patsy with a 200-mb subtropical jet streak during ET permitted extratropical cyclogenesis to occur. In both of these studies, ET was described as proceeding in a manner resembling archetypal Petterssen "Type-B" extratropical cyclogenesis, in which superposition of upper-tropospheric PVA above lower-tropospheric baroclinity results in deepening of the surface low (Petterssen and Smebye 1971).

The interaction of TCs with the mid-latitude circulation pattern they translate into during ET has also been recently studied (Bosart and Lackmann 1995, Browning et al. 1998, Carr and Elsberry 1999, Harr et al. 2000). Bosart and Lackmann (1995) described how Hurricane David (1979) altered an environment of pre-existing, weak baroclinity to permit extratropical redevelopment. They suggested that the combined effect of diabatic heating produced by David and warm advection downstream of the storm resulted in mid- and upper-tropospheric ridging downstream, whereas cold advection simultaneously

deepened a pre-existing mid-latitude, short-wave trough upstream. This "downstream ridging" produced a potential vorticity (PV) anomaly upstream of David that caused re-intensification of David through self-amplification. Browning et al. (1998) discussed the evolution of Hurricane Lili into an extratropical, warm-core cyclone through interaction with a stratospheric potential vorticity (PV) anomaly, and subsequent intrusion of cool, dry air that encircled the warm, moist air over the circulation center.

Harr et al. (2000) discussed how the character and phasing of mid-latitude synoptic patterns affect 30 ET cases that occurred during 1994-98 in the western North Pacific. They defined two characteristic synoptic patterns (*northwest* and *northeast*) based on the location of the upper-level PV maximum in the mid-latitudes relative to the TC at *transition time* (first synoptic time at or after the Joint Typhoon Warning Center (JTWC), Pearl Harbor, Hawaii, designated the storm as extratropical). Thirteen storms in the northwest pattern (Fig. I-2a) quickly coupled with the PV maximum associated with a short-wave trough located to the northwest of the storm center. By contrast, 17 storms entering the northeast pattern (Fig. I-2b) never completely coupled with the PV maximum located to the northeast of the storm center. Thus, storms in the northwest (northeast) pattern re-intensified more quickly (slowly) in the 36 h following transition time, and moved in a more meridional (zonal) direction.

The sequence of events that occur during ET has been examined and described using satellite imagery, NWP analyses, and radar reflectivity patterns. Bader et al. (1995) used infrared (IR) imagery to describe the transition of four Atlantic TCs into extratropical cyclones. In particular, they described the development of a convex-shaped, cirrus

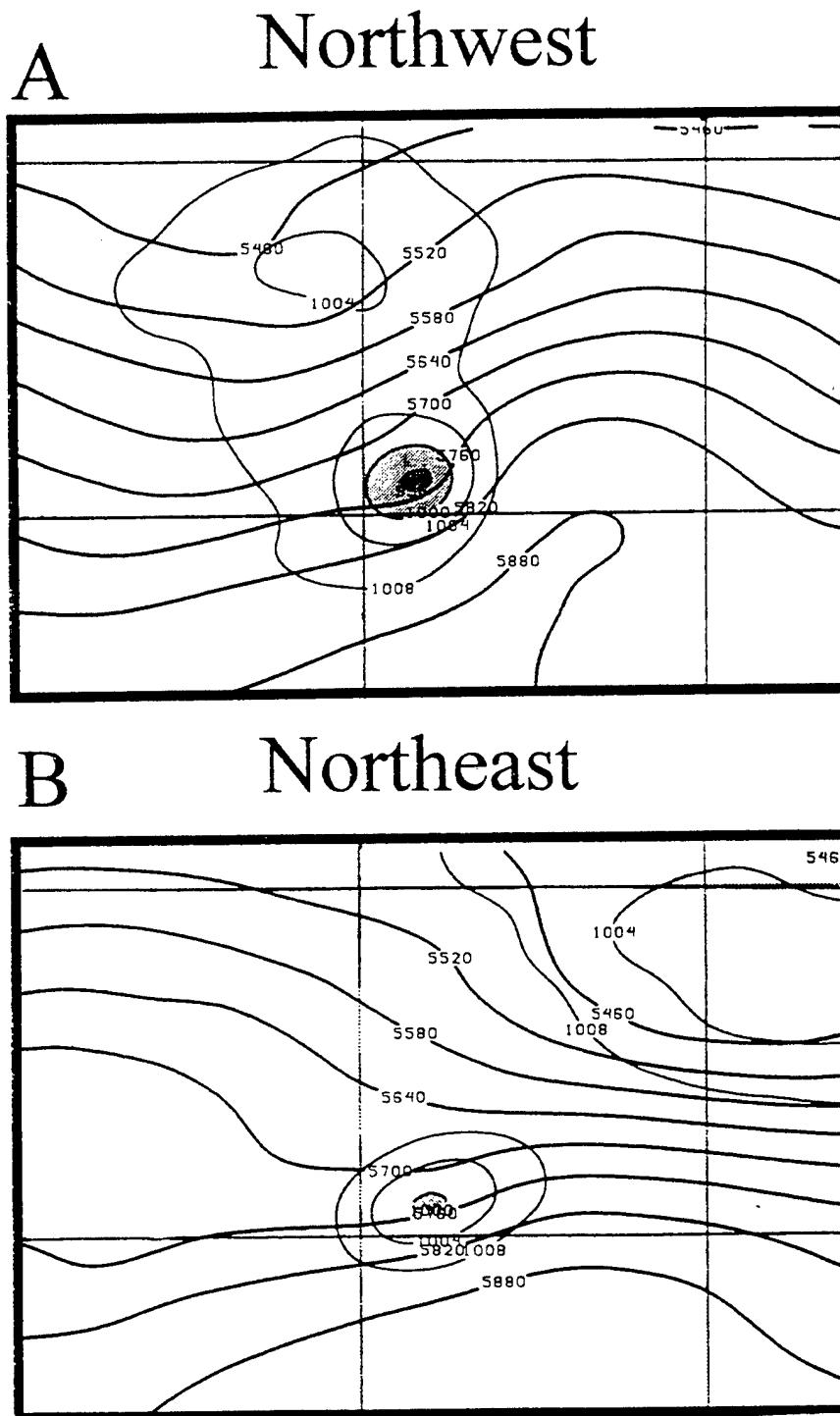


Fig. 1-2. Composite 500-mb height (60 m interval) and sea-level pressure (4 mb intervals, beginning at 1008 mb) analyses based on (a) 13 northwest cases, and (b) 17 northeast cases of ET in the western North Pacific (Harr et al. 2000).

outflow shield that could be observed once the storm translated into and interacted with the westerlies. They also suggested that as a TC translated poleward, it brought with it a southerly plume of warm, moist air that created a lower-tropospheric baroclinic zone, and noted that ET often occurred downstream of an upper-level short wave embedded in the pre-existing mid-latitude circulation.

Klein (1997) studied cases of ET in the western North Pacific that occurred during July through October 1994-96. He indicated that virtually all of these cases appeared in infrared (IR) imagery and NWP analyses to transform from a warm-core vortex into a baroclinic, extratropical cyclone in the same sequential fashion, and called this the *transformation stage*¹ of ET. He also defined a second stage called *re-intensification*, in which the transformed TC either redeepens if the upper troposphere is favorable for Petterssen Type-B extratropical cyclogenesis (as described by Bosart and DiMego (1982) and Sinclair (1993)), or dissipates.

B. REVIEW OF CHARACTERISTICS OF TROPICAL CYCLONES AND MID-LATITUDE CYCLONES

The process of ET is defined here to begin with a weakening TC translating poleward and being transformed into a baroclinic system, and ends once the TC remnants have re-intensified into a mid-latitude cyclone (Klein 1997, Klein et al. 2000a). Thus, it is important to distinguish between the physical characteristics of tropical cyclones and baroclinic lows.

¹ Transformation as described by Klein (1997) is analogous to Bosart and DiMego's predevelopment stage. Re-intensification in Klein (1997) is similar to the re-intensification and transformation stage of Bosart and DiMego, except that Klein requires the TC to have transformed into a baroclinic, cold-core low before re-intensification takes place.

A TC is a warm-core system that derives its energy from the latent heat release (LHR) produced by deep convection. Subsidence induced by this LHR increases the mean virtual temperature of the vertical column at the center of the TC, and thus reduces the SLP at the storm center. This decrease in SLP causes increased lower-tropospheric inflow of air with high values of equivalent potential temperature (θ_e) into the TC, and thus sustains deep eyewall convection, and maintains low central SLP and continued inflow of warm, moist air. The process described above produces a maximum radial temperature gradient that is located across the TC eyewall. Therefore, the pressure surfaces in the lower troposphere also have their maximum slope across the eyewall, which requires that the maximum winds associated with the TC be located above the planetary boundary layer (PBL) within the eyewall. As the lower-tropospheric parcels progress toward the center of the storm in an "in-up-and out" circulation, they gain moisture and heat from air-sea interaction, such that the parcels that reach the eyewall have the highest θ_e values and ascend to the highest elevations. As these parcels progress toward the eyewall, they only partially conserve angular momentum due to frictional dissipation. Thus, those parcels that reach the eyewall have also lost the most angular momentum. As they ascend and then progress outward in an outflow layer while more closely conserving angular momentum, those parcels in the eyewall have the smallest radial extent of cyclonic motion before turning to anticyclonic motion. Those parcels ascending in radial bands farther from the center have larger angular momentum, and will have a larger radial extent of cyclonic motion. Thus, the region of cyclonic winds in a TC resembles a pyramid extending upward into an anticyclone aloft.

A west-east cross-section (1° lat./long. resolution) of Navy Operational Global Atmospheric Prediction System (NOGAPS) isentropes and isotachs is depicted in Fig. I-3a for a weakening TC of average size and intensity. A warm core in the upper-troposphere (concave isentropes) is noticeable above the storm center, little vertical wind shear is present above the center, and the tropopause is above 150 mb. As expected, maximum winds are at inner radii near the surface. Notice also the pyramidal shape of the isotachs, which implies that the radius of cyclonic winds decreases with height as described earlier until an anticyclone exists in the upper troposphere.

The kinetic energy source for all extratropical cyclones is the baroclinic conversion of potential energy. An analogous NOGAPS west-east cross-section (1° lat./long. resolution) of a typical occluded mid-latitude cyclone is shown in Fig. I-3b. A "cold dome" of isentropes is west of the storm, and a lower tropopause is clearly evident over the center. Notice also the tight packing of isentropes in the vicinity of 300 mb and 200 mb, upstream and downstream of the storm, respectively. Large vertical wind shear exists near the storm center, where lower-tropospheric baroclinity is greatest, which is consistent with the thermal wind relationship. The polar jet centered between 300 mb and 250 mb is east of the storm center. In contrast to the TC, the maximum winds are indeed well away from the storm center, and increase in elevation to the jet level. A summary of the key characteristics of TCs and extratropical cyclones is presented in Table 1.

Given that the characteristics of TCs and mid-latitude cyclones are so different, it should be expected that significant changes will be observed in the distribution of gale-force winds, clouds, and precipitation as a storm progresses through ET. After

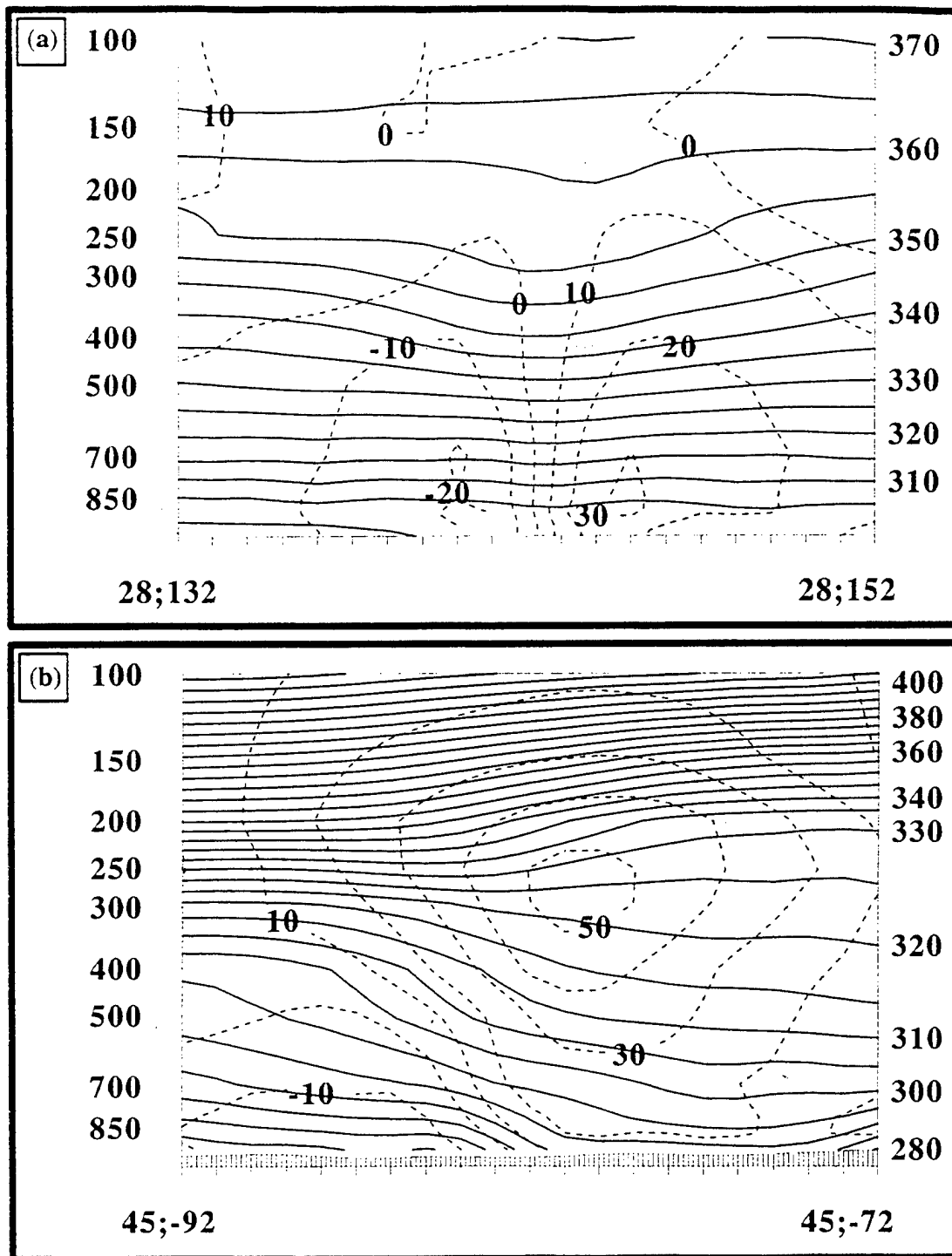


Fig. I-3. Vertical west-east cross-section of (a) a weakening western North Pacific typhoon, and (b) an occluding extratropical cyclone in the Northern Hemisphere. Solid contours represent isentropes (5 K interval) and dashed contours represent isotachs of v wind component (10 m/s interval).

Table 1. Summary of physical characteristics of TCs and extratropical cyclones.

Physical Characteristic	TCs	Extratropical Cyclones
Energy Process	Warm Core Energetics (LHR produced by deep central convection)	Baroclinic Conversion of Potential Energy
Location of RMW	In the eyewall, 10's of km from the storm center	100's of km from the center of low pressure
Vertical Wind Shear	Little vertical wind shear present near center	Increasing winds with height, with maximum vertical wind shear above greatest low-tropospheric baroclinity
Vertical Structure	Warm core with no tilt	Baroclinic tilt toward cold air, cold core

commencing the transformation stage of ET on 0000 UTC 27 June 1997, TY Peter still resembles a TC in enhanced IR imagery (Fig. I-4a). An area of 975-mb gale-force winds (Fig. I-4b) extends from 127°E to 133°E , and 22°N to 31°N . It is acknowledged that the resolution of this 1° lat./long. analysis is insufficient to properly depict the location of maximum winds, which are found in the eyewall of TY Peter. However, the horizontal extent of the gale-force wind field associated with the TC in Fig. I-4b is believed to be more accurately represented. A similar pattern of ocean wave heights exceeding 3 m (Fig. I-4b) is produced by the gale- and storm-force winds associated with TY Peter.

By 1200 UTC 29 June (Fig. I-5), Peter has completed the transformation stage of ET and has commenced re-intensification as a baroclinic low. Notice that the storm resembles an occluding extratropical cyclone (Fig. I-5a), complete with cloud patterns that would be expected to accompany lower-tropospheric fronts. The area of 975-mb gale-force winds (Fig. I-5b), which extends from 148°E to 165°E and 33°N to 51°N , is much larger than 60 h earlier, and has become elongated and comma-shaped, with regions of maximum wind located over 400 km from the storm center. These changes in the

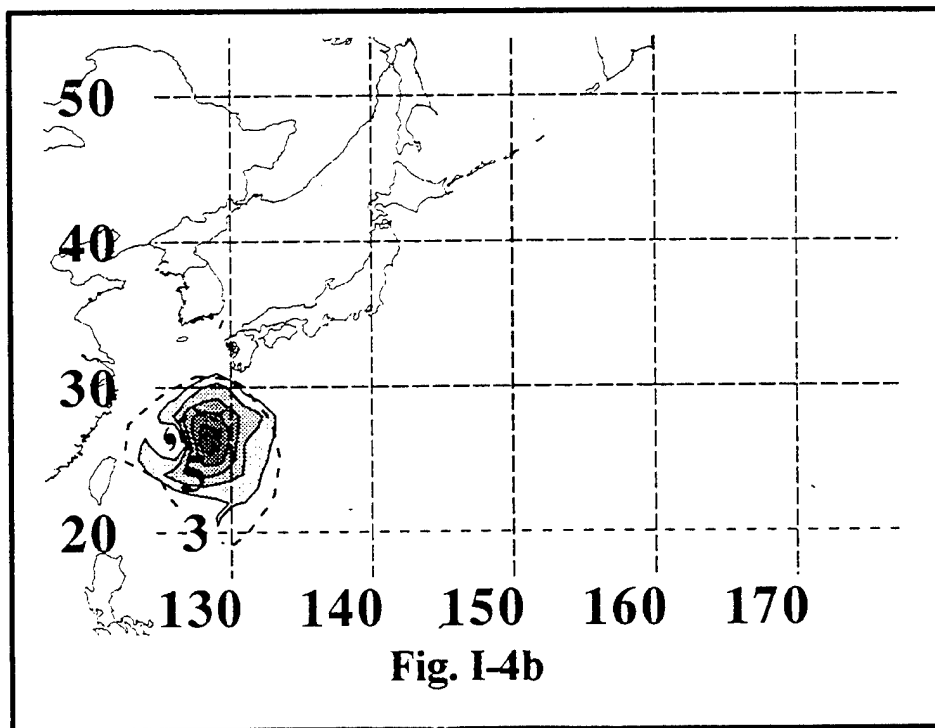
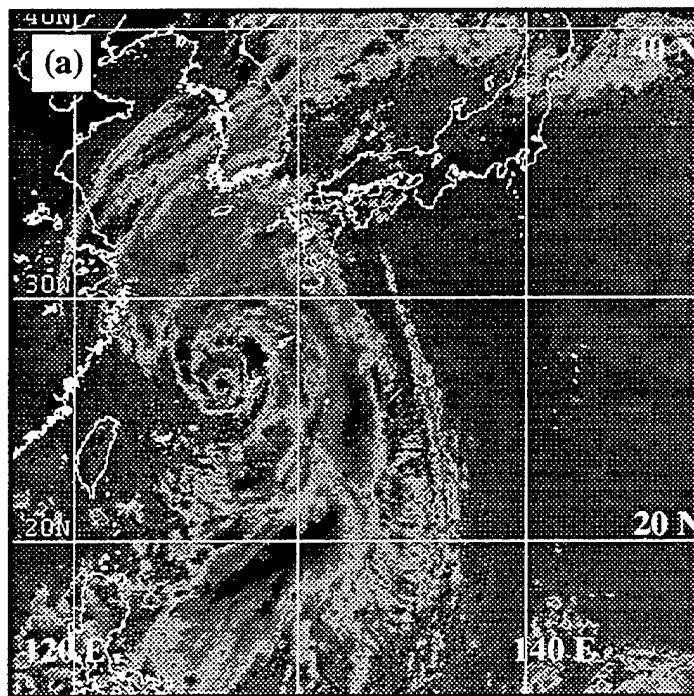


Fig. I-4. Infrared imagery of TY Peter at (a) 0032 UTC 27 June 1997, and (b) NOGAPS analysis of 975-mb winds (shaded, 5 kt interval beginning at 35 kt), and significant wave height (dashed, 2 m interval) at 0000 UTC 27 June 1997.

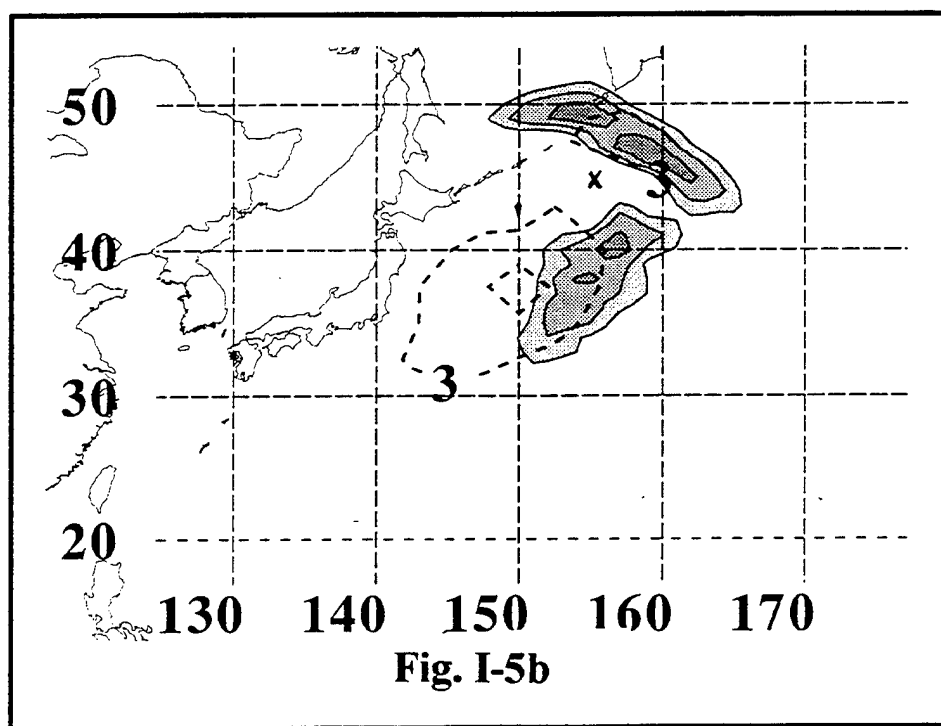
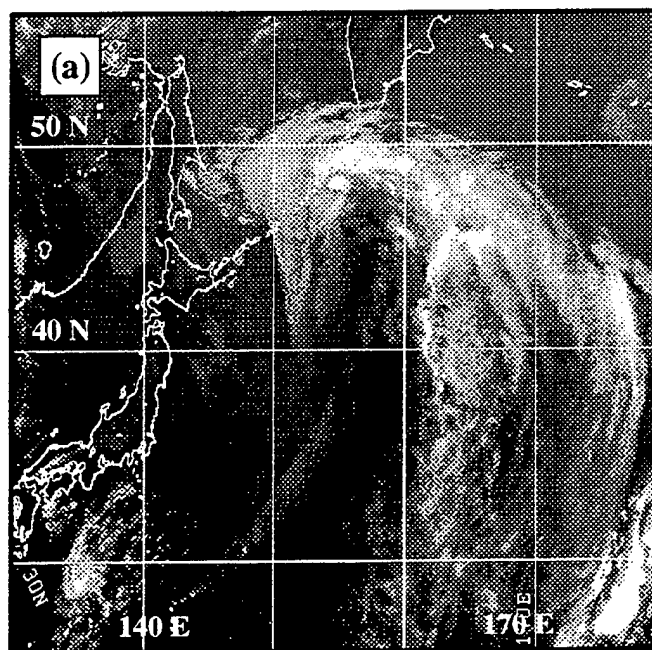


Fig. I-5. Infrared imagery of TY Peter at (a) 1232 UTC 29 June 1997, and (b) NOGAPS analysis of 975-mb winds (shaded, 5 kt interval beginning at 35 kt), and significant wave height (dashed, 1 m interval) at 1200 UTC 29 June. The location of the surface low center is marked "X."

observed winds produced a region of ocean wave heights exceeding 3 m (Fig. I-5b) that is also distributed differently compared to 60 h earlier².

The change in the distribution and intensity of precipitation that occurs during the ET of TY Peter is depicted in Fig. I-6 using the 85 GHz channel of the Special Sensor Microwave Imager (SSM/I), which can be regarded as a proxy for rainrate from convective clouds. At 0000 UTC 27 June (Fig. I-6a), TY Peter has rainbands in all quadrants that spiral inward to the storm center, with a ring of convection surrounding the center of the storm. By 1200 UTC 28 June (Fig. I-6b), a swath of clouds and precipitation north and east of the storm center wraps into the western quadrant, with relatively little clouds or precipitation evident in the southern half of the storm. Foley and Hanstrum (1994) showed that during ET off the western coast of Australia a broad swath of clouds and precipitation was likely to be observed poleward of the storm track, while high winds and relatively fewer clouds and precipitation were found equatorward of the storm track. The ET of TY Peter depicted in Figs. I-4 through I-6 is consistent with their results. As a TC undergoes ET, forecasters must anticipate these changes in cloud patterns, and locations of heavy precipitation. Similarly, the changes in gale- and storm-force winds, and pattern of significant wave heights have a direct impact on the type and timing of the severe weather advisories necessary to alert coastal and maritime interests to the changing nature of the threat to life and property. Issuing typhoon and tropical storm

² Bowyer (2000) described how the transition of Hurricane Luis in the Atlantic (1995) produced wave heights exceeding 10 m, with a maximum of 30 m. He attributed these extreme wave heights to the "trapped-fetch" phenomenon, in which a storm translates in resonance with the wave phase speed to generate wave heights far greater than expected by forecasters. Since a TC commencing ET typically accelerates as it translates poleward, it is believed likely that "trapped-fetch" conditions may be satisfied during the transformation stage in the western North Pacific as well.

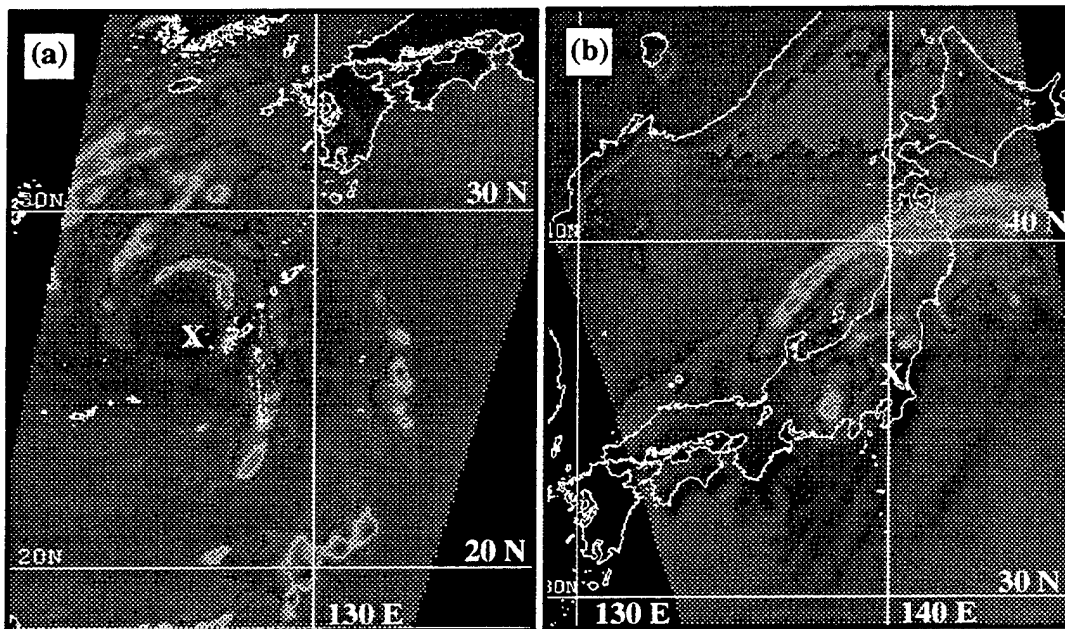


Fig. I-6. Special Sensor Microwave Imager (SSM/I) imagery, 85 GHz channel, of TY Peter at (a) 0000 UTC 27 June, and (b) 1200 UTC 28 June 1997. The storm center is marked "X."

warnings during ET, while better than disseminating no warning at all, will improperly focus preparations and precautionary measures based on the type of wind and precipitation patterns depicted in Figs. I-4b and I-6a rather than those in Figs. I-5b and I-6b.

C. RESEARCH GOALS AND HYPOTHESES

Klein (1997) and Klein et al. (2000a) suggested that the conceptual model of Matano and Sekioka (1971) did not adequately explain the evolution of a TC into a baroclinic low during ET because: (i) it was based only on surface pressure patterns, and thus failed to acknowledge the role of the mid- and upper-troposphere in ET; (ii) the model would have had to be heavily modified to permit classification of the 30 ET cases examined by Harr et al. (2000); and (iii) the model did not define any physical mechanisms

that satisfactorily describe how the three-dimensional structure and characteristics of a TC change during ET. Furthermore, no standard terminology is used to describe ET, which often leads to confusion. For example, the terms *transition* and *transformation* are often used interchangeably in the literature, and TCs that become extratropical are sometimes described as having undergone ET simply because they have translated into the mid-latitudes.

The primary objective of this study is to provide a description and explanation of the three-dimensional physical processes that result in the transformation of a TC into a baroclinic system during the transformation stage of ET, and the subsequent extratropical cyclogenesis that occurs during the re-intensification stage. Three main questions regarding the understanding of how the atmosphere evolves during ET must be addressed: (i) how can one recognize when a TC commences and completes the transformation stage of ET, and what physical processes are important in the evolution of a TC into a baroclinic low during transformation? (ii) what physical processes trigger the extratropical cyclogenesis that occurs during the re-intensification stage, and what are the relative contributions of the TC remnants and the mid-latitude circulation pattern to that re-intensification? and (iii) can the outcome of the re-intensification stage be anticipated before extratropical cyclogenesis occurs so that the ET cases that re-intensify only moderately can be distinguished from those that become the most intense?

Based on Klein (1997) and Klein et al. (2000a), it is hypothesized that the transformation stage of ET involves a common sequence of interactions for nearly every case of ET that occurs over the western North Pacific Ocean. The first goal is to

understand interactions between: (i) the outer and inner core circulations of the TC; (ii) a pre-existing, quasi-linear temperature and/or moisture gradient established by the mid-latitude circulation or surface boundary characteristics; (iii) the environmental flow in which the TC is embedded; and (iv) the synoptic-scale, mid-latitude circulation pattern. In this study, transformation is defined to begin with the interaction of the TC outer circulation with a pre-existing, mid-latitude baroclinic zone. It is believed that this interaction causes parcels in the TC outer circulation to ascend tilted isentropic surfaces of the baroclinic zone, release latent heat, then descend dry adiabatically at lower values of θ_e . Based on the thermal wind relationship, if the TC is interacting with lower-tropospheric baroclinity, it is also being affected by vertical wind shear, which will hasten the decay of the TC warm core and advect it downstream. During the transformation stage, the TC lower-tropospheric outer circulation evolves into a quasi-linear asymmetric circulation pattern through temperature and/or moisture frontogenesis. The final step in this sequence occurs when the lower-tropospheric circulation center of the storm becomes imbedded within the baroclinic zone so that cold, descending air undercuts warm, rising air at the storm center. At completion of transformation, the TC remnants will more closely resemble those of an extratropical cyclone (Fig. I-3b, Table 1). Because all transformations in the western North Pacific are believed to occur in this manner, a conceptual model will be developed that describes both the appearance and the step-by-step physical processes that are observed during the transformation stage of ET in the western North Pacific.

In this study, it is hypothesized that the transformed TC redeepens as a baroclinic cyclone during the re-intensification stage of ET through Petterssen "Type B" cyclogenesis (Petterssen and Smebye 1971). That is, once an upper-tropospheric PV anomaly becomes superposed over the lower-tropospheric baroclinity and cyclonic vorticity associated with the transformed TC, it initiates the extratropical cyclogenesis. Carlson (1991) listed four criteria that must exist for vigorous and explosive extratropical cyclogenesis to occur: (i) strong meridional baroclinity (and therefore vertical wind shear); (ii) vertical phase lag between the height and thermal fields, which implies that the upper-tropospheric perturbation is the triggering mechanism; (iii) relatively low static stability; and (iv) geographic location in the middle or high latitudes. These criteria will be used to determine if there is a "critical region" in the mid-latitude circulation pattern that is capable of supporting deep, and potentially explosive, Petterssen Type-B extratropical cyclogenesis during ET. If deep extratropical cyclogenesis is favored, then the final outcome of the re-intensification stage (in terms of storm intensity) is believed to depend primarily on the phasing of the transformed storm with this critical region. Thus, if the transformed TC translates into the critical region such that it couples in an optimum way with the upper-tropospheric PV anomaly, it achieves deep (and possibly explosive) extratropical re-intensification. Those TCs that fail to achieve optimal phasing with the critical region complete only a modest re-intensification.³

It is further hypothesized that if deep re-intensification is favored based on the criteria of Carlson (1991) presented above, an extratropical cyclone, perhaps even an

³ Definitions of deep and moderate re-intensification are provided in Chapter II.

intense and explosively deepening one, will develop in the same critical region identified in the control forecast even in the absence of the TC that completed ET. Therefore, the outcome of any re-intensification stage of ET in the western North Pacific could be anticipated based on the mid-latitude synoptic pattern (northwest or northeast, according to Harr et al. 2000) that the transformed storm has entered, and the phasing of the transformed storm with the critical region within that synoptic pattern.

In Chapter II, definitions of ET and its stages, including the beginning and end of each stage, are presented, and the data and method used to examine the 30 cases of ET that occurred during this five-year period are described. A conceptual model of the transformation stage of ET, based on detailed analysis of these 30 cases, is proposed in Chapter III. In Chapter IV, a brief climatology based on these cases is presented for the transformation stage and the subsequent cyclone characteristics of the re-intensification stage. In Chapter V, the re-intensification stage is studied, with emphasis on the role of the phasing between the translating TC and the mid-latitude circulation pattern. In Chapter VI, the conclusions of this study are summarized, forecaster rules of thumb are described, and areas of future research are discussed.

II. DATA AND ANALYSIS PROCEDURES

A. DATA SOURCES

In this study, 30 ET cases that occurred in the western North Pacific from 1 June through 31 October during 1994-98 are examined. These are the same 30 ET cases studied by Harr et al. (2000). All tropical cyclone tracks and intensities are from the JTWC post-storm ("best track") analyses. While cases occurring in 1994-95 are studied using Geostationary Meteorological Satellite (GMS-4 and -5) imagery only at 12-h intervals (00 UTC and 12 UTC), cases in 1996 (1997-99) are examined using GMS-5 imagery at 3-h (1-h) intervals. During 1997-99, the polar-orbiting SSM/I passes over tropical cyclones during ET are also available. Archived NOGAPS analyses and forecasts with 2.5° lat./long. resolution are available at 12-h intervals throughout the period studied. After 1 September 1996, 1° lat./long. NOGAPS analyses and forecasts at 6-h intervals are also available. Water vapor winds have been included as a data source in the NOGAPS analyses after 1 June 1996. Each analysis began no less than 72 h before the tropical cyclone became extratropical according to JTWC, and continued until at least 24 h after the transition appeared to be complete.

B. DEFINITIONS

Use of the terms "transition" and "transformation" during discussions of ET in the literature often produces confusion. The objective here is to describe ET in the western North Pacific as a process that occurs over a period of time, and involves a specific sequence of physical processes that can be observed and described by satellite imagery and

NWP analyses. Therefore, the term "transition" will only be used to describe the entire process of ET, and "transformation" will be used to define a stage of ET. As in Klein (1997), and based on review of the 30 ET cases, the transformation stage of ET is defined as an evolution of a TC into a baroclinic cyclone, while the re-intensification stage is the extratropical re-intensification of the transformed storm in a manner that resembles Petterssen Type-B extratropical cyclogenesis. Commencement of ET coincides with the beginning of the transformation stage of ET, which is defined to start when visible, infrared (IR), and water vapor imagery suggest an asymmetric appearance of clouds, and especially a widespread decrease of deep convection in the western quadrant of a poleward-moving TC. Simultaneously, the outermost edge of the TC circulation is impinging on a pre-existing mid-latitude baroclinic zone or front on the northern or northwestern side. Transformation is defined to be completed when the storm has the characteristics of a baroclinic cyclone in both satellite imagery and NWP analyses, and the center of the storm is imbedded in cold, descending air.

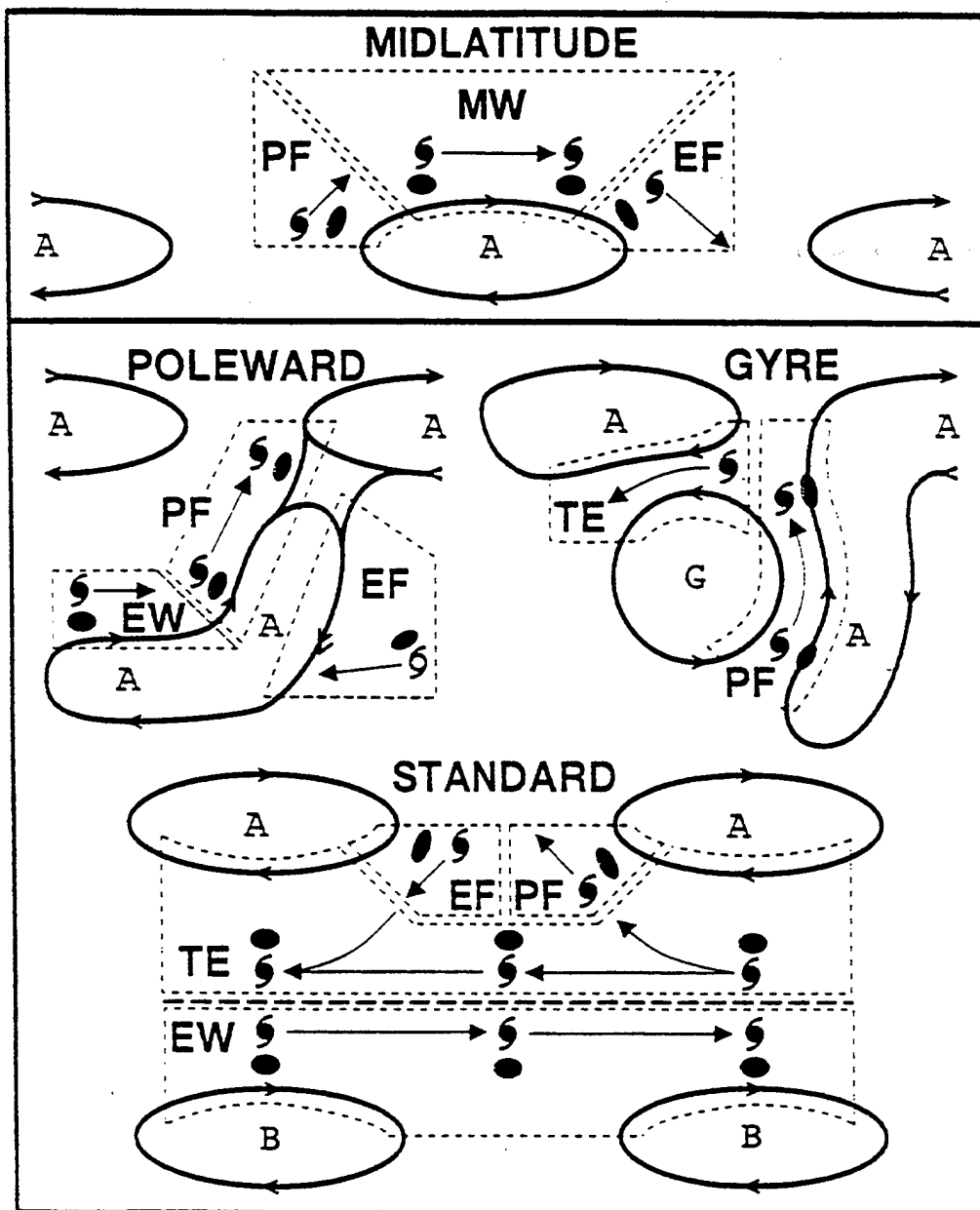
If the storm then deepens as a baroclinic cyclone, this re-intensification stage is defined to begin at the synoptic time when the transformed storm has achieved its highest central SLP at or after the completion of transformation. The re-intensification stage is defined to conclude at the synoptic time when the re-intensifying storm has achieved the deepest SLP before either filling or holding steady in the next analysis. Deep (moderate) re-intensification is defined to occur if the SLP achieved at the end of ET is below 980 mb (between 980 mb and 1000 mb). Since these SLP thresholds are empirically defined for the western North Pacific ETs, appropriate thresholds may vary in other basins. If the

tropical cyclone does not complete both the transformation and re-intensification stages, it will be classified as a "decayer." In this period, 14 tropical cyclones that became extratropical failed to complete ET and were classified as decayers. In Chapter III, STY Ivan is presented as an example of a decayer, and its characteristics are contrasted with those of storms that complete ET.

Most ET cases are also recurving TCs. Statistics and additional discussion of recurvature in ET will be presented in Chapter IV. In this study, recurvature is defined to occur as the TC passes through the subtropical ridge axis while simultaneously changing the direction of its translation so that it exhibits an eastward, rather than a westward, component of motion. Carr and Elsberry (1994) developed a systematic approach to TC track forecasting that included classification of TC tracks based on synoptic patterns and regions. Characteristic tracks were found in each synoptic pattern and region. Using the updated synoptic patterns and regions of Carr and Elsberry (1999) depicted in Fig. II-1, recurvature in cases of ET is achieved in one of two ways: (i) the TC progresses from the Standard pattern/Poleward Flow region to the Midlatitude pattern/Poleward Flow region; or (ii) the TC initially in the Standard pattern has a transition into a Poleward pattern, and the TC progresses from the Poleward pattern/Poleward Flow region into the Midlatitude pattern/Poleward Flow region.

It is also important to stress that in this study, designation by JTWC of a TC as extratropical does not mean that the TC has commenced ET. In the western North Pacific, a TC will be designated as extratropical by JTWC once it has lost its central dense overcast, and translates poleward of the polar jet axis. This JTWC designation is not

WESTERN NORTH PACIFIC SYNOPTIC PATTERNS AND REGIONS



MW = MIDLATITUDE WESTERLIES TE = TROPICAL EASTERLIES
 PF = POLEWARD FLOW EW = EQUATORIAL WESTERLIES
 EF = EQUATORWARD FLOW

Fig. II-1. The four synoptic patterns and five synoptic regions of Carr and Elsberry (1999) for the western North Pacific.

based on the physical characteristics of the TC, but rather on its appearance and location relative to the mid-latitude circulation pattern. It should not be construed to mean that the TC has "transitioned" out of the tropics, and therefore has completed ET. As indicated above, 14 other TCs that JTWC listed as extratropical failed to complete ET as defined here and are classified as decayers. The process of ET is better described as a sequence of events that cause the evolution of a TC into a baroclinic cyclone, rather as a single, discrete event that is defined by geography.

The 30 ET cases studied did become extratropical according to JTWC's definition, although in some of these cases the TC actually completed the transformation stage of ET before JTWC issued its final TC warning. In Table 2, the time of the final JTWC TC warning message for the 30 ET cases studied is compared with the time at which the transformation stage of ET was completed. At the time JTWC has issued its final TC warning, some of these 30 ET cases were as much as 18 h from completing the transformation stage, and one case completed transformation as much as 78 h earlier. In 12 (40%) of these 30 ET cases, JTWC issued their last TC warning an average of 21 h after the storm completed its transformation into a baroclinic cyclone. These 12 cases featured cloud, precipitation, and wind patterns similar to those depicted in the case of TY Peter in Figs. I-5a, I-5b, and I-6b during and just after the transformation stage. It should be obvious that at the time of the JTWC final TC warning, these 30 ET cases probably displayed a wide variety of physical characteristics, with just under half of them bearing more resemblance to a baroclinic cyclone than to a TC. Thus, it is possible in these 12 cases of ET that issuing a TC warning after completion of the transformation stage could

Table 2. List of 30 tropical storms (TS), typhoons (TY), and supertyphoons (STY) that completed ET during 1 June through 31 October 1994-98.

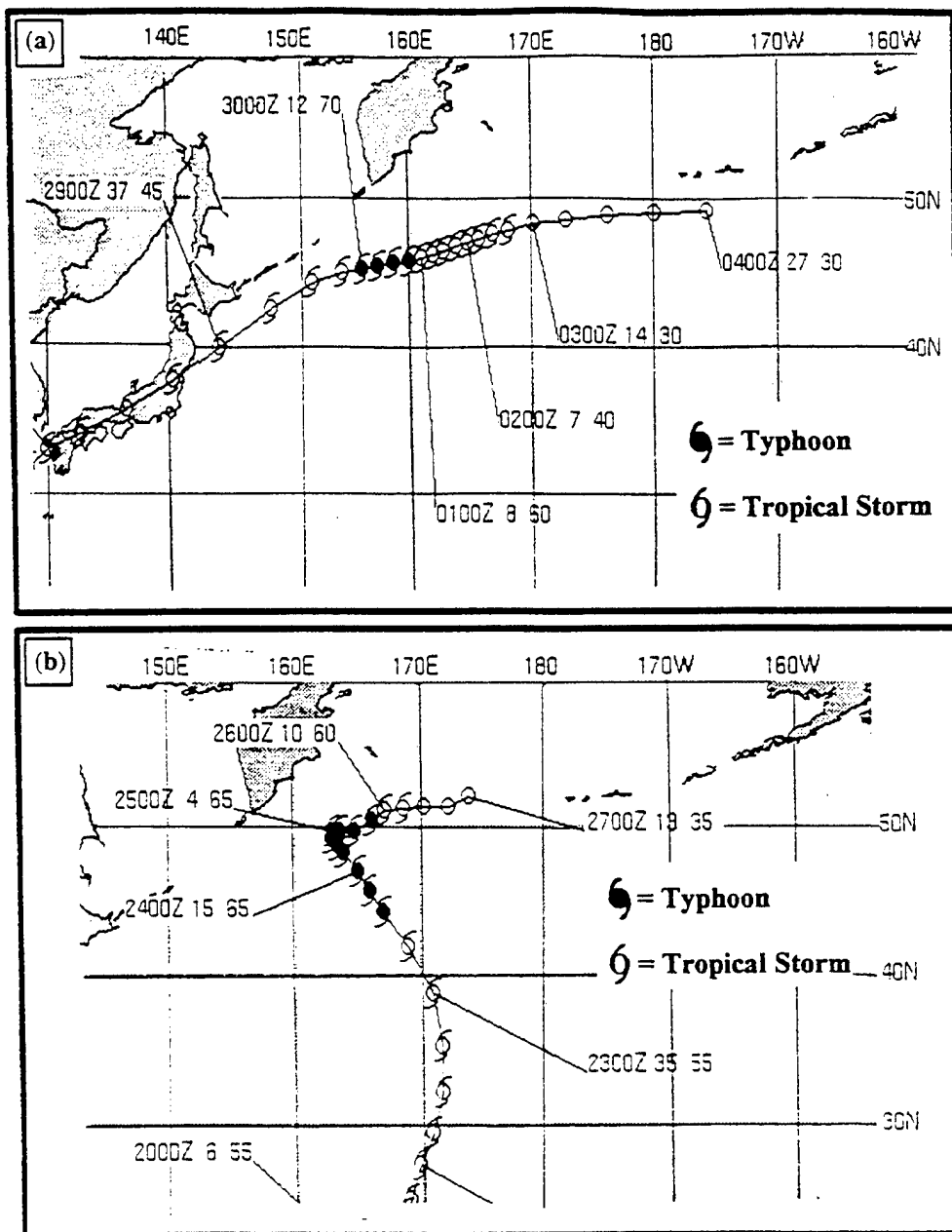
Name	JTWC Final Warning (YYMMDDHH)	Period of Transformation Stage (YYMMDDHH)	End of Re- intensification Stage (YYMMDDHH)
TY Zeke	94072412	94072312 to 94072500	94072700
TY Ivy	94090306	94090212 to 94090312	94090400
STY Melissa	94091806	94091612 to 94091900	94092400
TY Seth	94101118**	94100912 to 94101100	94101300
TS Janis	95082918**	95082412 to 95082612	95082800
STY Oscar	95091800	95091600 to 95091800	95091912
TY Polly	95092118	95091900 to 95092200	95092212
STY Ryan	95092412	95092200 to 95092412	95092512
STY Ward	95102212	95102012 to 95102212	95102400
TY Dan	96071206**	96070900 to 96071112	96071212
TY Joy	96080506	96080300 to 96080600	96080700
TY Kirk	96081606**	96081400 to 96081512	96081612
TY Orson	96090306	96090200 to 96090312	96090512
TY Tom	96092006	96091800 to 96092100	96092312
STY Violet	96092300	96092100 to 96092300	96092400
STY Yates*	96100118	96093012 to 96100212	96100500
TY Carlo	96102618**	96102400 to 96102512	96102600
STY Nestor	97061500**	97061300 to 97061412	97061512
TY Opal	97062106**	97061812 to 97062012	97062100
TY Peter	97062900	97062700 to 97062900	97063000
TY Tina	97080900	97080712 to 97081000	97081100
TY Yule	97082306**	97082100 to 97082300	97082412
STY Bing	97090500	97090300 to 97090500	97090600
TY David	97092006**	97091800 to 97091912	97092100
STY Ginger	97093006**	97092800 to 97093000	97093012
STY Joan	97102400	97102200 to 97102412	97092600
TY Rex	98090700**	98090500 to 98090612	98090712
TY Stella	98091612	98091500 to 98091700	98091900
TY Vicki	98092300	98092112 to 98092300	98092400
STY Zeb	98101800**	98101512 to 98101700	98101812

* Yates commenced ET in September 1996, but completed both stages of ET in October and thus is considered an October case.

** Cases in which the JTWC Final Warning Time came after completion of the transformation stage of ET.

incorrectly result in the anticipation of a tropical storm instead of a powerful, baroclinic cyclone, although it is acknowledged that such a warning is better than none at all.

In some instances, JTWC identifies these storms in their post-processed "best-track" analyses with typhoon symbols during extratropical re-intensification (Fig. II-2). By 0000 UTC 30 June 1997, Peter has completed the re-intensification stage of ET (Table 2), yet is depicted in Fig. II-2a as a typhoon, which falsely implies that the storm



NOTE: TC location depicted every 6 h and labeled hhhhZ ss iii where hhhh = hour, ss = TC translation speed (kt) and iii = TC intensity (kt).

Fig. II-2. Post-processed JTWC best-track analyses of TC motion and intensity for (a) TY Peter in June 1997, and (b) TY Yule in August 1997 (JTWC 1998).

strengthened as a tropical cyclone. Similarly, TS Yule is depicted at 1200 UTC 23 August 1997 in Fig. II-2b as if it has become a typhoon at 45°N, when in fact Yule has already completed the transformation stage of ET, and has begun extratropical re-intensification.

For these reasons, it is necessary to distinguish between how JTWC designates TCs as extratropical, and how ET and its stages are defined in this study. Use of the JTWC final warning time or designation of a TC as extratropical is not believed to be an appropriate tool for defining any aspect or stage of ET, since these terms only refer to a single moment in time when a TC may actually possess a wide range of physical characteristics, rather than describing a sequence of events that, at each step, defines the same set of physical processes occurring in the atmosphere.

C. METHOD

Although ET can occur in the western North Pacific at any time of the year, this study focuses on the months June through October to address the special threat posed to maritime interests by TCs undergoing ET. Many trans-ocean voyages during this period are planned at higher latitudes, which minimizes distances while avoiding TCs. However, an ET may lead to an unexpectedly strong mid-latitude cyclone at higher latitudes during these months, and therefore pose a threat to safe navigation. Cases during 1997-98 have been added to the Klein (1997) database so that this study includes 30 cases of ET occurring in the western North Pacific from 1 June through 31 October 1994-98.

In the transformation stage, satellite imagery and NWP analyses described in Chapter II.A were reviewed for each of the 30 ET cases. In particular, NOGAPS 2.5° and 1° lat./long. resolution analyses were used to prepare SLP charts, as well as plan-view

plots at mandatory levels and vertical cross-sections through the center of the storm of geopotential heights, temperature, moisture, NOGAPS-analyzed vertical motion, and winds. Various physical processes were studied during this stage, including interaction between the TC vortex and the pre-existing, mid-latitude baroclinic zone, lower-tropospheric temperature advection, lower-tropospheric frontogenesis, vertical motion, and response to vertical wind shear. The diagnostic calculations used to study these and any other physical parameters will be described in detail in Chap. III. Similarities between the cases were noted and used to define a three-step conceptual model in Chap. III that describes the appearance of the transformation stage of ET in the western North Pacific, and explains the physical processes that transform a TC into a baroclinic system.

In the re-intensification stage, three NWP forecasts were produced for each case of ET examined: (i) a control forecast in which the NOGAPS analysis from an observed ET case is used to define the initial conditions; (ii) a forecast using that same NOGAPS analysis, except with the TC removed from the analysis field, and (iii) a set of forecasts with the TC shifted to different locations relative to the synoptic-scale circulation patterns in the analysis. The control forecast initial conditions for the Navy Coupled Ocean-Atmosphere Model Prediction System (COAMPS) Version 2.0.13⁴ were prepared using the NOGAPS 2.5° lat./long. (for cases occurring before 1997) or 1° lat./long. (for cases occurring during and after 1997) analyses that coincide with Step 2 (defined in Chapter III) of the transformation stage. Diagnostic calculations of potential vorticity (PV),

⁴ The characteristics, specifications, and other details concerning COAMPS are described by Hodur (1997). Specific descriptions about the geographic domains and methodology used to produce these COAMPS forecasts will be presented in Chapter V.

positive vorticity advection (PVA), divergence, and vertical motion in the mid- and upper-troposphere will be used to define a critical region in the COAMPS control forecast where deep and potentially explosive extratropical cyclogenesis is favored, based on Carlson's criteria (Carlson 1991) and Petterssen Type-B extratropical cyclogenesis (Petterssen and Smebye 1971). The TC will be removed from the analysis field using a procedure developed by Kurihara et al. (1995) for use with the Geophysical Fluid Dynamics Laboratory (GFDL) model, with modifications engineered by Prof. Patrick Harr. This procedure will be described in detail in Chapter V, and is necessary to examine whether or not extratropical cyclogenesis would occur in the same critical region identified in the COAMPS control forecast, even in the absence of the TC that completed ET. Additional COAMPS forecasts will be completed with the initial location of the TC varied within the analysis field, so that the phasing of the translating TC and the critical region could be varied to produce deep (moderate) re-intensification when the TC achieved (did not achieve) proper phasing with the critical region.

III. TRANSFORMATION STAGE OF EXTRATROPICAL TRANSITION

A. TYPICAL SATELLITE IMAGERY

Klein (1997) suggested that the transformation stage of virtually every ET case could be described by a common sequence of infrared (IR) images. The IR images during the transformation stage of ET in the cases of STY Violet and TY Opal (Fig. III-1), STY Ginger and TY Stella (Fig. III-2), and TY Seth and TY Peter (Fig. III-3) illustrate features common to all of the cases. In all six cases, a marked decrease in deep cloudiness and rainbands outside the inner core in the western quadrant of the tropical cyclone occurs in the earliest IR image of the sequence (Figs. III-1a, III-1d, III-2a, III-2d, III-3a, and III-3d). The result is an asymmetric appearance of clouds and deep convection compared to the more symmetric structure during the mature stage of the tropical cyclone. Dry slots also appear between rainbands in the southern quadrant, and the cloudiness there is reduced compared to the eastern and northern quadrants.

In the second IR image of each sequence (Figs. III-1b, III-1e, III-2b, III-2e, III-3b, and III-3e), the dry slots appear to have expanded, and deep convection has nearly ceased in the southern quadrant, and is greatly reduced in the eastern quadrant as well. However, a large area of multi-layer cloud with imbedded deep convection appears in the northern quadrant, and extends around to the western quadrant. The TC outflow interacts with the polar jet to produce a cirrus "shield" (Bader et al. 1995) that features a sharp edge, which implies confluence between this outflow and the polar jet.

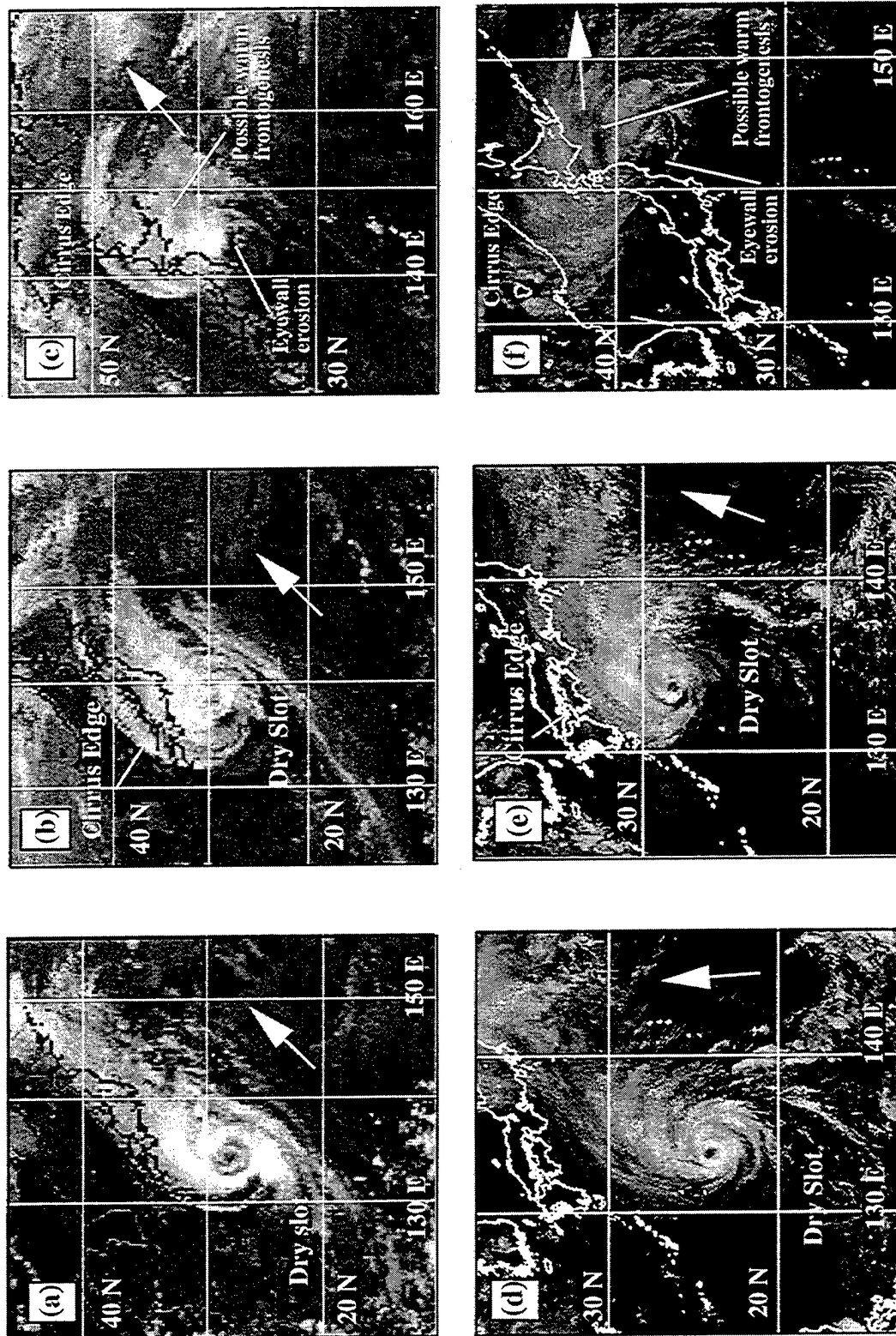


Fig. III-1. Infrared (IR) imagery of the transformation of STY Violet at (a) 0332 UTC 21 September, (b) 1832 UTC 21 September, and (c) 1232 UTC 22 September 1996, and TY Opal at (d) 1232 UTC 18 June, (e) 0432 UTC 19 June, and (f) 1232 UTC 20 June 1997. Notice the change in scale and domain in each imagery frame. The direction of storm motion is depicted by arrows to the right of the storm.

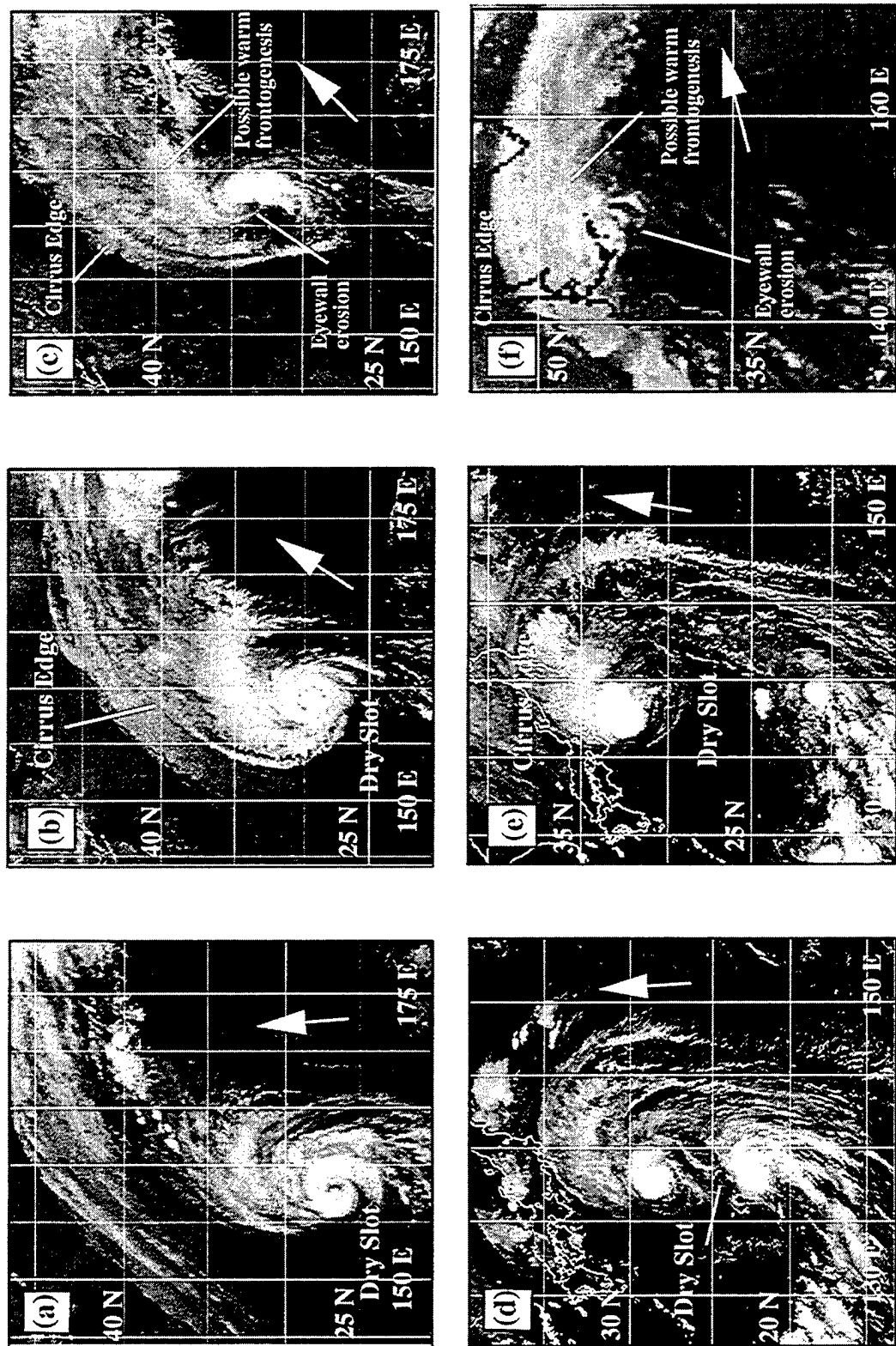


Fig. III-2. As in Fig. III-1, except for the transformation of STY Ginger at (a) 0332 UTC 28 September, (b) 0032 UTC 29 September, and (c) 1232 UTC 29 September 1997, and TY Stella at (d) 0032 UTC 15 September, (e) 1232 UTC 16 September, and (f) 1232 UTC 17 September 1998.

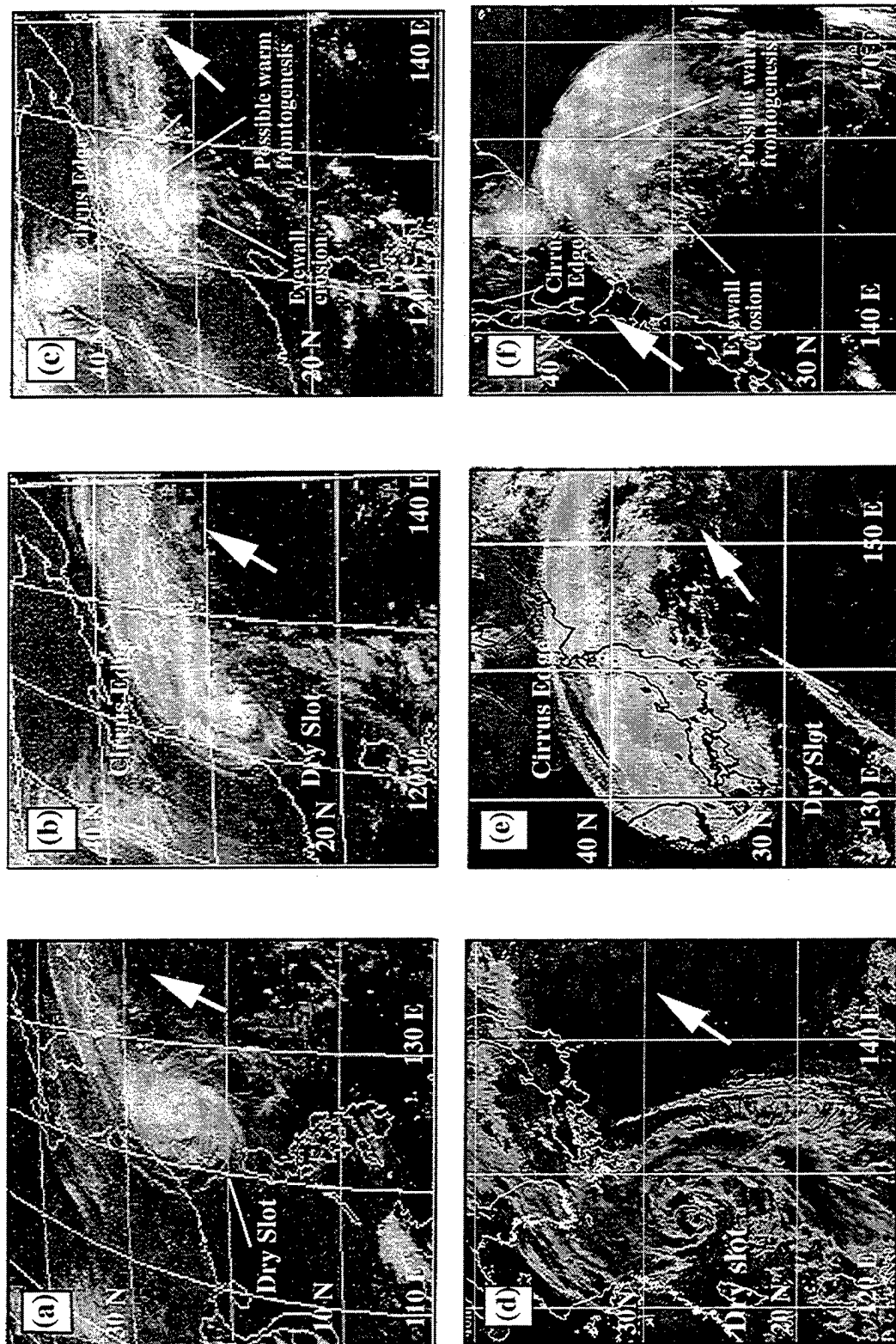


Fig. III-3. As in Fig. III-1, except for the transformation of TY Seth at (a) 1232 UTC 9 October, (b) 1232 UTC 10 October, and (c) 0032 UTC 11 October 1994 and TY Peter at (d) 0032 UTC 28 June, (e) 0032 UTC 28 June, and (f) 0032 UTC 29 June 1997.

The transformation of all six storms is nearly complete in the third IR image of each sequence (Figs. III-1c, III-1f, 1II-2c, 1II-2f, III-3c, and III-3f). Notice the erosion of inner-core deep convection to produce dry "gaps" in what was once the eyewall, particularly west of the storm center. In the outer circulation of the storm, little deep convection is evident anywhere except for that embedded in the large area of multi-layer cloud north and east of the storm center. A band of convective clouds extends from the western part of this multi-layer cloud region and begins to turn southward in the western quadrant of the storm. The cirrus shield described in Figs. III-1b, III-1e, 1II-2b, 1II-2e, III-3b, and III-3e is clearly visible, and the cloud patterns to the north and east of the storm center suggest the commencement of warm frontogenesis. By contrast, the cloud patterns south of the storm center suggest that at most only weak cold frontogenesis has begun. This is consistent with the conclusion of Harr and Elsberry (2000) that cold frontogenesis is typically less vigorous than the warm frontogenesis that occurs during ET.

Twelve of the 30 ET cases either made landfall, or translated close enough to land that the tropical cyclone outer circulation interacted with land, including five cases depicted in Figs. III-1 through III-3 (the lone exception is STY Ginger in Fig. III-2a-c). Despite the interaction with land, the transformation of these five storms appears similar to that of STY Ginger (Fig. III-2), whose track remained far from the coast of Japan. One important exception is that the eastern half of the inner core of STY Ginger remains fairly well organized, with spiraling rainbands that imply continued deep convection. In the 12 cases in which the tracks passed over or close to land, interaction with the terrain appeared to weaken the inner core sufficiently so that it appeared less well organized than

in the remaining 18 cases. This was the only difference in the satellite imagery or NWP analyses noted between cases that interacted with land, and those that did not. Presumably this similarity is because the physical processes during the transformation stage were of a large enough spatial scale that they were relatively unaffected by the small size of the Japanese islands. Whereas only one case of ET achieved landfall over continental Asia, three others passed close enough to China so that their outer circulations briefly interacted with land⁵.

During the transformation stage, the appearance in satellite imagery was not different for the northwest or northeast mid-latitude synoptic patterns. These synoptic patterns were defined at the synoptic time following the final JTWC TC warning message (Harr et al. 2000), which ensured that in most cases the transformation stage was completed, or nearly completed (Table 2). Indeed, the relevance of the synoptic pattern that a transforming TC eventually translates into becomes evident only during the re-intensification stage of ET, and will be examined in detail in Chapter V.

Miller and Lander (1997) discussed modifications to the Dvorak technique of estimating tropical cyclone intensity that could be applied during ET. Consider the sequences in Figs. III-1 through III-3 with respect to the apparent intensity of the transforming storm. In particular, a small eye with an inner eyewall is clearly evident in Fig. III-2a, as is a tight pattern of spiral banding throughout the inner circulation into the eyewall. This banding relaxes somewhat by 0032 UTC 29 September (Fig. III-2b) so that the storm appears to be less intense than 21 h earlier. By 1232 UTC 29 September (Fig.

⁵ The storm tracks of the 30 ET cases will be discussed in greater detail in Chapter IV.

III-2c), the western half of the inner circulation features an erosion of deep convection, although weaker spiral banding is still evident in the remaining inner circulation. Since it is proposed that this three-step IR image sequence is representative of the appearance of the transformation stage of ET in the western North Pacific, it should also be possible to employ satellite imagery to distinguish between different levels of storm intensity once ET has commenced. This does not mean that all tropical cyclones have the same intensity at each step of the imagery sequence of transformation depicted in Figs. III-1 through III-3. Instead, it suggests that all tropical cyclones experience the same systematic weakening during the transformation stage of ET, which allows the forecaster to use this three-step sequence, together with modified Dvorak techniques, to estimate storm intensity during transformation. Recall that by completion of the transformation stage, the wind field of the transformed storm changes drastically (Figs. I-4 and I-5), and the radius of maximum wind increases. Therefore, this technique should not be applied after Step 3, and will result in overestimating wind intensity during Step 3 if the maximum winds have already moved away from the center of the storm.

B. THE TRANSFORMATION OF TY DAVID (SEPTEMBER 1997)

Since a representative, three-step sequence of IR imagery (Figs. III-1 through III-3) can be identified that is similar for each of the 30 ET cases studied, it is hypothesized that the physical processes responsible for that appearance are also similar in these ET cases. The transformation of TY David (September 1997) is presented as an archetypal example of how NOGAPS 2.5° lat./long. resolution (for cases occurring in 1994 through 1996) and 1° lat./long. resolution analyses (for cases occurring in 1997-98) can be used to

diagnose and explain the physical processes that occur during the transformation stage of all 30 TCs that complete ET in the western North Pacific during 1 June through 31 October 1994-98. A three-step conceptual model, based on thorough review of these 30 ET cases, is proposed in Chapter III-C as a description of how virtually every case of ET that occurs over the western North Pacific completes the transformation stage of ET.

Even during the June through October period studied, a recurving tropical cyclone in the extreme western North Pacific may encounter a region of considerable baroclinity with a northeast-southwest orientation parallel to the east Asian coast. If the tropical cyclone recurves farther to the east, it will approach a more east-west oriented zone farther to the north over the open Pacific Ocean. It is the interaction of the TC circulation with the baroclinic zone and its associated vertical wind shear that initiates the transformation stage of ET. Consequently, some differences in ET timing may occur if the tropical cyclone moves poleward closer to the coast and interacts with the southwest-northeast baroclinic zone, instead of recurving farther eastward where the baroclinic zone is more east-west. Otherwise, the appearance in satellite imagery of the three steps of the transformation stage is not affected by the season (summer or autumn) in which the case of ET occurs.

At 0000 UTC 18 September, TY David is translating north-northwest over decreasing sea-surface temperatures (Fig. III-4a) as it approaches the Kuroshio that branches eastward from Honshu, Japan. A NOGAPS analysis of the air temperature at a height of 2 m (Fig. III-4b) suggests that except for a small area in the eastern quadrant of the storm, the sea surface is warmer than the air above it. Despite this, the amount of

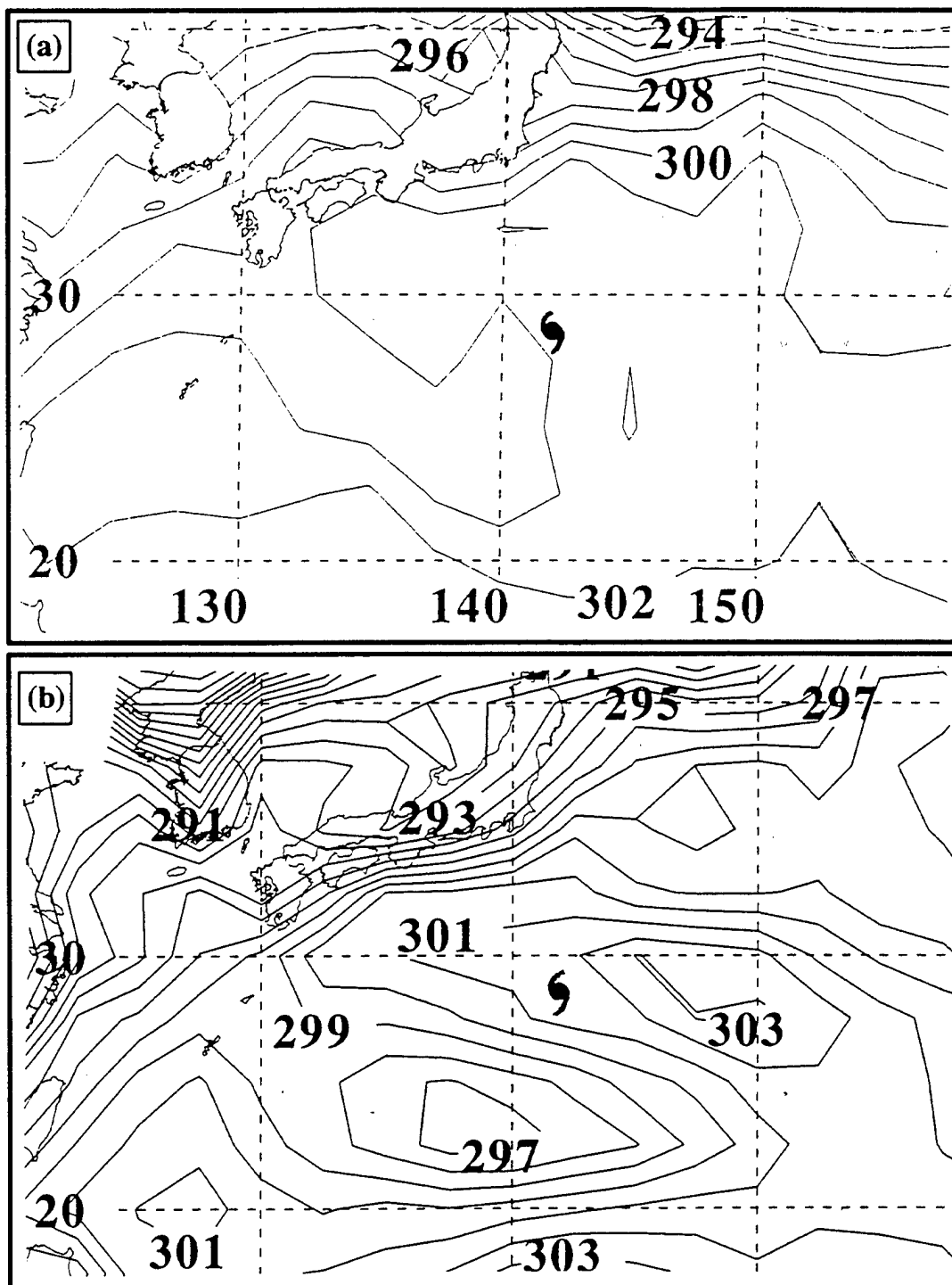


Fig. III-4. NOGAPS analysis of (a) sea-surface temperature (solid contours, 1 K interval) and (b) 2 m air temperature (solid contours, 1 K interval) at 0000 UTC 18 September 1997.

deep convection has decreased in the western quadrant by 0332 UTC 18 September (Fig. III-5a) compared to earlier IR imagery (not shown), and the resulting distribution of clouds and rainfall (with continued deep convection in the remaining quadrants) has become more asymmetric. Notice also the dry slot forming in the southern quadrant, and wrapping around into the eastern quadrant. Visible imagery (Fig. III-5b) reveals rows of cumulus in the western quadrant, and clearly depicts the location of the baroclinic zone. In this case, the island chain to the northwest may have locally added to the modified air flow characteristics in that quadrant of the circulation. Water vapor imagery (Fig. III-5c) confirms that the environmental flow to the west of David is dry, and that the western quadrant is drier than in the other quadrants at the same distance from the center. However, a SSM/I pass at 2259 UTC 17 September (Fig. III-5d) indicates the deep convection in the inner core of the storm is still quite symmetric.

The imagery in Fig. III-5 can be supplemented with the NOGAPS analysis of 1000 mb streamlines and equivalent potential temperature (θ_e) at 0000 UTC 18 September (Fig. III-6a) to confirm that the transformation stage of ET has begun. The outermost part of TY David's circulation is just beginning to impinge on a pre-existing baroclinic zone that is oriented from southwest to northeast in the Japan Sea. Whereas the large-scale environmental flow to the west of TY David is advecting cooler, drier air with low values of θ_e equatorward into David's circulation, the flow pattern is also locally being modified by the islands. Meanwhile, a poleward flow to the east of TY David maintains the inflow of warm, moist air into the eastern quadrant of the storm. As a result, tropical cyclone

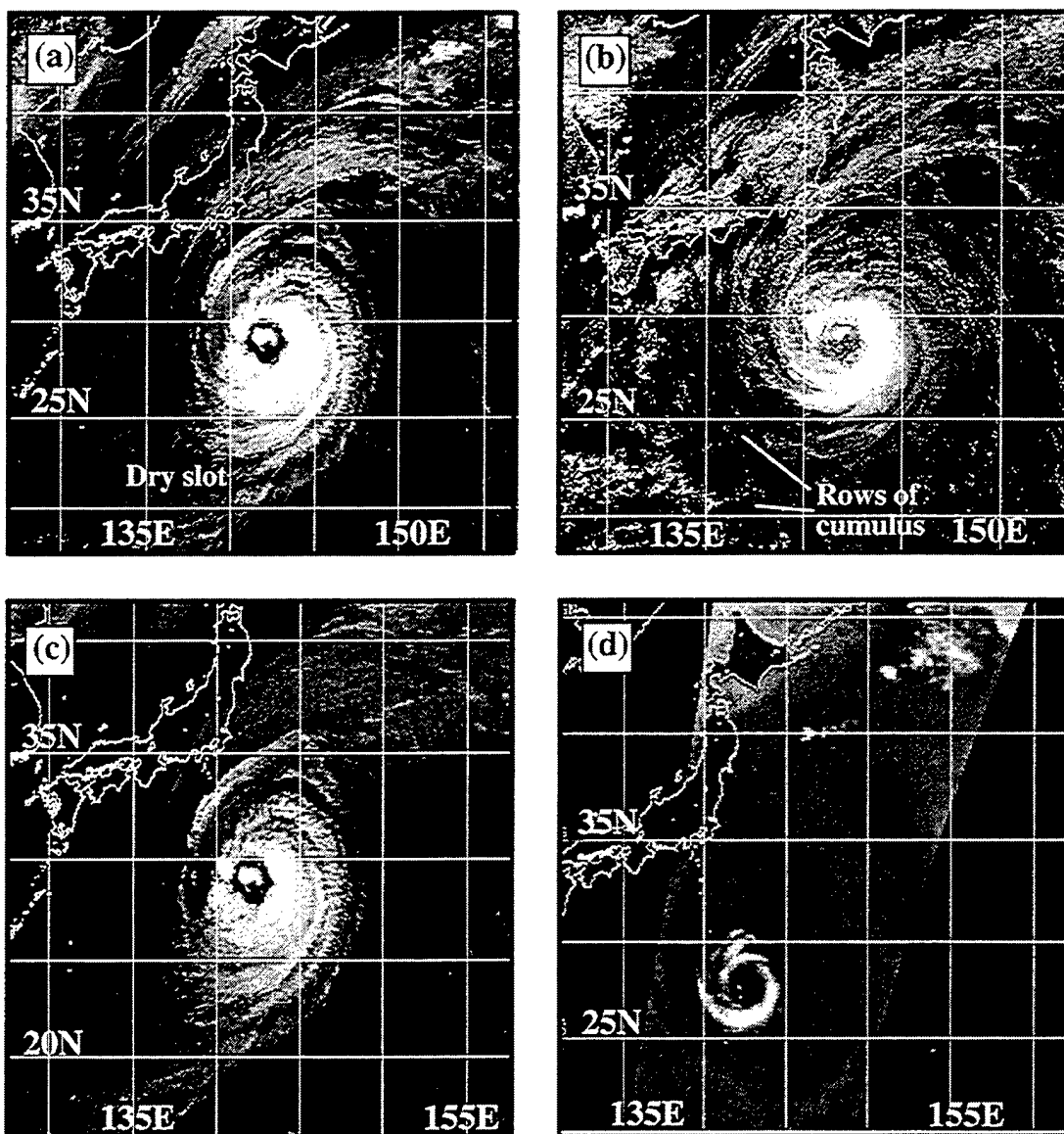


Fig. III-5. Step 1 of transformation of TY David depicted in (a) IR imagery, (b) visible imagery, and (c) water vapor imagery at 0332 UTC 18 September, and (d) 85 GHz SSM/I imagery at 2259 UTC 17 September 1997.

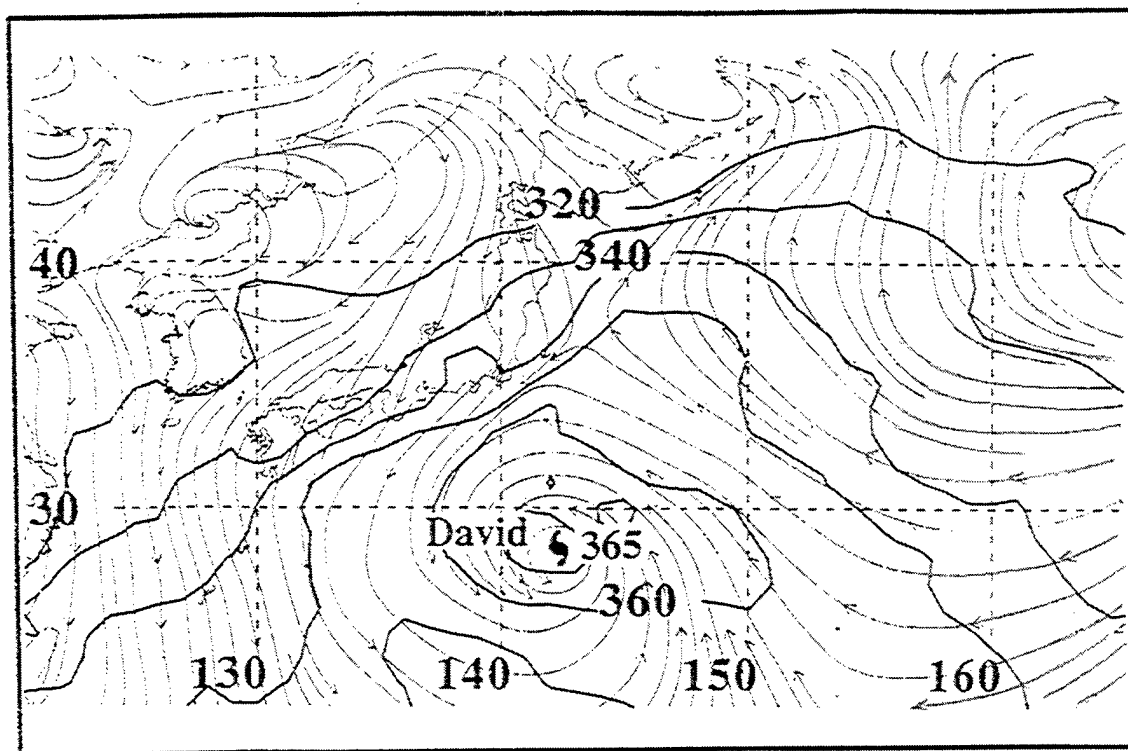


Fig. III-6. Step 1 of the transformation of TY David depicted at 0000 UTC 18 September 1997 in NOGAPS (a) analysis of equivalent potential temperature (heavy solid contours, 10 K interval except for 365 K isentrope) and streamlines at 1000 mb.

convection persists in the eastern and northern quadrants, and the storm exhibits an asymmetric pattern of deep convection (Fig. III-5). Thus, TY David has commenced Step 1 of the transformation stage of ET according to the definition presented in Chapter II.

Vertical west-to-east cross-sections through the storm center of θ_e and winds (Fig. III-7a), and PV and vertical motion (Fig. III-7b) from the NOGAPS analysis depict the predominantly tropical characteristics of TY David at 0000 UTC 18 September. Cross-sections of hydrostatic Ertel PV are prepared using

$$PV = -g(\zeta + f) * (\partial\theta / \partial p).$$

Cross-sections of vertical motion (ω) are prepared using NOGAPS model-derived vertical motion. It is acknowledged that the 1° lat./long. resolution of these cross-sections is

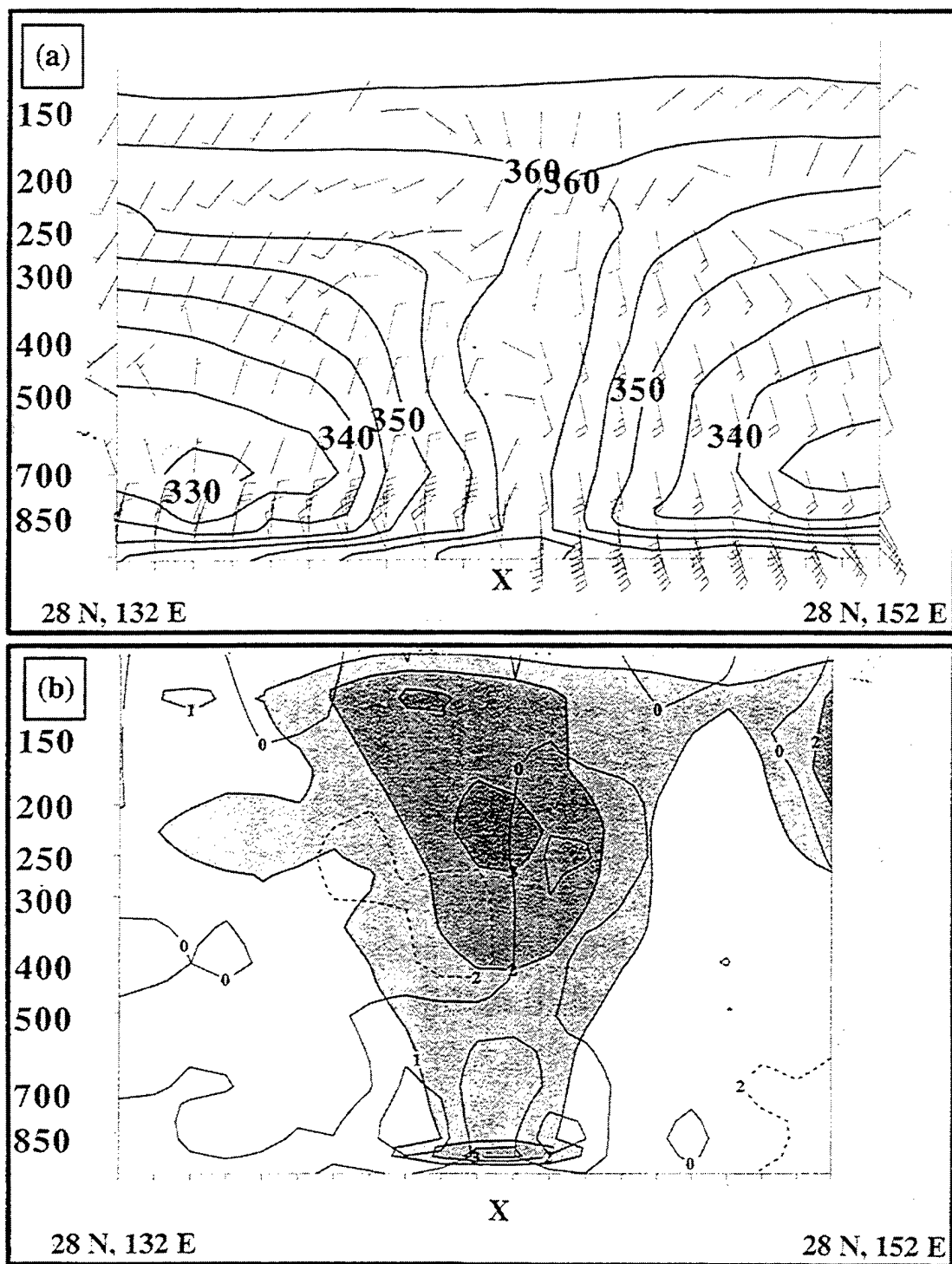


Fig. III-7. Step 1 of the transformation of TY David depicted at 0000 UTC 18 September 1997 in NOGAPS vertical east-west cross-sections through the center of TY David (marked "X") of (a) equivalent potential temperature (5 K interval) and winds (5 m/s interval), and (b) potential vorticity (shaded, in units of $10^{-6} \text{ m}^2 \text{ K} / (\text{s kg})$) and NOGAPS analyzed vertical motion ($2 \times 10^{-3} \text{ mb/s}$ interval), with ascent (descent) represented by solid (dashed) contours, and (c) hodograph of azimuthally averaged u and v wind components (m/s) around a circle with radius of 300 km from the storm center, at mandatory levels between 850 and 200 mb. The approximate distance between tick marks is 100 km.

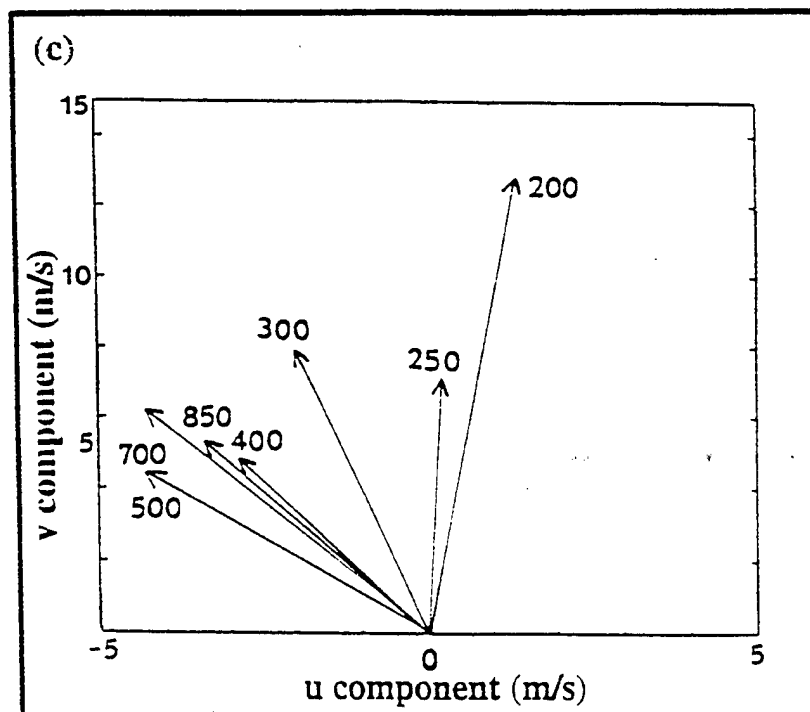


Fig. III-7 (continued).

insufficient to depict accurately the actual distribution of θ_e and PV in the inner core of the storm. However, these analyses provide a qualitative description of the physical processes occurring beyond the inner core of the storm during transformation, and should provide a quantitative description of physical processes occurring on a scale greater than 300 km. Furthermore, NOGAPS combines synthetic observations with previous model 6 h forecasts of the TC vortex that exist in the first guess field, as well as current observations (including water vapor winds) to develop the TC vortex in the analysis until JTWC determines that the TC has become extratropical. Thus, it is believed that NOGAPS will properly represent the TC vortex during the transformation stage, although such a representation is not solely the result of the synthetic TC observations.

At 0000 UTC 18 September, the NOGAPS analysis depicts a distinct warm core that extends up to 200 mb above David (Fig. III-7a). The 365 K isentrope of θ_e below

850 mb indicates that a warm, moist pool of lower-tropospheric air is associated with TY David. Notice also that the maximum winds are located in the lower troposphere, immediately on either side of the storm center. Two PV maxima, one near the surface and one associated with the upper-tropospheric warm core, are analyzed (Fig. III-7b), and upward vertical motion exists on either side of the storm center below 500 mb. An area of descent is also evident between 400 mb and 250 mb west of the storm center. This subsidence, combined with the intrusion of cooler, drier air into the western quadrant (Figs. III-5 and III-6), is believed responsible for the drastically reduced deep cloudiness in the western quadrant, and the formation of the dry slot southwest of the storm center (Fig. III-5).

Since TY David has begun to interact with a pre-existing baroclinic zone (Fig. III-6), it is worthwhile to examine the vertical wind shear associated with this lower-tropospheric baroclinity. Vertical wind shear was calculated at 0000 UTC 18 September by azimuthally averaging the u and v wind components (m/s) along a circle of 300 km radius, centered on the storm, at all mandatory levels from 850 mb to 200 mb (Fig. III-7c). The change in wind direction from southeasterly in the lower- and mid-troposphere to south-southwesterly in the upper troposphere is consistent with David's imminent recurvature through the subtropical ridge. Although very little vertical shear exists between 850 mb and 400 mb, the wind shear from 400 mb to 200 mb is nearly 7.5 m/s from the southwest.

Over the next 24 h, TY David recurved and began to translate north-northeastward until the center was less than 100 km from the lower-tropospheric

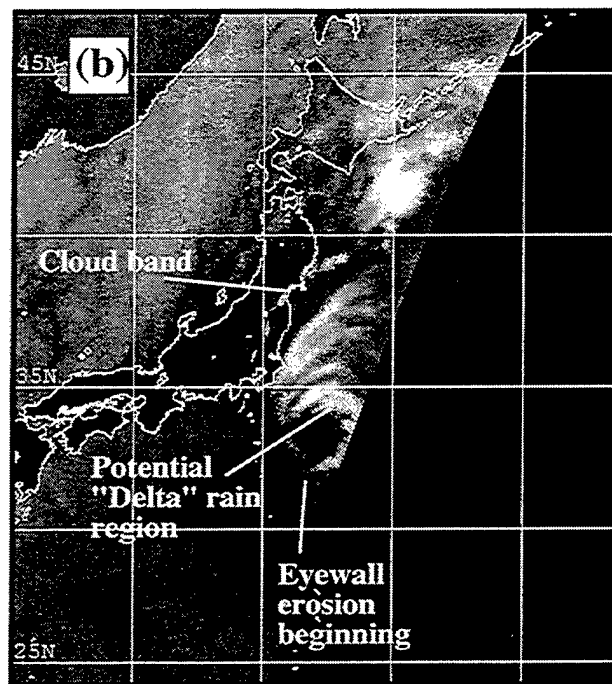
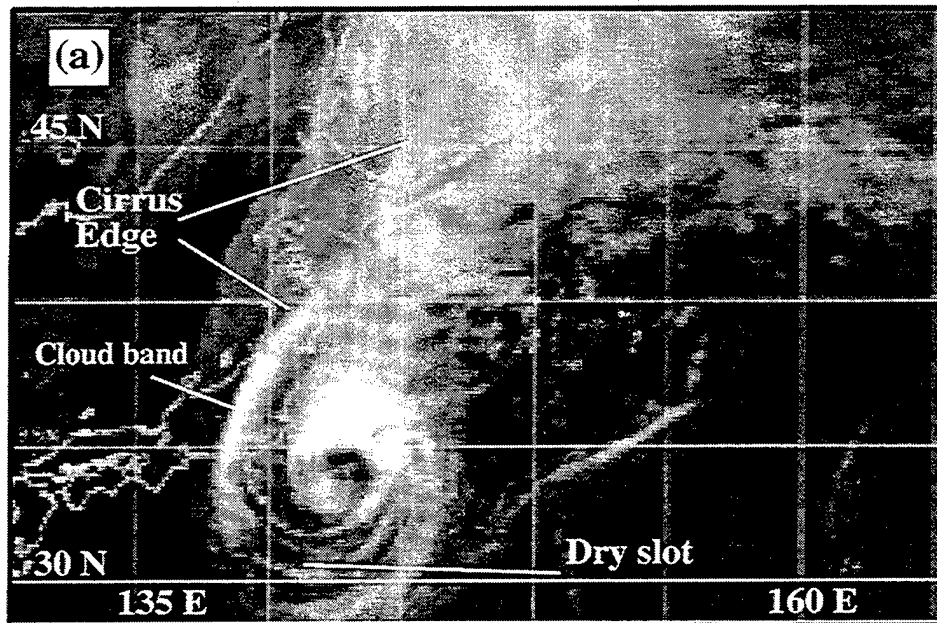


Fig. III-8. Step 2 of transformation of TY David depicted in (a) IR image at 2332 UTC 18 September, and (b) 85 GHz SSM/I image at 2216 UTC 18 September 1997.

baroclinic zone. Step 2 of David's transformation can be inferred from IR and SSM/I imagery. The same features noted in the satellite IR imagery at 0332 UTC 18 September (Fig. III-5) can again be readily identified at 2332 UTC 18 September (Fig. III-8a). An extensive dry slot is present in the southern quadrant (Fig. III-8a), and evidence of dry air is suggested in the SSM/I imagery at 2246 UTC 18 September (Fig. III-8b) even in the innermost circulation of the storm. Deep convection in the inner region appears to be eroding, particularly west and south of the storm center. A large cirrus shield (Fig. III-8a) indicates a strong upper-tropospheric outflow that is interacting with the polar jet (Bader et al. 1995). A large region of multi-layer cloud with embedded convection immediately north of the storm is evident in both the IR and SSM/I imagery (Fig. III-8). Notice that the triangular-shaped region of convection north of the storm center. Shimazu (1998) reviewed conventional radar reflectivity patterns during 16 typhoons that struck Japan, and in all seven cases in which a typhoon approached a mid-latitude frontal zone, a triangular-shaped "delta rain region" similar to the one depicted in Fig. III-8 was observed north of the storm center. A distinct cloud band northwest of the storm that extends around the storm into the western quadrant is also evident in Figs. III-8a and b.

The NOGAPS analysis of 1000 mb streamlines and θ_e at 0000 UTC 19 September (Fig. III-9a) depicts continuing equatorward (poleward) environmental advection of cooler, drier (warm, moist) air that has penetrated farther into the storm's outer circulation west (east) of the storm center than it did 24 h earlier. This advective process also affects the baroclinic zone during this period. At 0000 UTC 18 September, the poleward edge of the baroclinic zone (Fig. III-6, defined by the 320 K isentrope) east of

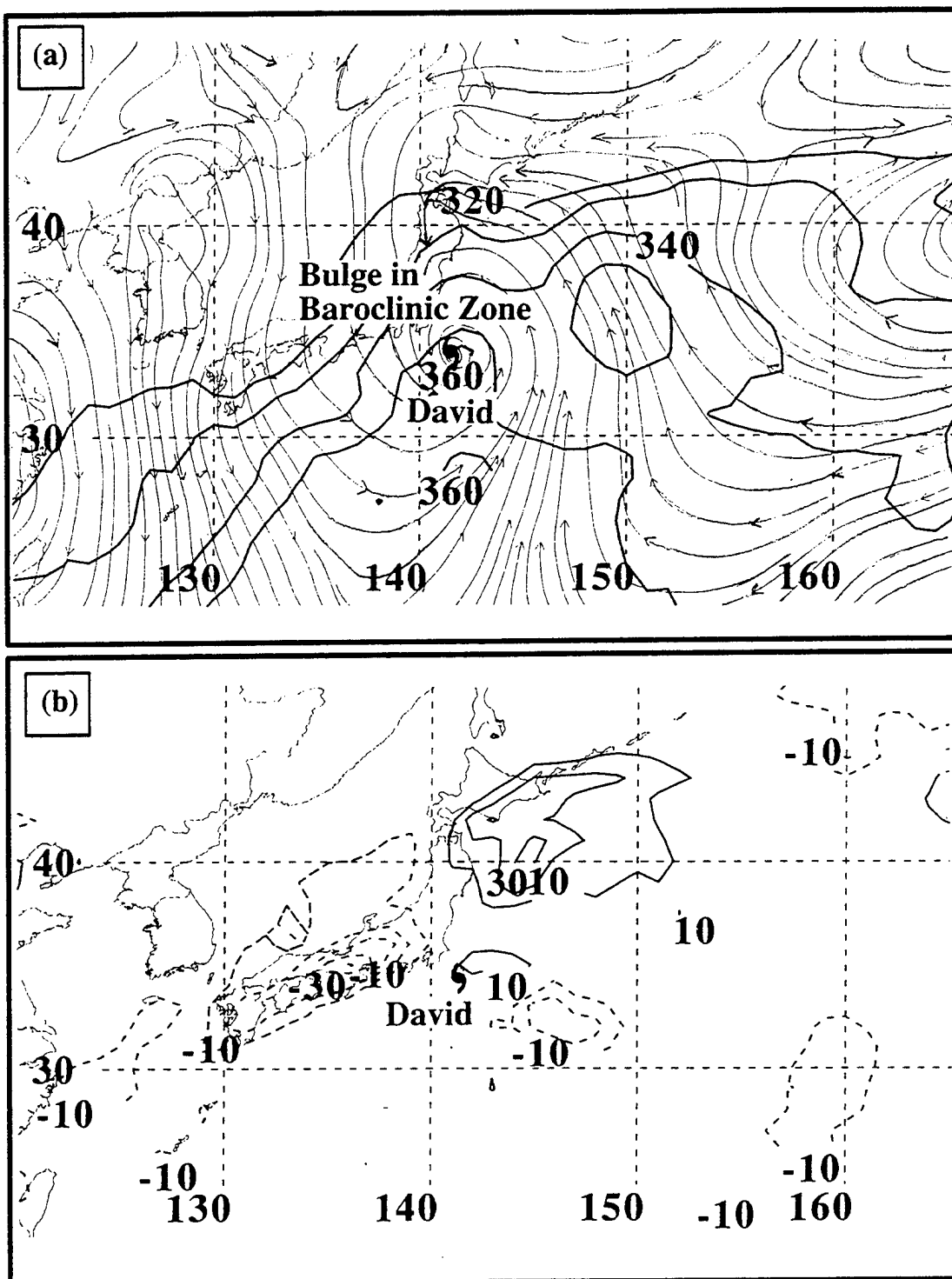


Fig. III-9. Step 2 of transformation of TY David at 0000 UTC 19 September 1997 depicted in NOGAPS (a) analysis of equivalent potential temperature (heavy solid contours, 10 K interval) and streamlines at 1000 mb, and (b) 850-mb warm (cold) temperature advection, represented by solid (dashed) contours (units 10^{-5} K/s).

135°E is located in the Japan Sea. By 0000 UTC 19 September, this isentrope has advanced southeast to the eastern coast of Japan (Fig. III-9a). In addition to the more southwest-to-northeast tilt, the isentropes in the baroclinic zone are more tightly packed directly to the west of the storm. Similarly, the gradient of isentropes has tightened east of 145°E along 42°N so that the low-level streamlines are lifted over an extensive east-west baroclinic zone north and east of the storm. Notice the circulation center is in a lower-tropospheric pool of higher θ_e values that has impinged on the baroclinic zone to form a bulge to the north of the storm (Fig. III-9a).

At 0000 UTC 19 September, cold (warm) advection (Fig. III-9b) is clearly evident west (northeast) of the storm associated with the equatorward (poleward) environmental air inflow with low (high) values of θ_e described earlier. On the larger scale, the lower-tropospheric temperature advection has maximum (minimum) values northeast (west) of the storm at 40°N, 145°E (35°N, 136°E), where the environmental θ_e gradient is the strongest. The warm advection region corresponds well with the swath of multi-layer cloud region (Fig. III-8) developing north and east of the storm. By contrast, the cold advection region west of the storm corresponds well with the dry region in Fig. III-8. A smaller scale warm/cold advection dipole is found to the east of David as the tropical cyclone circulation interacts with the adjacent thermal pattern.

Two important characteristics can be observed in the 500-mb analysis at Step 2 of the transformation stage. During Step 1, David's surface center is located beneath concentric, closed 500-mb contours, and is equatorward of the 5820-m contour associated with a short-wave trough to the northwest of the storm (Fig. III-10a). During Step 2 (Fig.

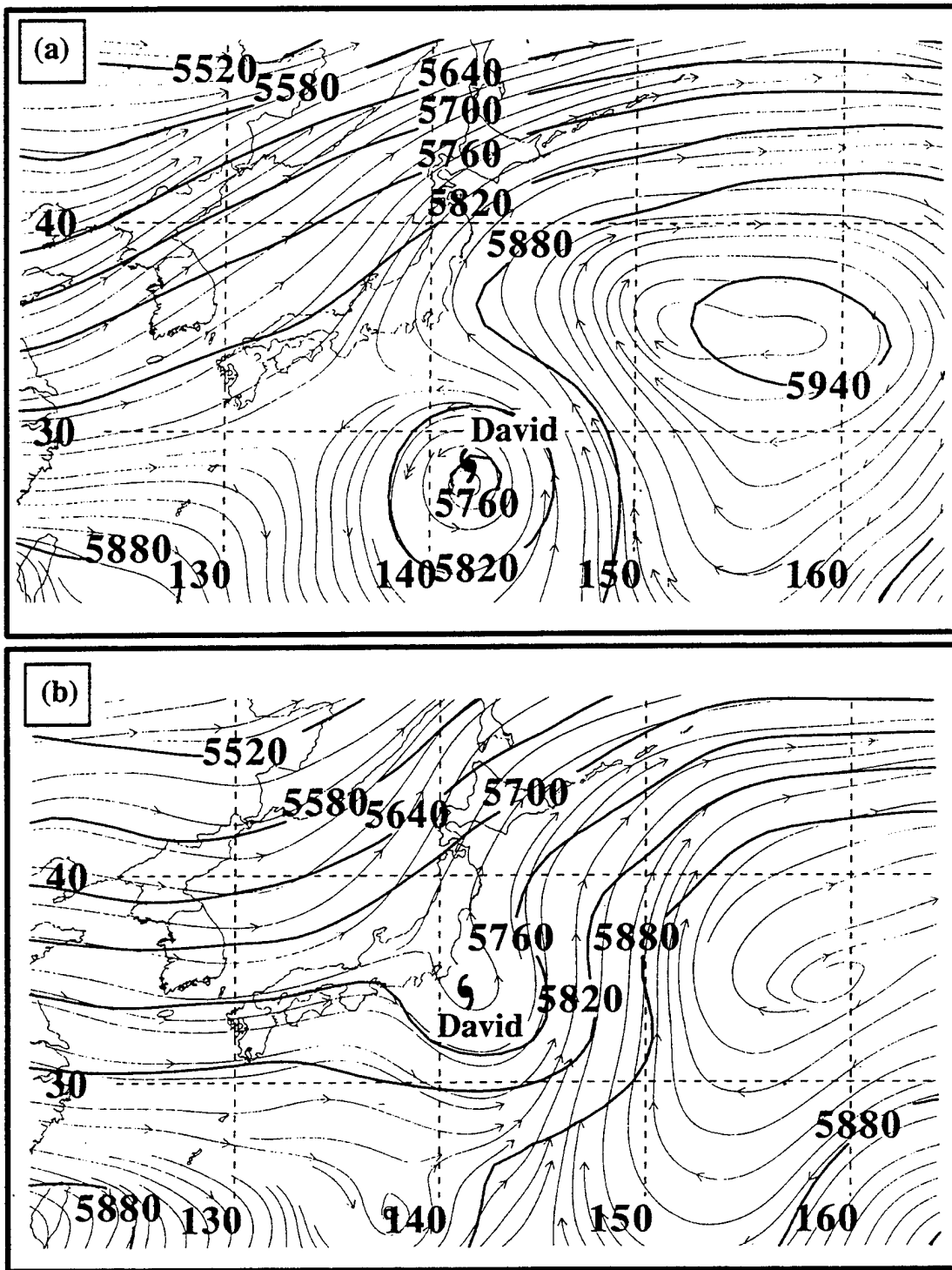


Fig. III-10. NOGAPS analysis of 500-mb isoheights (solid, 60 m interval) and streamlines at (a) 0000 UTC 18 September, and (b) 0000 UTC 19 September 1997.

III-10b), the closed contours associated with David 24 h earlier have combined with the approaching 500-mb trough so that David appears to be in an open wave. Furthermore, the streamlines associated with this short-wave trough have wrapped around the circulation of David, which indicates that David has become imbedded in the 500-mb westerlies. This open wave in the 500-mb isoheights was evident during Step 2 of the ET transformation stage in 26 of the 30 (87%) ET cases studied. If a 500-mb isoheight contour interval of 30 m is selected (not shown), a closed contour above David's surface center suggests that the warm core is still present. This is consistent with the persistence of inner-core convection in Fig. III-8. Nevertheless, forecasters should anticipate this open wave and streamline pattern in 500-mb isoheights during Step 2 of the transformation stage provided the standard interval of 60 m is used.

A southwest-northeast vertical cross-section through the storm center (Fig. III-11a) indicates that the closed 360 K θ_e contour that defined the upper-tropospheric warm core at 0000 UTC 18 September (Fig. III-7b) has been dispersed, and the lower- and mid-tropospheric warm core has been weakened. Also evident in Fig. III-11a is advection downstream of the tropical cyclone warm core (as defined by the 350 K contour) above 700 mb, and vigorous southerly winds northeast of the storm center below 400 mb (Fig. III-11a). A southwest-northeast vertical cross-section of PV and NOGAPS model-derived vertical motion (Fig. III-11b) indicates that ascent is analyzed northeast of the storm center (Fig. III-11b), which suggests that these air parcels ascend the tilted isentropic surfaces that are nearly east-west oriented (Fig. III-9a). This flow turns cyclonically (Fig. III-9a) and descends (presumably dry adiabatically) into the western

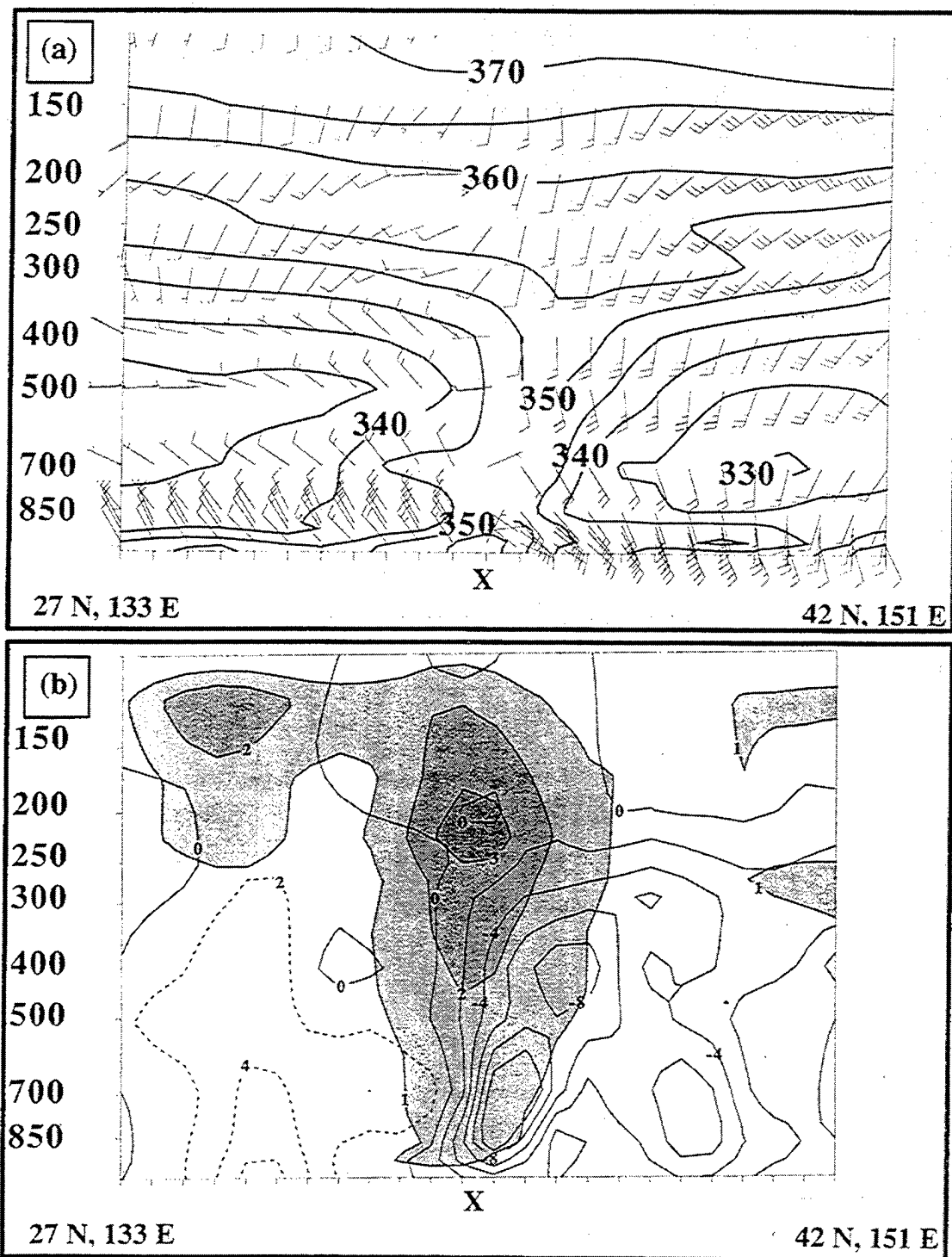


Fig. III-11. As in Fig. III-7a and b, except for vertical southwest-northeast cross-sections through the center (marked "X") at Step 2 of the transformation of TYDavid on 0000 UTC 19 September 1997. The approximate distance between tick marks is 100 km.

quadrant southwest of the storm center (Fig. III-11b). This air thus has lower values of θ_e , and subsequent advection into the southern quadrant close to the storm center is considered to be responsible for the erosion of deep convection observed there (Fig. III-8). Even though the upper-tropospheric warm core has been dispersed, a PV maximum is located between 250 mb and 150 mb (Fig. III-11b). Values of PV > 1 unit are found 300 km southwest of the storm center at 300 mb, but are 500 km northeast of it at 200 mb, so that PV is asymmetrically distributed relative to the storm center. Weakening of the lower-tropospheric winds is reflected in absence of the lower-tropospheric PV maximum that was present 24 h previously. Notice also the PV maximum above 150 mb southwest of the storm, which is an upper-tropospheric reflection of the approaching short-wave trough northwest of David in the 500-mb analysis (Fig. III-10b).

As during Step 1, environmental vertical wind shear was calculated at Step 2 (Fig. III-12a). The wind shear from 850 mb to 250 mb has increased in 24 h to nearly 9 m/s, and the winds at each level are from the southwest. According to the moist numerical simulations of Ritchie and Elsberry (1999) and Frank and Ritchie (1999), vertical wind shear should produce a tilt downstream of isentropic surfaces and contours of PV, and a vertical motion dipole with maximum ascent (descent) located downshear and left (upshear and right). Thus, it is suggested that this vertical shear flow is responsible for the advection of the upper-tropospheric warm core downstream (Fig. III-11a) and the asymmetry of the PV contour > 1 unit (Fig. III-11b). It is also believed that this shear contributes to the descent analyzed southwest of the storm center. However, a descent maximum at 900 mb (Fig. III-11b) is located where streamlines are believed to descend

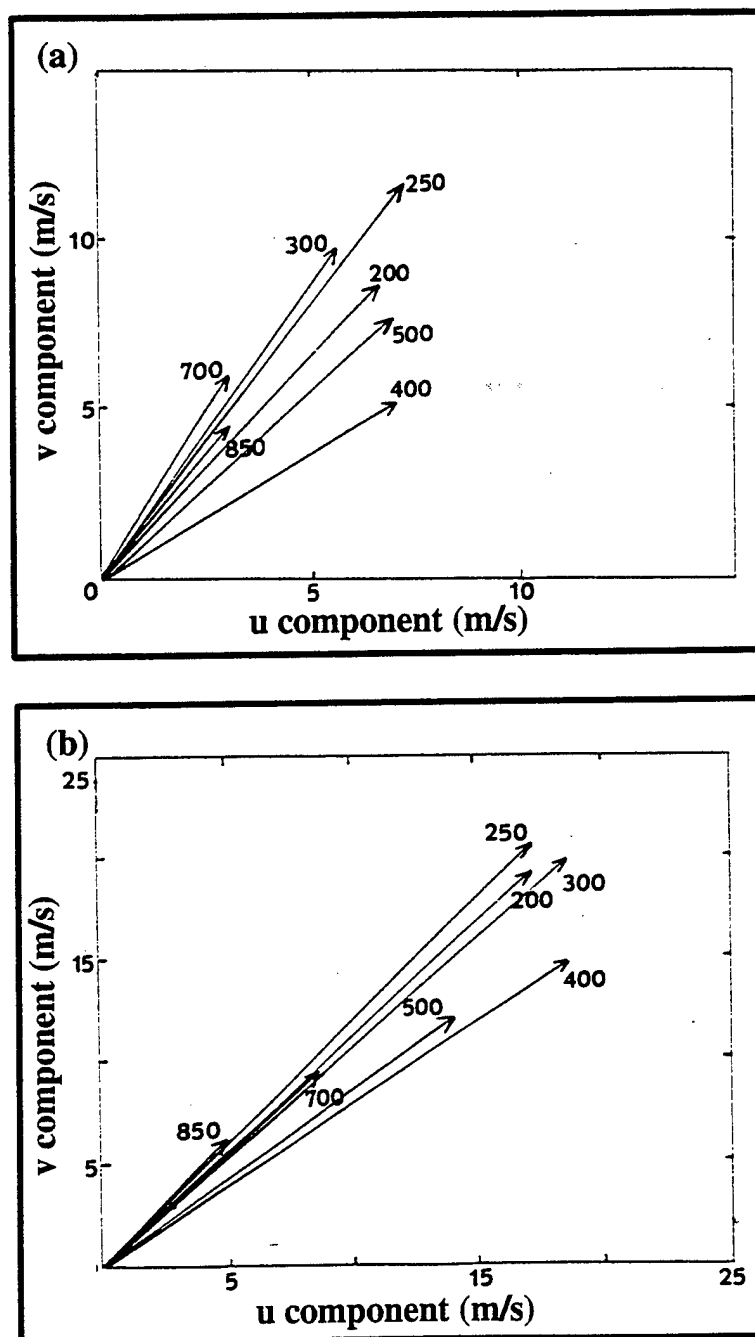


Fig. III-12. Hodograph of azimuthally averaged u and v wind components (m s^{-1}) around a circle with a radius of 300 km from the storm center, at mandatory levels between 850 mb and 200 mb at (a) 0000 UTC 19 September, and (b) 1200 UTC 19 September 1997. Notice the different wind scales on the abscissa and the ordinate in each case.

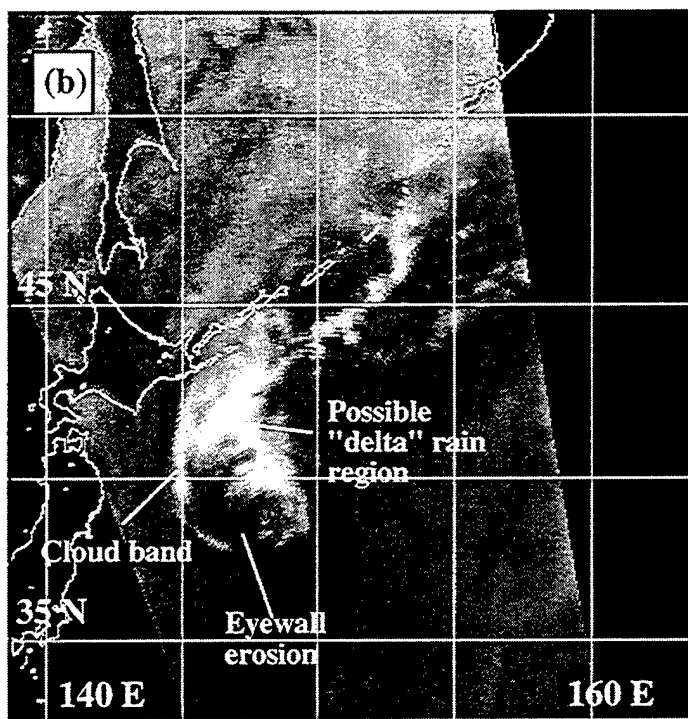
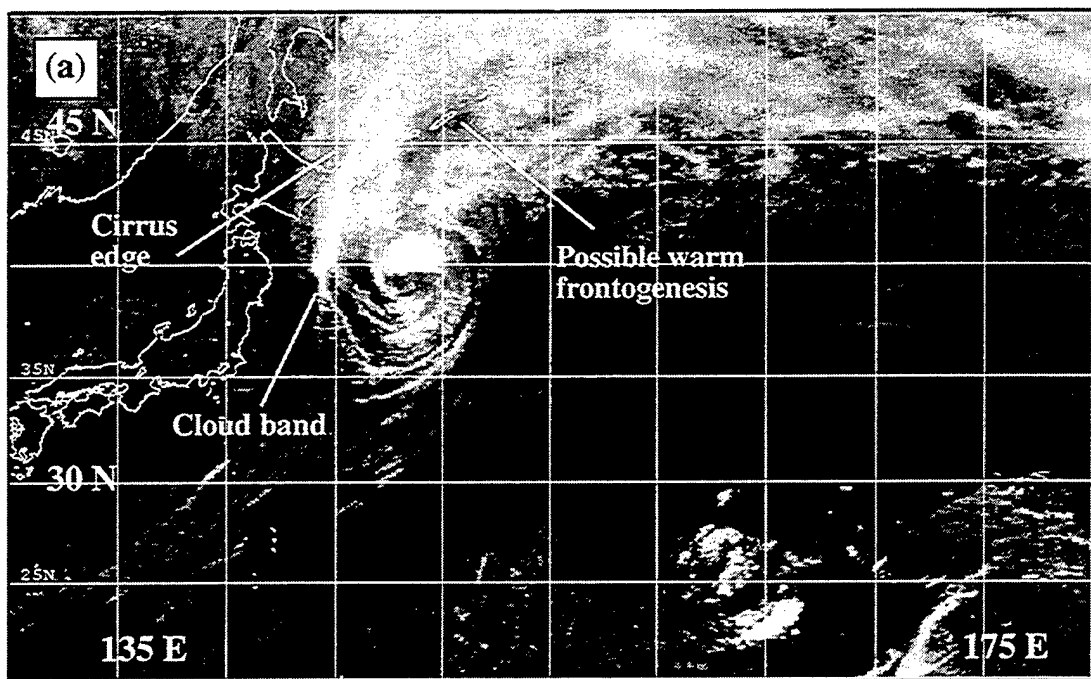


Fig. III-13. Step 3 of transformation of TY David depicted in (a) IR image at 1232 UTC 19 September, and (b) 85 GHz SSM/I image at 1120 UTC 19 September 1997.

dry adiabatically as they turn cyclonically into the western quadrant (Fig. III-9a). Since David is simultaneously interacting with vertical wind shear collocated with lower-tropospheric baroclinity, it is difficult to determine how much of the analyzed descent is due to vertical wind shear (Frank and Ritchie 1999) or lower-tropospheric baroclinic effects.

During the third step in the ET transformation, David continues to translate poleward. At 1232 UTC 19 September, significant deep convection is no longer evident in the outer western, southern, and eastern quadrants (Fig. III-13a). Instead, the remnants of TY David now more closely resemble a mid-latitude cyclone, with a large swath of multi-layer cloud that implies warm frontogenesis has commenced north and east of the center, but little evidence to suggest that cold frontogenesis may have commenced south of the center. Brightness values in the 85 GHz SSM/I image (Fig. III-13b), which are a proxy for rainfall from deep convective clouds, suggest greatly reduced rainrates in the southwestern portion of the inner core of the storm. However, remnants of the "delta rain region" that were evident 12 h earlier may be identified in Fig. III-13b slightly northwest of the storm center. Also evident in both Figs. III-13a and b is the distinct cloud band farther north and west of the storm center that was first described in Step 2. The region of deep convection north of the storm center is to the left of the vertical wind shear direction (Fig. III-13b). This location is consistent with the numerical simulations of Ritchie and Elsberry (1999) and Frank and Ritchie (1999) that have maximum values of ascent left of the direction of the vertical wind shear, even though the shear in this case is concentrated in the lower troposphere below 400 mb.

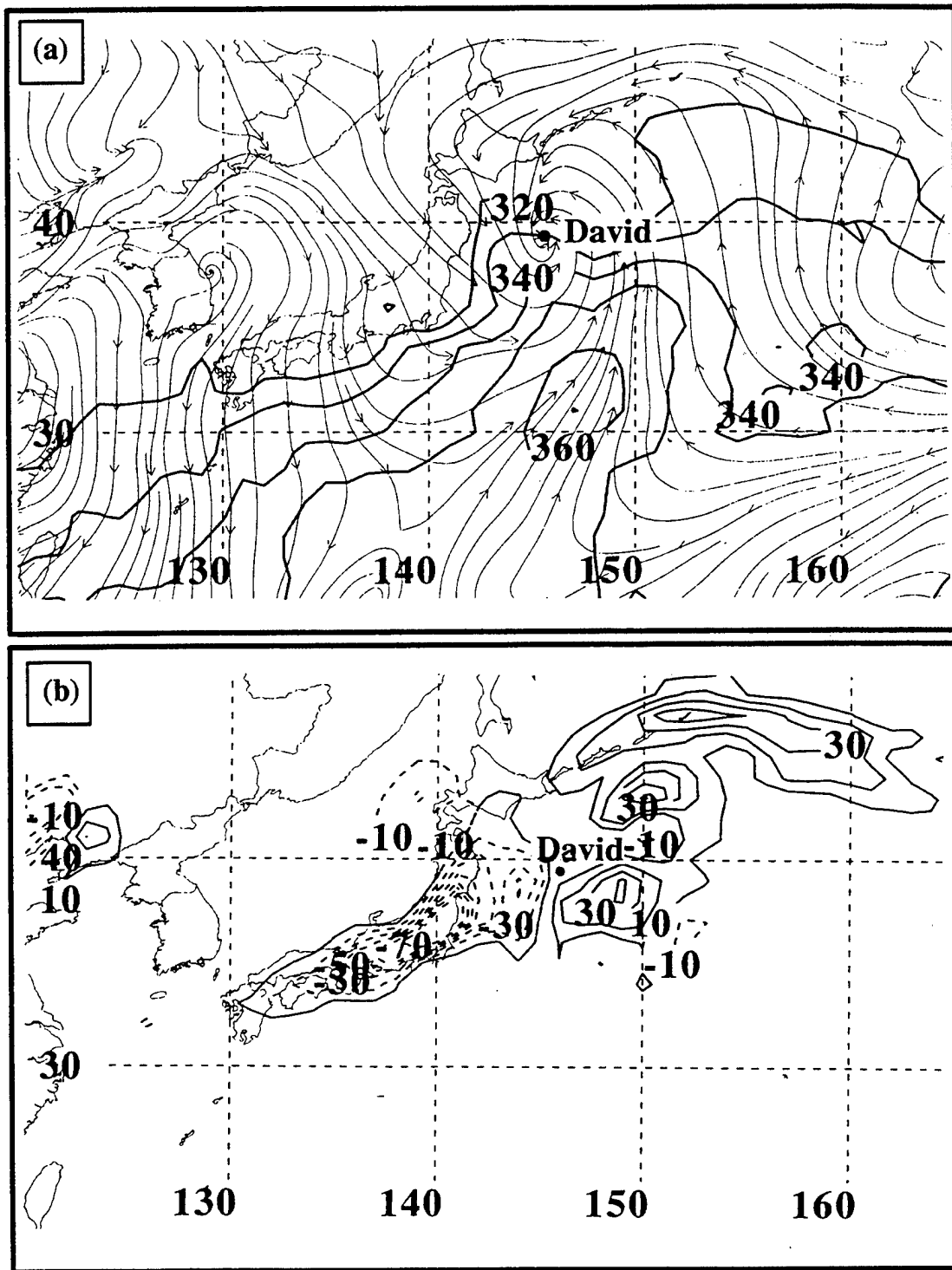


Fig. III-14. As in Fig. III-9, except for Step 3 of the transformation of TY David at 1200 UTC 19 September 1997.

As in the previous two steps of David's ET transformation, the 1000-mb analysis at 1200 UTC 19 September (Fig. III-14) again depicts equatorward (poleward) advection of cooler, drier (warm, moist) environmental air toward the inner core of the storm. Although the remnants of David's circulation center are clearly within the baroclinic zone, a small bulge of higher θ_e air remains associated with the center in the NOGAPS analysis. During the past 12 h, the θ_e gradient in the baroclinic zone east of the storm center from 145°E to 155°E has increased. Ascent of the poleward environmental flow over tilted isentropic surfaces is analyzed east and north of the storm (not shown), and (dry adiabatic) descent is implied where this flow turns cyclonically into the western quadrant and toward the inner core of the storm. These processes are responsible for the lack of deep convection in the western, southern, and eastern quadrants, and the erosion of convection in the southwest quadrant of the inner core (Fig. III-13b).

Calculations of lower-tropospheric frontogenesis by Harr and Elsberry (2000) suggest that vigorous warm frontogenesis and weak cold frontogenesis should be anticipated in most cases of ET. In this study, significant frontogenesis was typically not observed until Step 3 of the transformation stage. The satellite imagery in Fig. III-13, NOGAPS analyses of 1000-mb θ_e and streamlines (Fig. III-14a), and calculations of 850-mb temperature advection (Fig. III-14b) provide supporting evidence that lower-tropospheric frontogenesis may be commencing in Step 3 of TY David's transformation. Notice the large values of warm (cold) advection (Fig. III-14b) to the northeast (southwest) of the storm center.

Contributions to 900-mb frontogenesis may be examined using the Miller frontogenesis equation adapted by Carlson (1991)

$$d/dt(-\partial\theta/\partial y') = (\partial u/\partial y')(\partial\theta/\partial x') + (\partial v/\partial y')(\partial\theta/\partial y') + (\partial\omega/\partial y')(\partial\theta/\partial p) .$$

In this expression, the first (second) term on the right side represents contributions to lower-tropospheric frontogenesis due to horizontal wind shear (confluence) in the y' direction normal to the frontal zone in the direction of the cold air, and the third term on the right represents contributions due to vertical motion ("tilting" term). In this analysis, the diabatic term is not calculated. Based on Carlson (1991), it was expected that the confluence (horizontal shear) term would be the leading term where warm (cold) frontogenesis had commenced. The objective of this analysis is to illustrate how a forecaster could confirm quantitatively the frontogenesis implied in satellite imagery at any step of the transformation. Notice that a maximum in 900-mb frontogenesis due to the confluence term (Fig. III-15a) exists in a region of 900-mb streamline confluence and widespread, strong warm advection (Fig. III-14b) that corresponds well to the region labeled "possible warm frontogenesis" in Fig. III-13a. In Fig. III-15b, a maximum of 900-mb frontogenesis northeast of David is in a region of horizontal shear in the 900-mb streamlines, which corresponds well to the cloud band and delta rain region northeast of the storm center in both IR and SSM/I imagery (Fig. III-13). Notice that the shear term contributions (Fig. III-15b) do not indicate significant cold frontogenesis south of David.

A south-north cross-section along 150°E (Fig. III-15c) depicts a direct circulation (with an ascent maximum at 48°N) in the region where warm frontogenesis is indicated in the satellite imagery. Although the contribution of the tilting term is frontolytic in this

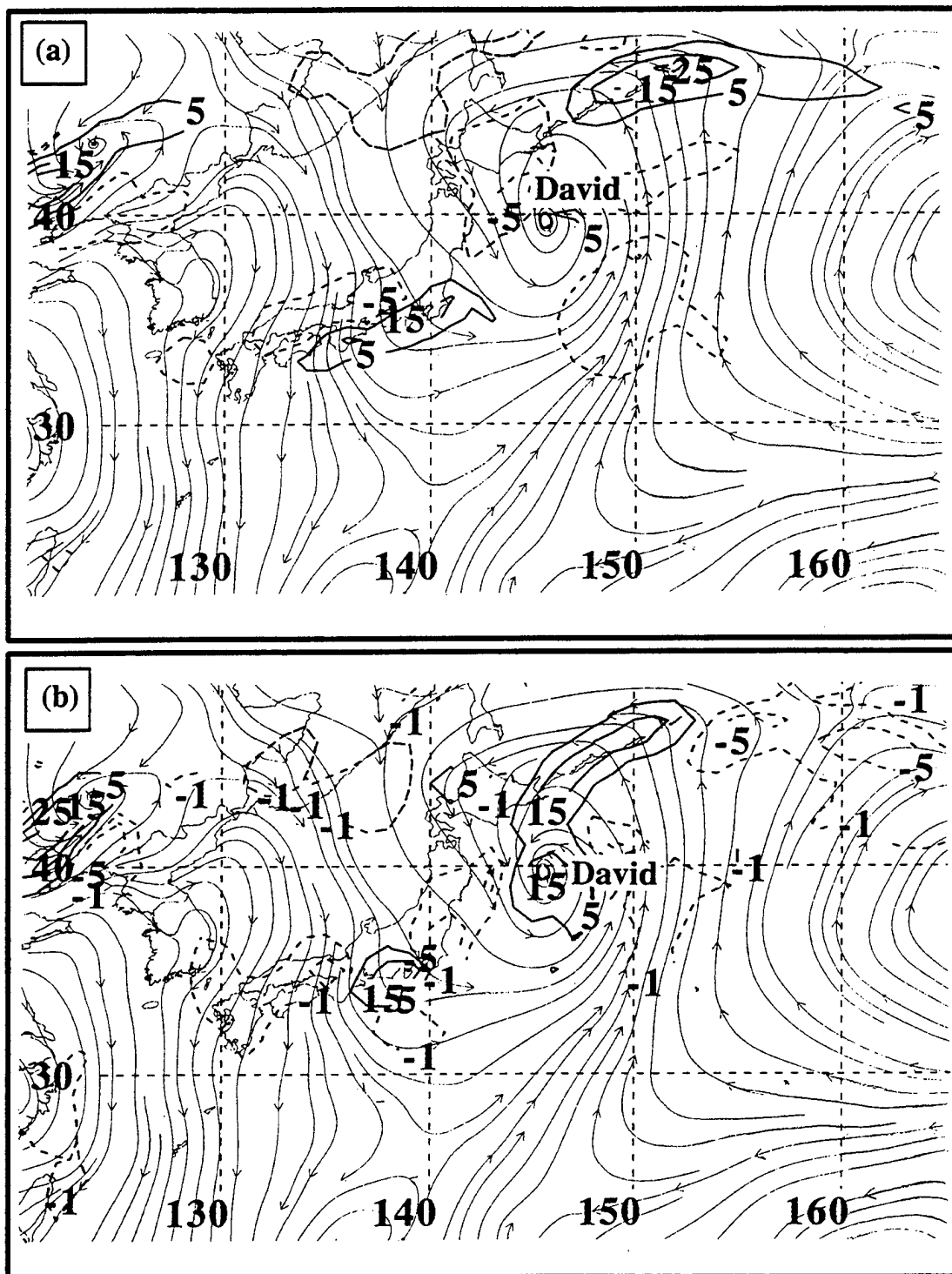


Fig. III-15. Calculations of 900-mb frontogenesis (interval $10 \times 10^{-10} \text{ K/(m s)}$), except for the $-1 \times 10^{-10} \text{ K/(m s)}$ contour), with solid (dashed) contours depicting frontogenetic (frontolytic) regions, and 900-mb streamlines at Step 3 of the transformation of TY David based on (a) confluence and (b) shear contributions at 1200 UTC 19 September 1997, and (c) vertical south-north cross-section of potential temperature (solid contours, 5 K interval) and NOGAPS analyzed vertical motion, with dashed (shaded) contours depicting ascent (descent) at a 2 (1) $\times 10^{-3} \text{ mb/s}$ interval.

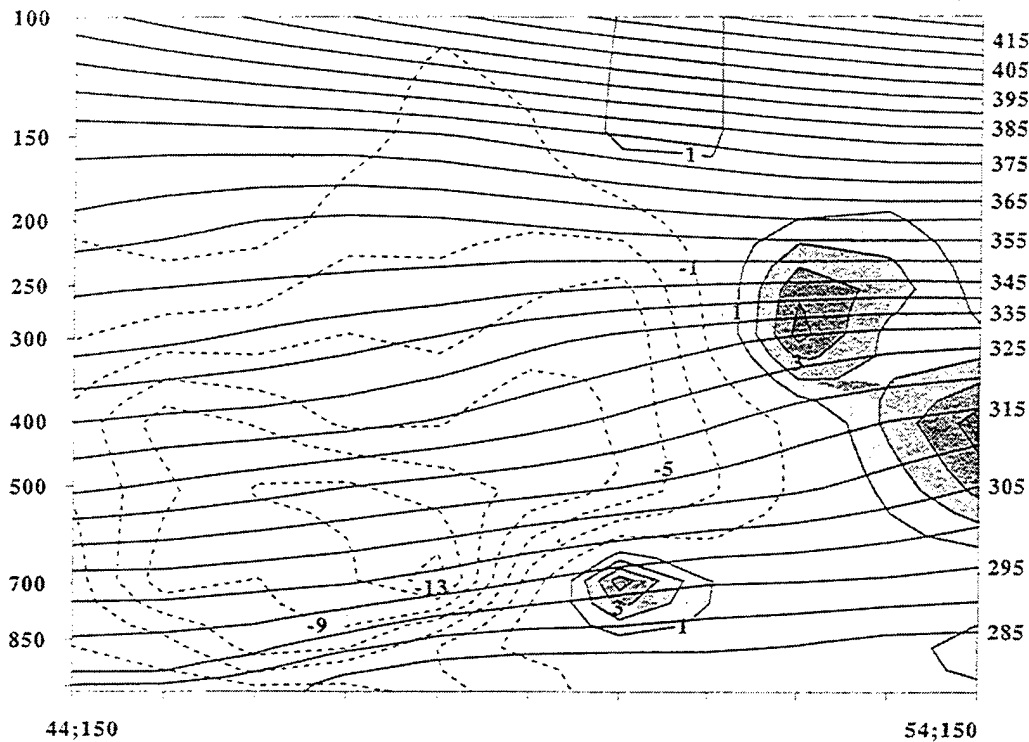


Fig. III-15 (continued).

location (-1.5×10^{-9} K/(m s) at 900 mb), the diabatic term (not calculated) is expected to be frontogenetic due to the latent heat release associated with the ascent of the warm, moist, poleward-flowing parcels that ascend these isentropic surfaces (Fig. III-14a), as in the calculations of Harr and Elsberry (2000).

With lower-tropospheric frontogenesis commencing, it is useful to consider what, if any, tropical characteristics remain in the remnants of David. An east-west vertical cross-section through the storm center at 1200 UTC 19 September (Fig. III-16a) indicates the continued existence of a pool of high θ_e air (>345 K) between 700 mb and 400 mb associated with the original tropical cyclone warm core. Although the central values have

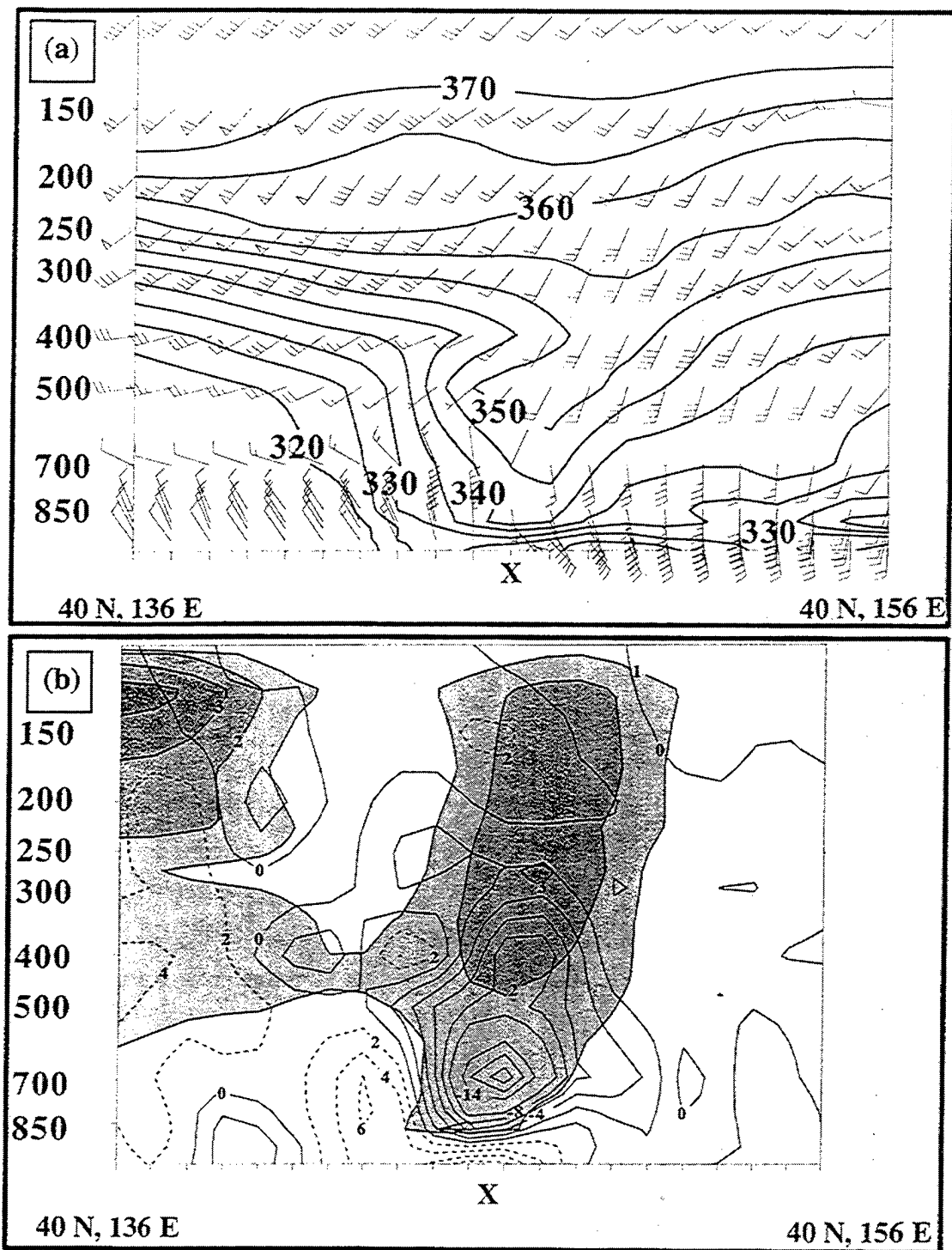


Fig. III-16. West-east cross-sections through the center as in Fig. III-7, except for 1200 UTC 19 September 1997.

decreased relative to the tropical cyclone warm core (>360 K) that existed 36 h earlier (Fig. III-7b), the environmental values have also decreased so that a distinct warm pool remains. The cold dome of isentropes west of David 12 h earlier has advanced eastward so that the storm center is in air with low values of θ_e that have undercut the higher θ_e air above. Wind speeds increase with height above 850 mb in the western half of the cross-section, which according to the thermal wind equation is consistent with the location of the cold dome. Notice also the southerly jet east of the storm between 700 mb and 400 mb, as well as the backing (veering) of winds west (east) of the storm center. This is consistent with the dipole of lower-tropospheric maximum (minimum) temperature advection directly east (west) of David (Fig. III-14b).

In Fig. III-16b, descent west of the storm has undercut ascent at the storm center, and the maximum descent corresponds to the intrusion of lower θ_e air that is the leading edge of the cold dome to the west (Fig. III-14a). The largest values of ascent are at 700 mb just east of the storm center, which is also the location of the southerly jet (Fig. III-16a). A PV maximum in the upper troposphere west of the storm is associated with the short-wave trough northwest of the storm. The connection of PV contours associated with David to those of the upstream, upper-tropospheric PV maximum (Fig. III-16b) suggests that David is about to couple with the short-wave trough. The PV values associated with David have decreased in the past 12 h, and are tilted to the east. Vertical wind shear at 1200 UTC 19 September (Fig. III-12b) indicates southwesterly flow at all levels, and an 850-mb to 250-mb vertical wind shear in excess of 20 m/s, which is more than double the value observed 12 h earlier. These larger values of wind shear are

believed to be the cause of the continued downstream advection of the top of the warm core (Fig. III-16a), as well as the increased tilt of the PV contours downshear (Fig. III-16b). This tilt is consistent with that in Hurricane Isidore simulated by DeMaria and Huber (1998) using the Geophysical Fluid Dynamics Laboratory (GFDL) model at $1/6^\circ$ lat./long. resolution. Again, it is difficult to separate how much of the analyzed ascent east of the storm center is due to the tilting of PV contours (Frank and Ritchie 1999) or lower-tropospheric baroclinic effects.

Visualization software (Vis5D) was used in conjunction with NOGAPS 1° lat./long. analyses and 6-h NOGAPS forecasts of 3-dimensional winds to produce four geographic trajectories of air parcel motion through David from 0000 UTC 18 September through 1200 UTC 19 September (Fig. III-17). Trajectory 1 depicts southerly flow originating in the eastern quadrant of David that ascends as it progresses poleward and then turns to the east. Notice the resemblance of this trajectory to a warm conveyor belt of an extratropical cyclone (Carlson 1991), and its relationship to the multi-layer cloud region in Fig. III-13, the warm advection region in Figs. III-9b and III-14b, and the southerly jet in Fig. III-8a. This trajectory represents the poleward transport of warm, moist environmental air around David's circulation at outer radii, and its ascent over tilted isentropic surfaces of the baroclinic zone north of David. Trajectory 2 originates north and east of the storm center, wraps cyclonically around the center of circulation, and then ascends and turns to the northeast. The path of this trajectory corresponds with the distinct cloud band northwest of the storm at 0000 UTC 19 September (Fig. III-8). Thus, it is believed that this cloud band is produced when parcels in the eastern quadrant travel

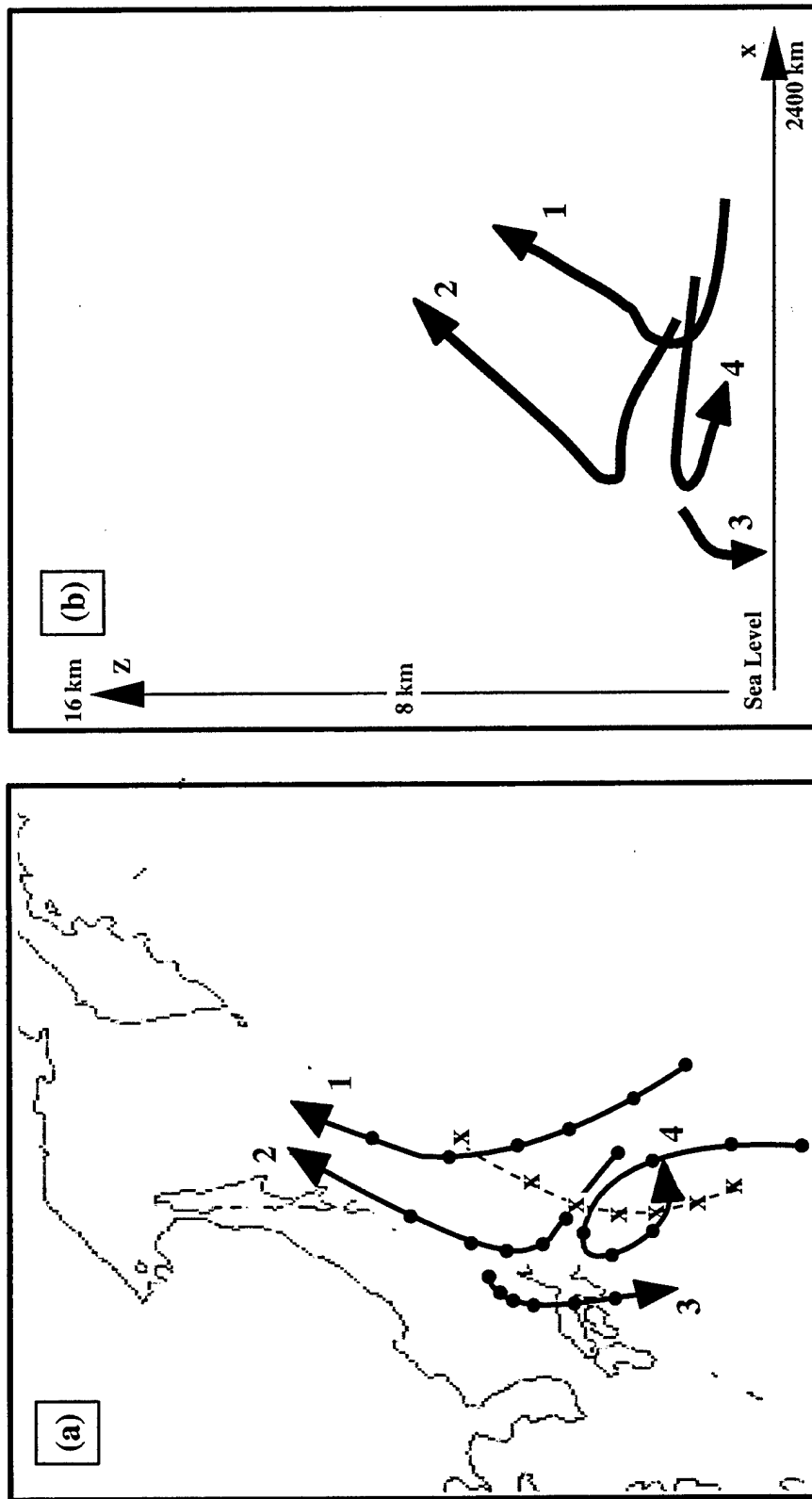


Fig. III-17. Four geographic trajectories depicting (a) plan view, and (b) elevations of parcels projected onto a west-east cross section, facing north, of airflow through TY David from 0000 UTC 18 September to 1200 UTC 19 September 1997. In the plan view plot, the location of parcels every 6 h is depicted by small dots, while the path of TY David is marked by a dashed line, and the location of the storm marked in 6 h intervals with an "x."

poleward, turn cyclonically north of the storm center while ascending over tilted isentropic surfaces in the baroclinic zone, then turn to the northeast and ascend over under-cutting cold, dry air descending northwest of the storm center.

Trajectory 3 in Fig. III-17 originates in the baroclinic zone northwest of the storm center, and descends as it travels equatorward into the western quadrant. The path of this trajectory is consistent with the dry regions in water vapor imagery (Fig. III-5c), the descent west of the storm center at 0000 UTC 19 September (Fig. III-11b), and the cold advection regions in Figs. III-9b and III-14b. Thus, this trajectory represents the equatorward advection of cooler, drier environmental air to the west of David. Trajectory 4 originates in the southern quadrant, turns cyclonically through the eastern quadrant, ascends slightly in the northern quadrant, then continues cyclonically into the western quadrant and descends, finally turning to the east far to the south of the translating storm. The path of this trajectory in the western quadrant of David is consistent with the descent in Fig. III-11b, and the continued cold advection west of David (Fig. III-9b).

At 1200 UTC 19 September, the center of David is located in cold, descending air. Thus, the transformation of TY David is complete based on the definitions presented in Section 2. Notice the appearance of fronts and erosion of inner-core tropical cyclone convection (Fig. III-13), the advection downstream of a weakening, upper-tropospheric warm core (Fig. III-16a), and the under-cutting descent into the storm center (Fig. III-16b) that is associated with an advancing cold dome. Given this baroclinic structure, convection is no longer hypothesized to be the primary energy source of David, which has become an extratropical cyclone. Re-intensification begins almost immediately, as the

remnants of David couple with an upper-level trough to its northwest, and rapidly redeepen to 966 mb⁶.

C. A CONCEPTUAL MODEL OF THE TRANSFORMATION STAGE OF EXTRATROPICAL TRANSITION

A summary of the physical processes observed in NWP analyses of the three steps of the transformation stage of ET is presented in Tables 3 and 4. Every ET studied commenced when the TC interacted with pre-existing mid-latitude baroclinity while at the same time translating over lower SST's. In all but three ET cases, warm (cold) temperature advection exceeding $5 (-5) \times 10^{-5}$ K/s was observed during Step 2 of the transformation stage. In the three cases (TY Ivy, TS Janis, TY Joy) that were the exception, TY Ivy and TY Joy completed Step 2 of transformation in the warm sector (that is, downstream of the lower-tropospheric cold front) of a pre-existing mid-latitude low, which limited the amount of colder environmental air that was ingested into the western quadrant of these storms (not shown). TS Janis had a weak lower-tropospheric circulation pattern associated with it during Step 2, which resulted in a small value of cold advection that surpassed the criterion only after the baroclinic zone TS Janis became imbedded in featured an increased gradient of isentropes during Step 3.

During Step 2 of transformation, all but two ET cases also featured a dipole of vertical motion with ascent (descent) east (west) of the storm center. The two cases where this dipole was not observed until Step 3 (TY Ivy, TY Joy) completed transformation after frontolysis of the pre-existing, upstream cold front discussed above

⁶ The re-intensification of TY David as a baroclinic cyclone will be discussed in Chapter V.

Table 3. Physical processes observed in NOGAPS 2.5° lat./long. resolution analyses of 18 ET cases during 1994-97.

Name	Onset of 850-mb Warm/Cold Advection Dipole*	Onset of Ascent/Descent Dipole	Onset of 900-mb Frontogenesis**
TY Zeke	Step 2	Step 2	Step 3
TY Ivy	Step 3	Step 3	below threshold
STY Melissa	Step 2	Step 2	Step 2
TY Seth	Step 2***	Step 2***	Step 3
TS Janis	Step 3	Step 3	Step 3
STY Oscar	Step 2	Step 2	Step 2
TY Polly	Step 2	Step 2	Step 2
STY Ryan	Step 2	Step 2	Step 3
STY Ward	Step 2	Step 2	below threshold
TY Dan	Step 2	Step 2	Step 2
TY Joy	Step 3	Step 2	Step 3
TY Kirk	Step 2	Step 2	Step 3
TY Orson	Step 2	Step 2	Step 3
TY Tom	Step 2	Step 2	Step 2
STY Violet	Step 2	Step 2	Step 3
STY Yates	Step 2	Step 2	below threshold
TY Carlo	Step 2	Step 2	below threshold
TY Opal	Step 2	Step 2	Step 3

Table 4. Physical processes observed in NOGAPS 1° lat./long. resolution analyses of 12 ET cases during 1997-98.

Name	Onset of 850- mb Warm/Cold Advection Dipole*	Onset of Ascent/Descent Dipole	Onset of 900-mb Frontogenesis**	Down- shear tilt of θ_e surfaces w/ height in Step 2	Down- shear tilt of PV surfaces w/ height in Step 2	Onset of Vertical Shear > 5 m/s from 850 mb to 200 mb
STY Nestor	Step 2	Step 2	Step 2	Y	Y	Step 1
TY Peter	Step 2	Step 2	Step 3	Y	Y	Step 1
TY Tina	Step 2	Step 2	Step 2	Y	Y	Step 2
TY Yule	Step 2	Step 2	below threshold	Y	Y	Step 2
STY Bing	Step 2	Step 2	Step 3	Y	Y	Step 2
TY David	Step 2	Step 2	Step 3	Y	Y	Step 1
STY Ginger	Step 2	Step 2	Step 3	Y	Y	Step 1
STY Joan	Step 2	Step 2	Step 3	Y	Y	Step 1
TY Rex	Step 2	Step 2	below threshold	Y	Y	Step 2
TY Stella	Step 2	Step 2	Step 2	Y	Y	Step 1
TY Vicki	Step 2	Step 2	Step 3	Y	Y	Step 1
STY Zeb	Step 2	Step 2	below threshold	Y	Y	Step 2

SUPPLEMENTAL NOTES FOR TABLES 3 AND 4:

*Based on earliest diagnosis of a value of at least $\pm 5 \times 10^{-5} \text{ K s}^{-1}$. The dipole of temperature advection described in Chapter III.C.1 was observed in all 30 cases during Step 2, but in the 3 cases where "Step 3" is listed, the cold advection term failed to meet the selected diagnostic criterion.

**Based on earliest diagnosis of a value of at least $10 \times 10^{-10} \text{ K m}^{-1} \text{ s}^{-1}$. The patterns of frontogenesis described in Chapter III.C.1 were observed in all 30 cases, but in the 7 cases where "below threshold" is listed, the frontogenesis terms failed to meet the selected diagnostic criterion.

***After Step 1 was determined, the timing of Step 2 was established using only IR satellite imagery since NWP analyses for TY Seth were not available again until Step 3 had been completed. The dipole of temperature advection and vertical motion was observed in the NOGAPS 12-h forecast that verified at the time of Step 2.

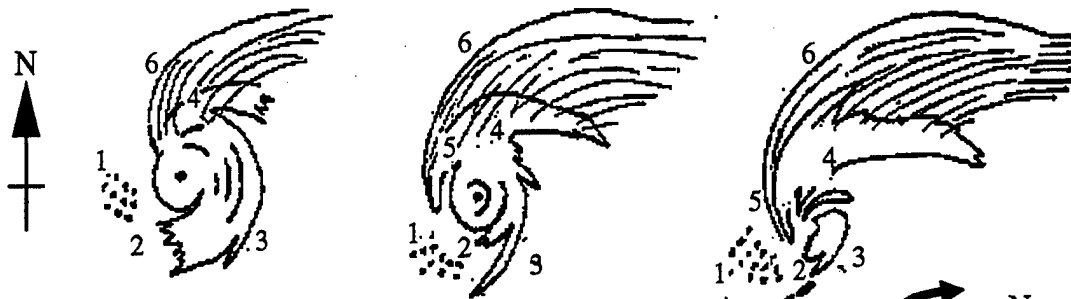
permitted the storms to become imbedded in the cold, descending air upstream of the front. In eight ET cases, lower-tropospheric frontogenesis $> 10 \times 10^{-10} \text{ K}/(\text{m s})$ was diagnosed during Step 2, and in 15 additional ET cases during Step 3. Frontogenesis was observed during Step 3 in the remaining seven cases, but was below the threshold criterion. In the 12 ET cases studied using NOGAPS $1^\circ \text{ lat./long.}$ resolution analyses (Table 4), vertical shear greater than 5 m/s from 850 mb to 200 mb was observed no later than Step 2 of transformation, and caused the θ_e and PV surfaces to tilt downstream during Steps 2 and 3⁷.

In Figs. III-1 through III-3 and in the case of TY David, recall that similar features (such as asymmetric cloud patterns, dry slots, the cirrus plume, "delta" rain regions, and eyewall erosion and the appearance of possible warm frontogenesis in Step 3) were observed in IR imagery in each of these seven cases during the transformation stage. In Appendix A, IR imagery of the three steps of the transformation stage is included for the remaining 23 ET cases studied. Notice the similar appearance of these features during the transformation stage, so that the sequence of the images from Step 1 through Step 3 also looks nearly the same in each case. Furthermore, the physical processes that are summarized in Tables 3 and 4 (temperature advection, vertical motion dipoles, and frontogenesis) are all consequences of the interaction of the TC with a pre-existing, lower-tropospheric mid-latitude baroclinic zone, and proceed in a similar fashion during the transformation of all 30 ET cases. Thus, the physical processes and diagnostic criteria

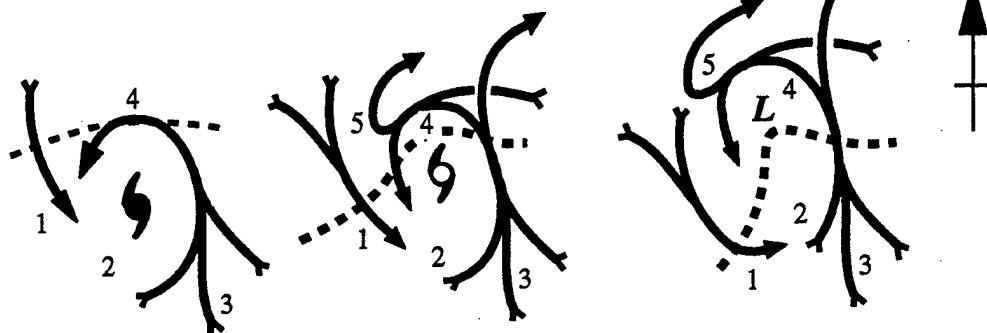
⁷ These 12 cases were studied using NOGAPS $1^\circ \text{ lat./long.}$ resolution analyses. The remaining 18 ET cases were studied using NOGAPS $2.5^\circ \text{ lat./long.}$ resolution. This grid spacing of nearly 250 km was insufficient to permit azimuthal averaging of the u and v wind components on a circle of 300 km radius from the storm center.

Conceptual Model of Transformation Stage of ET in the Western North Pacific

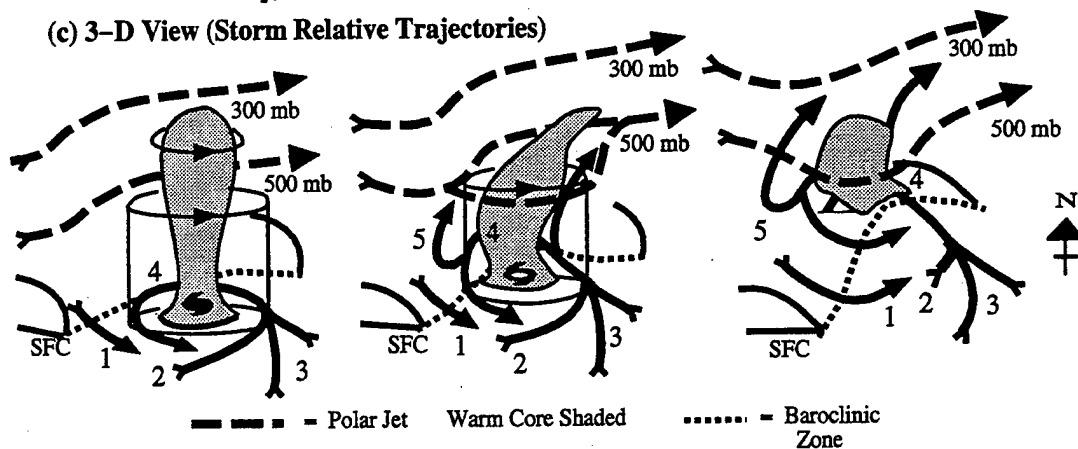
(a) Infrared Imagery



(b) Plan View (Storm Relative Trajectories)



(c) 3-D View (Storm Relative Trajectories)



STEP 1

STEP 2

STEP 3

Labelled Areas (BOLD numbering):

1. Environmental equatorward flow of cooler, drier air (with corresponding rows of cumulus). 2. Decreased tropical cyclone convection in the western quadrant (with corresponding dry slot) in Step 1, which extends throughout the southern quadrant in Steps 2 and 3. 3. Environmental poleward flow of warm, moist air is ingested into tropical cyclone circulation, which maintains convection in the eastern quadrant, and results in an asymmetric distribution of clouds and precipitation in Steps 1 and 2. In Steps 2 and 3, this flow or southerly jet also ascends tilted isentropic surfaces. 4. Ascent of warm, moist inflow over tilted isentropic surfaces associated with baroclinic zone (dashed line) in middle and lower panels. 5. Ascent (undercut by dry adiabatic descent) that produces cloudbands wrapping westward and equatorward around the storm center. Dry adiabatic descent occurs close enough to the circulation center to produce erosion of eyewall convection in Step 3. 6. Cirrus shield with a sharp cloud edge if confluent with polar jet.

Fig. III-18. Conceptual model of transformation stage of ET in the western North Pacific.

described in Tables 3 and 4 should prove useful to forecasters when determining when Steps 2 and 3 of ET are occurring or have been completed.

Based on the similarity of all 30 ET cases in satellite imagery and NWP analyses during transformation, a conceptual model (Fig. III-18) is proposed that describes and explains the similar physical processes that occurred during virtually every transformation stage of ET studied in the western North Pacific.

In Step 1 (Fig. III-18), the tropical cyclone commences the transformation stage as it translates poleward over lower SSTs (not shown), and its outer circulation begins to impinge on a pre-existing mid-latitude baroclinic zone. As interaction with the baroclinic zone begins, colder, drier, environmental equatorward flow (labeled 1 in Fig. III-18, compare to Fig. III-6) exists to the west of the tropical cyclone. Thus, little deep convection is evident in the outer circulation of the western quadrant of the tropical cyclone, and a dry slot forms in the southwestern quadrant (labeled 2 in Fig. III-18, compare to Figs. III-5 and III-6), with decreased deep convection. As this cooler, drier air is heated and moistened by surface fluxes from the relatively warm ocean, rows of cumulus may be observed. Environmental poleward flow to the east of the tropical cyclone (labeled 3 in Fig. III-18, compare to Fig. III-5) advects warm, moist air into the southern and eastern quadrants of the tropical cyclone, which maintains deep convection in these quadrants. Thus, an early indicator of transformation is an asymmetric appearance of tropical cyclone cloud patterns, similar to that observed in Figs. III-1 through III-3, Fig. III-5, and Appendix A. This environmental, poleward flow turns cyclonically and interacts with a pre-existing baroclinic zone (labeled 4 in Fig. III-18,

compare to Fig. III-6) to produce ascent over tilted isentropic surfaces. Since the storm is also beginning to interact with vertical wind shear associated with the polar jet, a cirrus shield (labeled 6 in Fig. III-18, compare to Figs. III-1 through III-3, Fig. III-5, and Appendix A) is observed in IR imagery.

In ET cases that occur during the early summer months (June and July), the branch of the Kuroshio Current that runs along the Asian coast to Japan is located farther equatorward than during the late summer and early autumn. In the case of TY Peter (Fig. III-19), the SST analysis at 0000 UTC 27 June 1997 had lower temperatures between 20°N and 30°N compared to autumn ET cases such as TY David (compare the 301 K contours in Figs. III-4 and III-19). It is likely that the lower SST's observed in early summer ET cases contribute to the decreased convection observed in the western quadrant. However, even in these summer ET cases the convection persists in the other quadrants, and seasonal differences are not obvious in the appearance of the transformation stage IR imagery sequence (Figs. III-1 through III-3, III-5, III-8, III-13, and Appendix A).

In Step 2 (Fig. III-18), the tropical cyclone is located just equatorward of the baroclinic zone. Cyclonic rotation of the baroclinic zone to a southwest to northeast orientation (even if not already pre-existing) occurs as environmental flow of cooler, drier (warm, moist) air continues west (east) of the storm (labeled 1 and 3, respectively, compare to Fig. III-9). This produces a dipole of lower-tropospheric, cold (warm) temperature advection (Tables 3 and 4) to the west (east). Notice also the expansion of the dry slot (labeled 2 in Fig. III-18, compare to Fig. III-8) into the southern quadrant.

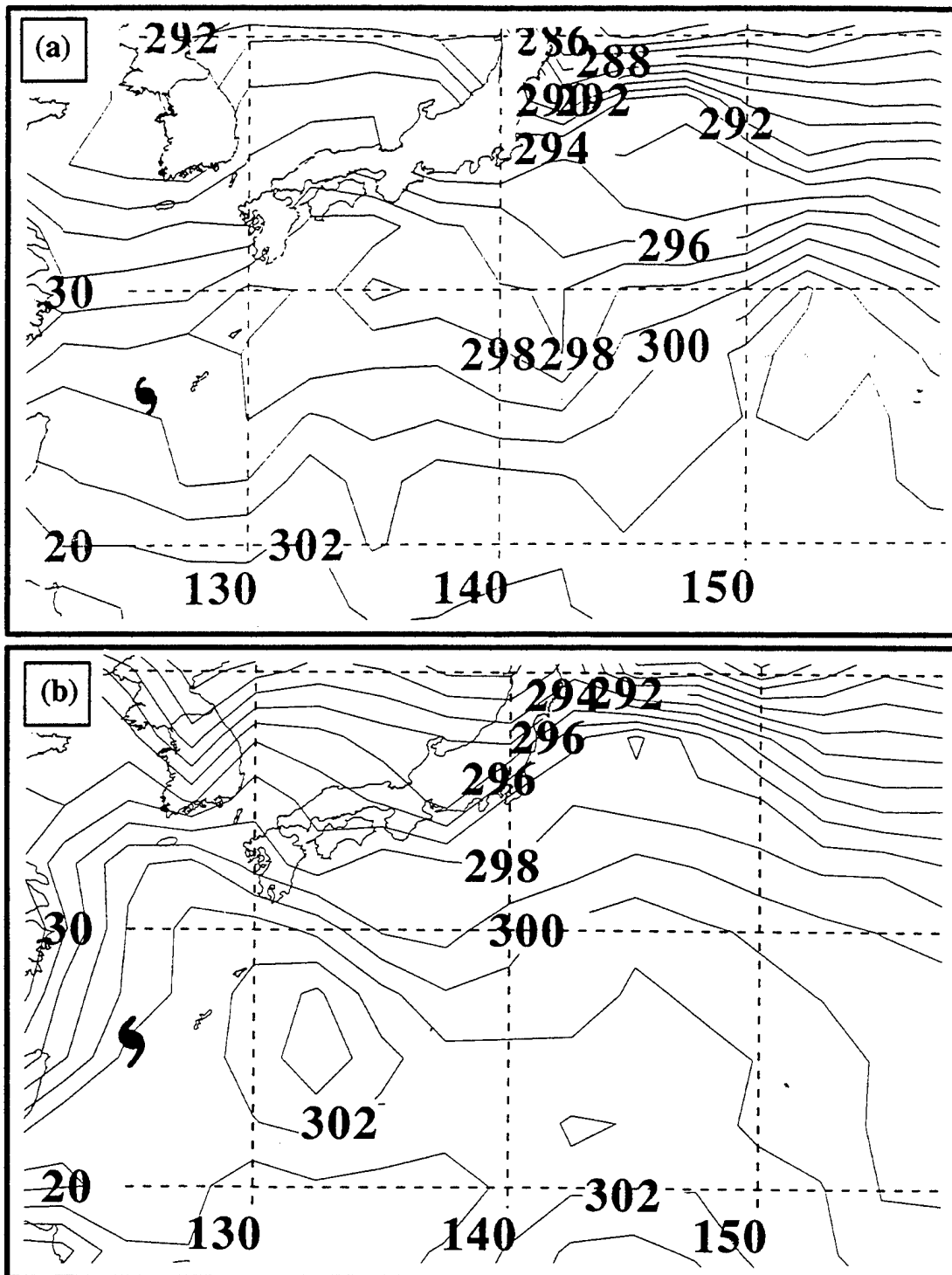


Fig. III-19. (a) Sea-surface temperature (K) and (b) 2-m air temperature (K) as in Fig. III-4, except for TY Peter at 0000 UTC 27 June 1997.

Environmental poleward flow of warm, moist air east of the storm now advances to the baroclinic zone and ascends over tilted isentropic surfaces poleward of the storm (labeled 4 in Fig. III-18, compare to Figs. III-9 and III-11). Some of these ascending parcels turn cyclonically, and then descend into the western quadrant (Fig. III-18c, Step 2, compare to Fig. III-17). The (presumed dry adiabatic) descent west of the storm center is the subsidence branch of a vertical motion dipole (Tables 3 and 4) in combination with the ascent to the east. At the same time, other parcels continue their ascent to the mid-troposphere and turn anticyclonically to the northeast (labeled 5 in Fig. III-18, compare to Fig. III-17). Finally, narrow bands of convection may extend southwestward from the northern quadrant to a point west of the storm center, which is generally in a region of cooler, drier environmental inflow and descent that otherwise inhibits deep convection (compare to Fig. III-8).

During this step, the storm is affected by vertical wind shear associated with the baroclinic zone, and a cirrus shield with a sharp cloud edge (labeled 6 in Fig. III-18, compare to Fig. III-8) appears as the warm, upper-tropospheric outflow of the transforming storm becomes confluent with the polar jet, which is still well poleward of the storm at this time. However, the onset of vertical wind shear to the south of the jet begins to "ventilate" the storm by advecting the top of the upper-tropospheric warm core downstream (Fig. III-18c, Step 2). Even though the 500-mb westerlies approach and wrap around the weakening mid-tropospheric warm core (as in Fig. III-10), deep convection persists in the tropical cyclone inner core.

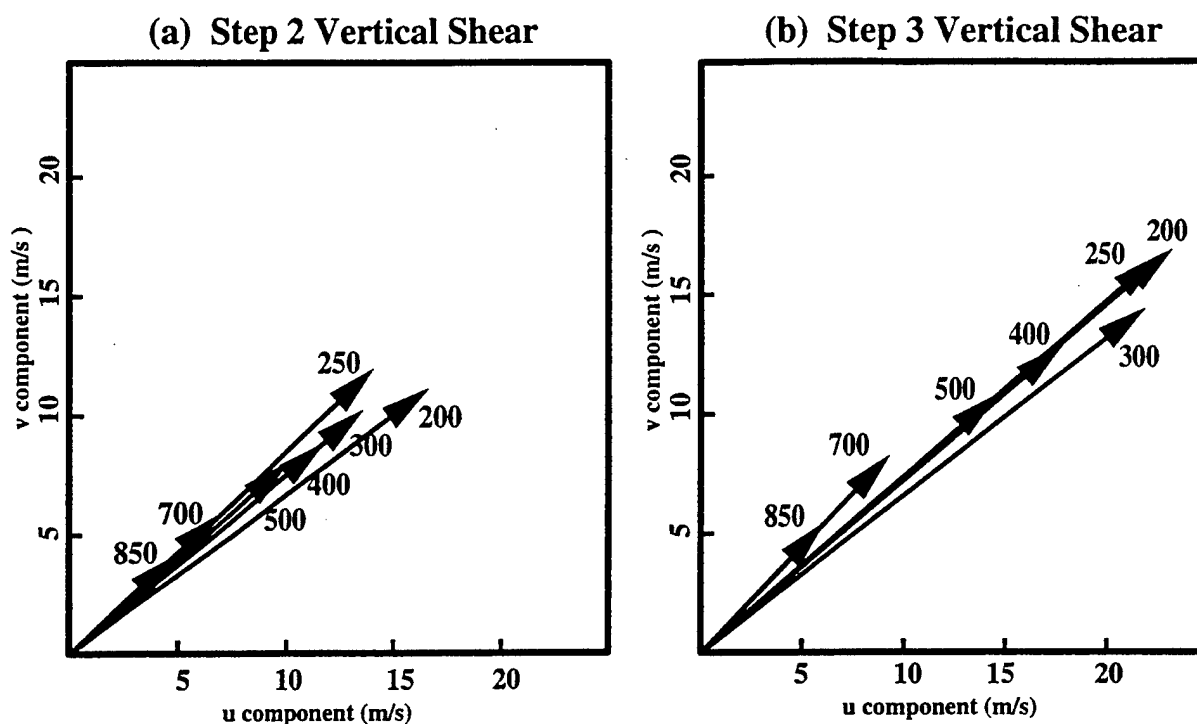


Fig. III-20. Azimuthally averaged u and v wind components (m/s) around a circle with radius of 300 km from the storm center at mandatory levels between 850 and 200 mb, for 12 ET cases occurring during 1994-98 at (a) Step 2, and (b) Step 3 of the transformation stage.

Vertical wind shear for 12 ET cases during 1997-98 (including TY David) was calculated by azimuthally averaging the u and v wind components along a circle of 300 km radius centered on the storm, at all mandatory levels from 850 mb to 200 mb (Fig. III-20). The mean vertical shear during Step 1 (not shown) in the 12 ET cases is small and from the southwest, which suggests that these storms have either just recurved, or have entered the Poleward/Poleward Flow pattern/region (Carr and Elsberry 1999) in association with a reverse-oriented monsoon trough (Fig. II-1). Notice that while the direction of the shear

is predominantly from the southwest in Step 2 (Fig. III-20a), the greatest change in velocity occurs in the layer between 700 mb and 500 mb. During Step 3 (Fig. III-20b), the vertical wind shear is again from the southwest with a significant increase in velocity between 850 mb and 300 mb, and the maximum shear is in the layer between 700 mb and 400 mb. This tendency for the maximum vertical wind shear to be concentrated in the middle troposphere was observed in 10 of these 12 cases. In one of the remaining two cases, the vertical shear increases the same amount at each level, and in the other, the vertical shear is greatest between 400 mb and 250 mb. Although vertical wind shear is believed to be responsible for the dispersal of the upper-tropospheric warm core, it is the concentration of maximum wind shear in the middle troposphere that may be responsible for the downstream tilt of the PV contours in these ET cases (as in Figs. III-11 and III-16).

Step 3 (Fig. III-18) is the logical conclusion of the continuation of the physical processes described in Step 2 (Tables 3 and 4) as the storm center becomes imbedded in the baroclinic zone. Vertical wind shear increases, SST values under the storm decrease (not shown), cold (warm) advection is produced by equatorward (poleward) environmental flow west (east) of the storm, and the interaction of the tropical cyclone circulation with the baroclinic zone produces ascent over tilted isentropic surfaces to the north, and then (dry adiabatic) descent to the northwest and west, as all of these processes continue as described in Step 2, Tables 3 and 4, and Figs. III-13 through III-17 in the case of TY David. Although increased vertical wind shear (Table 4) is believed to be responsible for continued advection downstream of the remnants of the upper-

tropospheric warm core, a weaker lower-tropospheric warm core remains over the surface center (shaded, in the lower right panel of Fig. III-18c, compare to Fig. III-16). Meanwhile, dry adiabatic descent west of the storm center of parcels that have previously ascended the baroclinic zone progressively weakens tropical cyclone inner-core convection and eventually produces eyewall erosion in the western and southern quadrants.

The transformed tropical cyclone now resembles an extratropical cyclone in that a large swath of multi-layer cloud that resembles a warm front exists on the poleward side, with a weaker cloud band to the southeast that resembles a cold front. Ascent northwest of the storm center is undercut by (dry adiabatic) descent, and produces a swath of clouds that now extends from the large region of multi-layer clouds north and east of the storm center and wraps around toward the western side of the storm. The environmental poleward flow of warm, moist air on the east side ascends over the baroclinic zone and joins the strong southwesterly jet aloft that resembles a warm conveyor belt of an extratropical cyclone (Carlson 1991).

D. THE DECAY OF SUPERTYPHOON IVAN (OCTOBER 1997)

As in the case of TY David, all of the other 29 cases of completed ET from 1 June through 31 October 1994-98 eventually became imbedded in a pre-existing, mid-latitude baroclinic zone. Thus, it appeared that interaction of a tropical cyclone with a mid-latitude baroclinic zone was an essential component in each step of the transformation stage of ET. During that period, 14 tropical cyclones were designated extratropical by JTWC that subsequently failed to complete ET; i.e., they did not complete both the

transformation and re-intensification stages. Satellite imagery of these dissipating extratropical storms often resembles the first two steps in the sequence of the transformation stage (as depicted in Figs. III-5 and III-8 in the case of TY David).

STY Ivan is not classified as an ET case because it failed to complete the transformation stage of ET according to the definitions in Section 2. At 1232 UTC 24 October 1997 (Fig. III-21a), satellite IR imagery suggests that STY Ivan may be in Step 2 of the transformation stage of ET. Notice the asymmetric cloud patterns characterized by the lack of tropical cyclone convection in the western and southern quadrants, and the presence of cloud bands that extend west and south from the northern quadrant. A weak cirrus shield also extends from the over-running cloud bands over the multi-layer cloud swath northeast of the storm center. Ivan is possibly beginning to interact with a baroclinic zone associated with a pre-existing cold front located 750 km to the northwest (Figs. III-21a and III-21b). Vertical cross-sections through the center of the storm at 1200 UTC 24 October (Figs. III-21c and d) reveal that the original tropical cyclone warm core is evident only below 400 mb, and that a PV maximum is located above the storm center in the lower troposphere, with ascent (descent) well to the east (west) of the storm center. Vertical wind shear from 500 mb to 200 mb of 9 m/s appears to be responsible for advecting the warm core downstream (Fig. III-21c), and for the tilt of PV contours to the east above 300 mb (Fig. III-21d). All of these features are similar to those analyzed during Step 2 of the transformation of TY David.

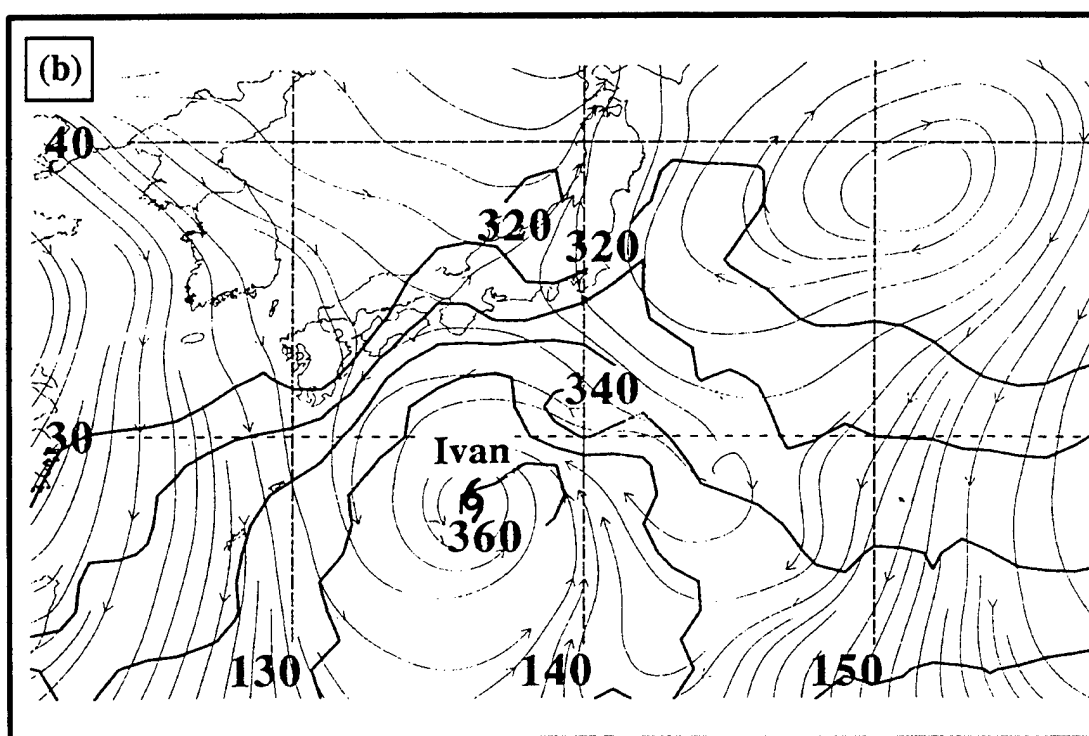
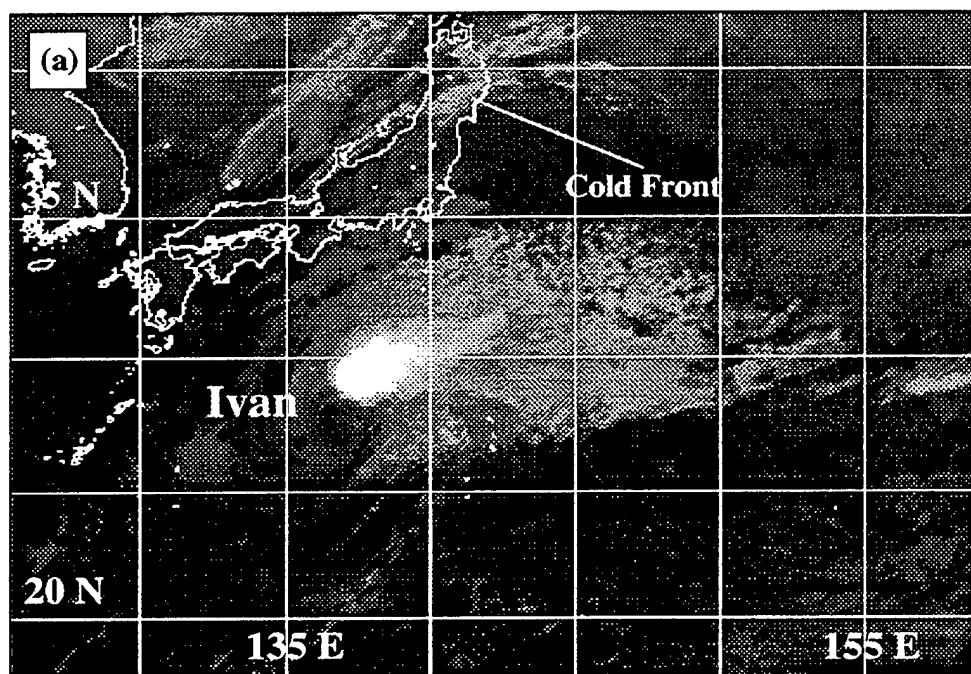


Fig. III-21. Infrared imagery of STY Ivan at (a) 1232 UTC 24 October 1997, and (b) 1000 mb streamlines and equivalent potential temperature contours as in Fig. III-6, (c) vertical cross-section through the center of equivalent potential temperature and wind, and (d) PV and vertical motion as in Fig. III-7, except for 1200 UTC 24 October 1997.

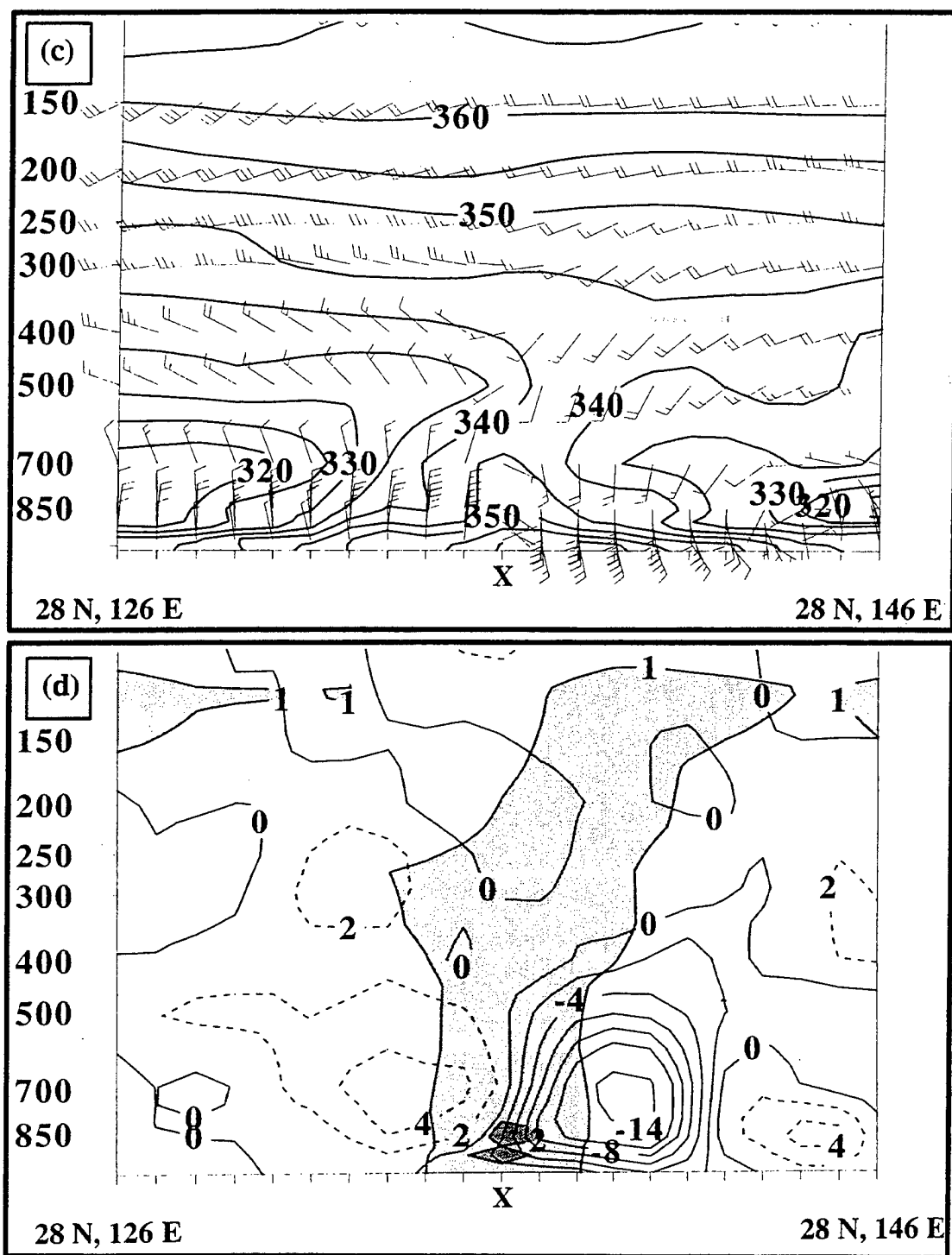


Fig. III-21 (continued).

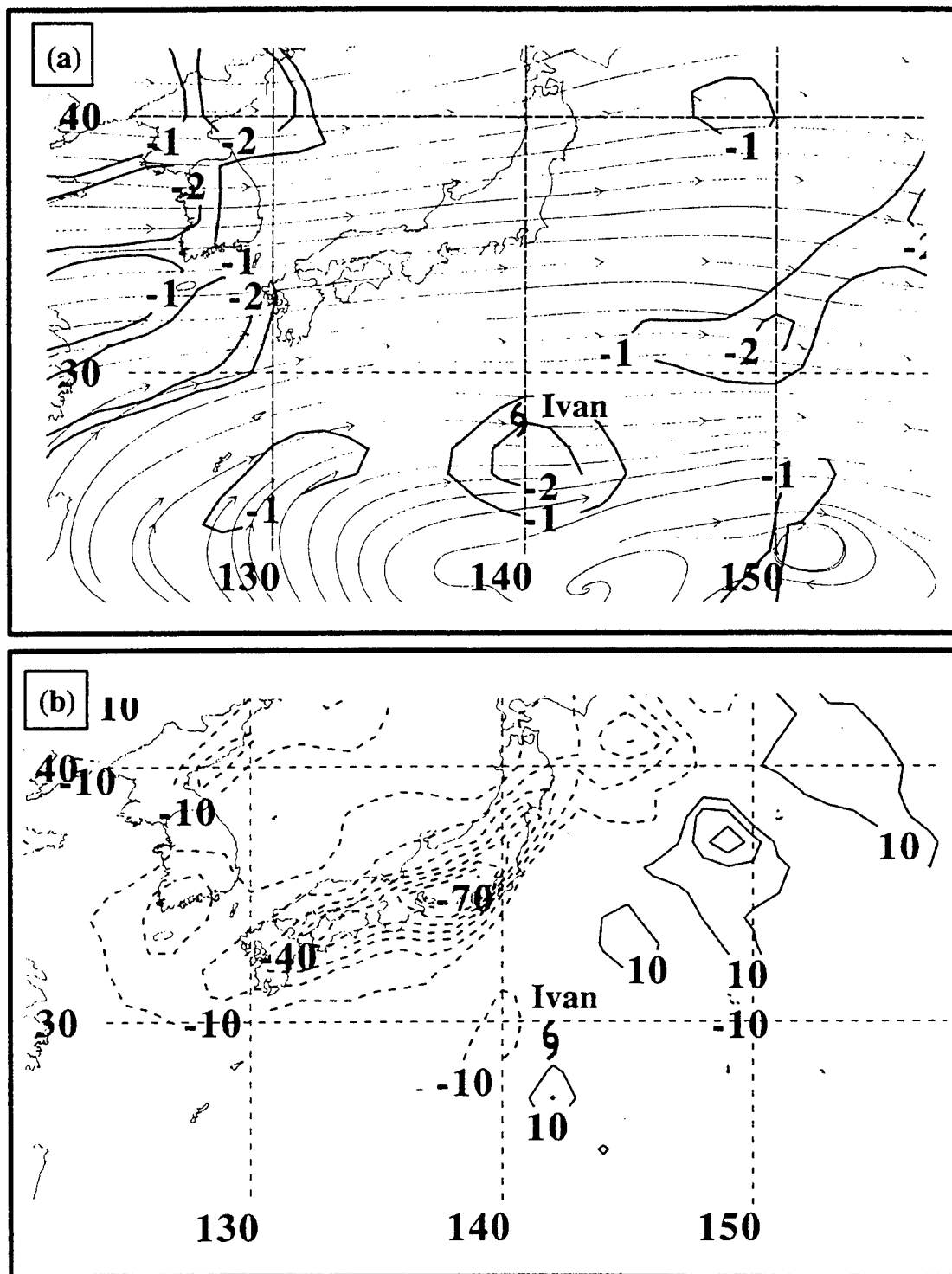


Fig. III-22. (a) NOGAPS 200-mb analysis at 0000 UTC 25 October 1997 of streamlines and divergence (heavy solid contours, in intervals of $1 \times 10^{-1} \text{ s}^{-5}$), and (b) 850-mb temperature advection as in Fig. III-9b, except for 1200 UTC 25 October 1997.

The NOGAPS 200-mb analysis at 0000 UTC 25 October (Fig. III-22a) indicates upper-tropospheric streamline confluence above Ivan, and an area of convergence. By 1200 UTC 25 October (Fig. III-22b), Ivan has translated east, and moved away from the baroclinic zone to the northwest. Notice that the significant dipole of cold and warm advection evident in Fig. III-22b is not associated with Ivan, but with the cold front to the northwest. At this time, Ivan appears in IR imagery to be weaker (Fig. III-23a) than it was 12 h earlier, as no vigorous convection appears anywhere in the storm circulation. No cirrus shield is evident in this region of a polar jet, which is consistent with the absence of deep convective outflow from Ivan. Unlike TY David (Fig. III-14a), Ivan does not translate into or become embedded in the baroclinic zone to the northwest (Figs. III-22b and III-23b). Notice also that the surface streamline pattern associated with Ivan (Fig. III-23b) does not exhibit a closed circulation. Unlike TY David (Fig. III-14a), little or no ascent of warm, moist poleward flow over tilted isentropic surfaces is analyzed in the north or east quadrants of Ivan's outer circulation.

Vertical, west-to-east cross-sections through the storm center at 1200 UTC 25 October (Figs. III-23c and III-23d) indicate that a weak remnant of the warm core remains in the lower troposphere below 500 mb, and is being advected downstream. The lower-tropospheric pool of high θ_e air associated with Ivan's center 12 h earlier has weakened (Fig. III-23c). Unlike David (Fig. III-16a), Ivan's center is not imbedded in an advancing cold dome, but remains in a pool of higher θ_e air. Under-cutting descent is not observed at the storm center (Fig. III-23d), and only a shallow, closed PV contour below 850 mb remains at the storm center. A broad area of descent is above the storm center, which is

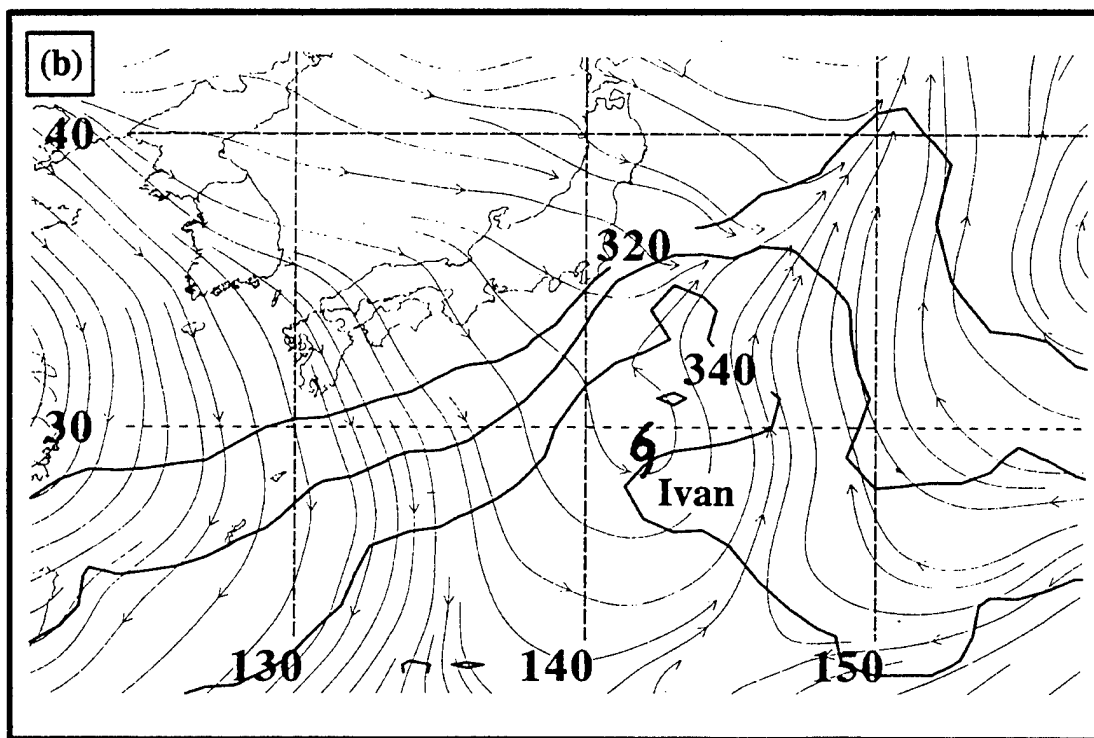
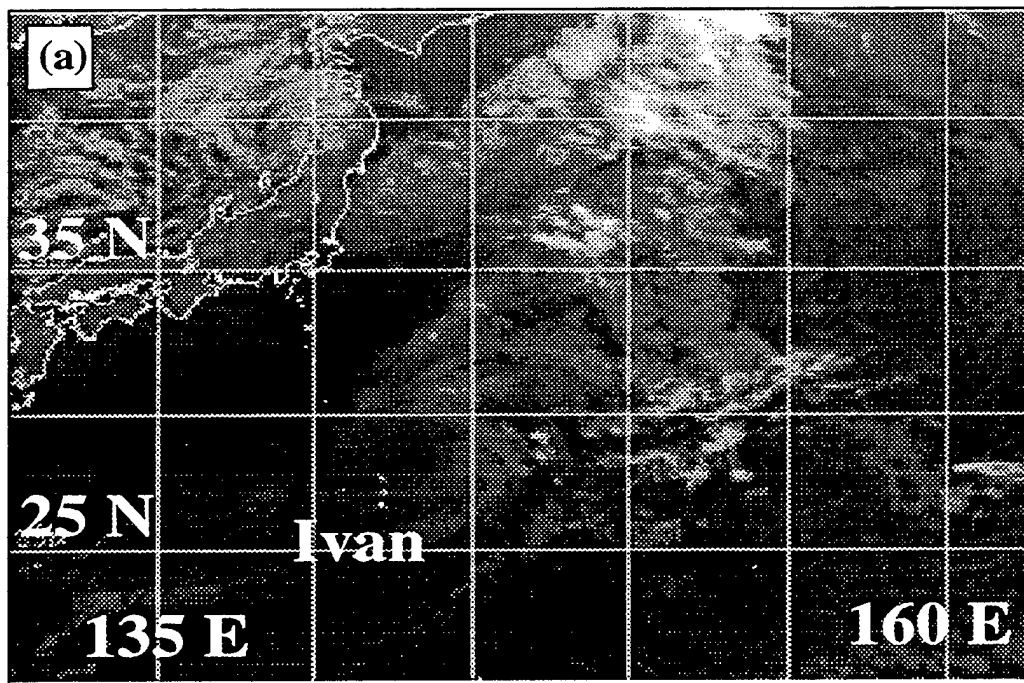


Fig. III-23. (a) Infrared satellite imagery, (b) 1000-mb streamlines and equivalent potential temperature, (c) vertical cross-section of equivalent potential temperature and winds, and (d) PV and vertical motion, as in Fig. III-21, except for (a) 1232 UTC 25 October, and (b) through (d) 1200 UTC 25 October 1997.

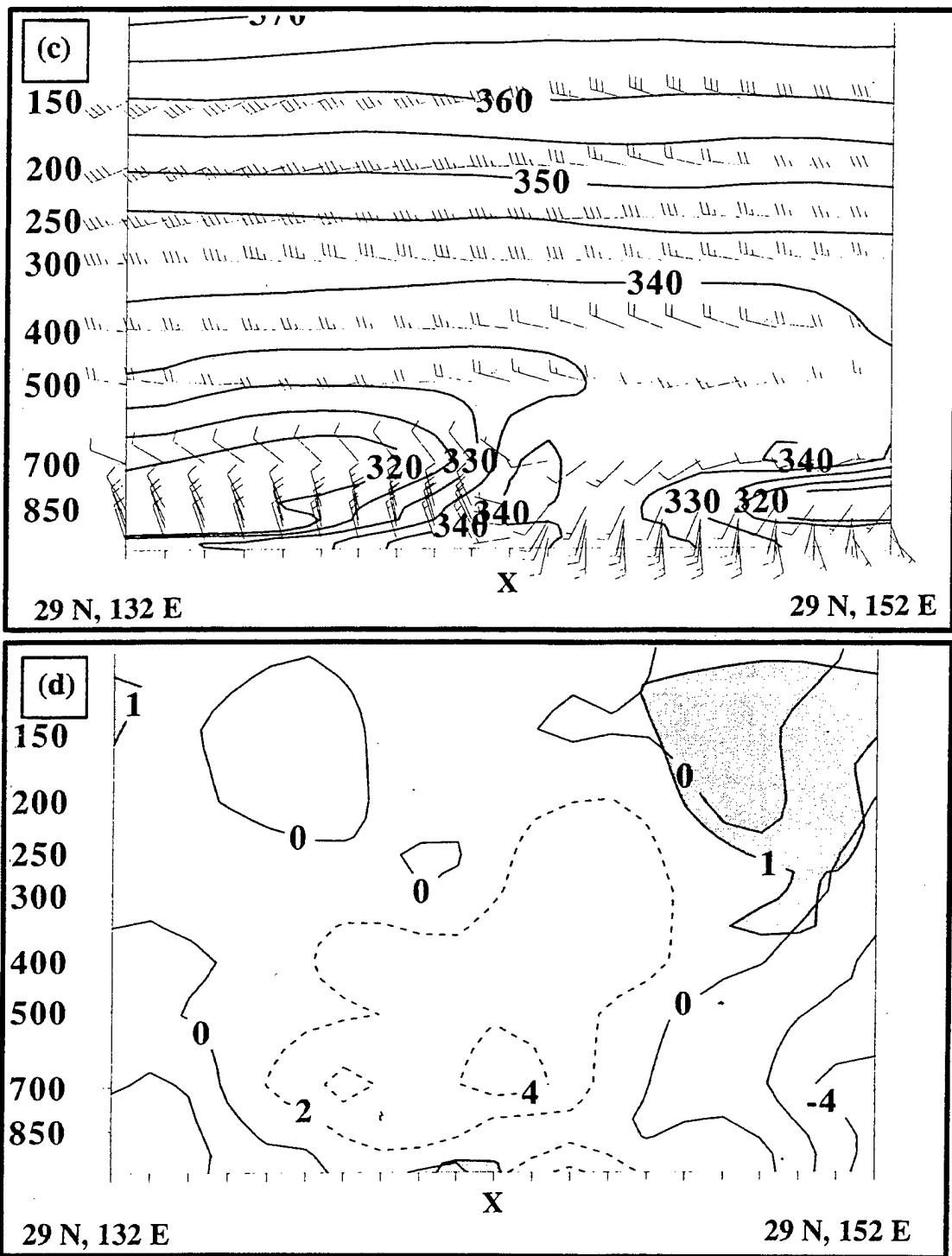


Fig. III-23 (continued).

consistent with the 200-mb convergence analyzed 12 h earlier (Fig. III-22a), and deep convection is not present anywhere in the storm circulation (Fig. III-23a).

Even though the IR imagery at 1232 UTC 24 October (Fig. III-21a) resembles Step 2 of the transformation stage, Ivan fails to complete ET as defined in Section 2. Ivan does not become a baroclinic low, and is in strong westerly flow with vertical wind shear values in excess of 13 m/s from 500 mb to 200 mb, so it simply dissipates over lower SSTs (not shown) and beneath upper-tropospheric convergence. Unlike TY David, Ivan does not translate poleward into a baroclinic zone, and its center never becomes imbedded in a cold dome. Instead, Ivan was steered zonally, and moved away from lower-tropospheric baroclinity (Figs. III-22b and III-23b) so that interaction with a pre-existing, mid-latitude baroclinic zone did not occur. Thus, ascent of warm, moist, poleward flow over tilted isentropic surfaces is not observed.

With the exception of two storms (STY Winnie during August 1997 and TY Waldo during September 1998) that dissipated over land, the remaining 11 cases designated as extratropical by JTWC that failed to complete ET behaved similarly to Ivan. The example of STY Ivan thus suggests that satellite imagery can be used in conjunction with NWP analyses and vertical cross-sections to distinguish “decayers” from real ET cases based on the conceptual model (Fig. III-18) of the transformation stage of ET.

THIS PAGE INTENTIONALLY LEFT BLANK

IV. CLIMATOLOGY OF EXTRATROPICAL TRANSITION

A. STATISTICS

In the period from 1 June through 31 October during 1994-98, 30 out of 112 (27%) tropical cyclones in the western North Pacific completed ET as defined above (Table 5). The SLP of the tropical cyclone in the NOGAPS analysis at the commencement of ET is not representative of the actual central SLP, since the resolution of the NOGAPS analyses is too coarse to permit accurate depiction of the tropical cyclone inner core. Thus, the central SLP of the tropical cyclone recorded at commencement of ET (Table 5, column 2) was based on the JTWC post-storm analyses. By the end of transformation, the SLP values in the NOGAPS analyses were in better agreement with those reported by JTWC. Therefore, the SLPs in the NOGAPS analyses at the completion of transformation (Table 5, column 2) and the end of re-intensification (Table 5, column 3) are recorded.

An annual average of six completed transitions occurred from the 22 tropical cyclones that were observed during 1 June through 31 October 1994-98. The annual and monthly distributions of ET cases are depicted in Table 6. Nearly half of all transitions (14 out of 30) occurred during September.

The translation poleward of TCs during ET can be described in terms of the synoptic patterns and regions of Carr and Elsberry (1994, 1999) that were introduced in Chapter II (Fig. II-1). From 1 June through 31 October during 1994-98, 39 tropical cyclones were in the Poleward pattern (Fig. II-1) after translating north of 30°N , and 20

Table 5. List of tropical storms (TS), typhoons (TY), and supertyphoons (STY) that completed ET during 1 June through 31 October 1994-98, including SLPs and durations of each stage of ET.

Name/Commencement of ET (YYMMDDHH)	SLP at Start of Transformation Stage (mb) / SLP at Completion of Transformation Stage (mb) / Duration (h) of Transformation	SLP at Completion of Re-Intensification Stage (mb) / Duration (h) of Re-Intensification Stage
TY Zeke / 94072312	984 / 997 / 36	990 / 48
TY Ivy / 94090212	996 / 997 / 24	994 / 12
STY Melissa / 94091612	933 / 981 / 60	969 / 48**
TY Seth / 94100912	939 / 998 / 36	981 / 24**
TS Janis / 95082412	989 / 1002 / 48	1001 / 36
STY Oscar / 95091600	898 / 980 / 48	959 / 24**
TY Polly / 95091900	954 / 988 / 72	987 / 12
STY Ryan / 95092200	910 / 1003 / 60	998 / 12**
STY Ward / 95102012	916 / 999 / 48	1002 / 12**
TY Dan / 96070900	967 / 994 / 60	986 / 12
TY Joy / 96080300	972 / 1004 / 72	1001 / 24
TY Kirk / 96081400	949 / 987 / 36	985 / 24
TY Orson / 96090200	972 / 986 / 36	975 / 24**
TY Tom / 96091800	980 / 998 / 72	974 / 60
STY Violet / 96092100	962 / 984 / 48	987 / 12**
STY Yates / 96093012*	962 / 995 / 48	977 / 48**
TY Carlo / 96102400	938 / 997 / 36	991 / 12
STY Nestor / 97061300	938 / 996 / 36	993 / 24
TY Opal / 97061812	954 / 990 / 48	989 / 12
TY Peter / 97062700	976 / 986 / 48	977 / 24
TY Tina / 97080712	980 / 996 / 60	993 / 24
TY Yule / 97082100	984 / 999 / 48	984 / 36
STY Bing / 97090312	949 / 993 / 36	996 / 12**
TY David / 97091800	976 / 988 / 36	966 / 36
STY Ginger / 97092800	927 / 984 / 48	974 / 12
STY Joan / 97102200	927 / 997 / 60	967 / 36
TY Rex / 98090500	984 / 984 / 36	975 / 24
TY Stella / 980901500	976 / 980 / 48	963 / 36**
TY Vicki / 98092112	954 / 1004 / 36	1003 / 12**
STY Zeb / 98101512	962 / 987 / 36	984 / 36

* Yates commenced ET in September 1996, but completed both stages of ET in October and thus is considered an October case.

**In these cases, the re-intensification stage did not begin when the transformation stage was completed. In these cases, the SLP recorded at the end of transformation continued to increase or hold steady, then decreased once the re-intensification stage began. For this reason, some cases have SLPs at the end of transformation that are actually higher than those recorded at the end of re-intensification.

Table 6. Number of ET cases occurring per month and year during 1 June through 31 October 1994-98.

Year	June	July	August	September	October	Total
1994	0	1	0	2	1	4
1995	0	0	1	3	1	5
1996	0	1	2	3	2	8
1997	3	0	2	3	1	9
1998	0	0	0	3	1	4
Total # ET Cases	3	2	5	14	6	30
Total # TCs by Month	6	22	31	30	23	112

(51%) of these later completed ET (Table 7). These 20 cases began ET in either the Poleward pattern/Poleward Flow (PF) region or in the Midlatitude pattern/PF region (Fig. II-1), and thus represent 67% of all the ET cases studied. The ten remaining ET cases (33%) were in the Standard pattern/Poleward Flow region (S/PF, Fig. II-1) at the time ET commenced. This larger percentage of ET cases emanating from the Poleward synoptic pattern rather than from the Standard pattern may be a special characteristic of the western North Pacific that may not reflect conditions in other regions.

Of these 30 ET cases, 25 were recurving tropical cyclones, while the remaining five translated poleward in a reverse-oriented monsoon trough and were later labelled as recurvers after passing through the subtropical ridge axis into the Midlatitude (M) pattern (Carr and Elsberry 1999). Riehl (1972) determined that most recurving tropical cyclones had achieved their peak intensity at or within 24 h of recurvature. The 25 completed ET cases that were recurvers commenced the transformation stage an average of 18 h after recurvature, with an average intensity of 85 kt (peak TC intensity for all 30 ET cases is 105 kt). Only one of the 30 completed ET cases had a peak intensity of less than typhoon

intensity. Other recurving tropical cyclones failed to complete ET and were classified as decayers (the example of STY Ivan is presented in Chapter III-D) as defined earlier.

The average durations (in h) of each of these stages, as well as the total duration of ET, are given in Table 7 and depicted in Fig. IV-1. The average interval between steps 1 and 2 is 30 h (Fig. IV-1), with a range of 12 h to 60 h in these 30 cases. Step 3 typically occurs after another 16 h, with a range from 12 h to 36 h. The means and standard deviations of the SLP at each step, and the time elapsed between steps, are depicted in Fig. IV-1. After completing the re-intensification stage, 11 cases achieved a SLP that was below 980 mb, 15 cases achieved a final SLP between 980 mb and 1000 mb, and four cases had a SLP above 1000 mb. The 11 deepest cases included six cases of rapid deepening (Carlson 1991). Even for these small samples, the 11 cases that re-intensified below 980 mb were statistically deeper, based on a student t-test at a 99% confidence level, than the 15 cases that achieved a final SLP between 980 mb and 1000 mb.

Table 7. Mean characteristics of 30 ET cases from 1 June through 31 October during 1994-98.

Trait	Mean Value (Standard Deviation)
1. Peak intensity during lifespan as a tropical cyclone:	105 kt (31)
2. Size (major and minor axes) at commencement of transformation:	1524 km (470), 1255 km (337)* 1273 km (414), 947 km (228)**
3. SLP at commencement of transformation (JTWC Best Track Data):	957 mb (25)
4. SLP at completion of transformation (NOGAPS analyses):	993 mb (7)
5. Duration of transformation:	46 h (12)
6. SLP at completion of ET (NOGAPS analyses):	984 mb (12)
7. Duration of re-intensification:	28 h (15)
8. Total time elapsed during ET:	81 h (27)

* Based on diameter of outermost closed isobar at sea-level.

**Based on diameter of closed contour of $1 \times 10^{-5} \text{ s}^{-1}$ units of relative vorticity at 1000 mb.

Timeline of events during Extratropical Transition in the Western North Pacific

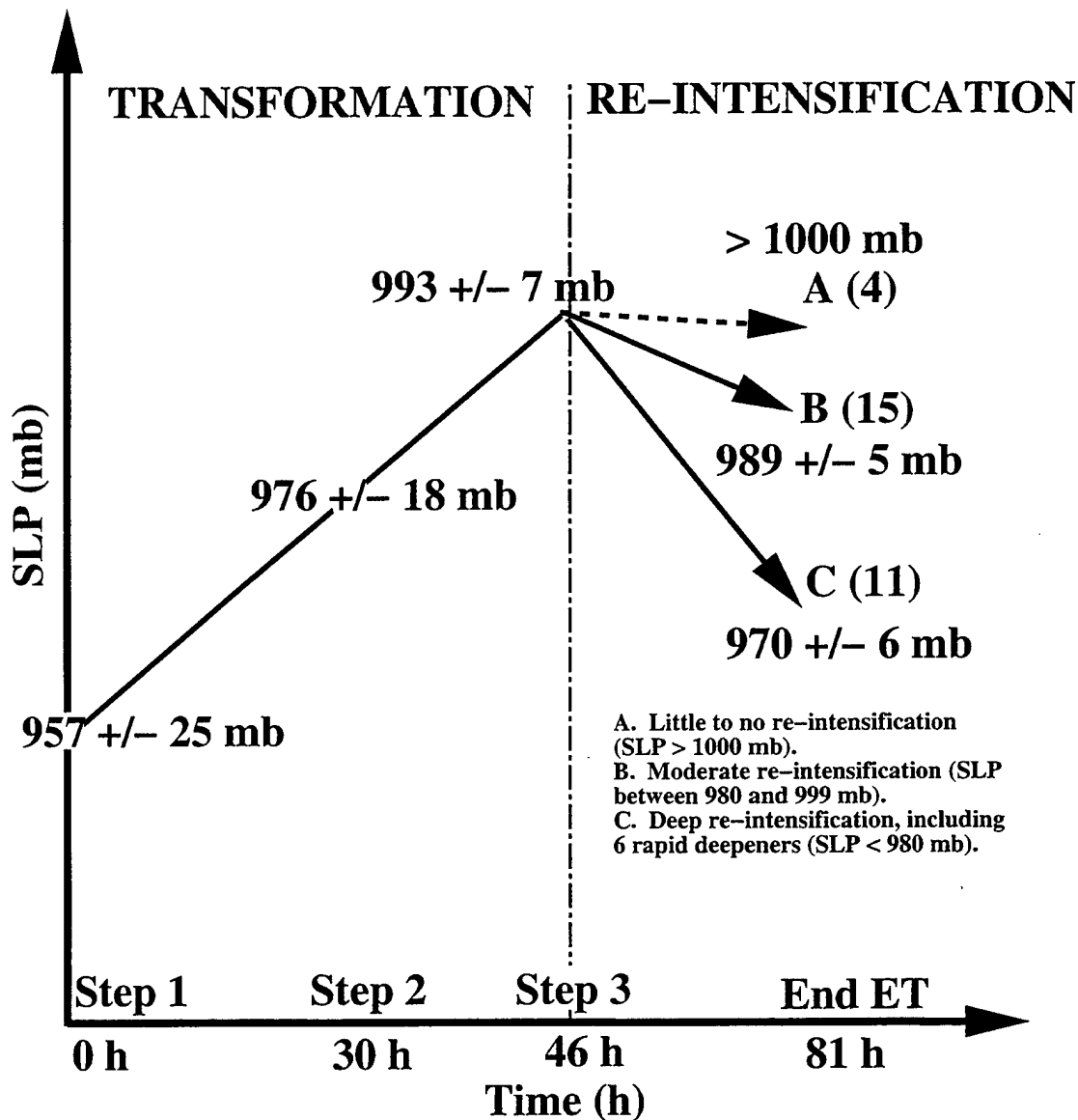


Fig. IV-1. Schematic of the evolution of ET in the western North Pacific based on 30 cases that occurred from 1 June through 31 October during 1994-98. The times on the abscissa are subsequent to the beginning of the transformation stage. Means \pm standard deviation of SLP are listed for each step of the transformation stage, and at the conclusion of the re-intensification stage, with the number of cases observed in each of the three outcomes of re-intensification depicted in the parentheses.

At the time ET commenced, the size of the tropical cyclone (Table 8) was defined using two criteria: length (in km) of the major and minor axes of the outermost closed sea-level isobar, and of the 1000-mb relative vorticity contour equal to $1 \times 10^{-5} \text{ s}^{-1}$. Based on both criteria, the size of the tropical cyclone did not appear to play a distinctive role in its subsequent ET (Tables 5 and 6). That is, the initial size of the tropical cyclone had no correlation with the duration of any stage of ET, or the total duration of ET. No effect of size could be detected, in that different size storms were as likely to redeepen below 980 mb as they were to achieve a final intensity between 980 mb and 1000 mb.

Peak intensity (kt) and the minimum SLP of the tropical cyclone at the beginning of the transformation stage (based on JTWC best-track analyses) also do not appear to play a distinctive role in determining the final SLP of storms that complete ET (Table 8). Of the 11 deepest cases of re-intensification, six were typhoons and five were supertyphoons. Some weak typhoons (e.g., TY Peter and TY Stella) with peak intensities of 65 kt became powerful baroclinic cyclones after completing ET, while some supertyphoons (e.g., STY Ward and STY Ryan) did not re-intensify significantly (Table 5). Since only one tropical storm completed ET, it is more likely that a typhoon will be able to survive the vertical wind shear and poleward translation over lower SSTs during the transformation stage and maintain a circulation that will eventually complete ET.

Of the 30 ET cases, 13 translated into a northwest pattern (Fig. IV-2a) and 17 translated into a northeast pattern (Fig. IV-2b) according to the definitions of Harr et al. (2000). The type of mid-latitude synoptic pattern (northwest or northeast) that a tropical

Table 8. Intensity, size, synoptic pattern/region at commencement of ET, and synoptic pattern at commencement of re-intensification, of 30 cases of ET occurring from 1 June through 31 October 1994-98.

Name	Peak Intensity (kt) / Intensity (kt) at Commencement of Transformation Stage	Size (km) of Major and Minor Axes at Commencement of Transformation Stage*	Synoptic Pattern at Commencement of ET, and Commencement of Re-Intensification Stage**
TY Zeke	65 / 55	864 by 816 / 1320 by 850	P / NE
TY Ivy	75 / 40	1280 by 1120 / 1174 by 1091	P / NW
STY Melissa	135 / 110	2208 by 1488 / 2332 by 1522	P / NE
TY Seth	120 / 105	1440 by 1200 / not available	S / NW
TS Janis	55 / 50	960 by 960 / 850 by 830	S / NE
STY Oscar	140 / 140	1440 by 1200 / 1420 by 1100	P / NE
TY Polly	90 / 90	2304 by 1680 / 2100 by 975	P / NE
STY Ryan	130 / 130	1776 by 1392 / 1085 by 850	P / NE
STY Ward	140 / 125	912 by 864 / 1331 by 880	S / NE
TY Dan	75 / 75	2080 by 1200 / 1481 by 1026	P / NE
TY Joy	75 / 70	1560 by 1120 / 1100 by 875	P / NW
TY Kirk	95 / 95	1280 by 1120 / 1153 by 1125	P / NE
TY Orson	115 / 70	1880 by 1200 / 1491 by 1027	S / NE
TY Tom	75 / 60	1600 by 1488 / 1573 by 871	P / NW
STY Violet	130 / 80	1920 by 1760 / 1587 by 934	P / NW
STY Yates	130 / 80	960 by 720 / 930 by 809	S / NE
TY Carlo	105 / 105	1488 by 1248 / 942 by 913	P / NW
STY Nestor	140 / 105	1488 by 1200 / 650 by 554	S / NE
TY Opal	90 / 90	2016 by 1680 / 1170 by 1100	S / NE
TY Peter	65 / 65	1100 by 1056 / 1021 by 925	P / NW
TY Tina	90 / 60	824 by 808 / 690 by 685	P / NE
TY Yule	65 / 55	1920 by 1600 / 1500 by 1242	P / NW
STY Bing	135 / 95	1800 by 1673 / 1282 by 884	P / NE
TY David	95 / 65	2640 by 2160 / 1583 by 955	S / NW
STY Ginger	145 / 115	1680 by 1440 / 1310 by 1116	S / NE
STY Joan	160 / 115	1200 by 960 / 388 by 350	P / NW
TY Rex	115 / 55	1312 by 1264 / 1593 by 997	P / NW
TY Stella	65 / 65	1576 by 1264 / 1318 by 1230	S / NW
TY Vicki	90 / 90	826 by 768 / 837 by 683	P / NE
STY Zeb	155 / 80	1392 by 1152 / not available	P / NW

*The size of the major and minor axes is listed based on the diameter of the outermost closed isobar at sea-level, followed by a second set of values based on the diameter of the closed contour of $1 \times 10^{-5} \text{ s}^{-1}$ units of relative vorticity at 1000 mb.

**Synoptic pattern at commencement of ET based on Carr and Elsberry (1994), with "P" for TCs in the Poleward synoptic pattern and "S" for TCs in the Standard synoptic pattern. Synoptic pattern at "transition time" based on Harr and Elsberry (2000), with "NE" for transformed storms entering the "Northeast" synoptic pattern and "NW" for those entering the "Northwest" synoptic pattern.

cyclone translated into is defined at or just prior to commencement of the re-intensification stage of ET (i.e., at or just after what Harr et al. (2000) call "transition time"). Storms in the northwest pattern (Fig. IV-2a) generally exhibited a more meridional track, while most of those in the northeast pattern (Fig. IV-2b) had an anticyclonic curvature that resulted

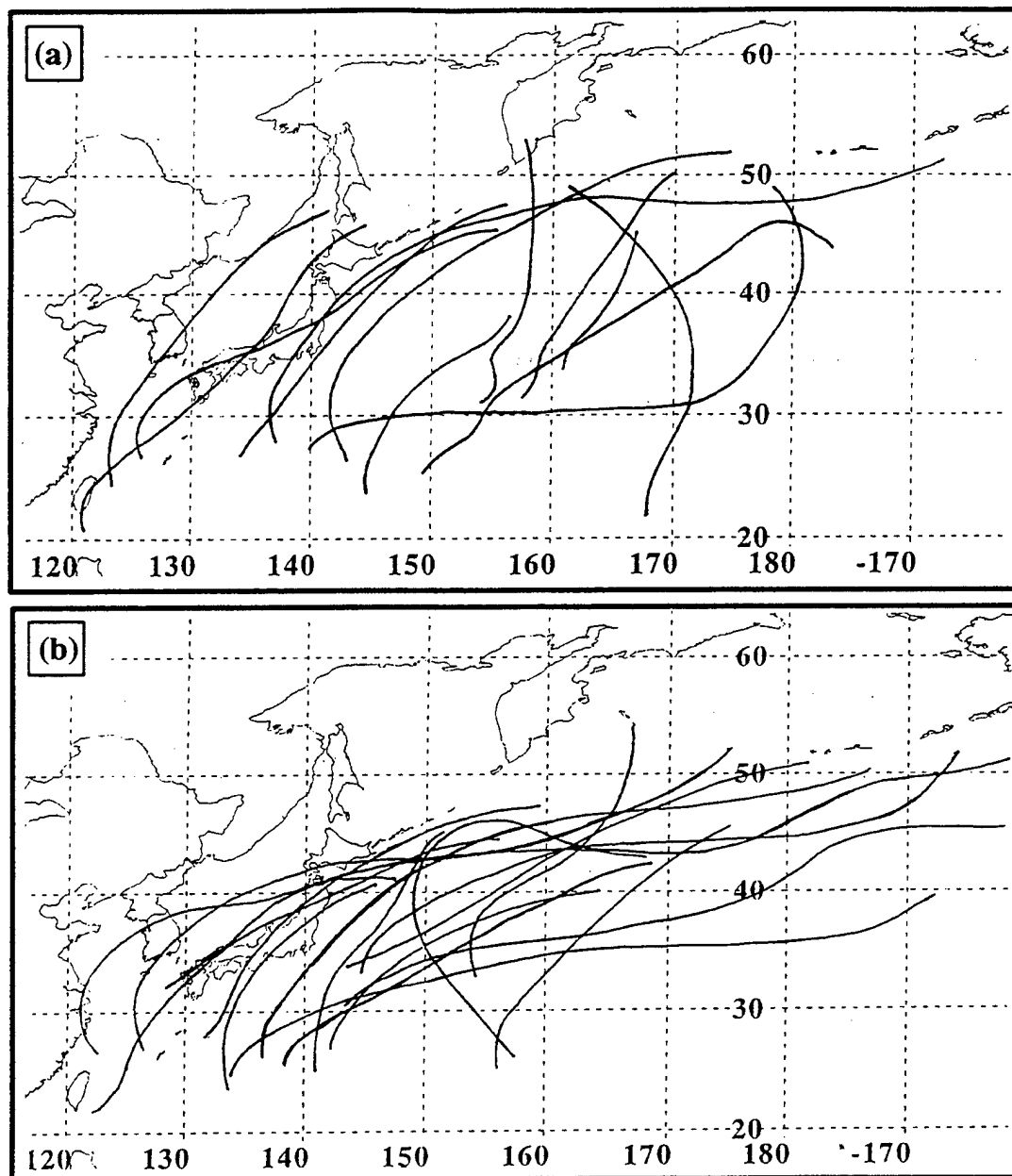


Fig. IV-2. Storm tracks of the 30 cases of ET from the commencement of the transformation stage until completion of the re-intensification stage that occurred from 1 June through 31 October during 1994-98. Tracks depict the paths of (a) 13 cases that translated into the northwest pattern and (b) 17 cases that translated into the northeast pattern as defined by Harr et al. (2000).

in a more zonal track. During the transformation stage of ET, tropical cyclones that eventually translated into a northeast pattern exhibited the same characteristics in NWP analyses and satellite imagery as those that later translated into a northwest pattern. In terms of size (km), peak intensity (kt), or intensity of the tropical cyclone at commencement of transformation, no significant differences were found between ET cases translating into a northwest pattern versus those that translated into a northeast pattern. Thirty-six hours after beginning of the re-intensification stage, the 13 northwest cases were statistically deeper (at a 95% confidence level) than the 17 northeast cases. Thus, a forecaster should anticipate a different track orientation and intensity of ET (at least for 36 h) based on the mid-latitude pattern into which the tropical cyclone is translating as it completes the transformation stage.

Five ET cases that occurred during 1 June through 31 October 1994-98 translated into a northeast pattern and achieved deep, and in some cases, explosive re-intensification. In these five cases, the TC translated into an evolving mid-latitude circulation pattern that resembled a northeast pattern at what Harr et al. (2000) call "transition time," but later resembled the northwest pattern as the storm re-intensified (Fig. I-2). In these five northeast cases, rapid, eastward translation of the transformed TC and evolution of the synoptic pattern so that 500-mb PVA and 200-mb divergence arrive in phase with the lower-tropospheric remnants of the storm, permitted Petterssen Type-B extratropical cyclogenesis that resulted in deep re-intensification well after the transformation stage had been completed. Their initially slow (or even lack of) re-intensification after completing the transformation stage of ET should not lull forecasters into dismissing any possibility of

subsequent deep (and even rapid) re-intensification. This topic will be discussed in greater detail in Chapter 5.

B. MERGERS

Matano and Sekioka (1971) defined a type of ET they called a "compound transition" in which a pre-existing mid-latitude cyclone and a TC translating poleward merged so that the mid-latitude cyclone appeared to "usurp the tropical vortex." During 1 June through 31 October 1994-98, four of 30 (13%) ET cases (TY Joy, TY Peter, TY Yule, and STY Joan) resembled the compound transition described by Matano and Sekioka (1971). At 1200 UTC 24 October 1997 (not shown), STY Joan was to the southwest of a nearby incipient, mid-latitude low that formed at the triple point of an occluding parent cyclone. STY Joan then began to intensify as an extratropical cyclone while interacting with that triple-point low (Fig. IV-3). The two vortices rotate counterclockwise around each other (Figs. IV-3a through IV-3e) until the cloud pattern associated with Joan becomes dominant and appears to absorb the pre-existing low (Fig. IV-3f). At 0000 UTC 24 October, the 500-mb absolute vorticity field associated with Joan (Fig. IV-4) is smaller, although more intense, than that associated with the incipient low. Ritchie and Holland (1993) numerically simulated the interaction between vortices of different sizes and intensities (in terms of relative vorticity). In the case in which a smaller, but more intense "vortex patch" interacts with a larger, weaker system, the larger system is sheared into a long vorticity filament, and wraps around the more intense vortex, which is only weakly affected by the interaction. The tracks of Joan and the pre-existing,

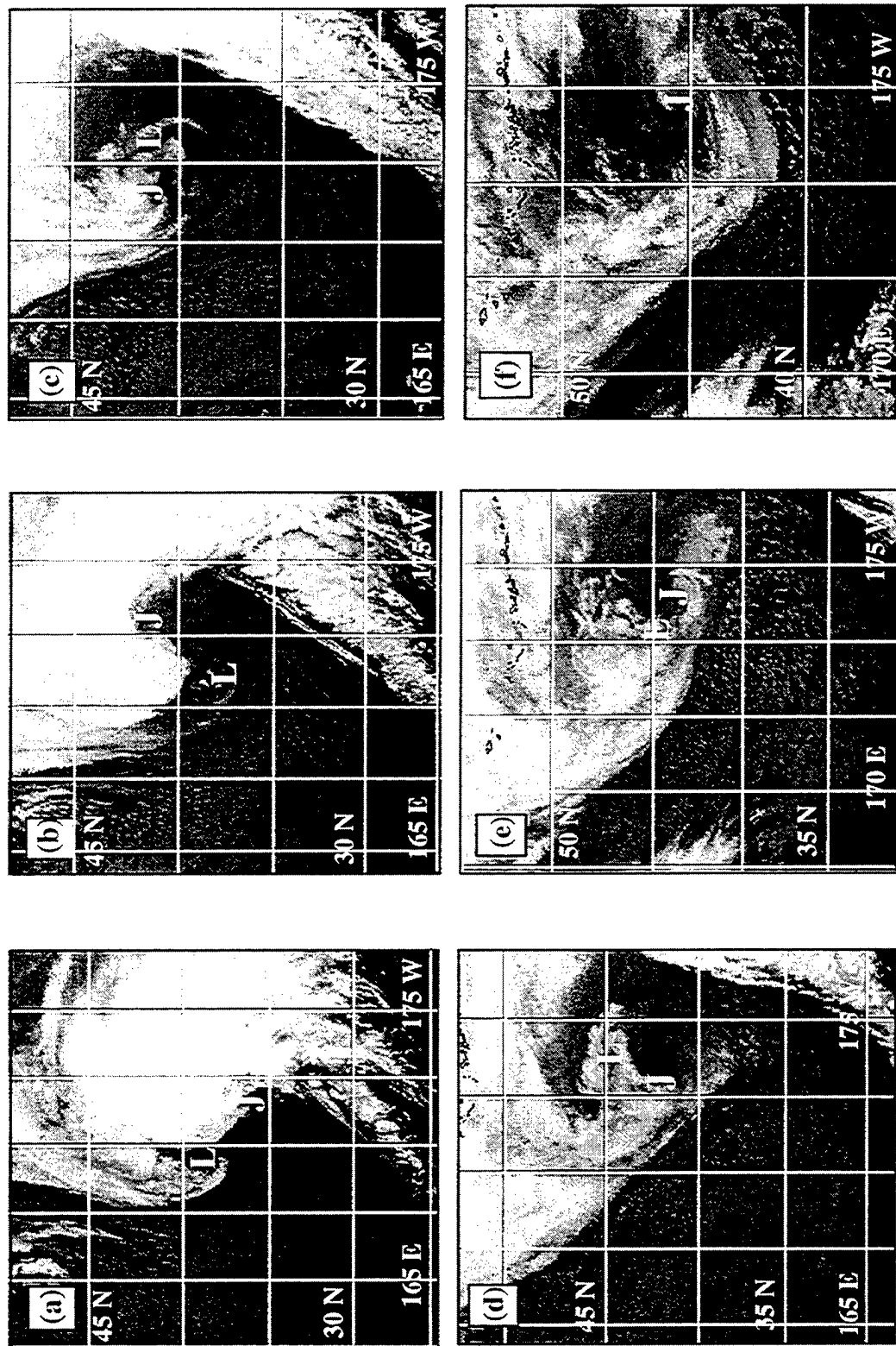


Fig. IV-3. The re-intensification of STY Joan as a baroclinic cyclone during ET, after completing the transformation stage, in IR imagery at (a) 0032 UTC 25 October, (b) 0632 UTC 25 October, (c) 1232 UTC 25 October, (d) 1832 UTC 25 October, (e) 0032 UTC 26 October, and (f) 0632 UTC 26 October 1997. Notice the interaction between Joan (marked "J") and a pre-existing, mid-latitude low (marked "L").

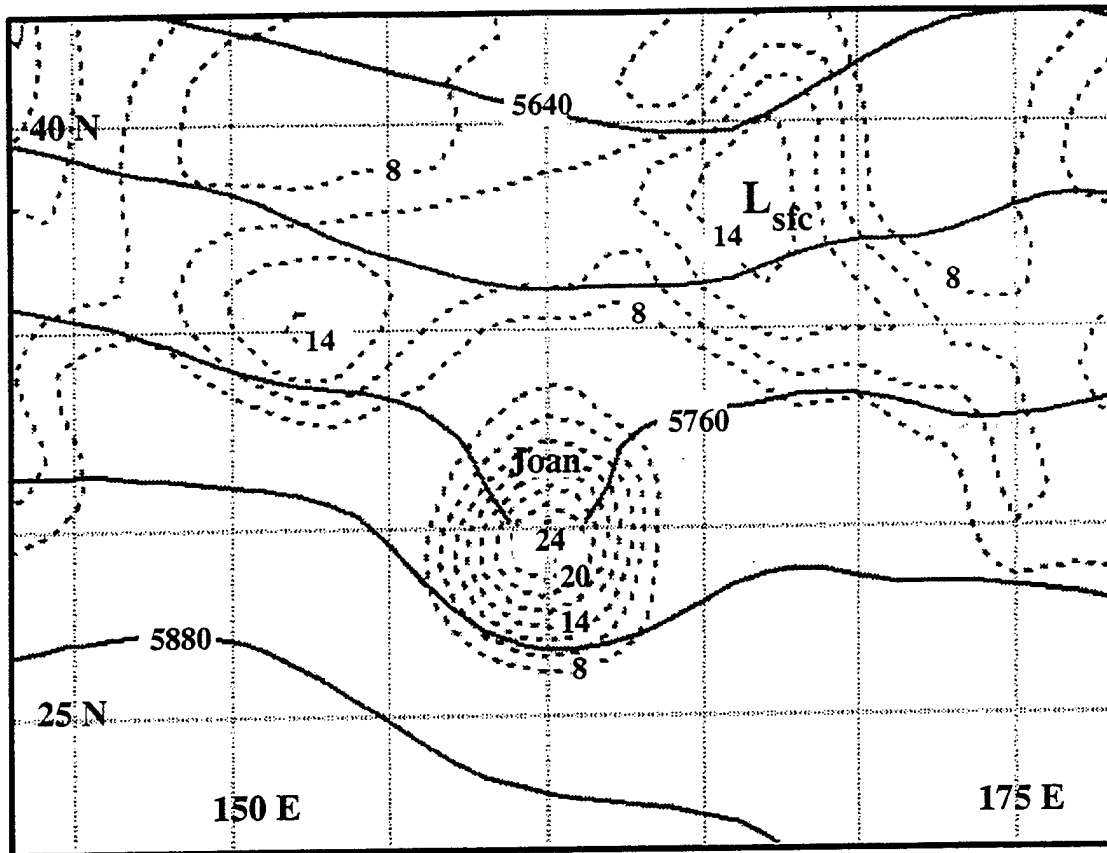


Fig. IV-4. NOGAPS analysis of 500-mb height contours (solid, 60 m interval) and absolute vorticity (dashed, $2 \times 10^{-5} \text{ s}^{-1}$ interval) during the transformation of STY Joan at 0000 UTC 24 September 1997. A mid-latitude low (labelled "L") is to the northeast of Joan.

incipient cyclone during their interaction (Fig. IV-3), and the outcome of the interaction, in which Joan was the dominant vortex and appeared to absorb the pre-existing low into its circulation pattern, are consistent with these numerical simulations of Ritchie and Holland (1993).

Each of these four cases completed the transformation stage of ET (recall the IR imagery of the transformation of TY Peter in Fig. III-3) and became a baroclinic cyclone as described by the conceptual model (Fig. III-16) before they later "merged" (according to the model of Matano and Sekioka 1971) with a pre-existing, mid-latitude cyclone

during the re-intensification stage. Thus, no difference has been found in this sample between the compound and complex cases defined by Matano and Sekioka (1971) during the transformation stage of ET, and these cases are adequately described by the conceptual model proposed in Chapter III.C.2. The compound transition defined by Matano and Sekioka (1971) presumed that the pre-existing mid-latitude cyclone would "usurp" the tropical vortex. In three of these four cases, the tropical vortex actually dominated the interaction, as illustrated in the case of STY Joan (Figs. IV-3 and IV-4), with only one (TY Joy, a midget typhoon) being incorporated into the circulation pattern of a pre-existing, mid-latitude cyclone. In this study, the impact of these vortex interactions during the re-intensification stage of ET will not be examined.

THIS PAGE INTENTIONALLY LEFT BLANK

V. RE-INTENSIFICATION STAGE OF EXTRATROPICAL TRANSITION

A. BACKGROUND

In Chapter III, the transformation stage of ET was described mainly as an interaction between a TC and pre-existing, lower-tropospheric baroclinity, together with its associated vertical wind shear. The physical processes that were observed during the transformation stage (lower-tropospheric temperature advection, establishment of a vertical motion dipole, dispersal of the warm core, ascent and descent along the tilted isentropic surfaces of a baroclinic zone, and lower-tropospheric frontogenesis) all were a consequence of interaction with that baroclinity. If the transformed storm begins to deepen as a baroclinic cyclone, the re-intensification stage of ET commences. As the re-intensification stage begins, the θ_e gradient of this lower-tropospheric baroclinity has already increased as a result of the interaction with the TC during the transformation stage (Figs. III-6, III-9a, and III-14a). Lower-tropospheric warm frontogenesis (Fig. III-15, and Tables 3 and 4) that began during transformation continues and strengthens as the re-intensification stage commences (Harr and Elsberry 2000).

The transformed storm also enters either the northwest or the northeast mid-latitude circulation described by Harr et al. (2000). In the northwest pattern, the storm couples with a short-wave trough to the northwest such that potential energy is efficiently converted to kinetic energy. In the northeast pattern, the storm does not couple with a weaker trough to the northwest. Rather, the interaction with the large-scale circulation destroys kinetic energy, although the system continues to translate eastward and may later

couple with a primary mid-latitude cyclone to the northeast. At the beginning of the re-intensification stage, the wind and precipitation in the TC remnants are already asymmetric (Chap. I, Figs. I-4 and I-5). By definition, the re-intensification stage ends after a deepening to a minimum SLP before holding steady or filling in the next analysis.

Carlson (1991) listed four criteria that must exist for vigorous and explosive (>12 mb decrease in sea-level pressure (SLP) in 12 h) extratropical cyclogenesis to occur: (i) strong meridional baroclinity (and therefore vertical wind shear); (ii) vertical phase lag of the height and thermal fields, which implies that the upper-tropospheric perturbation is the triggering mechanism; (iii) relatively low static stability; and (iv) geographic location in the middle or high latitudes. If all of these criteria are satisfied, deep, and potentially explosive Petterssen Type-B extratropical cyclogenesis (Petterssen and Smebye 1971) may result. Warrenfeltz and Elsberry (1988) studied the effects of superposition of an upper-tropospheric PV maximum above a lower-tropospheric PV maximum, and illustrated that the phasing of these translating upper- and lower-level PV anomalies played an important role in determining the rate of extratropical cyclogenesis that resulted. In many prior ET cases, extratropical re-intensification of the TC remnants is similar to Petterssen Type-B extratropical cyclogenesis, with positive vorticity advection (PVA) and upper-tropospheric divergence above a TC that has already been transformed into a baroclinic cyclone (DiMego and Bosart 1982, Sinclair 1993, Foley and Hanstrum 1994, Klein 1997, and Harr et al. 2000).

In Chapter IV, three possible outcomes for storms that completed ET are listed: (i) deep re-intensification (SLP less than 980 mb at completion of ET); (ii) moderate re-

intensification (SLP greater than 980 mb, but less than 1000 mb at completion of ET); and (iii) little re-intensification (SLP greater than 1000 mb after completion of ET). Because of their destructive potential, cases of deep and/or rapid re-intensification are of the greatest interest to mariners and those who live or work near the ocean coast.

It is hypothesized that deep re-intensification during ET is likely if the four criteria presented by Carlson (1991) are satisfied (Klein et al. 2000b). If Petterssen Type-B extratropical cyclogenesis is the method by which a TC re-intensifies after completing the transformation stage of ET, the TC must translate poleward and arrive at some critical location where PVA and upper-tropospheric divergence exist in the mid-latitude circulation pattern. In this study, the term "proper phasing" means the TC remnants arrive at this critical location in the mid-latitude circulation pattern. *The specific hypothesis is that phasing of the poleward-translating TC remnants with an eastward translating and evolving mid-latitude circulation will provide mid- and upper-tropospheric support for a Petterssen Type-B extratropical cyclogenesis that determines the magnitude of the re-intensification.* A critical region is defined in which Carlson's cyclogenesis criteria are satisfied, which specifically involves superposition of upper-tropospheric divergence and cyclonic vorticity advection over a lower-tropospheric PV maximum. Based on the observational study, this region will be defined as a volume of the atmosphere in which the 200-mb divergence $> 3 \times 10^{-5} \text{ s}^{-1}$, 500-mb PVA has a maximum $> 50 \times 10^{-10} \text{ s}^{-2}$, and the dipole of 925-mb temperature advection $> \pm 10 \times 10^{-5} \text{ K s}^{-1}$.

The final SLP achieved at the end of the re-intensification stage (which coincides with the end of ET according to the definitions presented in Chapter II) is listed in Chap.

IV (Table 5), along with the mid-latitude synoptic circulation pattern (Harr et al. 2000) it entered before re-intensification began. Six cases of deep re-intensification were observed in the northwest pattern. Harr et al. (2000) used TY David as an archetypal example of the re-intensification that occurs in the northwest pattern. At 0000 UTC 19 September 1997, analysis of layer-averaged PV (Fig. V-1a) between 925 mb and 700 mb (shaded) and 500 mb and 300 mb (solid contours) indicates that TY David is southeast of an upper-tropospheric PV maximum. TY David is interacting with a baroclinic zone to the north (Fig. V-1d), is downstream of a 500-mb local maximum of PVA (Fig. V-1b), and is southwest of an area of upper-tropospheric divergence (Fig. V-1c). If David is to complete the re-intensification stage of ET, the mid-tropospheric PVA (Fig. V-1b) and upper-tropospheric divergence (Fig. V-1c) must become superposed above the lower-tropospheric dipole of temperature advection (Fig. V-1d) to produce a critical region that supports Petterssen Type-B extratropical cyclogenesis. At this time, David has not yet completed the transformation stage of ET, but it is translating into a northwest mid-latitude circulation (Harr et al. 2000) so that it is expected to phase with that critical region.

Over the next 24 h, David completes the transformation stage of ET and translates northeastward to a critical region southwest of the tip of Kamchatka (Fig. V-2a). At this time, David is imbedded in a baroclinic zone (Fig. V-2d) near the center of a dipole of cold (warm) advection to the west (east). David is in a 500-mb ridge/trough couplet, is in a region of 500-mb PVA (Fig. V-2b), and is also beneath 200-mb divergence (Fig. V-2c) associated with the equatorward entrance region of a polar jet streak. Notice that the

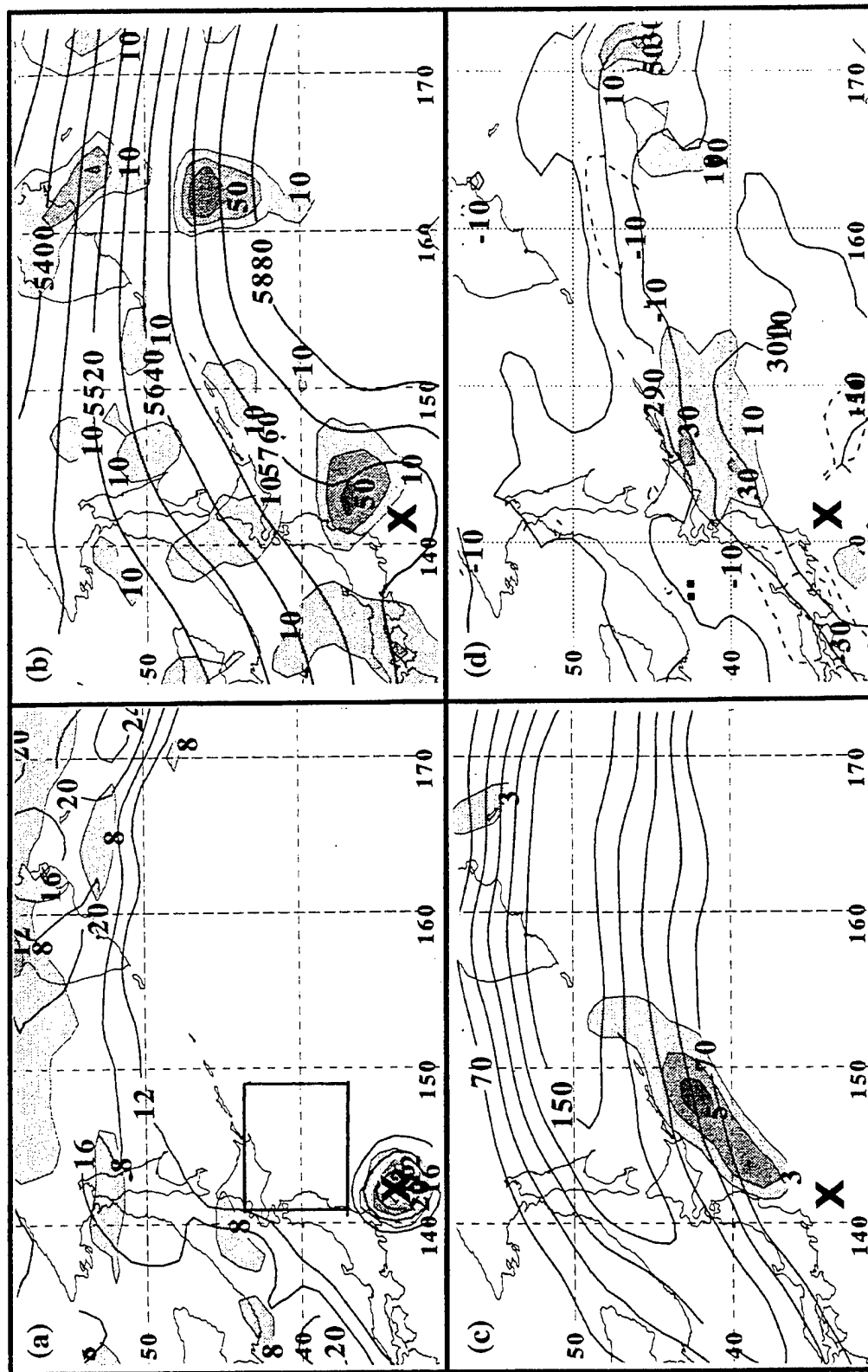


Fig. V-1. The ET of TY David at 0000 UTC 19 September 1997, depicted in NOGAPS analyses of (a) layer-averaged PV between 925 mb and 700 mb (shaded, interval $4 \times 10^{-7} \text{ K m}^2 \text{ s}^{-1} \text{ kg}^{-1}$, beginning at $8 \times 10^{-7} \text{ K m}^2 \text{ s}^{-1} \text{ kg}^{-1}$), and 500 mb to 300 mb (solid contours, interval $4 \times 10^{-7} \text{ K m}^2 \text{ s}^{-1} \text{ kg}^{-1}$, beginning at $12 \times 10^{-7} \text{ K m}^2 \text{ s}^{-1} \text{ kg}^{-1}$), (b) 500-mb isotherms (solid contours, 60 m interval) and positive vorticity advection (shaded, $20 \times 10^{-5} \text{ s}^{-1}$ interval, beginning at $10 \times 10^{-5} \text{ s}^{-1}$), (c) 200-mb isotachs (solid, 20 kt interval beginning at 70 kt) and divergence (shaded, $1 \times 10^{-5} \text{ s}^{-1}$ interval, beginning at $3 \times 10^{-5} \text{ s}^{-1}$), and (d) 925-mb temperature advection, with warm advection represented by shaded contours ($20 \times 10^{-5} \text{ K s}^{-1}$ interval, beginning at $10 \times 10^{-5} \text{ K s}^{-1}$), and isentropes of 925-mb potential temperature (thick solid contours, 5 K interval). The critical region is depicted by a solid box in (a), and the storm location is denoted with an "X."

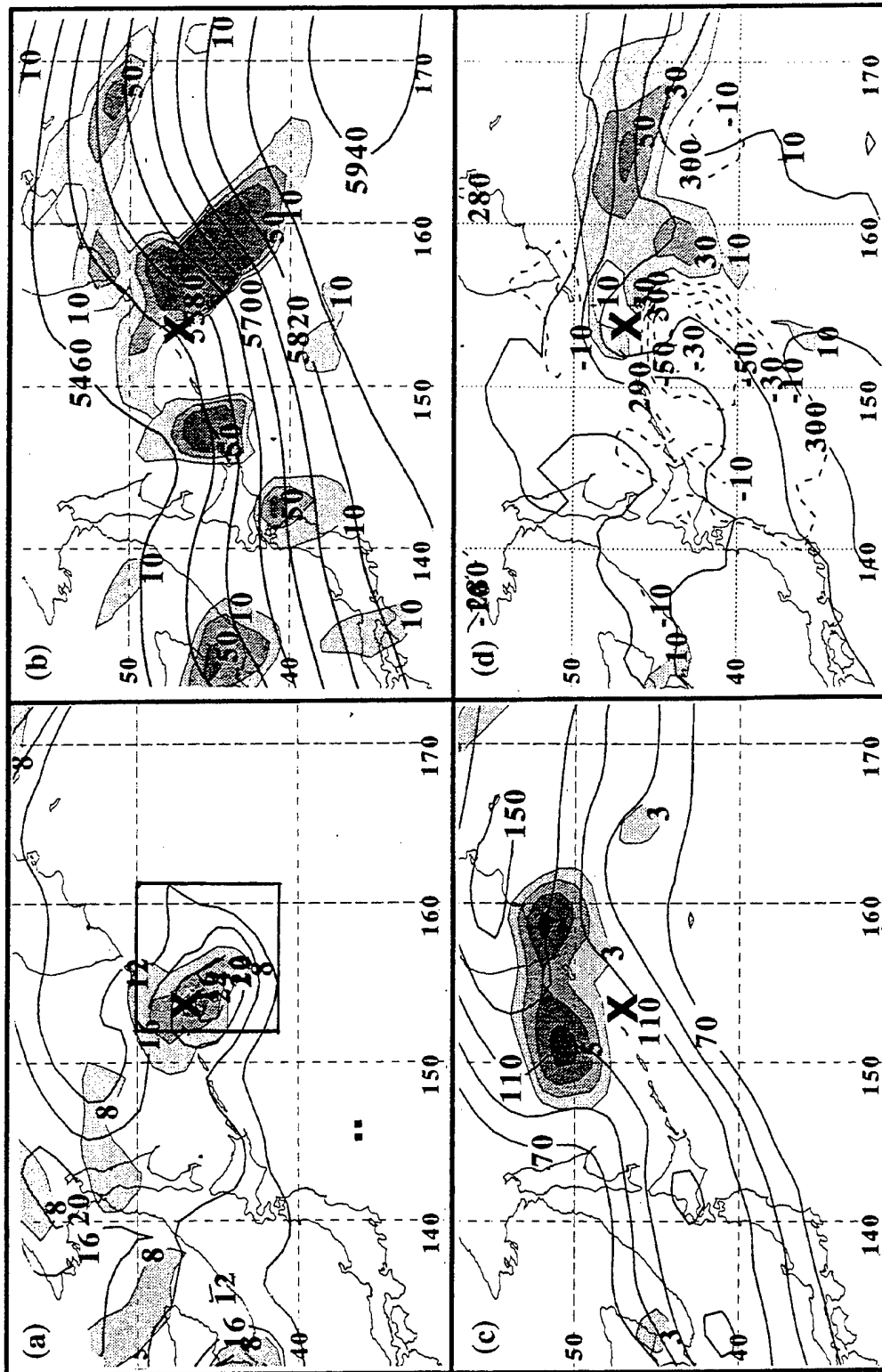


Fig. V-2. (a) Layer-averaged PV between 925 mb and 700 mb (shaded) and 500 mb to 300 mb (solid contours), (b) 500-mb isotherms and PVA, (c) 200-mb isotherms and divergence, and (d) 925-mb warm advection and isentropes of potential temperature as in Fig. V-1, except for NOGAPS analysis of TY David at 0000 UTC 20 September 1997.

upper-tropospheric PV maxima that was northwest of David 24 h earlier is now superposed above David (Fig. V-2a). As David translates poleward and transforms, it enters a northwest mid-latitude circulation pattern in phase with parameters (divergence, PVA, temperature advection) that define a critical region, then remains in that critical region for 36 h (not shown). While within this critical region, David completes the re-intensification stage of ET and deepens 21 mb in 24 h, including a 12-h period of rapid deepening, until it achieves a SLP of 966 mb (not shown).

Seven ET cases that entered the northwest pattern either did not phase with a critical region, or phased with a critical region for only a short time, so that they achieved only moderate to little re-intensification. At 0000 UTC 4 September 1994, TY Ivy is far to the southeast of the upper-level PV maximum (Fig. V-3a). Notice that a dipole of cold and warm advection (Fig. V-3d) is present, but is much weaker than that associated with David, as is the 500-mb PVA above Ivy (Fig. V-3b). The 200-mb jet streak and associated divergence above Ivy is also weaker than in the case of David (Fig. V-3c), and the lower-tropospheric PV maxima associated with Ivy is much weaker than with TY David (Fig. V-2a). Consequently, no critical region (as defined by the diagnostic criteria presented earlier) is present in Fig. V-3, and Ivy clearly never phases with a critical region, and achieves a weak re-intensification of only 3 mb.

Harr et al. (2000) used TY Opal as an archetypal example of the remaining 17 ET cases that completed re-intensification in the northeast pattern. At 0000 UTC 20 June 1997, TY Opal is interacting with weak lower-tropospheric baroclinity (Fig. V-4d). Whereas Opal is upstream of a 500-mb trough (Fig. V-4b), it is still positioned in a weak

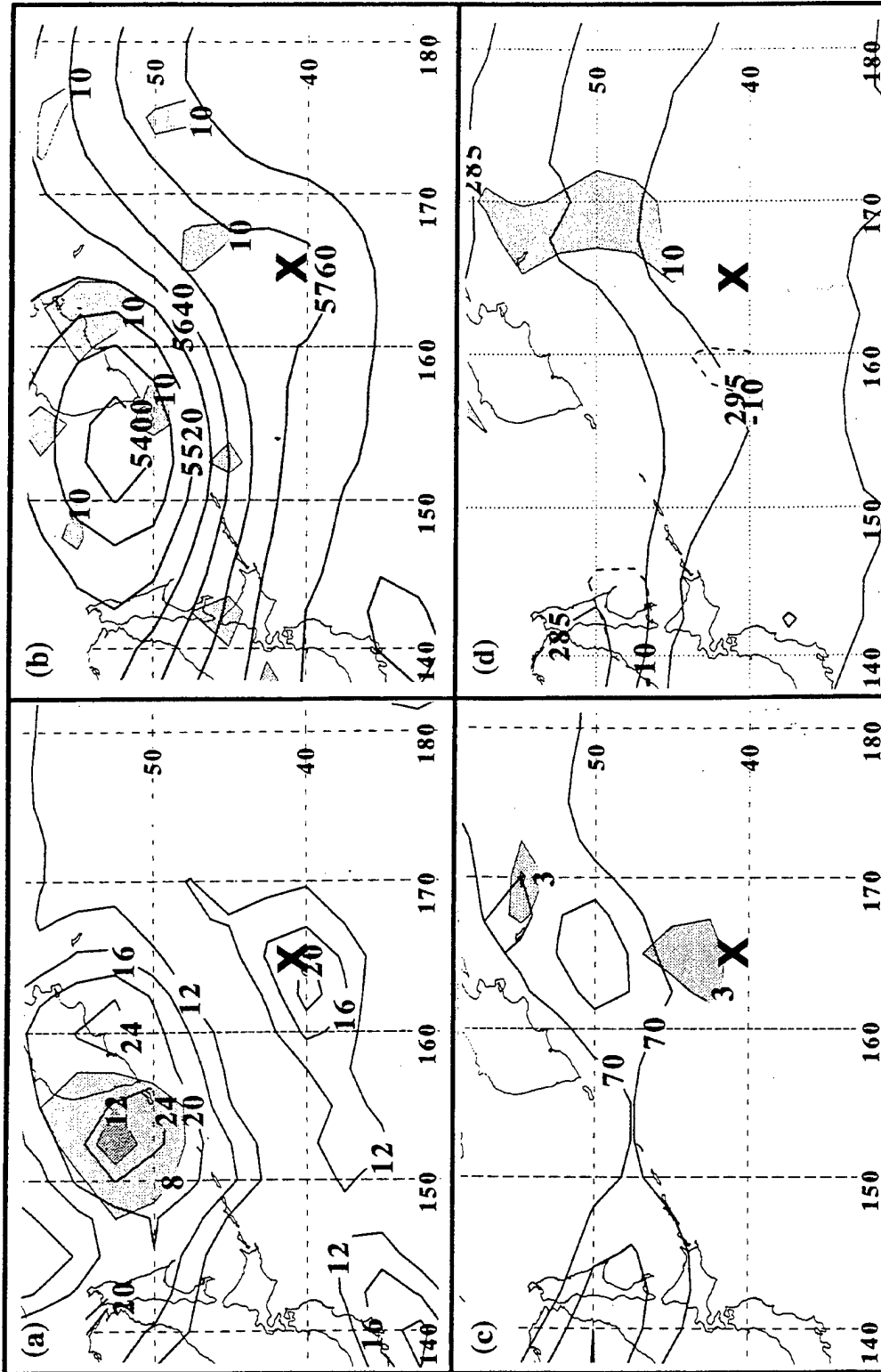


Fig. V-3. (a) Layer-averaged PV between 925 mb and 700 mb (shaded) and 500 mb to 300 mb (solid contours), (b) 500-mb isotherms and PVA, (c) 200-mb isotachs and divergence, and (d) 925-mb warm advection and isentropes of potential temperature as in Fig. V-1, except for NOGAPS analysis of TY Ivy at 0000 UTC 4 September 1994.

500-mb ridge-trough couplet (Fig. V-4b) and beneath 200-mb divergence (Fig. V-4c) associated with the equatorward entrance region of a weak polar jet streak. Notice that Opal is also far to the southwest of the 500-mb to 300-mb layer-averaged PV maximum (Fig. V-4a). Twenty-four hours later, Opal is within a weak lower-tropospheric dipole of temperature advection (Fig. V-5d), and a weakening 500-mb ridge-trough couplet and PVA that is far weaker (Fig. V-5b) than that associated with David (Fig. V-2b). Opal is also lagging upstream of the maximum region of 200-mb divergence (Fig. V-5c) and remains southwest of the main 500-mb to 300-mb layer-averaged PV maximum (Fig. V-5a). While Opal did interact with a critical region in the mid-latitude synoptic circulation pattern for 12 h (not shown), it only re-deepened 1 mb before beginning to weaken and dissipate.

Harr et al. (2000) suggest that storms entering a northeast synoptic pattern only weakly interact with the local PV maximum associated with a weak trough northwest of the storm. Rather, the strongest interaction is with the northerly flow behind the primary trough to the northeast, which results in destruction of kinetic energy associated with the TC remnants (e.g., TY Opal in Fig. V-5). Thus, deep re-intensification should not be expected during the first 36 h in the northeast pattern. However, five cases were found in which a transformed TC later did achieve deep re-intensification after passing through the northeast synoptic circulation pattern to eventually re-intensify in a northwest pattern downstream. One of these (STY Ginger) actually resembled re-intensification in a northwest pattern from the start after the weak short-wave northwest of the storm deepened, and Ginger later coupled with it (not shown).

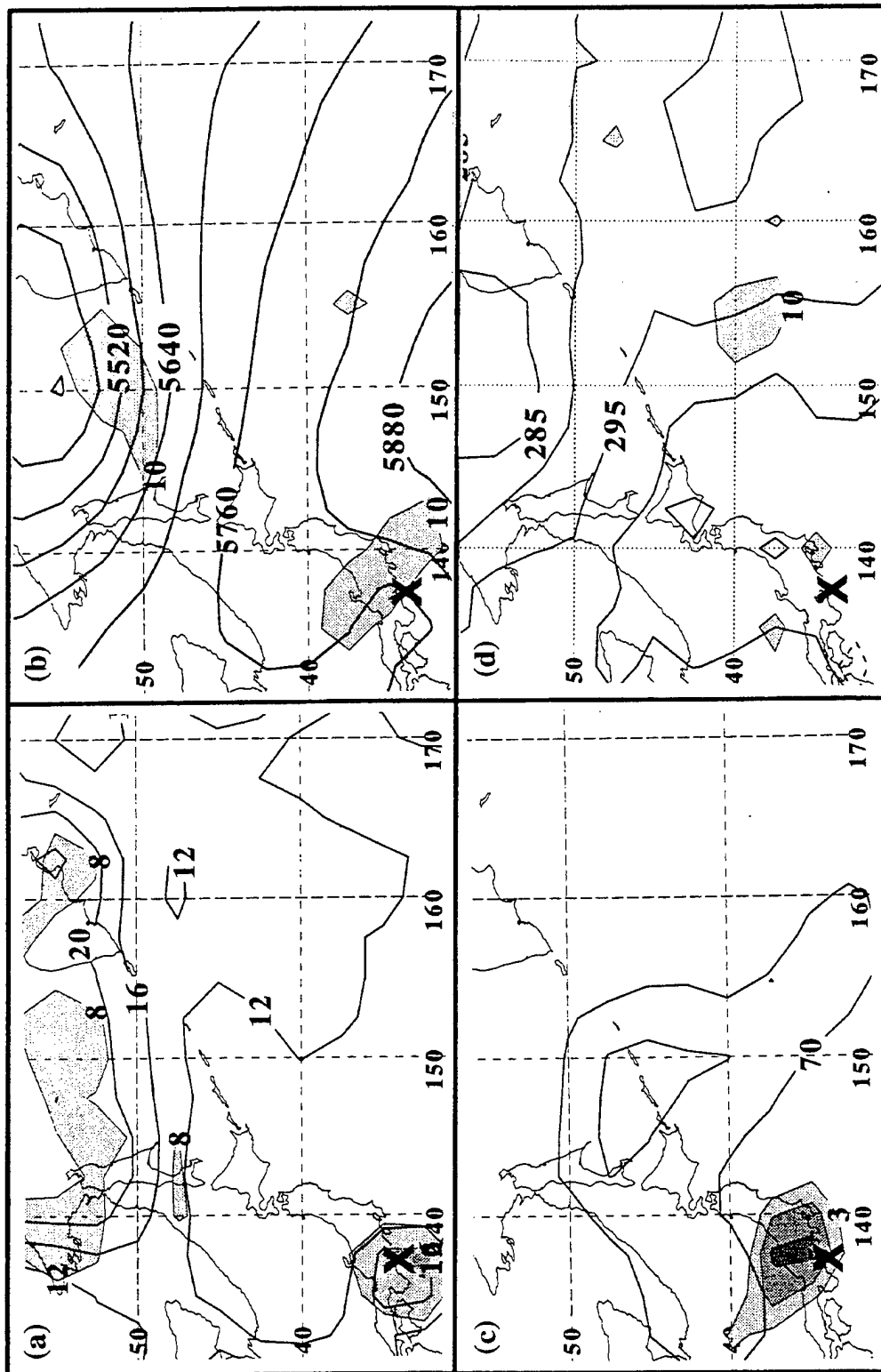


Fig. V-4. (a) Layer-averaged PV between 925 mb and 700 mb (shaded) and 500 mb to 300 mb (solid contours), (b) 500-mb isoheights and PVA, (c) 200-mb isotachs and divergence, and (d) 925-mb warm advection and isentropes of potential temperature as in Fig. V-1, except for NOGAPS analysis of TY Opal at 0000 UTC 20 June 1997.

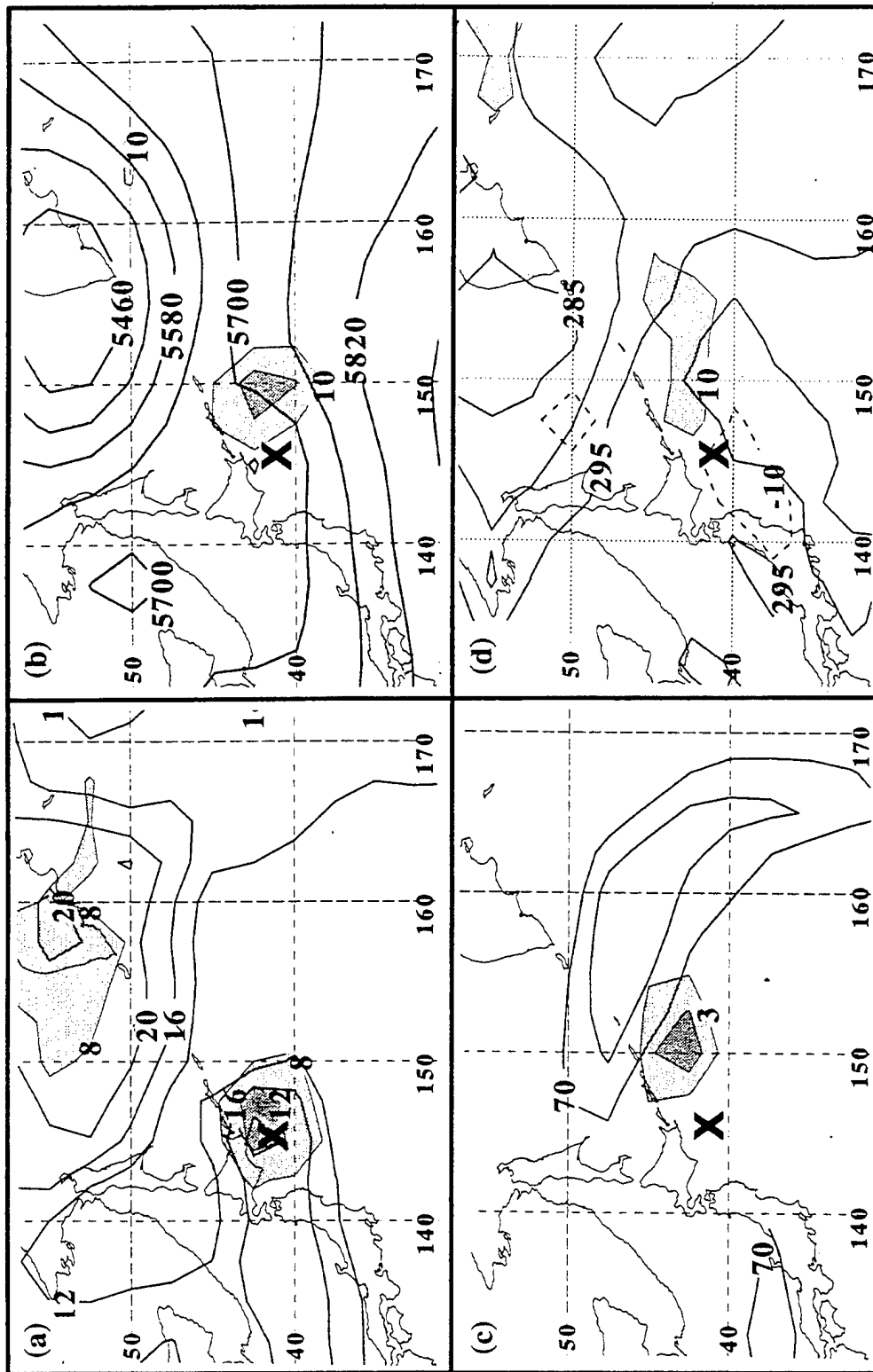
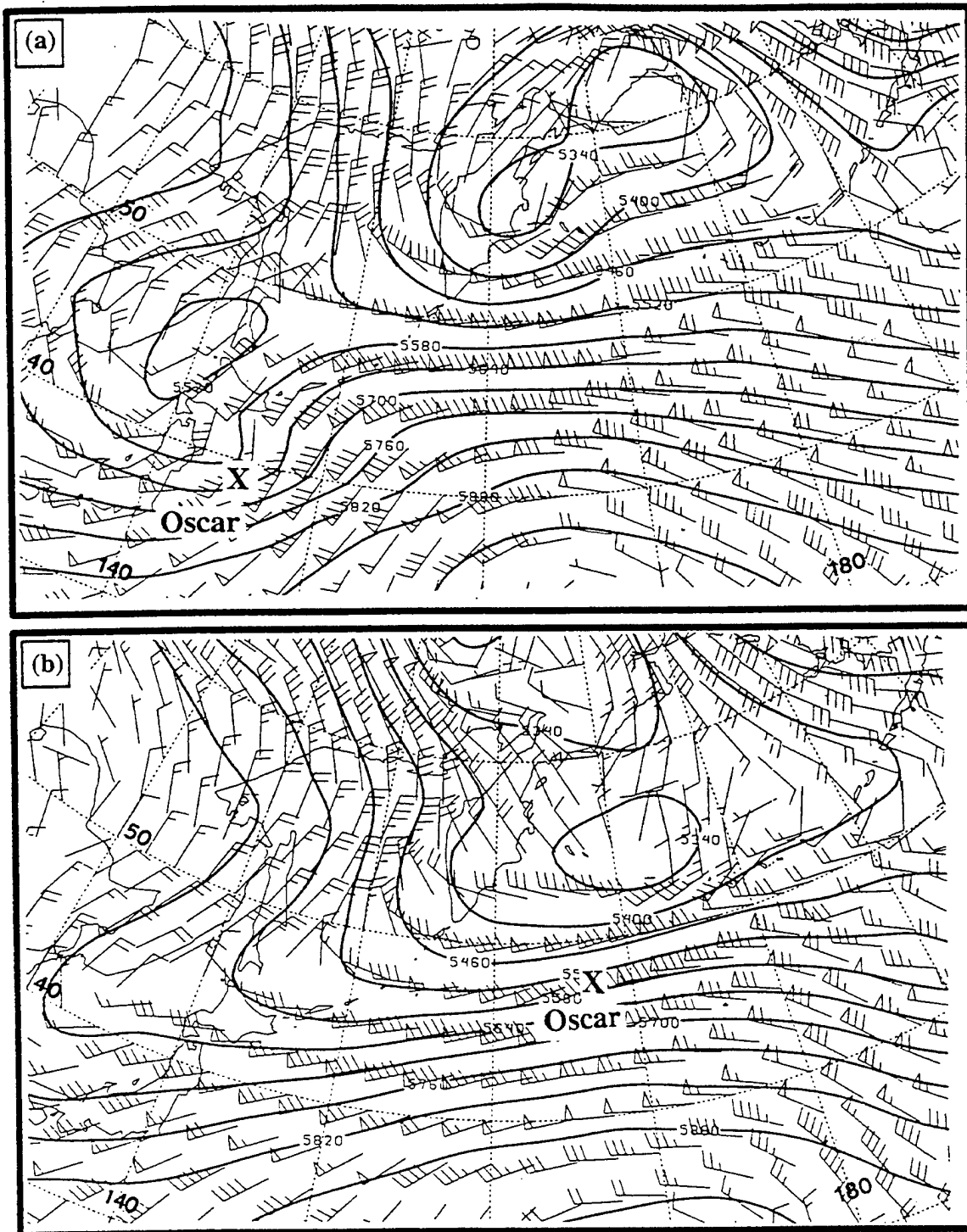


Fig. V-5. (a) Layer-averaged PV between 925 mb and 700 mb (shaded) and 500 mb to 300 mb (solid contours), (b) 500-mb isoheights and PVA, (c) 200-mb isotachs and divergence, and (d) 925-mb warm advection and isentropes of potential temperature as in Fig. V-1, except for NOGAPS analysis of TY Opal at 0000 UTC 21 June 1997.

Therefore, STY Ginger is better described as having re-intensified in a northwest rather than a northeast pattern.

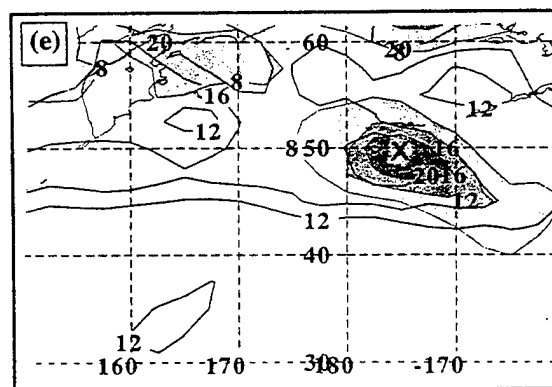
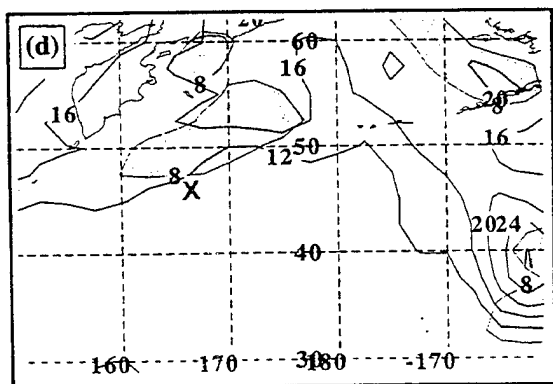
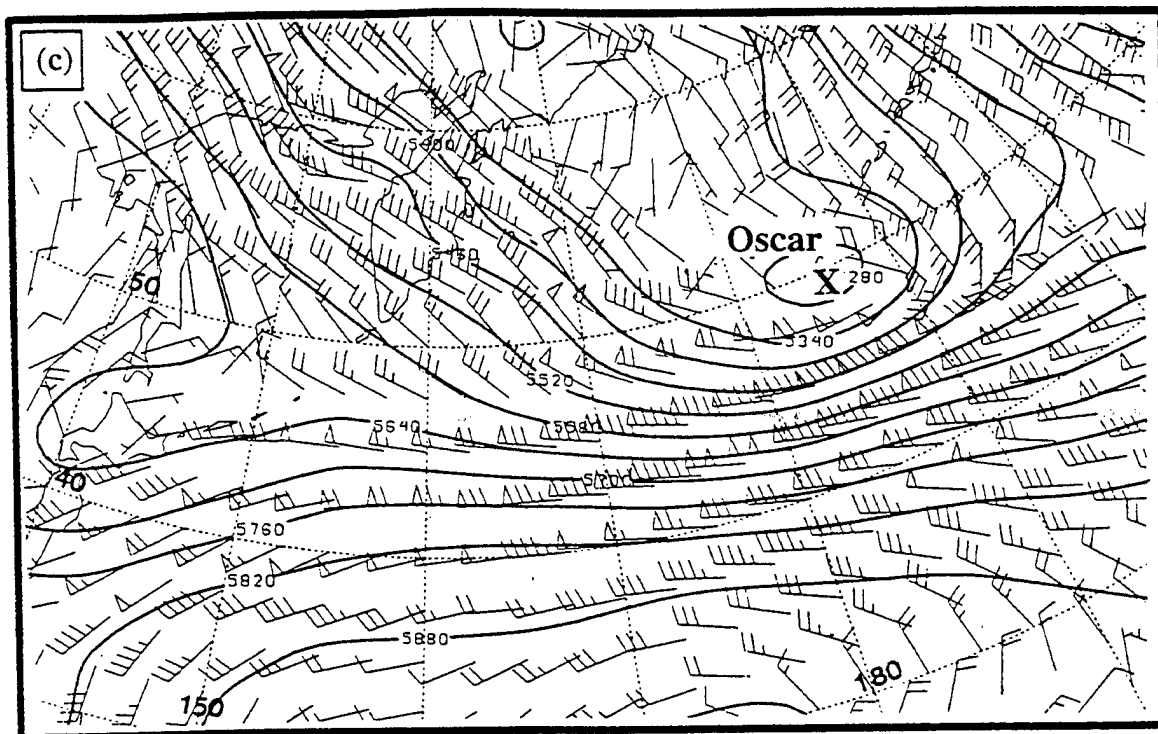
Three cases of deep re-intensification in the northeast pattern (STY Melissa, TY Orson, and STY Yates) were similar to STY Oscar during September 1995 (Fig. V-6), which transformed, and then rapidly translated into a northeast pattern of 500-mb isoheights that had evolved over 48 h into a northwest pattern when the storm re-intensified. As Oscar began to re-intensify at 1200 UTC 18 September (Fig. V-6b), it had been translating downstream at 41 knots and then began to couple with an upper-tropospheric PV maxima to the northeast (Fig. V-6d). By 1200 UTC 19 September, this upper-level PV maxima (Fig. V-6e) has intensified and is superposed above the lower-level PV maximum that is associated with Oscar. In the 24-h period that Oscar interacted with the critical region implied by the 500-mb to 300-mb layer-averaged PV maximum, deep and rapid re-intensification occurred and Oscar achieved a final SLP of 959 mb after deepening 28 mb in 24 h (not shown). Thus, it is possible for a northeast case to achieve deep re-intensification, but only if the transformed storm rapidly translates downstream in strong zonal flow and survives long enough to arrive in phase with a downstream critical region as the synoptic circulation pattern evolves and better resembles a northwest rather than the original northeast pattern.

In all 30 completed ET cases, the transformed TC arrived in the mid-latitude circulation pattern in phase with some critical region of the atmosphere that supported extratropical cyclogenesis according to the Pettersson Type-B mechanisms. The previous examples (Figs. V-1 through V-6) suggest that the outcome of the re-intensification stage



X = Surface Center

Fig. V-6. The ET of STY Oscar with solid contours depicting 500-mb isoheights (60 m interval) and winds (5 kt interval) at (a) 1200 UTC 17 September, (b) 1200 UTC 18 September, and (c) 1200 UTC 19 September 1995, and layer-averaged PV as in Fig. V-1a, except for STY Oscar at (d) 1200 UTC 18 September and (e) 1200 UTC 19 September 1995.



X = Surface Center

Fig. V-6 (continued).

of ET depends on: (i) whether or not the transforming TC arrives in phase with the critical region in the mid-latitude circulation pattern; and (ii) how well that critical region satisfies Carlson's criteria (that is, the magnitudes of lower-tropospheric temperature advection, 500-mb PVA, and upper-tropospheric divergence that exist in the critical region); and (iii) how long the transformed TC remains in that critical region. For example, the critical region in the case of TY David (Fig. V-2) appeared to satisfy Carlson's criteria more strongly than the support for extratropical cyclogenesis that is depicted in the cases of TY Ivy (Fig. V-3) and TY Opal (Fig. V-5). In particular, David moved into a region with large values of lower-tropospheric meridional baroclinity, 500-mb vorticity advection, and upper-tropospheric divergence. Whereas some of the elements are present or nearby TY Opal at 1200 UTC 20 June 1997 (not shown), they do not satisfy the criteria for a critical region.

Unfortunately, the observational analysis of the re-intensification stage of these 30 ET cases is not conclusive that deep re-intensification cases only occur in the critical regions that most closely fit Carlson's criteria, and when transformed TCs remained in those critical regions the longest. No threshold for lower-tropospheric baroclinity, 500-mb PVA, and upper-tropospheric divergence could be found that would closely satisfy Carlson's criteria, and at the same time include all cases of deep re-intensification, while excluding all cases of little to moderate re-intensification. Furthermore, STY Ginger completed its deep re-intensification in 12 h (Table 5), so it was possible to achieve deep re-intensification after only a brief period of time within the critical region.

B. HYPOTHESES

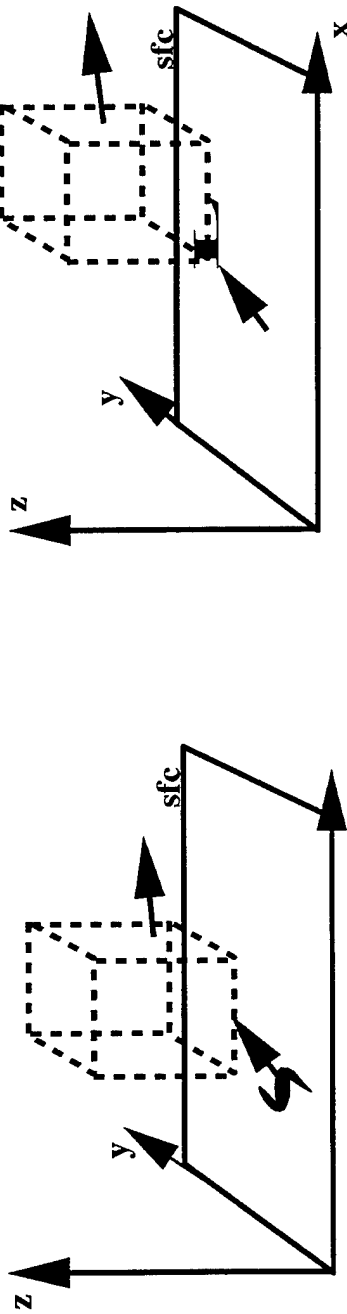
1. Phasing of the TC and the Critical Region

It is hypothesized that the principle factor that determines whether or not deep re-intensification will occur is whether or not the transformed TC enters a critical region in the mid-latitude circulation pattern, and how long the transformed storm remains within that critical region. Consequently, optimal support for deep and/or rapid Petterssen "Type-B" extratropical cyclogenesis is hypothesized to exist if the transformed TC phases with the critical region of the mid-latitude circulation pattern with the largest values of lower-tropospheric temperature advection, mid-tropospheric PVA, and upper-tropospheric divergence.

Based on this superposition hypothesis, a simple conceptual model (Fig. V-7) would appear to describe two contrasting scenarios: (i) the TC arrives in the mid-latitude circulation pattern in phase with the critical region, couples with it, and re-intensifies as a baroclinic cyclone; or (ii) the TC fails to arrive in phase with the critical region (if a region meeting all criteria exists), does not couple with it, and thus does not significantly re-intensify. In Scenario One (Fig. V-7a), the transformed TC and the critical region in the mid-latitude circulation pattern have both translated so that the TC remnants enter the critical region. That is, upper-tropospheric divergence, mid-tropospheric PVA, lower-tropospheric baroclinity and the transformed TC are superposed, and therefore the cyclone re-intensifies. Even if a critical region is present and translates downstream with the same course and speed, what is different in Scenario Two (Fig. V-7b) is the initial location or translation of the TC remnants has changed such that a coupling does not occur and only

CONCEPTUAL MODEL OF PHASING BETWEEN THE CRITICAL REGION AND THE TC DURING THE RE-INTENSIFICATION STAGE OF ET IN THE WESTERN NORTH PACIFIC

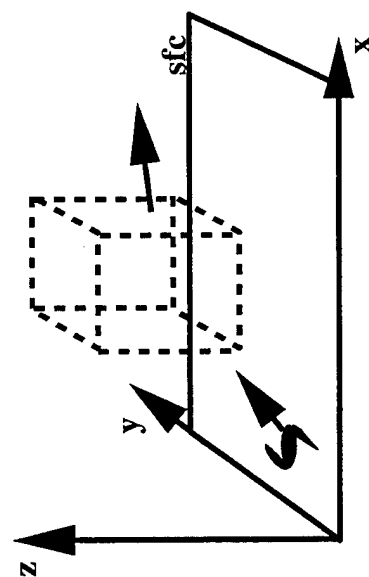
(a) SCENARIO ONE: TC ARRIVES IN PHASE WITH CRITICAL REGION



Time " t " and critical region depicted with dashed lines

Time " $t + \Delta t$ ", critical region depicted with dashed lines, "L" for transformed TC

(b) SCENARIO TWO: TC DOES NOT ARRIVE IN PHASE WITH CRITICAL REGION



Time " t " and critical region depicted with dashed lines

Time " $t + \Delta t$ ", critical region depicted with dashed lines, "L" for transformed TC

Fig. V-7. Conceptual model of the phasing between the critical region in the mid-latitude circulation pattern and the TC during the re-intensification stage of ET, depicting (a) TC vortex and critical region at initial time " t " both translate so that after a period of Δt hours, the transformed TC is located within the critical region, and (b) at initial time " t ," the TC vortex is displaced and has a different translation direction and speed, while the critical region moves in the same direction and at the same speed as in (a), so that the TC does not arrive in the critical region after " Δt " hours.

minimal re-intensification is achieved. In this simple and static superposition model, the upper-tropospheric divergence and mid-tropospheric PVA are not modified by the interaction with the transformed TC. As will be demonstrated below, the interaction is not always static. Nevertheless, the key aspect in the re-intensification will be how the TC remnants phase with the mid-latitude circulation.

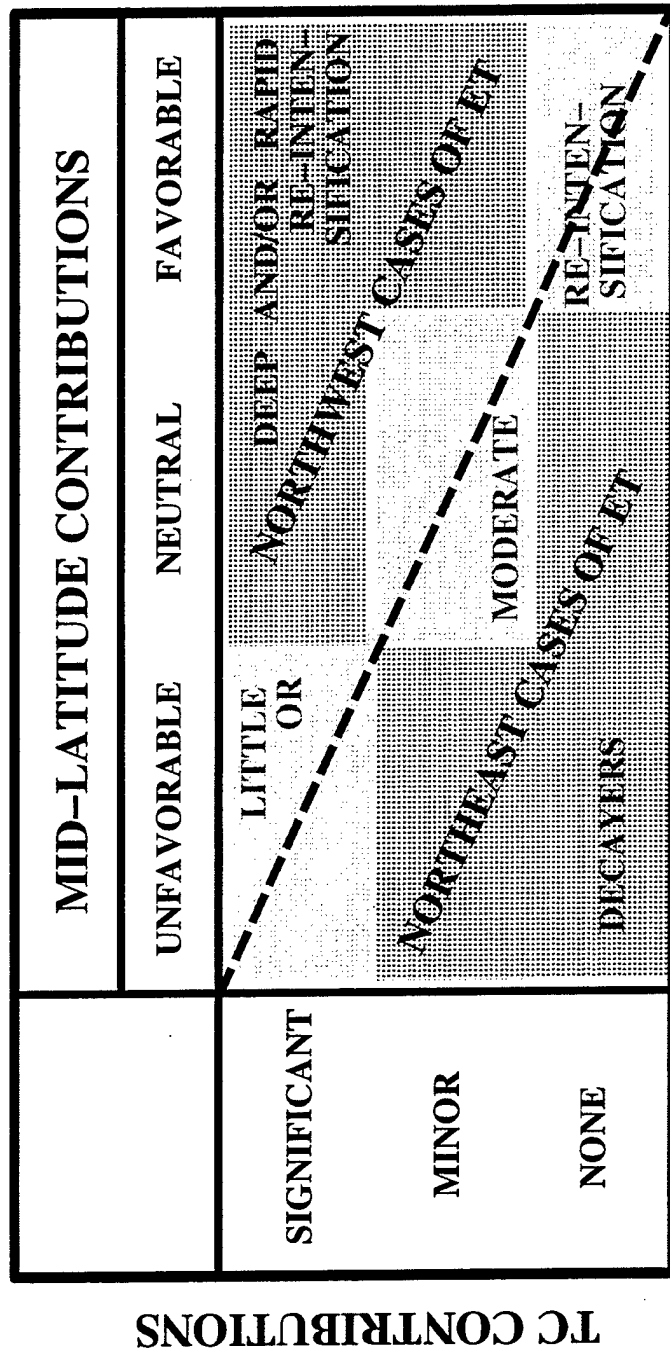
This hypothesis and conceptual model (Fig. V-7) imply that the SLP at the end of the re-intensification stage depends on whether or not a poleward-moving TC arrives in the mid-latitude circulation pattern in phase with the optimal critical region, and thus the outcome of the re-intensification stage will be altered if the TC is displaced from its initial position so that its phasing with the critical region is also changed. This aspect of the hypothesis will be tested in a mesoscale numerical model by first generating a control forecast, and then generating other forecasts after displacing the initial TC position such that the phasing of the TC with the critical region is altered. The objective is to achieve more (less) deepening relative to the control when the initial TC produces more (less) optimal phasing between the TC and the critical region. Specifically, simulations in which the TC achieved deep re-intensification will be displaced so that they resemble Scenario Two in Fig. V-7b and do not phase with the critical region, and thus will not deepen as much. Cases with only moderate deepening due to less than optimal phasing will be shifted in such a way as to better phase with the critical region, and thus deepen more. Finally, decayers (described in Chap. III) will be displaced so that they more resemble Scenario One in Fig. V-7a in that they phase better with the critical region and achieve at least moderate re-intensification. The ability to shift the TC position in such a way to

change the phasing with the mid-latitude critical region and thus change the re-intensification will be considered to be a validation of the superposition hypothesis.

2. Contributions of the Mid-Latitude Circulation Pattern and the TC during the Re-Intensification Stage

The mid-latitude circulation contribution to the re-intensification stage of ET has been defined above in terms of the characteristics of the critical region in the mid-latitude circulation. Thus, it is hypothesized that even if the TC was not present, extratropical cyclogenesis would occur strongly, moderately, or not at all depending on the existence and character of the critical region. This hypothesis will be tested in a numerical model by removing the TC vortex from the initial conditions of the simulation. It is expected that strong (weak) extratropical cyclogenesis will occur even without the TC in cases where an optimal (less than optimal) critical region is present. If no critical region is present, then only weak extratropical cyclogenesis will occur in the absence of the TC. A *favorable* mid-latitude contribution to the re-intensification stage (Fig. V-8) will be defined when a critical region is forecast in the numerical simulation in which the TC has been removed (hereafter "no-TC" simulation) so that moderate or strong extratropical cyclogenesis occurs within it. The mid-latitude contribution to the re-intensification stage will be described as *neutral* if no critical region is forecast, and only weak extratropical cyclogenesis occurs in the no-TC simulation. If a ridge is built at or just downstream of the location where the TC was in the control simulation, the mid-latitude contribution to the re-intensification stage will be described as *unfavorable* (Fig. V-8).

RE-INTENSIFICATION STAGE OF ET IN THE WESTERN NORTH PACIFIC



MID-LATITUDE CONTRIBUTION CHARACTERIZATION

FAVORABLE: In "no-TC" simulation, a critical region is forecast, and significant extratropical cyclogenesis (ETC) occurs in absence of transitioning TC.

NEUTRAL: In "no-TC" simulation, no critical region is forecast, but weak ETC is predicted.

UNFAVORABLE: In "no-TC" simulation, anticyclogenesis occurs in transitioning TC domain.

TC CONTRIBUTION CHARACTERIZATION

SIGNIFICANT: TC contributes proper phasing with critical region AND interacts optimally with lower baroclinity to maximize baroclinic conversion.

MINOR: TC does not phase with critical region, and thus lacks optimal upper-tropospheric support for ETC, and TC does interact optimally with lower-tropospheric baroclinity.

NONE: TC does not phase with critical region and interacts minimally or not at all with upper PV and lower-tropospheric baroclinity.

Fig. V-8. Characterizations of the mid-latitude circulation pattern and TC contributions to the re-intensification stage of ET depicted as a matrix, where the combinations of these contributions produce one of three different outcomes: (i) Deep and/or rapid re-intensification (upper right; SLP at the end of ET < 980 mb); (ii) little to moderate re-intensification (along diagonal; SLP at the end of ET > 980 mb); and (iii) decay of the TC without completing ET (lower left). Northwest and northeast cases of ET (Harr et al. 2000) are separated by a dashed line.

A simple characterization of the TC remnants contribution to the re-intensification stage of ET in Fig. V-8 will first be in its phasing with the mid-latitude circulation critical region. An optimal phasing that results in coupling of the transformed TC with the upper-tropospheric PV anomaly in the critical region and optimal interaction with lower-tropospheric baroclinity will be defined as a *significant* contribution by the TC to the re-intensification stage of ET. In cases in which the TC does not phase with the critical region so that interactions between the transformed TC and the upper-tropospheric PV anomaly and lower-tropospheric baroclinity are less than optimal, the TC contribution will be defined as *minor*. If the transforming TC interacts minimally, or not at all with the upper-tropospheric PV anomaly and the lower-tropospheric baroclinity within the critical region, the TC contribution will be described as *none*.

3. Combinations of Mid-Latitude and TC Contributions and Their Impact on the Outcome of the Re-Intensification Stage

In Fig. V-8, the contributions of the mid-latitude circulation and by the TC to the outcome of the re-intensification stage of ET are depicted in a matrix. Based on the definitions above, a *favorable* mid-latitude contribution in combination with a *significant* TC contribution will support deep extratropical cyclogenesis ($SLP < 980$ mb) during the re-intensification stage of ET. The combinations of a *favorable* mid-latitude contribution with a *minor* TC contribution, or a *neutral* mid-latitude contribution with a *significant* TC contribution, will also produce deep re-intensification. In cases of an *unfavorable* mid-latitude contribution, little to moderate intensification ($SLP > 980$ mb at the end of ET) may still be possible in the event of a *significant* TC contribution. If the mid-latitude

contribution is *favorable*, little to moderate re-intensification should also be possible even if the TC contribution is classified as *none*. Given a *neutral* mid-latitude contribution, little to moderate re-intensification (decay) will occur if the TC contribution is *minor* (*none*). Based on the climatology in Chap. IV, the three combinations of mid-latitude and TC contributions that are above (below) the dashed line in Fig. V-8 will tend to be the northwest (northeast) ET cases as defined by Harr et al. (2000).^c The three combinations along the diagonal line may be either a northwest or northeast case.

C. METHOD

1. Experimental Framework

Nine of the ET cases that occurred between 1997-99 in the western North Pacific were studied in detail using NOGAPS 1° lat./long. analysis fields to initialize Coupled Ocean/Atmosphere Mesoscale Prediction System (COAMPS) forecasts of the re-intensification stage of ET. The characteristics, specifications, and other details concerning COAMPS are described by Hodur (1997). The COAMPS model has an Arakawa "C" grid staggering of mass and momentum variables, and includes high resolution topographic databases over land. A sophisticated boundary layer model is included to address the air-sea fluxes. An ocean prediction model is not used in this study. Explicit moist physics are used for grid-scale saturation, and the Kain-Fritsch scheme is used for sub-grid-scale convection. Forty vertical levels and two nested grids are used in this study. The outer mesh has a 90 km horizontal grid size, and the inner nested grid size is 30 km (Fig. V-9), with two-way interaction between the grids. The inner grid domain is

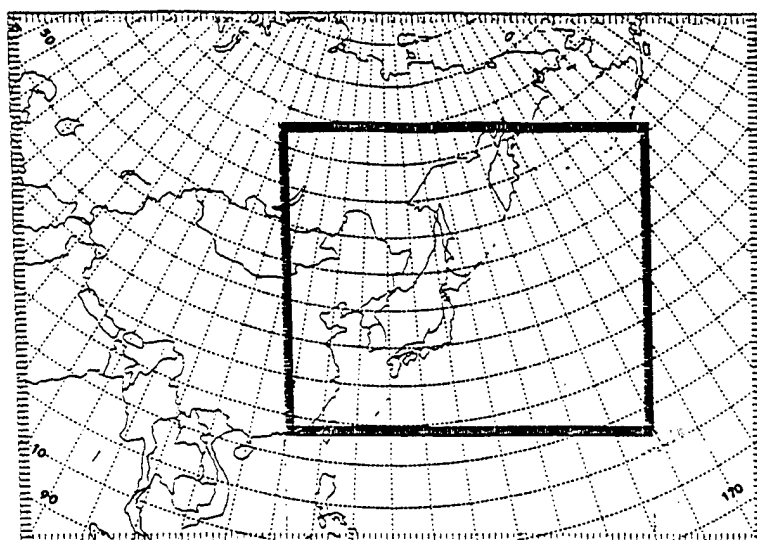


Fig. V-9. Outer- and inner-grids of COAMPS domain with 90 km and 30 km grid intervals respectively.

approximately 5490 km by 4590 km so that the entire track of any ET case is contained within the 30 km grid.

Based on the hypotheses discussed in Chap. V-B, several COAMPS forecasts will be completed for each case. The first is the control forecast, in which the NOGAPS analysis at Step 2 of the transformation stage of ET will be used to initialize a COAMPS forecast of the re-intensification stage that concludes at the end of ET. As described in Chap. V-B and Fig. V-8, a no-TC COAMPS simulation after removal of the TC vortex from the initial NOGAPS analysis will be used to characterize the mid-latitude circulation contribution to the extratropical cyclogenesis in the absence of the TC. The control forecast will also be the basis for judging whether or not subsequent COAMPS simulations of the re-intensification stage produce more (less) deepening as a result of displacing the initial position of the TC vortex to produce a more (less) favorable phasing with the critical region identified in the mid-latitude circulation pattern. That is, the TC

will be shifted in a manner that preserves the basic TC track as in the control forecast, but improves (delays or prevents) its coupling with the known critical region so that a deeper (higher) SLP is predicted compared to the control forecast.

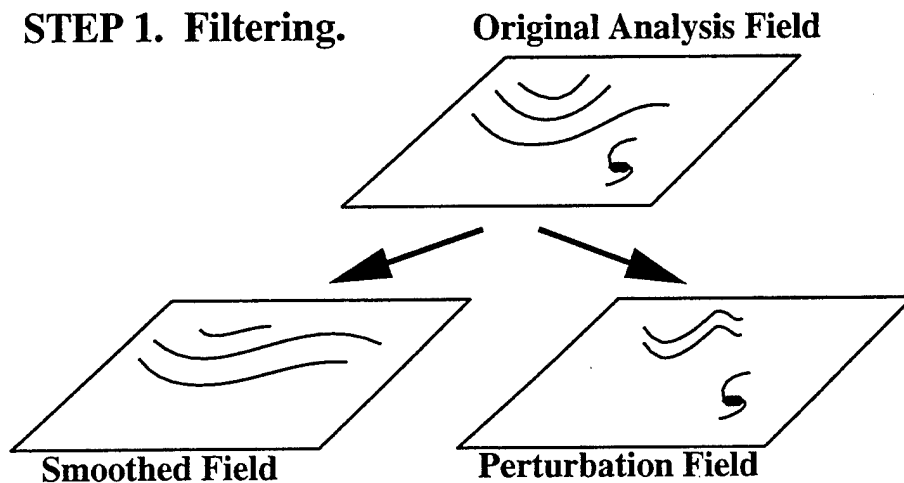
2. Vortex Removal and Displacement

To remove the TC vortex from the NOGAPS analysis field, a technique developed by Kurihara et al. (1995) for use with the Geophysical Fluid Dynamics Laboratory (GFDL) Hurricane Prediction model will be employed with modifications engineered by Prof. Patrick Harr. As depicted by Step 1 of the flow chart in Fig. V-10, this technique first uses a low-pass filter to separate the 850-mb wind analysis field into a basic (filtered) field and a perturbation field that is the difference between the original and filtered fields. In this study, the strongest filtering option was used so that perturbations whose wavelength < 900 n mi would be completely removed from the basic field. In Step 2, the 850-mb perturbation wind field is searched outward along 24 radial spokes that start from the gridpoint nearest the TC center for radial and tangential wind components that decrease with radial distance from the local maxima near the TC center. The outer limit of the TC wind field domain along a specified radial spoke is defined at that grid point at which the tangential wind achieves a local minimum, and/or the radial gradient of tangential wind is less than $4 \times 10^{-6} \text{ s}^{-1}$.

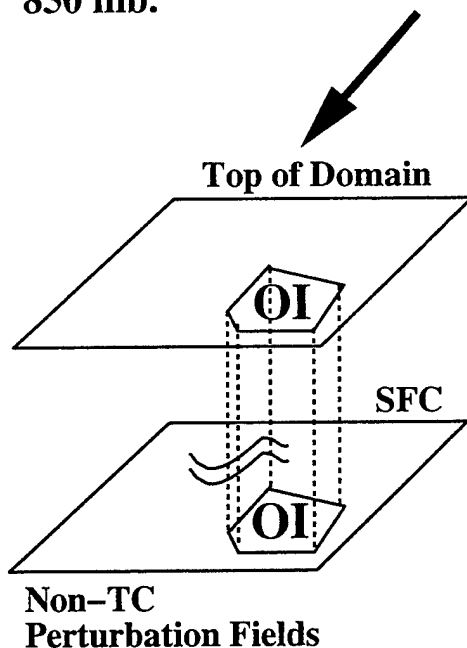
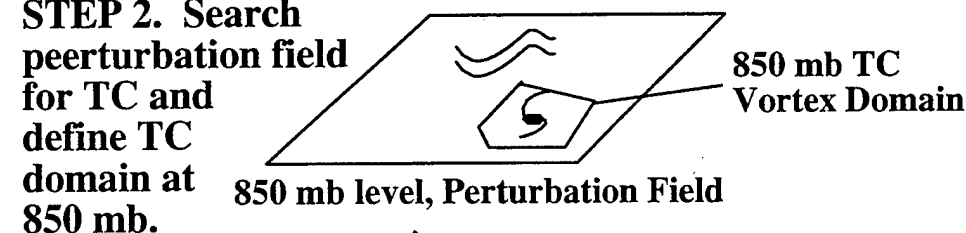
After this TC domain is identified along the 24 spokes in the 850-mb perturbation wind field, Step 3 of the procedure (Fig. V-10) involves removal of the TC vortex from

REMOVING AND RELOCATING THE TC VORTEX

STEP 1. Filtering.



STEP 2. Search perturbation field for TC and define TC domain at 850 mb.



STEP 3. Create the Non-TC perturbation field. All physical parameters (u, v, w, p, T , and moisture) are set to zero in the TC domain cylinder at all levels. A smoothly-varying field is created by using OI with respect to the Perturbation Field.

Fig. V-10. Five steps in the procedure to remove and/or relocate the TC from the initial NOGAPS analysis field before ingest into the COAMPS model.

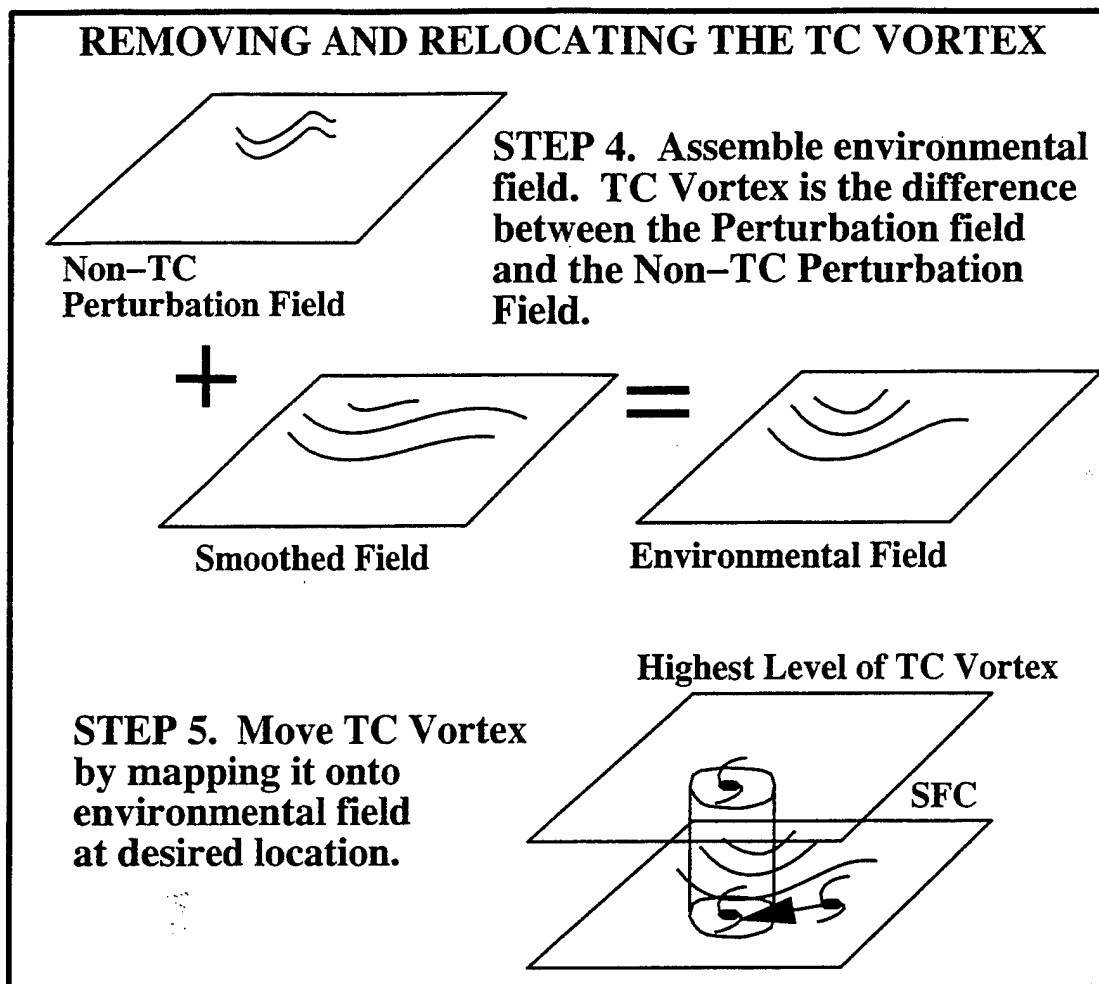


Fig. V-10 (continued).

the perturbation field by setting equal to zero all winds (also height, moisture, and temperature) at gridpoints within this domain at each vertical level. Replacement values for these variables within the TC domain are then obtained through an optimum interpolation while holding fixed the boundary values along the periphery of the TC domain. The result is a smooth field that blends with the fixed boundary values around the TC domain, and thus with the perturbation field values outside the TC domain that remain unchanged. In Step 4 (Fig. V-10), the "non-TC perturbation" field is added to the basic (filtered original field) field to define an "environment field" free of the TC vortex.

Whereas the gridpoint values outside the TC domain will be unchanged, the original values within the TC domain are now decomposed into an environment field and (by subtraction) the TC vortex as represented in the NOGAPS analysis. This decomposition is an important step because that environment field (without the TC) is used to initialize the no-TC forecast to determine whether an extratropical cyclone would have developed, which is the basis for defining the mid-latitude circulation pattern contribution (Fig. V-8) as described above.

The TC vortex (difference between the original perturbation field and the non-TC perturbation field) is then specified by the wind, height, temperature, and moisture values at the gridpoints within the TC domain. Because the TC vortex is defined as a perturbation relative to the environment, it can be moved (Step 5 in Fig. V-10) by changing the gridpoint indices of the boundaries of the TC domain, and then adding this vortex perturbation to a similarly defined environment field within the same domain centered on the desired location. That is, the existing environmental field gridpoint values within this shifted domain are set to zero, an optimum interpolation is done to match the boundary values, and the values of the TC vortex field gridpoints are substituted in the place of whatever analyzed values were within the shifted domain. Since the perturbed winds, heights, moisture, and temperature values are shifted, no re-balancing is required, and the small imbalances are rapidly dispersed as gravity waves.

The example of TY David at 0000 UTC 18 September 1997 (Fig. V-11) is presented as representative of the NOGAPS 1° lat./long. resolution analysis fields used to initialize COAMPS simulations after Steps 1 through 4 of the procedure depicted in Fig.

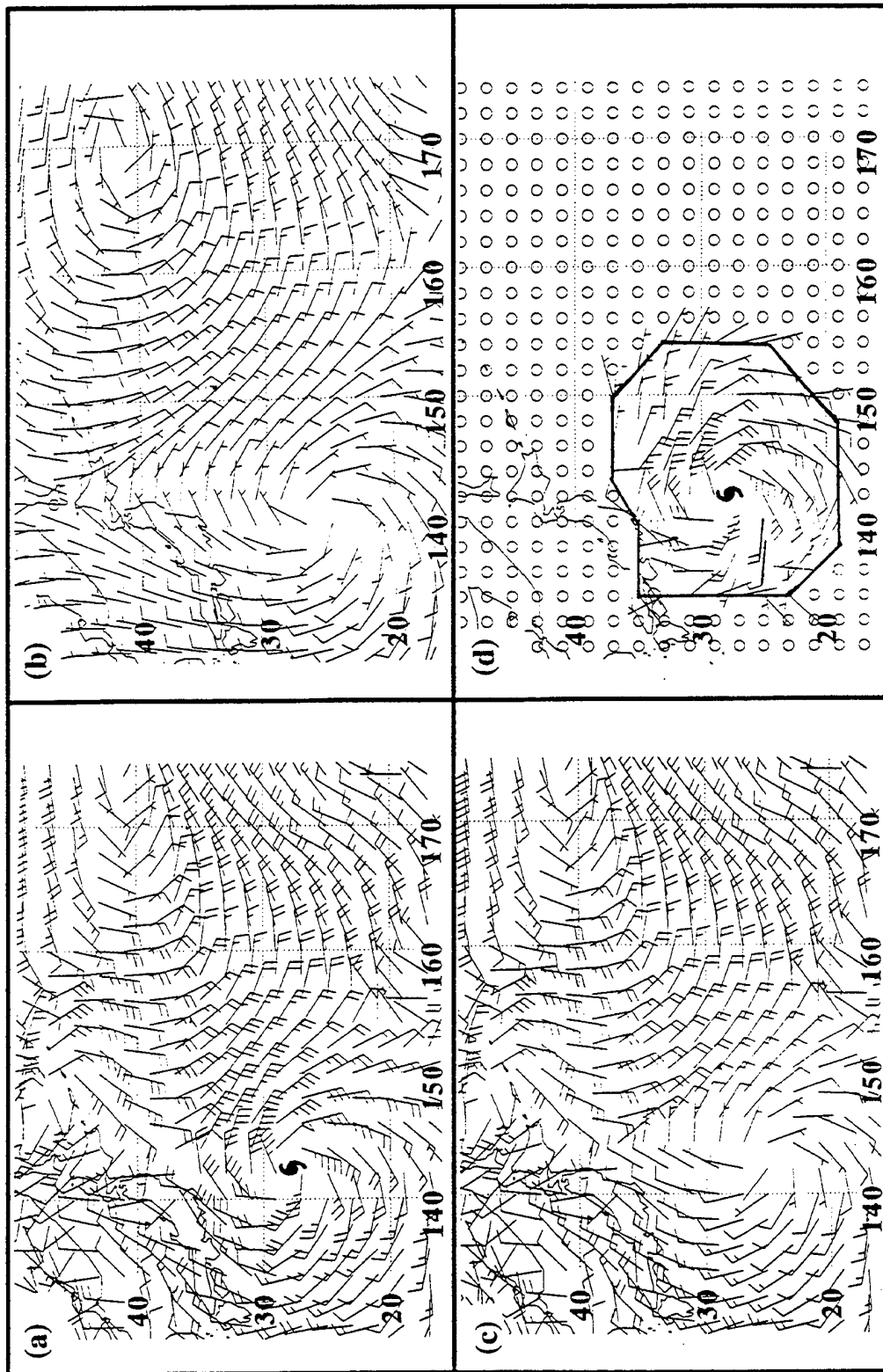


Fig. V-11. Analyses of 850-mb winds (full barb = 10 kt) in the case of TY David at 0000 UTC 18 September 1997 depicting (a) NOGAPS analysis field, (b) basic wind field after filtering using the procedure described in Step 1 of Fig. V-10, (c) environment field that remains after Step 4 of Fig. V-10, and (d) TY David vortex wind field.

V-10. The most obvious difference between the 850-mb analysis field (Fig. V-11a) and the basic (Fig. V-11b) and environment (Fig. V-11c) fields is the absence of TY David. After removal of TY David, a cyclonic circulation remains between the subtropical ridge over the western North Pacific and a high over Asia. Notice that the weak cyclone near 45° N, 150° E in the 850-mb wind analysis field (Fig. V-11a) is also removed from the basic field by the filtering (Fig. V-11b), but is not removed in the environment field (Fig. V-11c) that is used to initialize the “no-TC” run because it lies outside of the TC domain (Fig. V-11d). The subtropical ridge wind speeds are also damped in the basic field (Fig. V-11b), but are identical to the initial analysis in the environment field outside of the TC domain. The TY David 850-mb wind field (Fig. V-11d) is defined within the irregular TC domain and is asymmetric. Examples of the “displaced-TC” fields produced in Step 5 of Fig. V-9 will be discussed later in this chapter.

3. Perturbed Fields in the no-TC and “displaced-TC” Simulations

Recall that the initial no-TC and “displaced-TC” fields outside of the TC domain are unchanged from the original fields. The question is how the removal or shifting of the TC would propagate into, or otherwise change, the adjacent fields early in the forecast. If the vortex removal technique is done properly, the only significant changes from the control forecast should be in the vicinity of the transforming storm, without significant gravity waves that modify the environment. In a forecast of STY Bart initialized at 0000 UTC 24 September 1999, the initial (Fig. V-12a) and 90-minute forecast (Fig. V-12b) 500-mb isoheight control minus no-TC difference fields have large values near the location of the transforming storm. However, the mid-latitude circulation and the subtropical ridge

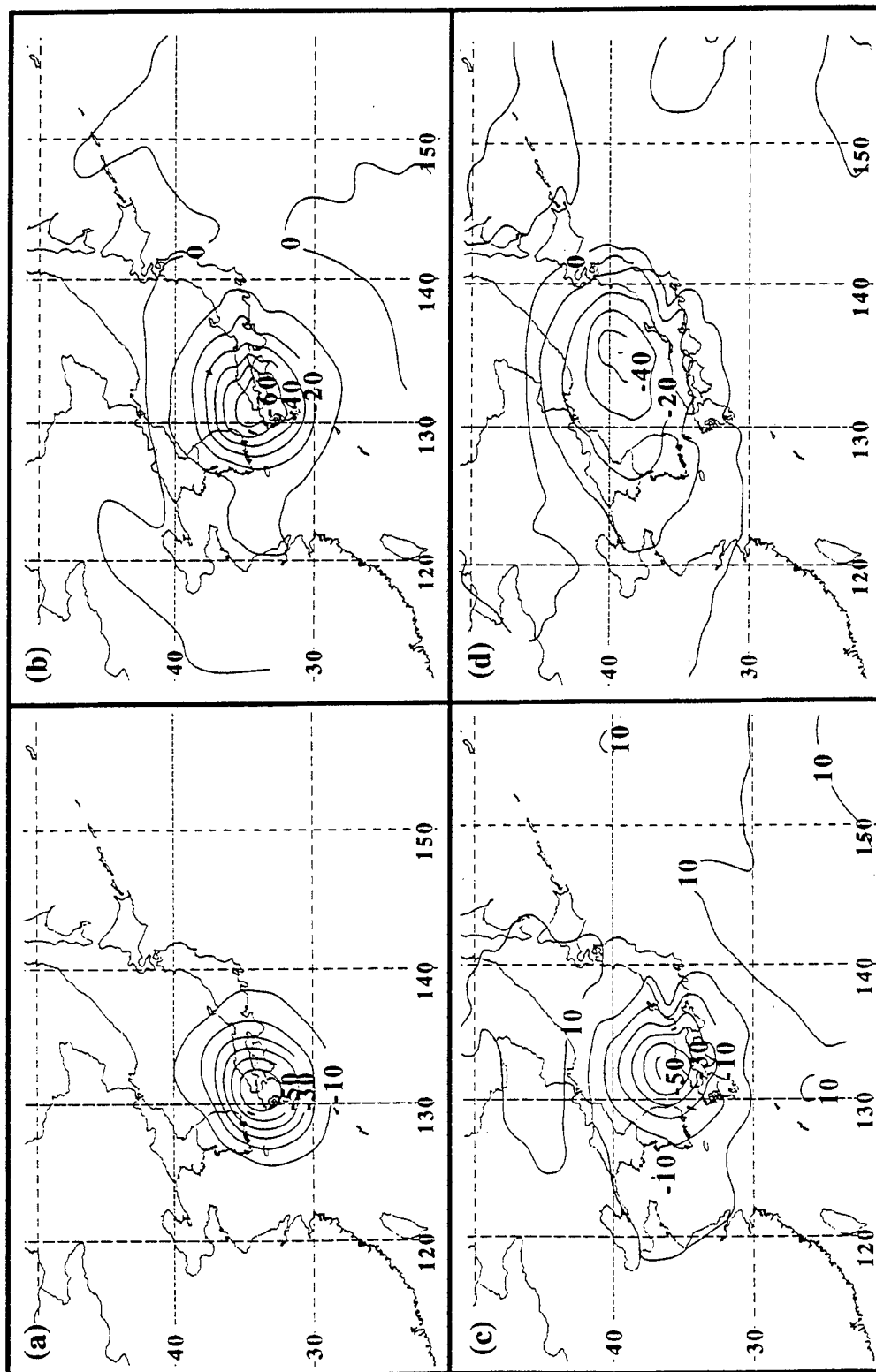


Fig. V-12. COAMPS (a) initial, (b) 90-minute forecast, (c) 6-h forecast, and (d) 12-h forecast of the difference between the control forecast and "no-TC" simulation 500-mb isoheights (10 m interval) in the case of STY Bart initialized at 0000 UTC 24 September 1999.

are nearly the same away from the storm, and only small amplitude gravity waves are emanating from the TC region.

Six hours into the control and no-TC forecasts (Fig. V-12c), the significant height differences are again centered on the transforming storm, although a large area of values exceeding 10 m is found southeast of the location of the transforming storm. These 500-mb height perturbations southeast of the TC in the control forecast are consistent with the Rossby wave dispersion (Carr and Elsberry 1994), in which a dispersive TC circulation produces ridging to the rear and right of its track. Another area of ridging northeast of the storm is consistent with the physical processes described in Step 2 of the transformation stage (recall Fig. III-26). The concave contours near 36° N, 138° E (Fig. V-12c) provide evidence of small amplitude gravity waves. After 12 h (Fig. V-12d), the differences between the COAMPS control forecast and no-TC simulation outside of the region of the removed TC vortex are less than about 10 m. Similar small differences are found in the wind, temperature, and moisture fields (not shown) away from the immediate vicinity of the TC domain. Thus, the vortex removal technique did not generate significant gravity waves in the no-TC forecasts.

In a similar "displaced-TC" simulation, STY Bart was displaced two gridpoints equatorward and two grid points to the west (approximately 150 n mi) in the NOGAPS 1° lat./long. analysis. As expected, a dipole pattern (Fig. V-13a) is found with height decreases in the new TC location and rises in the region of the original TC position. These height decreases are reduced in magnitude and areal extent 6 h later (Fig. V-13b). Although the height rises have a larger maximum, their areal extent has decreased. Small

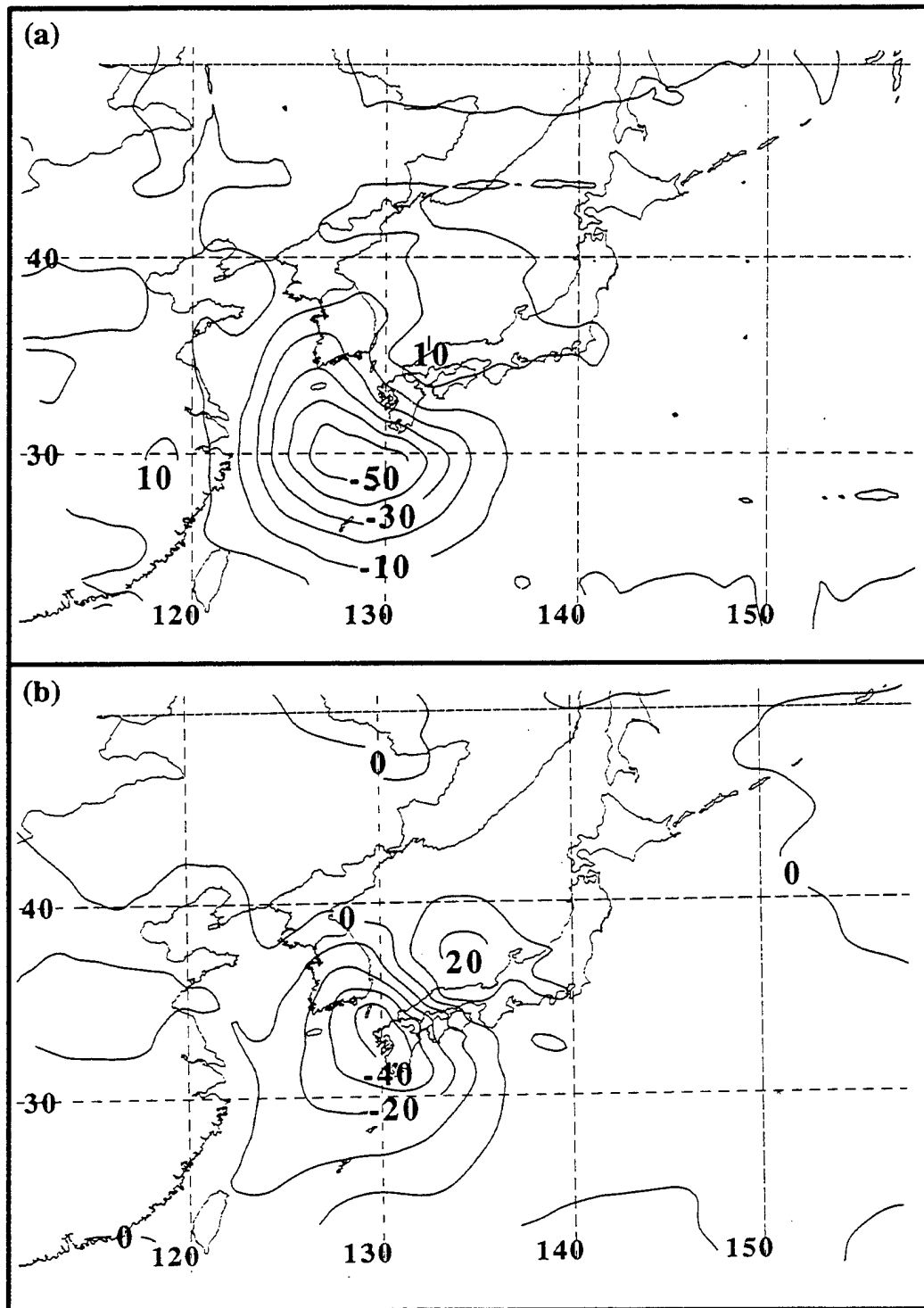


Fig. V-13. As in Fig. V-12, except for the (a) initial and (b) 6-h forecast of the 500-mb isoheight difference between the control forecast and "displaced-TC" simulation in which STY Bart has been moved two gridpoints equatorward and two grid points westward.

ripples in the height contours over and downstream of Japan are evidence of small amplitude gravity waves that arise since the flow across the topography has been changed due to the TC being displaced. Outside of the TC domain, the differences between the COAMPS control forecast and "displaced-TC" simulation after six hours are less than about 10 m. As in the case of the no-TC simulations, similar small differences are found in the wind, temperature, and moisture fields (not shown) away from the immediate vicinity of the TC domain. Therefore, the vortex movement technique also did not generate significant gravity waves propagating away from the modified region in the model.

D. CHARACTERIZATION OF THE MID-LATITUDE CONTRIBUTION TO THE RE-INTENSIFICATION STAGE: THE CONTROL FORECASTS AND NO-TC SIMULATIONS

Nine COAMPS control forecasts that included three with deep re-intensification, four with little or moderate re-intensification, and two with a decay of the TC without completing ET will be used to illustrate the influence of the mid-latitude circulations in the re-intensification stage by comparing them to the nine no-TC simulations. Recall the contribution (favorable, neutral, or unfavorable) of the mid-latitude circulation pattern to the re-intensification stage of ET will be characterized by the degree of mid-latitude cyclogenesis in the no-TC simulations. Specifically, the mid-latitude circulation contribution will be defined as "favorable" if cyclogenesis occurs in the mid-latitudes even in the absence of the TC. Continued existence of a weak low with no significant cyclogenesis in the mid-latitudes will be defined as "neutral," and anticyclogenesis in the mid-latitudes will be defined as "unfavorable."

1. Favorable Mid-Latitude Circulation Contributions

In the case of the no-TC simulation of STY Bart initialized at 0000 UTC 24 September 1999 (Fig. V-14a), the removal of the cyclone with a SLP = 987 mb has left a broad region of low SLP with the minimum SLP = 1006 mb near 37° N, 130° E. By 24 h in the no-TC simulation (Fig. V-14b), surface pressures have decreased to the northeast, and the surface trough is now oriented southwest to northeast with the minimum SLP = 1007 mb near 44° N, 140° E. This position is just to the north of where the remnants of STY Bart were in the control forecast, which had filled from 987 to 998 mb during the 24 h. Extratropical cyclogenesis was forecast in the 24-48 interval (Fig. V-14c) in both the control and the no-TC forecasts. In the control forecast (not shown), the transformed STY Bart remnants deepened 15 mb to 983 mb and the track turned poleward to about 50° N, 145° E. In the no-TC forecast shown, an extensive east-west trough is predicted with the minimum SLP = 1001 mb. Thus, the new cyclone moved zonally and deepened 6 mb in 24 h (Fig. V-14c). In both the control and no-TC forecasts, the cyclogenesis begins west of Hokaido Island and continues northeastward to the tip of Kamchatka. The gradient in the SLP contours at 24 h (Fig. V-14b) suggests a strong southerly flow into this region, which would provide warm advection in the lower troposphere to support cyclogenesis. Although the storm in the control forecast deepened more and had a more meridional track with a final position farther north and west than in the no-TC simulation (Fig. V-14c), it is argued that the mid-latitude circulation was already favorable for cyclogenesis.

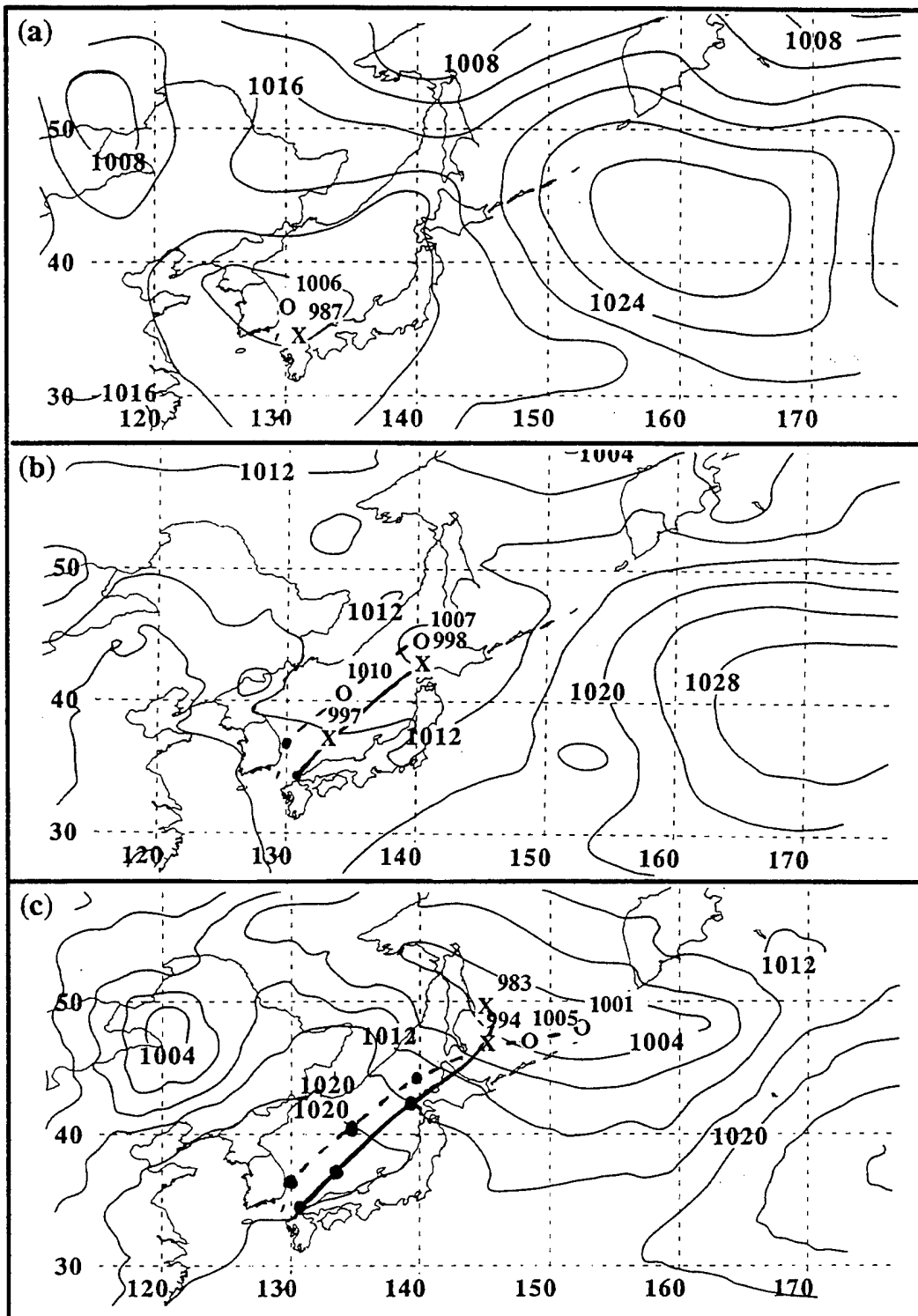
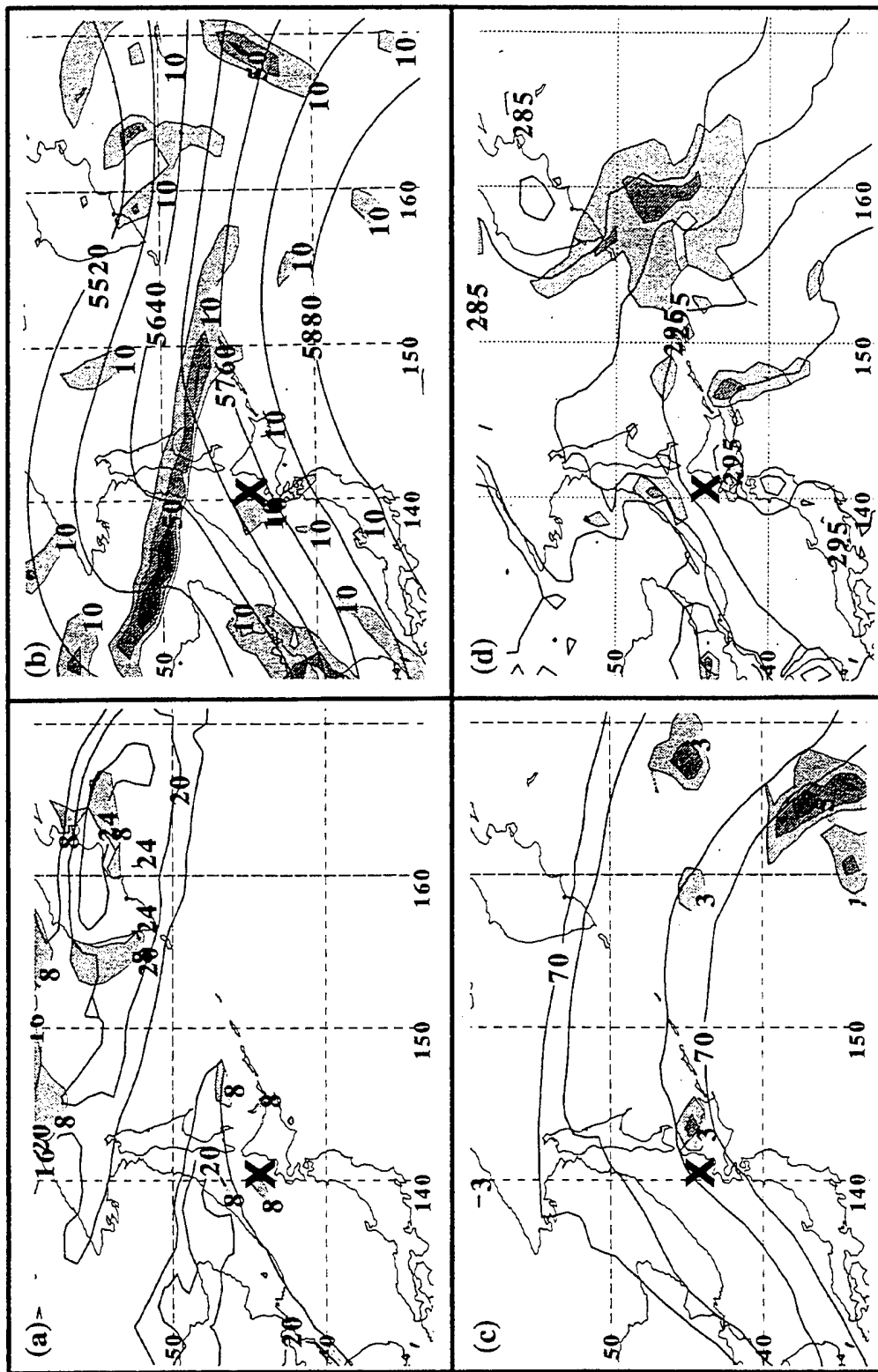


Fig. V-14. COAMPS (a) initial, (b) 24-h forecast, and (c) 48-h forecast of SLP (solid, 4 mb interval) in the STY Bart "no-TC" simulation initialized at 0000 UTC 24 September 1999. The track and initial, 12-h, 24-h, 36-h, and 48-h forecast positions of STY Bart (weak surface perturbation) in the control forecast ("no-TC" simulation) are depicted by black dots connected with a thick black (dashed) line. At each interval, the SLP of the storm in the control forecast and the perturbation in the "no-TC" simulation are also plotted.

Prior to the beginning of cyclogenesis in the STY Bart no-TC simulation, only a small lower-tropospheric PV maximum of $8 \times 10^{-7} \text{ K m}^2 \text{ s}^{-1} \text{ kg}^{-1}$ has developed near 44°N , 140° E (Fig. V-15a) where the incipient SLP center is evident in the no-TC simulation (Fig. V-14b). However, an upper-tropospheric PV maxima of 20 units is found to the northwest. A weak short-wave trough is evident at 500 mb to the northwest of the lower-tropospheric PV center, with maximum PVA $> 50 \times 10^{-10} \text{ s}^{-2}$ (Fig. V-15b) oriented east-west along 50° N . Although no well-defined jet streak is evident at this time, a > 90 kt jet stream is present (Fig. V-15c) over the incipient lower-tropospheric PV maximum. A small, weak ($3 \times 10^{-5} \text{ s}^{-1}$) divergence center is present about 4° long. east of the lower-tropospheric PV maximum. As suggested above in conjunction with the lower-tropospheric flow pattern in Fig. V-14b, warm advection of about $30 \times 10^{-5} \text{ K s}^{-1}$ (Fig. V-15d) is beginning to occur along a southwest to northeast oriented baroclinic zone in the Japan Sea. Thus, prior to the beginning of cyclogenesis at 24 h in the no-TC simulation, the stage is set for a Petterssen Type-B cyclogenesis of a low center on a baroclinic zone with approaching upper-tropospheric support. However, the conditions of 500-mb PVA, upper-tropospheric divergence, and lower-tropospheric warm advection that are the criteria for a critical region are not yet met.

Only slight differences exist between the control forecast and the no-TC simulation at 24 h. The lower-tropospheric PV maximum of $8 \times 10^{-7} \text{ K m}^2 \text{ s}^{-1} \text{ kg}^{-1}$ associated with the transformed STY Bart is in a similar location, but larger in areal extent (not shown) than the one evident in the no-TC simulation. The amplitude of the 500-mb ridge-trough couplet is somewhat larger in the control forecast (not shown), so that larger values of



500-mb PVA are near 45° N, 140° E than those depicted in the no-TC simulation (Fig. V-15b). The warm advection and gradient of isentropes between 130° E and 140° E is also larger in the control forecast (not shown).

Twelve hours later, the cyclone in the no-TC simulation has begun to intensify, deepening 2 mb as it translated east-northeast to a position near 150° E (Fig. V-14c). The lower-tropospheric PV maximum of $8 \times 10^{-7} \text{ K m}^2 \text{ s}^{-1} \text{ kg}^{-1}$ (Fig. V-16a) has increased in size in 12 h and is located east of the storm center. The upper-level PV maxima has increased by 4 units in 12 h and is found northwest of the storm center. The 500-mb ridge-trough couplet has amplified and moved 600 n mi downstream (Fig. V-16b) so that 500-mb PVA $> 50 \times 10^{-10} \text{ s}^{-2}$ is oriented northwest to southeast between 150° E and 160° E. A small closed contour of 110 kt at 200 mb (Fig. V-16c) is located near 49° N, 164° E, which suggests the presence of a weak jet streak, and a large region of divergence $> 5 \times 10^{-5} \text{ s}^{-1}$ is also found between 150° E and 160° E, and widespread warm advection with values $> 30 \times 10^{-5} \text{ K s}^{-1}$ (Fig. V-16d) is also evident in the same region. Thus, a critical region can be found in the no-TC simulation (Fig. V-16a) southwest of the tip of Kamchatka between 150° E and 160° E, and the center of this intensifying extratropical cyclone is just west of that critical region. By 48 h, this cyclone moved farther downstream (Fig. V-14c) and entered this critical region, which had also translated to the east (not shown), and achieved a SLP of 997 mb at 60 h while remaining within this critical region (not shown), which suggests the cyclone would have continued to deepen.

Recall that in the control forecast the re-intensifying storm moves more poleward from 24-48 h (Figs. V-14b and c) than the cyclone in the no-TC simulation. At 36 h in the

control forecast, STY Bart had already commenced the re-intensification stage of ET (Fig. V-17). A large, east-west oriented region of lower-tropospheric $PV > 8 \times 10^{-7} \text{ K m}^2 \text{ s}^{-1} \text{ kg}^{-1}$ (Fig. V-17a) is between 140° E and 150° E equatorward and southeast of two upper-level PV maxima > 24 units. The amplitude of the 500-mb ridge-trough couplet (Fig. V-17b) is slightly greater than the one evident in the no-TC simulation (compare the 5580 m and 5520 m contours in Figs. V-16b and V-17b). In this control forecast, a small region of $PVA > 30 \times 10^{-10} \text{ s}^{-2}$ (Fig. V-16b) is above the re-intensifying storm, with a large area of $PVA > 50 \times 10^{-10} \text{ s}^{-2}$ farther upstream than in the no-TC simulation. A well-defined jet streak is found at 200 mb (Fig. V-17c), and the 200-mb divergence maximum associated with the equatorward entrance region (near 48° N , 152° E) is also farther upstream than the 200-mb divergence maximum in the no-TC simulation. The warm advection in both the control forecast and the no-TC simulation is nearly the same, except that maximum values $> 30 \times 10^{-5} \text{ K s}^{-1}$ (Fig. V-17d) extend farther west to nearly 150° E in the control forecast, and a smaller warm advection maxima is also located northeast of the storm near 50° N , 145° E . Therefore, the critical region found in the control forecast (Fig. V-17a) is west of the no-TC simulation critical region at 36 h (Fig. V-16a), which is consistent with the location of the re-intensifying storm that is also west of the cyclone in the no-TC simulation (Fig. V-14c).

Significant 500-mb PVA (Fig. V-17b) and 900-mb warm advection (Fig. V-17d) are predicted at 42 h in the control forecast beneath weak 200-mb divergence (not shown) above the re-intensifying storm near 46° N , 144° E . Thus, the storm in the control forecast continues to deepen and achieves a final SLP of 982 mb at the 54-h interval (not

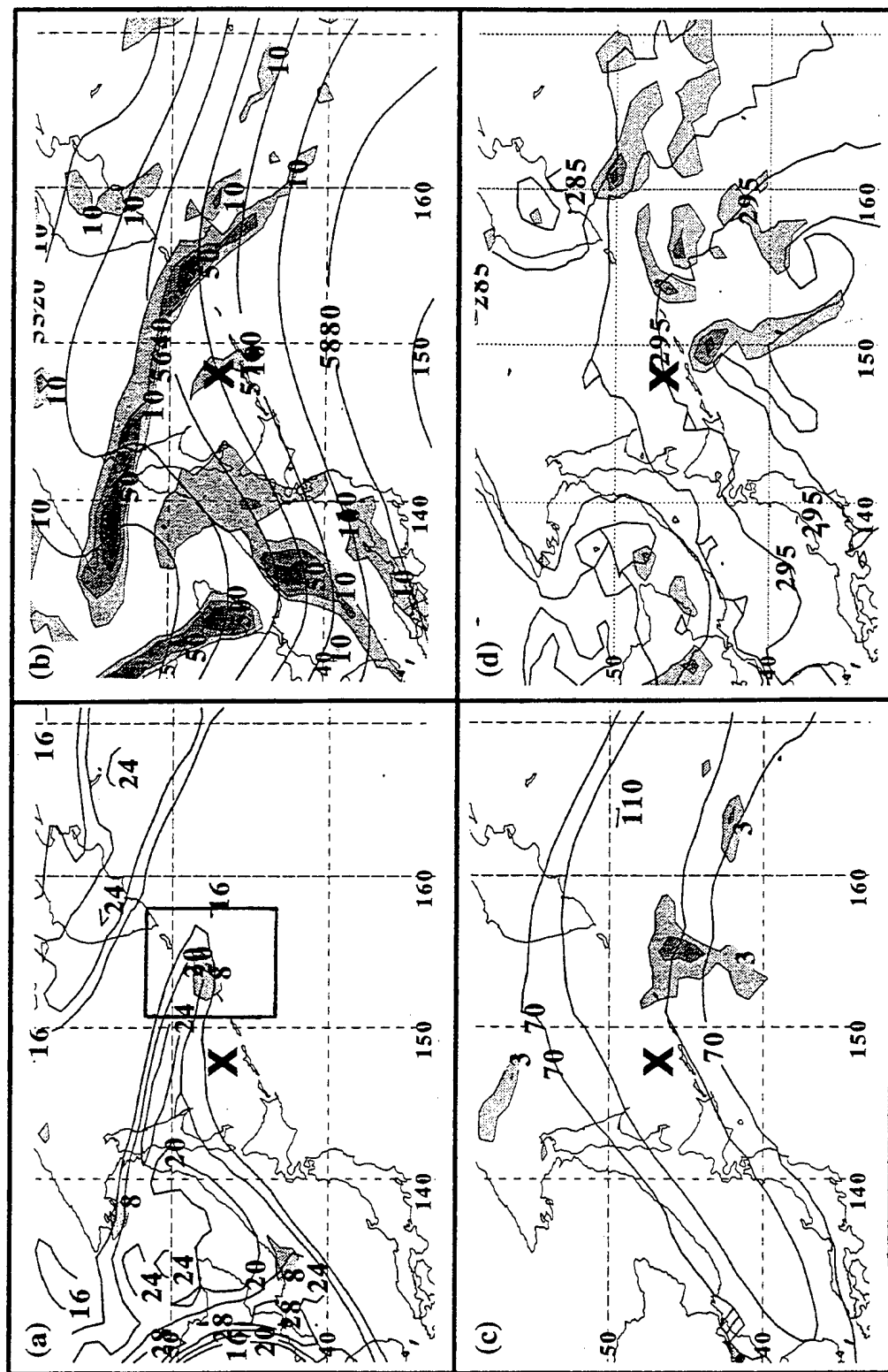


Fig. V-16. (a) Layer-averaged PV between 925 mb and 700 mb (solid contours), (b) 500-mb isotherms and PVA, (c) 200-mb isotherms and divergence, and (d) 925-mb warm advection and isentropes of potential temperature as in Fig. V-15, except for 36-h interval. The critical region is depicted by a solid box in (a), and the storm location is denoted with an "X."

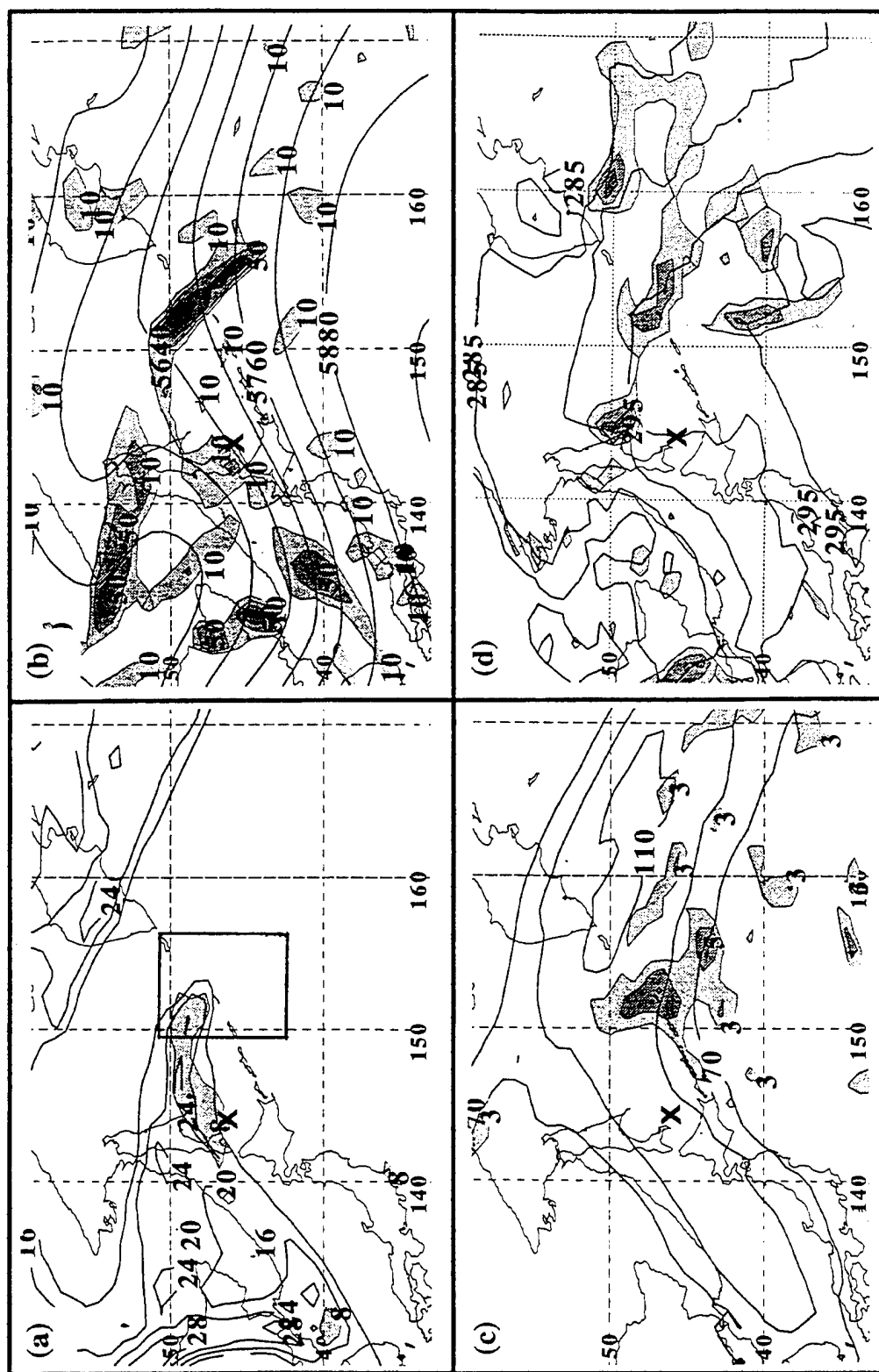


Fig. V-17. As in Fig. V-15 except for 36-h interval of STY Bart control forecast initialized at 0000 UTC 24 September 1999. The critical region is depicted by a solid box in (a), and the storm location is denoted with an "X."

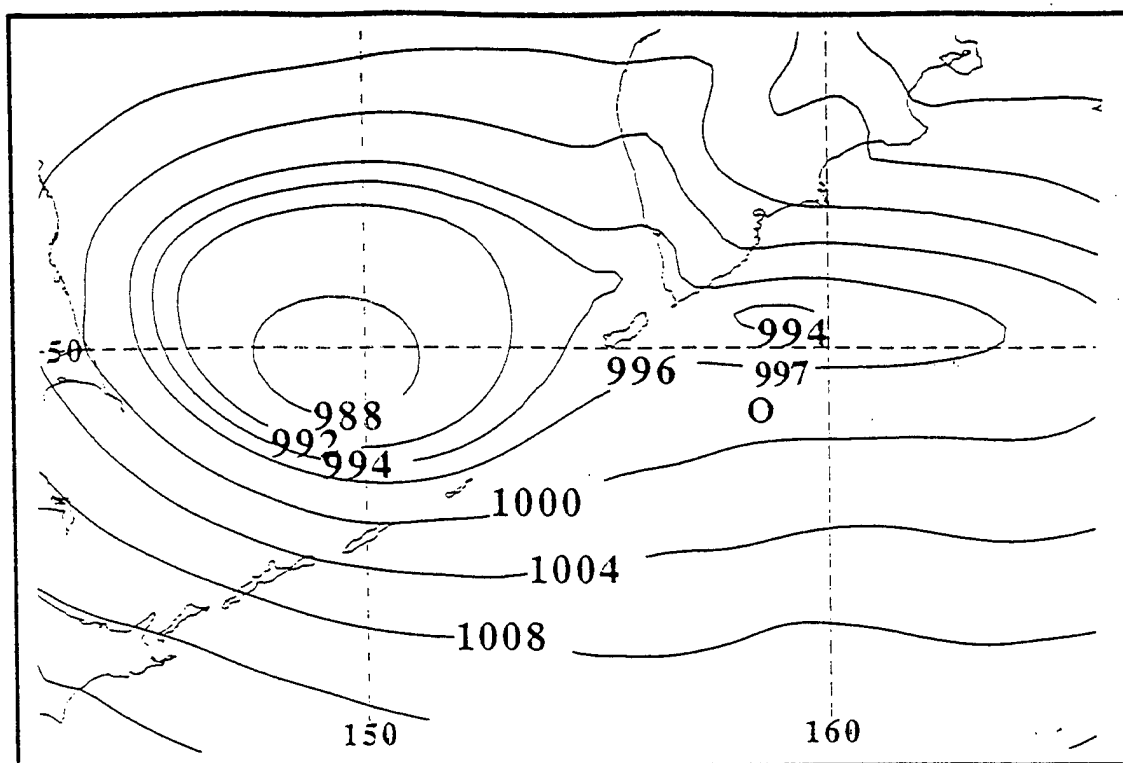


Fig. V-18. The COAMPS 60-h control forecast of SLP (solid, 4 mb interval, except for 994 mb contour) in the case of STY Bart initialized at 0000 UTC 24 September 1999. The location of the storm at 60 h in the no-TC simulation is marked "O," with intensity listed in mb.

shown), even though the critical region is downstream (not shown). At 60 h in the control forecast, this critical region initiated a separate extratropical cyclogenesis at 51° N, 159° E (Fig. V-18), which is east of the storm that completed ET (at 50° N, 149° E), and 120 n mi poleward of the location of the extratropical cyclone at 60 h in the no-TC simulation.

The fundamental differences between the no-TC simulation and the control forecast are: (i) the phasing of the transforming TC with the short-wave trough over Manchuria and the Japan Sea in the control forecast results in extratropical cyclogenesis

that produces a moderately deep extratropical cyclone near 50° N, 145° E (Fig. V-14c); (ii) the location of the critical region at 36 h in the control forecast is somewhat farther west than in the no-TC simulation (compare Fig. V-16a to V-17a), and (iii) the initiation of a separate extratropical cyclogenesis at 60 h in the control forecast (Fig. V-18), which occurs later and farther downstream than the extratropical cyclogenesis in the no-TC simulation (Figs. V-14 through 16). Thus, the extratropical cyclogenesis that occurs in the no-TC simulation is defined to be significant, and the mid-latitude contribution to the re-intensification stage is classified as "favorable." The differences, along with those that will be discussed in the comparison of the STY Bart control forecast to the "displaced-TC" simulations, will be the basis for determining the TC contribution to the re-intensification stage and will be discussed in further detail later in this Chapter.

The no-TC simulations in the cases of TY David (September 1997) and TY Stella (September 1998) also forecast significant extratropical cyclogenesis with the TC removed (Appendix B), and along with STY Bart, the mid-latitude contribution to the re-intensification stage in these cases is classified as "favorable" based on the definitions presented earlier.

2. Neutral Mid-Latitude Circulation Contributions

In the no-TC simulation of STY Ginger initialized at 1200 UTC 29 September 1997 (Fig. V-19a), the removal of the TC with a SLP = 978 mb leaves a broad region of low SLP with the minimum SLP = 1003 mb near 38° N, 161° E. By 24 h in the no-TC simulation (Fig. V-19b), the surface trough has translated east-northeast, is oriented southwest to northeast, and has filled with the minimum SLP = 1010 mb near 40° N, 170°

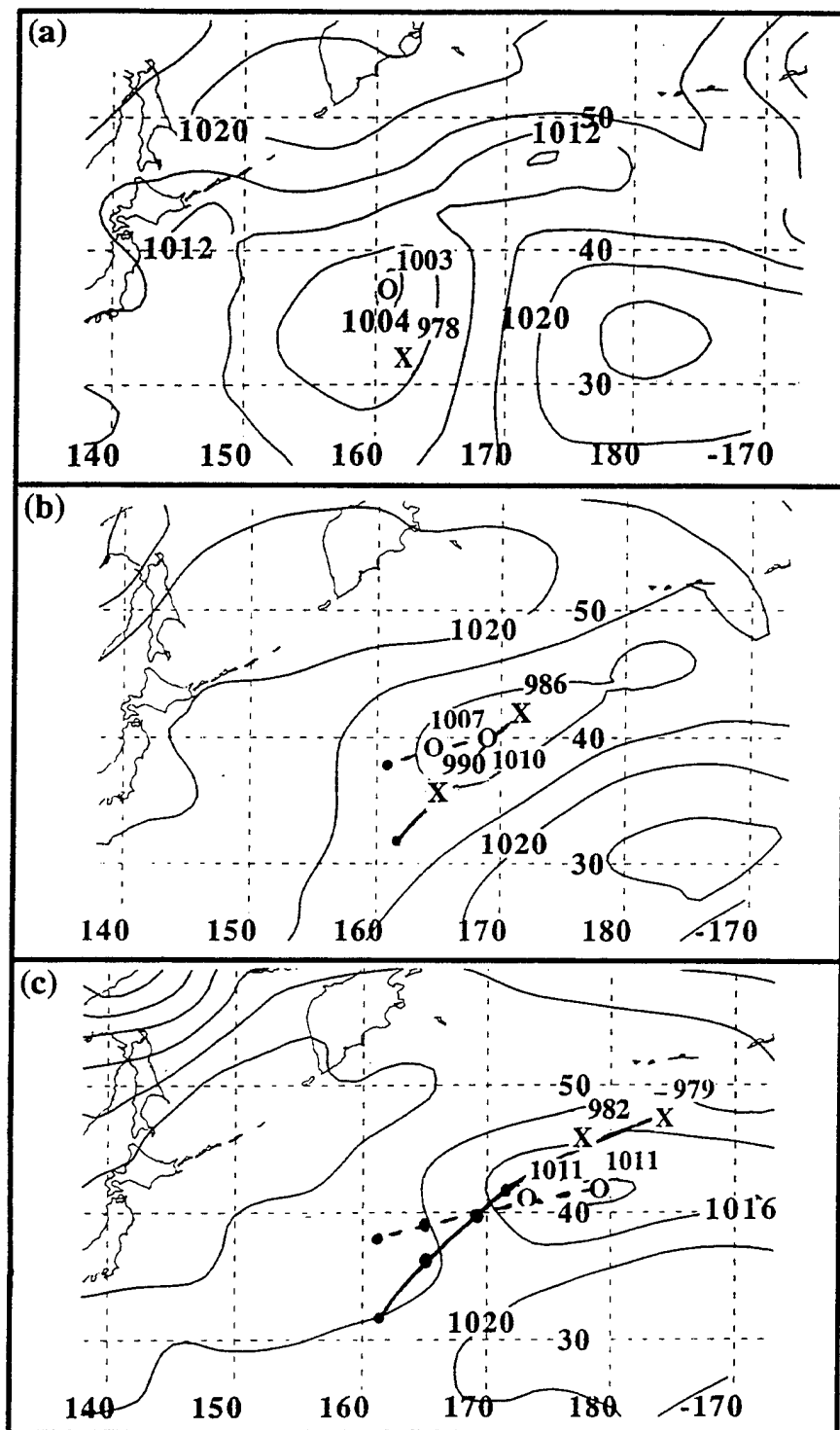


Fig. V-19. COAMPS (a) initial, (b) 24-h forecast, and (c) 48-h forecast of SLP as in Fig. V-14, except for STY Ginger initialized at 1200 UTC 29 September 1997.

E. This position is 200 n mi southeast of where the remnants of STY Ginger are in the control forecast, which has filled 12 mb during the first 12 h of the control forecast, then re-intensifies with a deepening of 4 mb to a SLP = 986 mb by 24 h. Extratropical cyclogenesis is forecast to continue in the 24-48 interval (Fig. V-19c) in the control forecast, and the transformed STY Ginger deepens 7 mb to a SLP = 979 mb and translates northeastward to 48° N, 176° W. In the no-TC forecast shown, the surface trough is predicted to fill 1 mb to 1011 mb over the 24-36 interval, then remain steady at 48 h and move east-northeastward between two adjacent ridges (Fig. V-19c) to 41° N, 179° E. By 48 h, this perturbation in the no-TC simulation does appear to become better organized with two closed SLP contours⁸. At the end of ET in the control forecast (48 h), the storm is predicted to be 32 mb deeper (Fig. V-19c) and translate northeastward. By contrast, the surface trough in the no-TC simulation only slowly deepens, with weak extratropical cyclogenesis forecast from 48-60 h (not shown).

At 36 h in the no-TC simulation (Fig. V-20a), a small area of lower-tropospheric $PV > 8 \times 10^{-7} \text{ K m}^2 \text{ s}^{-1} \text{ kg}^{-1}$ is at 41° N, 170° E, which is about 200 n mi west of the center of the surface perturbation (Fig. V-19c), and an upper-level PV maxima > 20 units is found to the northwest. A short-wave trough is also evident to the northwest (Fig. V-20b) with a small region of $PVA > 10 \times 10^{-10} \text{ s}^{-2}$ near 40° N, 168° E, which is also upstream of the surface perturbation center. No well-developed jet streak is forecast at 200 mb, although a small area of 200-mb divergence $> 3 \times 10^{-5} \text{ s}^{-1}$ (Fig. V-20c) is superposed above the 500-mb PVA. A large region of 925-mb warm advection $> 10 \times$

⁸ The 1016 mb isobar is closed, although Fig. V-19c does not extend far enough eastward to demonstrate this.

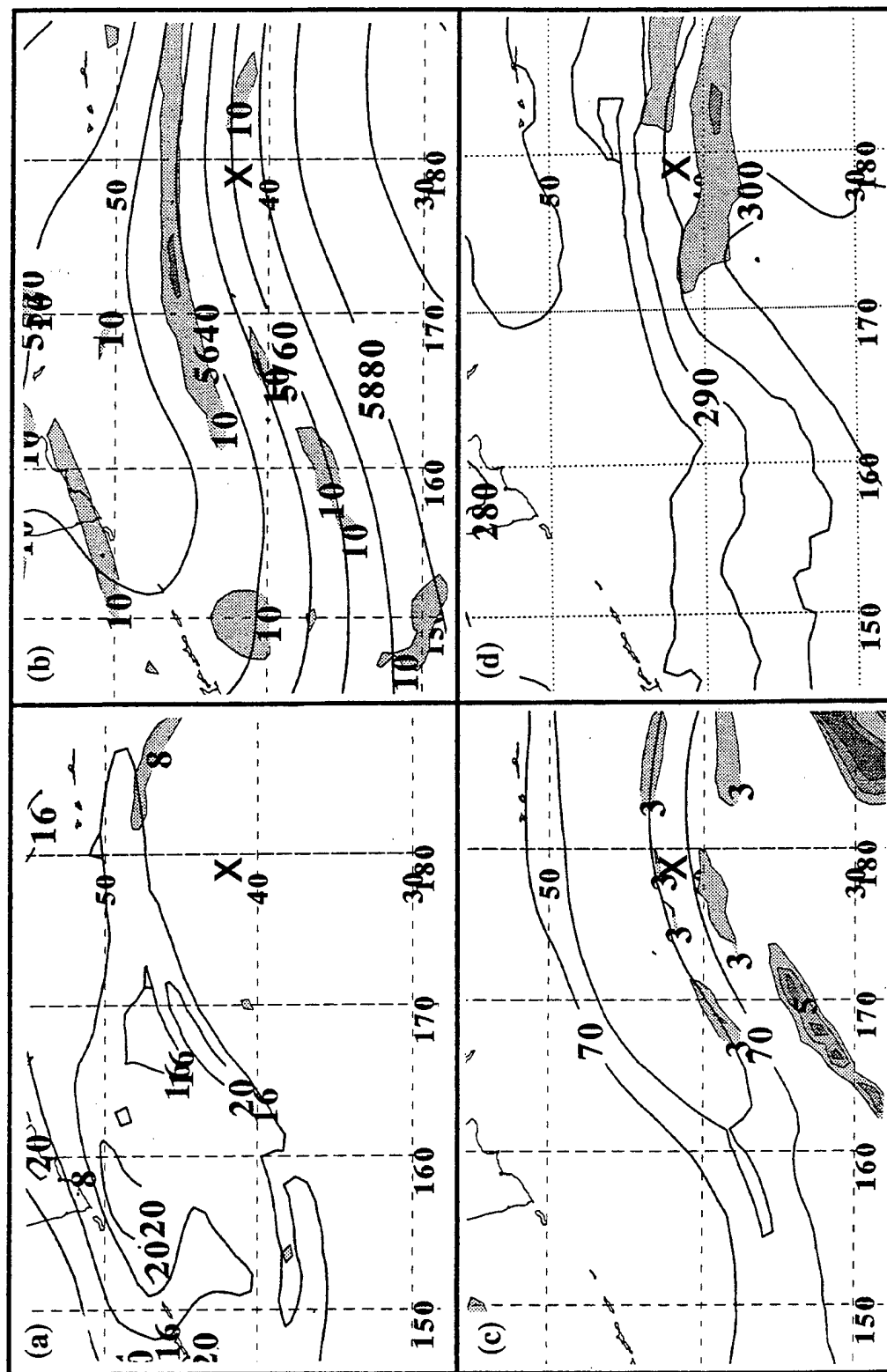


Fig. V-20. (a) Layer-averaged PV between 925 mb and 700 mb (shaded) and 500 mb to 300 mb (solid contours), (b) 500-mb isoheights and PV, (c) 200-mb isotachs and divergence, and (d) 925-mb warm advection and isentropes of potential temperature as in Fig. V-15, except for 36-h interval of STY Ginger no-TC simulation initialized at 1200 UTC 29 September 1997. The storm location is denoted with an "X."

10^{-5} K s^{-1} (Fig. V-20d) associated with the weak surface perturbation is predicted east of 40° N , 170° E . While no critical region is evident at 36 h, upper-tropospheric support for extratropical cyclogenesis is approaching lower-tropospheric baroclinity, so that Petterssen Type-B cyclogenesis is predicted by the end of the no-TC simulation (not shown).

At 36 h in the control forecast (Fig. V-21), STY Ginger has already commenced the re-intensification stage of ET (see SLP in Fig. V-19c). The deepening storm is farther poleward (notice the location of the lower-tropospheric PV maxima near 46° N , 178° W in Fig. V-21a) than the weak perturbation in the no-TC simulation (Fig. V-20a). An upper-tropospheric PV maximum > 24 units is immediately to the northwest of the re-intensifying storm, and the 5520 m 500-mb height contour has advanced equatorward (Fig. V-21b) to form a 500-mb trough northwest of the transforming storm so that 500-mb PVA $> 50 \times 10^{-10} \text{ s}^{-2}$ is superposed above the storm. Unlike the no-TC simulation, the 200-mb jet maximum downstream from the storm is predicted to be 5° lat. farther poleward (Fig. V-21c), and is split so that 200-mb divergence $> 5 \times 10^{-5} \text{ s}^{-1}$ is east of the re-intensifying storm between 180° and 170° W . The storm is forecast to penetrate farther into the lower-tropospheric baroclinity represented by the 925-mb isentropes than in the no-TC simulation (compare Fig. V-21d to Fig. V-20d). In particular, the 290 K and 295 K isentropes are predicted to move farther equatorward east of 170° E , with warm advection $> 10 \times 10^{-5} \text{ K s}^{-1}$ (Fig. V-21d) east of 180° . A critical region is thus evident (Fig. V-21a) immediately downstream from the re-intensifying storm, and the storm is forecast to deepen 3 mb in 6 h after it enters this critical region (not shown).

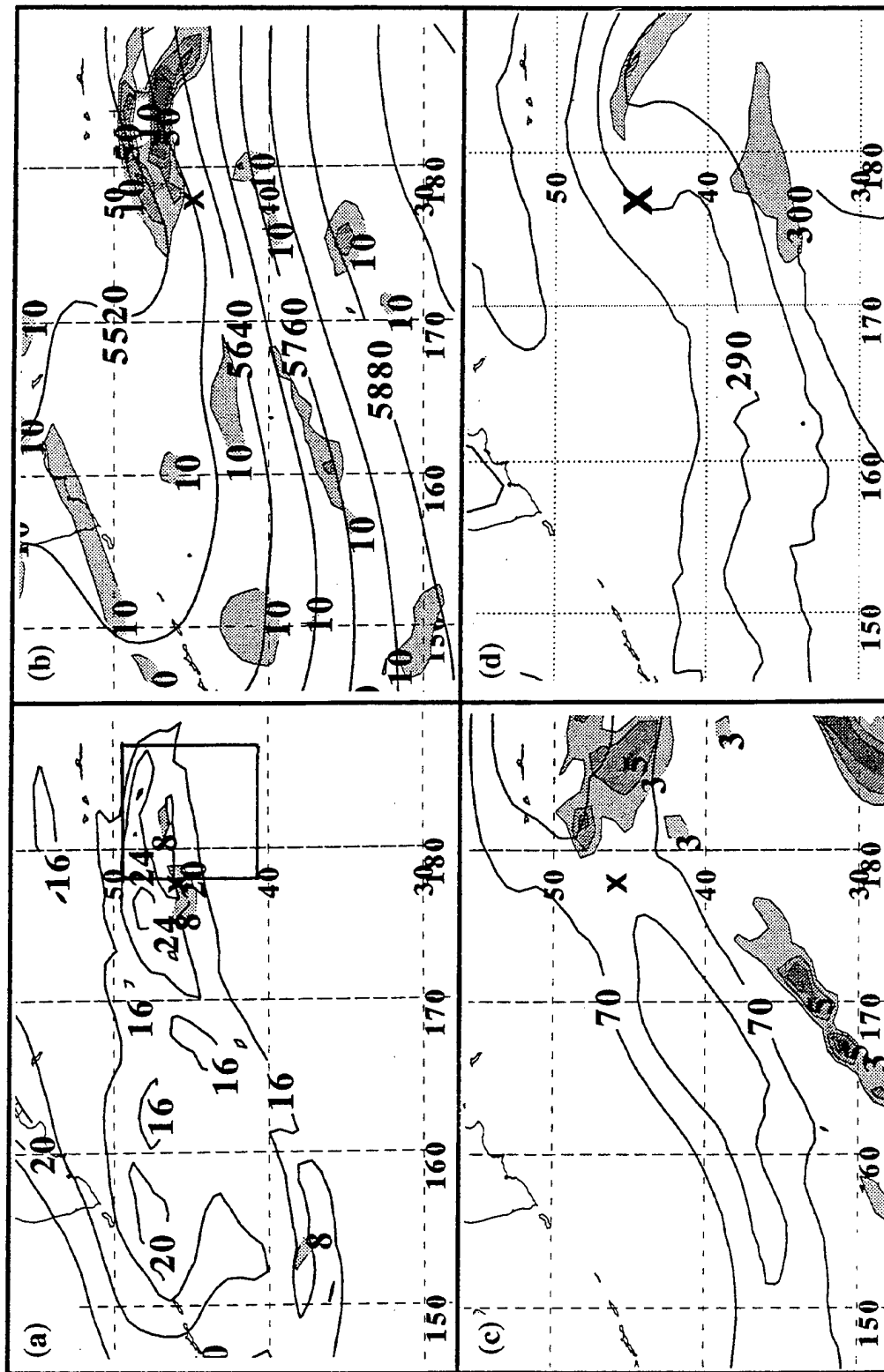


Fig. V-21. (a) Layer-averaged PV between 925 mb and 700 mb (shaded) and 500 mb to 300 mb (solid contours), (b) 500-mb isotherms and PVA, (c) 200-mb isotherms and divergence, and (d) 925-mb warm advection and isentropes of potential temperature as in Fig. V-20, except for 36-h interval of STY Ginger control forecast initialized at 1200 UTC 29 September 1997. The critical region is depicted by a solid box in (a), and the storm location is denoted with an "X".

Distinct differences between the no-TC simulation and the control forecast at the 36-h interval imply that the TC has made specific contributions to the re-intensification stage of the ET of STY Ginger. These include: (i) the phasing of the transforming TC and the mid-latitude circulation pattern in the control forecast produces a 500-mb ridge-trough couplet, 200-mb jet, and lower-tropospheric baroclinic zone that are markedly different from the no-TC simulation (compare Fig. V-20 and Fig. V-21); (ii) that these circulation interactions results in a critical region at 36 h in the control forecast, but not in the no-TC simulation; and (iii) the control forecast therefore predicts ET with deep re-intensification to 979 mb, while only weak cyclogenesis is forecast in the no-TC simulation. These differences between the control forecast and no-TC simulation strongly suggest that in the control forecast the phasing of STY Ginger with a pre-existing short-wave trough to the northwest and an associated lower-tropospheric baroclinic zone is responsible for modifying the parameters that define the critical region, with over-threshold values of 500-mb PVA, 200-mb divergence, and increased lower-tropospheric baroclinity compared to the below-threshold values in the no-TC simulation. Whereas deep extratropical cyclogenesis is predicted in the control forecast, only weak cyclogenesis in a different location is forecast in the no-TC simulation, and no critical region is predicted to exist.

Because only weak cyclogenesis in the absence of a critical region is forecast in the no-TC simulation, the mid-latitude contribution in this case to the re-intensification stage of ET is classified as "neutral" based on the definitions presented earlier. The cases of TY Rex (September 1998), TY Vicki (September 1998), and STY Oliwa (September 1997) also have a neutral mid-latitude contribution to the re-intensification stage of ET

(Appendix B), because they too exhibited only weak extratropical cyclogenesis, if any, in each of those no-TC simulations.

3. Unfavorable Mid-Latitude Circulation Contribution

In the no-TC simulation of STY Bing initialized at 0000 UTC 4 September 1997 (Fig. V-22a), the removal of the TC with a SLP = 978 mb left a weak trough at 38° N, 145° E adjacent to a subtropical ridge cell that extends eastward to at least 170° W. Over the next 24 h in the no-TC simulation (Fig. V-22b), this surface trough is forecast to fill as the subtropical ridge builds to a SLP = 1026 mb at 35° N, 179° W. At the same time in the control forecast (not shown), STY Bing is predicted to translate east-northeastward to 42° N, 161° E and fill 20 mb to 998 mb (Fig. V-22b) during its transformation. Over the next 24 h of the no-TC simulation, the subtropical ridge continued to build (Fig. V-22c) until a separate closed contour of 1024 mb is evident at 44° N, 158° E. During this period of the control forecast (not shown), the transformed remains of STY Bing are predicted to translate east-northeastward to 51° N, 178° W and hold steady at 998 mb for 12 h, then deepen 8 mb in 12 h to achieve a SLP = 990 mb at 48 h (Fig. V-22c). STY Bing is forecast to move northeastward through this 48-h period and begin its re-intensification after 24 h (Fig. V-22b) so that by the 48-h interval (Fig. V-22c) it has deepened 8 mb. As the subtropical ridge built during the first 48 h of the no-TC simulation, notice that the cyclone at 54° N, 142° E at the initial time (Fig. V-22a) is forecast to weaken in 24 h (Fig. V-22b) and continue to fill and move eastward off chart during the 24-48 h interval.

At 36 h in the STY Bing no-TC simulation, no regions of lower-tropospheric PV > $8 \times 10^{-7} \text{ K m}^2 \text{ s}^{-1} \text{ kg}^{-1}$ are predicted anywhere south of 50° N near where the control

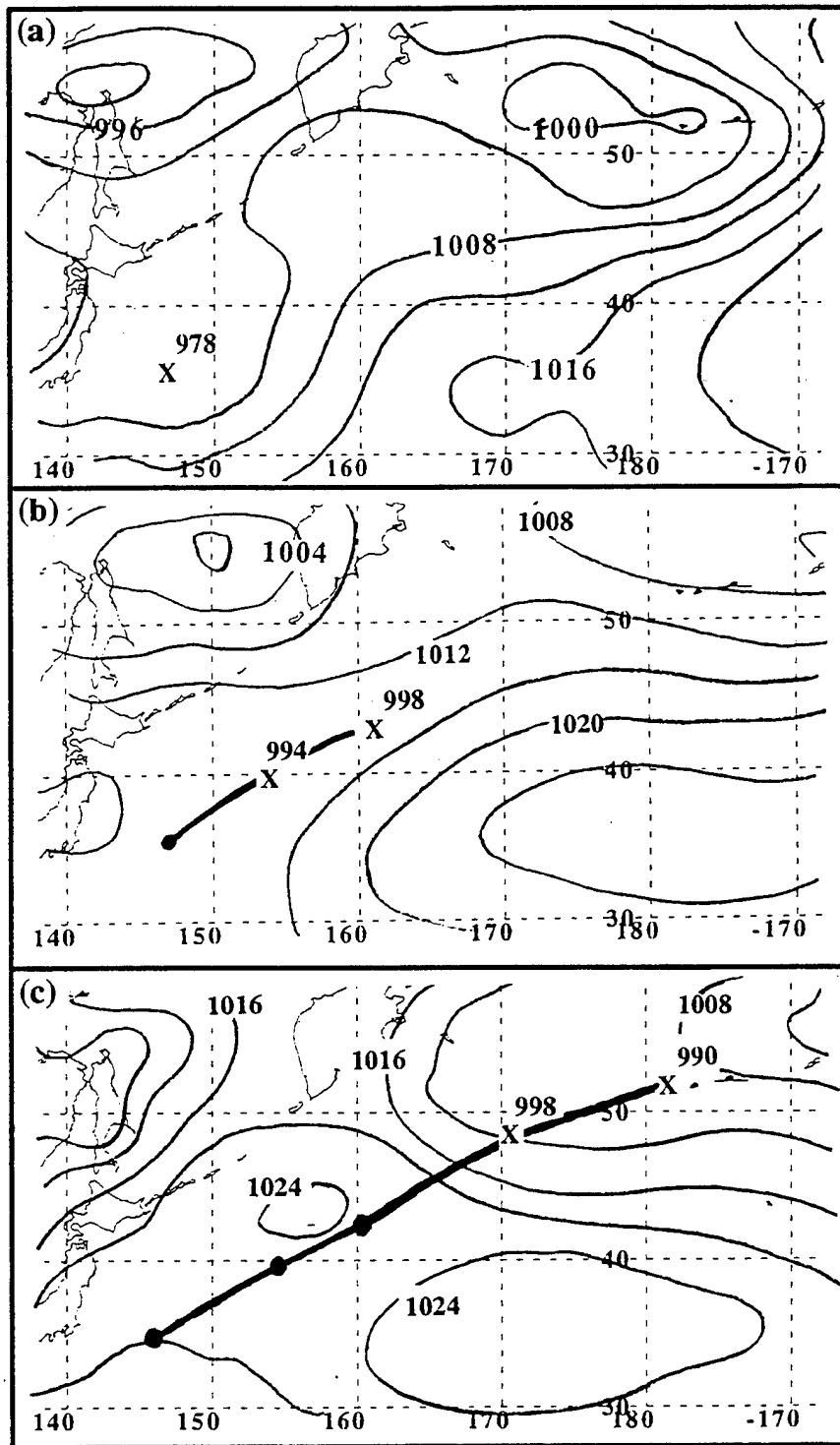


Fig. V-22. COAMPS (a) initial, (b) 24-h forecast, and (c) 48-h forecast of SLP as in Fig. V-14, except for STY Bing initialized at 0000 UTC 4 September 1997.

forecast has a re-intensification (Fig. V-23a). A 500-mb ridge east of 170° E (Fig. V-23b) is forecast to amplify. Zonal isentropes and zonal flow with no significant warm advection (Fig. V-23d) are predicted. Rather than a critical region being forecast in the STY Bing no-TC simulation, anticyclogenesis (Fig. V-22) is predicted.

At 36 h in the control forecast (Fig. V-24), distinct differences are predicted compared to the no-TC simulation, as there were in the case of STY Ginger. An upper-level PV maxima > 28 units is found north-northwest of the storm center (Fig. V-24a). The 500-mb ridge-trough couplet is amplified in the control forecast (compare the 5580 m and 5640 m contours in Fig. V-24b versus in Fig. V-23b). Values of 500-mb PVA are also larger in the control forecast, with maximum values $> 50 \times 10^{-10} \text{ s}^{-2}$ at 49° N, 172° E. Furthermore, the 200-mb jet streak is forecast farther poleward (Fig. V-24c) with divergence $> 4 \times 10^{-5} \text{ s}^{-1}$ associated with the equatorward entrance region superposed above the 500-mb PVA and the surface center. Values of 925-mb warm advection $> 50 \times 10^{-5} \text{ K s}^{-1}$ (Fig. V-24d) are predicted near the storm center. Thus, a critical region (Fig. V-24a) is evident at 36 h in the control forecast, and the STY Bing remnants are within it. In the following 30 h, the remnants of Bing deepened 16 mb and achieved a moderate re-intensification to 982 mb.

The phasing of the transforming STY Bing with the short-wave trough to the northwest results in the critical region at 36 h in the control forecast, while no critical region is forecast in the STY Bing no-TC simulation beyond 36 h. Because anticyclogenesis is predicted in the no-TC simulation, the mid-latitude contribution is classified as "unfavorable." One other case (TY Tina, August 1997) resembled STY Bing,

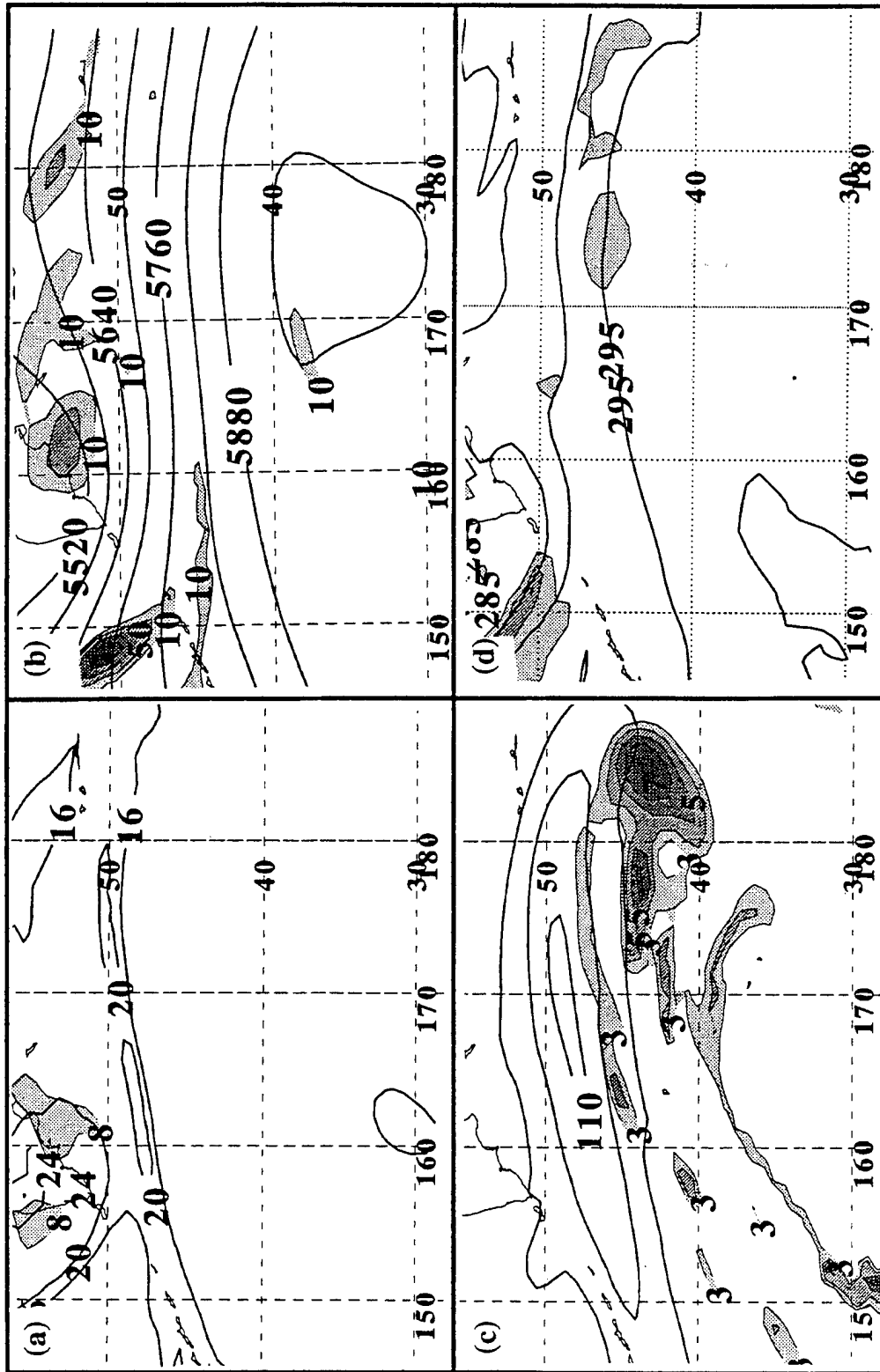


Fig. V-23. (a) Layer-averaged PV between 925 mb and 700 mb (shaded) and 500 mb to 300 mb (solid contours), (b) 500-mb isoheights and PVA, (c) 200-mb isotachs and divergence, and (d) 925-mb warm advection and isentropes of potential temperature as in Fig. V-15, except for 36-h interval of STY Bing no-TC simulation initialized at 0000 UTC 4 September 1997.

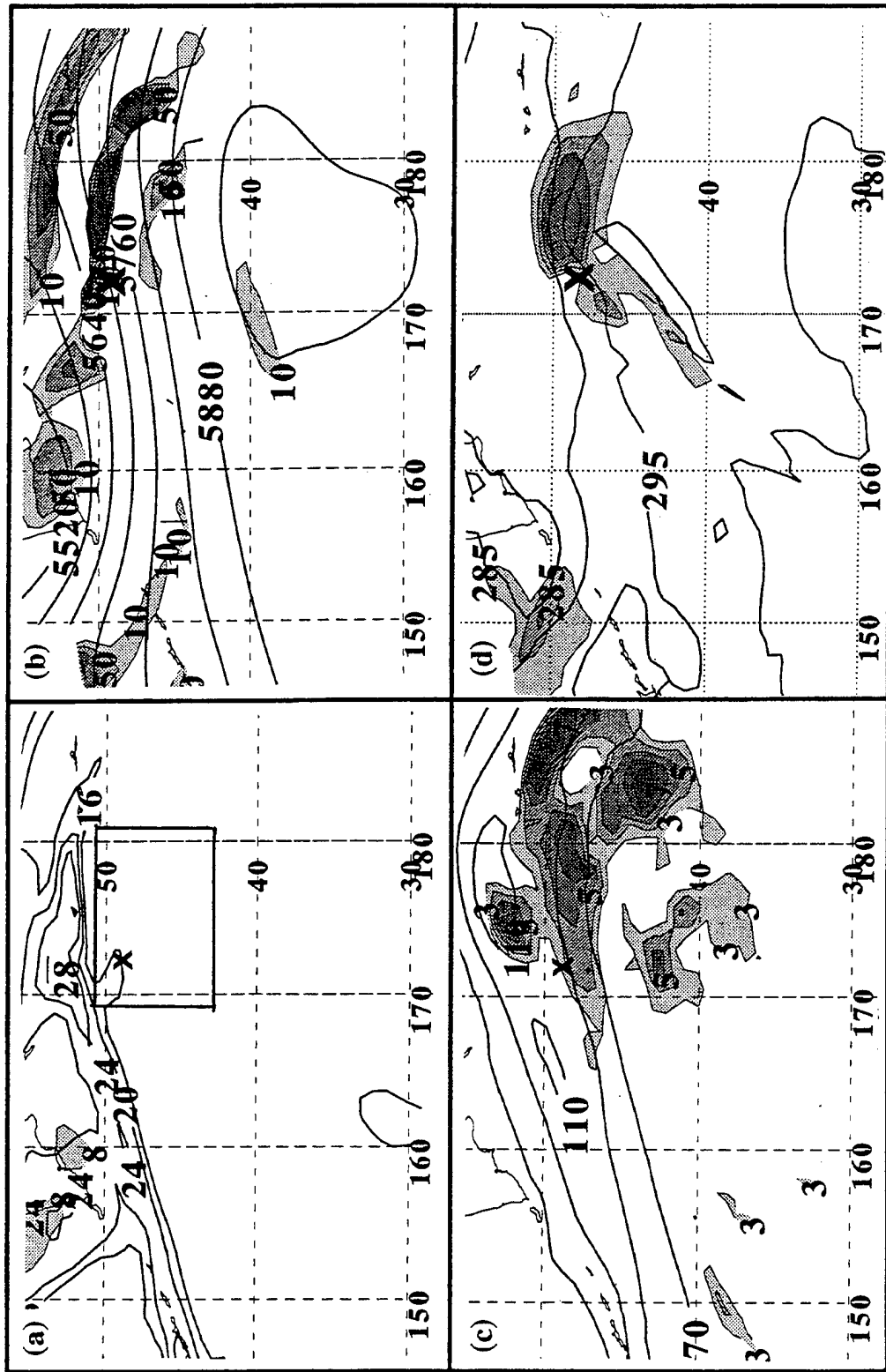


Fig. V-24. (a) Layer-averaged PV between 925 mb and 700 mb (shaded) and 500 mb to 300 mb (solid contours), (b) 500-mb isoheights and PVA, (c) 200-mb isotachs and divergence, and (d) 925-mb warm advection and isentropes of potential temperature as in Fig. V-23, except for 36-h interval of STY Bing control forecast initialized at 0000 UTC 4 September 1997. The critical region is depicted by a solid box in (a), and the storm location is denoted with an "X."

with anticyclogenesis evident in the no-TC simulation (Appendix B), so that the mid-latitude contribution to the re-intensification stage in the case of TY Tina is also classified as unfavorable.

In summary, the contributions of the mid-latitude circulation pattern have been described and classified based on the amount of extratropical cyclogenesis forecast in the COAMPS no-TC simulations. In cases in which the mid-latitude contribution is favorable, a critical region is found in both the no-TC simulation and the control forecast, and extratropical cyclogenesis occurs within that critical region. In the case of TY David, an ET with a deep re-intensification (final SLP = 977 mb) is predicted in the control forecast in the same location as a comparatively weaker extratropical cyclogenesis in the no-TC simulation (Appendix B). In the case of STY Bart, a separate cyclogenesis occurred apart from the ET in the control run. In the case of TY Stella, the presence of the TC in the control run appeared to matter very little, since it barely re-intensified during its ET. Whereas a separate extratropical cyclogenesis is forecast in the same location as in the cyclogenesis predicted in the no-TC simulation, only a 2 mb difference in intensity at the end of the no-TC and control forecasts (not shown).

In cases in which the mid-latitude contribution is defined to be neutral, no critical region is predicted in the no-TC simulation, although the atmosphere is forecast to support at least weak extratropical cyclogenesis. However, the STY Ginger (Fig. V-19) and TY Rex (Appendix B) control forecasts predict ET with deep re-intensification, which implies that the interaction of the TC with the mid-latitude circulation pattern and

associated pre-existing lower-tropospheric baroclinity in those cases is sufficient to produce a deep cyclogenesis that would not have occurred in the absence of the TC.

In cases in which the mid-latitude contribution is defined to be unfavorable, anticyclogenesis is forecast in the no-TC simulation. In one case (STY Bing), the contribution of the TC was sufficient to produce a moderate re-intensification that did not occur in the no-TC simulation.

These no-TC simulations suggest that in some cases little if any extratropical cyclogenesis will be observed in the atmosphere if it were not for the TC that completed ET. Furthermore, these results demonstrate that the interaction of the TC and the mid-latitude circulation pattern produces different outcomes within the same category of the mid-latitude contribution (the columns depicted in Fig. V-8). This TC contribution will be evaluated further by displacing the TC vortex so that its phasing and interaction with the mid-latitude circulation pattern are altered. These evaluations will consider: (i) whether the translating TC phases with a critical region so that the transformed storm redeepens through Petterssen Type-B extratropical cyclogenesis; and (ii) whether or not that phasing results in an optimal interaction between the TC and the mid-latitude circulation pattern and lower-tropospheric baroclinity to produce rapid and/or deep extratropical cyclogenesis.

E. THE "DISPLACED-TC" SIMULATIONS

Recall that the primary objective here is to demonstrate that proper phasing of the TC with the critical region in the mid-latitude circulation pattern determines the outcome of the re-intensification stage of ET. In cases in which the phasing between the TC and

the critical region is forecast to be more (less) optimal, the storm will be predicted to be deeper (weaker) than in the control forecast. In this section, the control forecast will be compared to "displaced-TC" simulations in which the TC is moved from its initial position to produce either a more or less favorable phasing with the critical region diagnosed in the control forecast at the time re-intensification is predicted to begin. This comparison will test the superposition hypothesis, and also provide further insight into the physical mechanisms related to the TC contribution to the re-intensification stage of ET.

1. STY Bart, Mid-Latitude "Favorable" Contribution

As described earlier in Chap. V-D, the location of the critical region at 36 h in the control forecast of the ET of STY Bart is predicted to be between 149° E and 157° E (Fig. V-17a). After some sensitivity tests with different initial positions, it was decided that displacing STY Bart so that it was farther north and east at the initial time would result in a better phasing between Bart and the critical region, since such a displaced vortex should advance poleward into the mid-latitude circulation pattern faster. Specifically, the vortex is displaced two gridpoints poleward and two grid points to the east (about 150 n mi to the northeast; hereafter referred to as Bart-NE) so that it would arrive in the critical region sooner, which according to the hypothesis should cause the storm to deepen more than in the control. In another simulation, the vortex is displaced two gridpoints equatorward and two gridpoints to the west (about 150 n mi to the southwest; hereafter referred to as Bart-SW) so that it would not phase with the critical region, which according to the hypothesis should cause the storm to re-intensify less than in the control. However, the Bart-SW simulation actually deepens more than the control, and the Bart-NE simulation deepens

less. Therefore, comparison of the Bart-SW simulation to the control will be discussed first.

The initial SLP in the Bart-SW simulation is about 4 mb higher than in the control forecast (Fig. V-25a), although the SLP does not increase as much during the transformation stage, and the Bart-SW vortex completes its transformation 6 h earlier. After 6 h, the Bart-SW simulation is always deeper than the control forecast. Bart-SW is forecast to begin the re-intensification stage at 18 h (Fig. V-25a) when it has a SLP = 996 mb and is at 40° N, 135° E, while the control cyclone begins to re-intensify at 24 h when it has a SLP = 998 and is at 41° N, 140° E. From 18 h until 54 h, the Bart-SW cyclone deepens 22 mb (Fig. V-25a) including a period of rapid deepening from 36 h to 48 h (14 mb SLP decrease in 12 h), and translates northeastward so that its track is farther poleward (Fig. V-25b) than either the control forecast or the Bart-NE simulation. The displacement to the SW results in a distinctly larger rate of deepening than in the control forecast so that the minimum SLP = 973 mb (982 mb) at 54 h in the Bart-SW (control) forecast, at which time the Bart-SW cyclone is at 52° N, 146° E (Fig. V-25b), which is 100 n mi poleward of the storm in the control.

At 36 h in the Bart-SW simulation, the storm is at 48° N, 143° E (Fig. V-26a), where a region of lower-tropospheric $PV > 8 \times 10^{-7} \text{ K m}^2 \text{ s}^{-1} \text{ kg}^{-1}$ is found. The cyclone in Bart-SW is 120 n mi farther poleward than the control, and an upper-level PV maxima > 28 units (which is 4 units greater than in the control forecast) is to the northwest. The Bart-SW cyclone is associated with a deepening 500-mb short-wave trough (Fig. V-26b). Although the pattern of 500-mb isoheights is nearly the same in both the Bart-SW and the

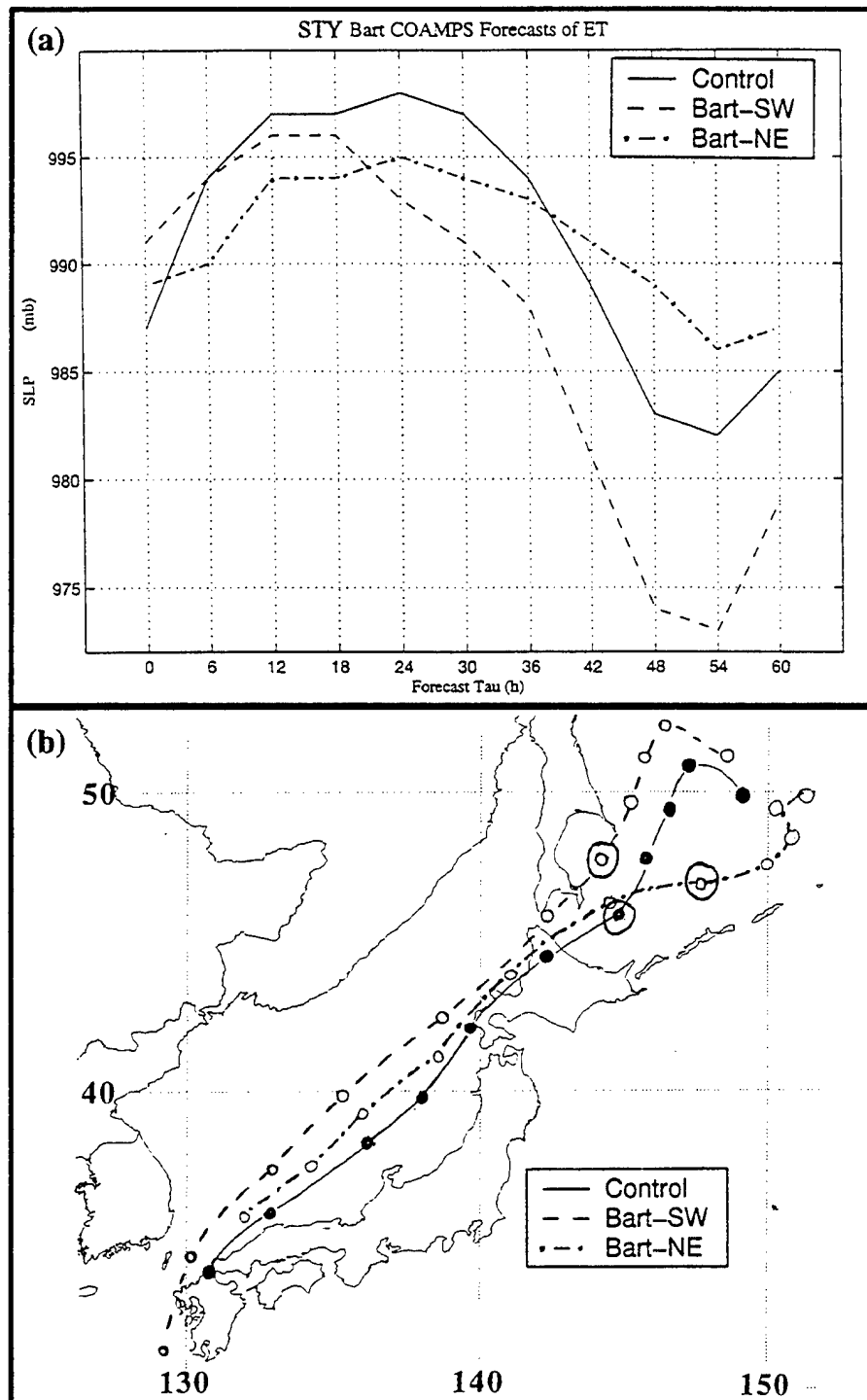


Fig. V-25. The control forecast and displaced-TC simulations in the case of STY Bart initialized at 0000 UTC 24 September 1999 depicting (a) the SLP of the storm in the control forecast, Bart-SW simulation, and Bart-NE simulation (interval 6 h), and (b) the storm tracks each 6 h for the control (solid, filled dots), Bart-SW (dashed, open circles) and Bart-NE (dashed-dot, open circles). The 36-h positions are circled for later discussion.

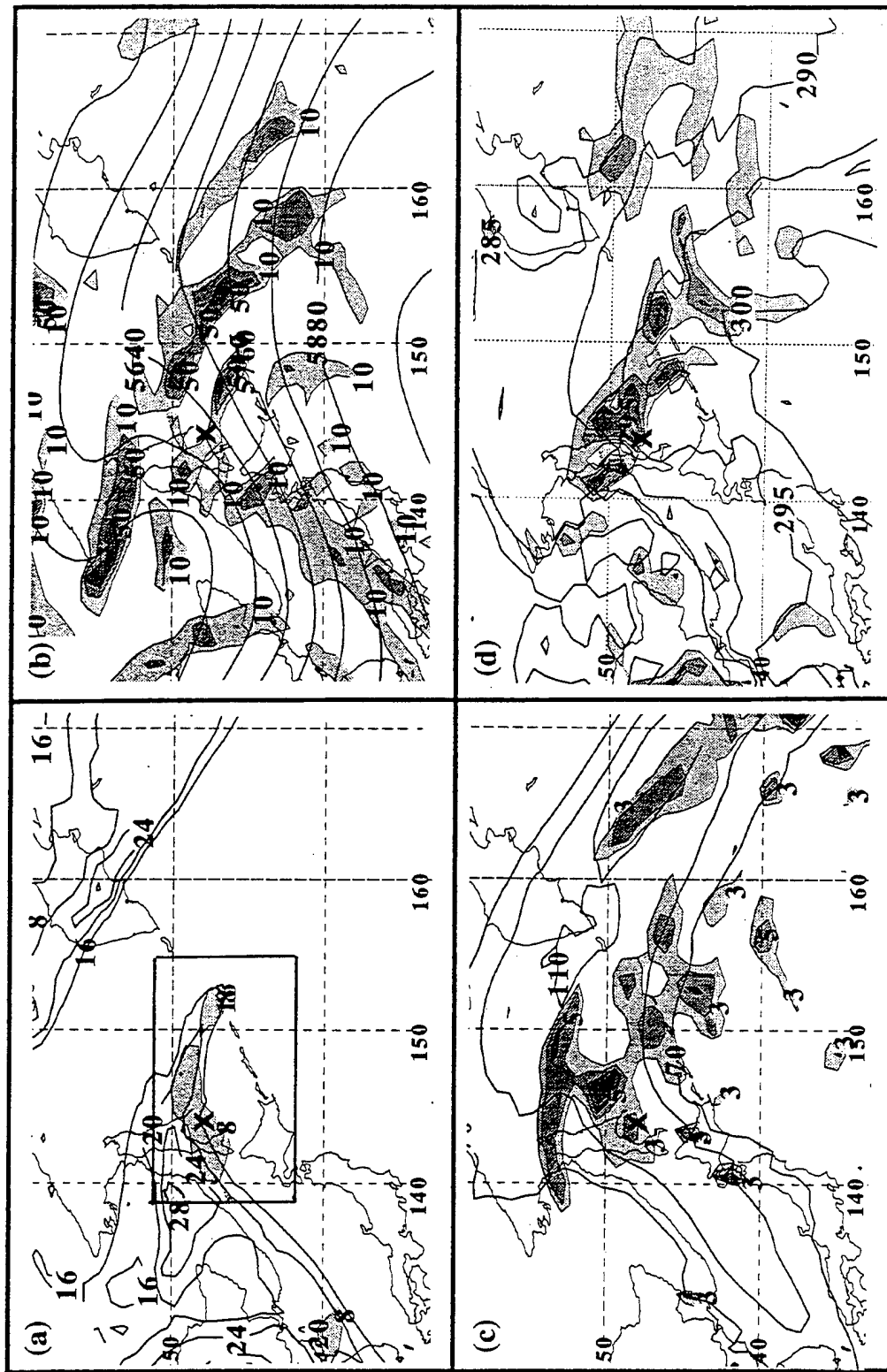


Fig. V-26. (a) Layer-averaged PV between 925 mb and 700 mb (shaded) and 500 mb (solid contours), (b) 500-mb isoheights and PVA, (c) 200-mb isotachs and divergence, and (d) 925-mb warm advection and isentropes of potential temperature as in Fig. V-15, except for 36-h interval of Bart-SW simulation initialized at 0000 UTC 24 September 1999. The critical region is depicted by a solid box in (a), and the storm location is denoted with an "X."

control forecast, the Bart-SW cyclone is near a region of 500-mb PVA with values $> 50 \times 10^{-10} \text{ s}^{-2}$ at 47° N , 146° E (Fig. V-26b), which is slightly larger than those in the control. The western edge of the 200-mb jet streak predicted in the Bart-SW case is 200 n mi farther upstream than in the control (compare Fig. V-26c versus Fig. V-17c), so that unlike the control forecast, the storm is beneath 200-mb divergence $> 4 \times 10^{-5} \text{ s}^{-1}$ (Fig. V-26c) associated with the equatorward entrance region of a 110-kt jet streak. The cyclone in Bart-SW is also in a tighter gradient of 925-mb isentropes than the control (compare Fig. V-26d versus Fig. V-17d). Notice the location of the 295 K isentrope west of the storm (which is farther equatorward in the Japan Sea than in the control) and east of the storm along 143° E (farther west than the control), and a closed contour of 300 K southeast of Bart-SW at 46° N , 148° E . In the Bart-SW simulation, the highest values of lower-tropospheric warm advection $> 50 \times 10^{-5} \text{ K s}^{-1}$ are immediately adjacent to the storm center, which is 20 units higher than the maximum nearly 300 n mi north of the storm in the control.

Thus, the western edge of the critical region in the Bart-SW simulation is 500 n mi farther west than in the control (compare Fig. V-26a versus Fig. V-17a). Unlike the storm in the control forecast, which is more than 300 n mi upstream from the critical region, the Bart-SW cyclone is predicted to be within a critical region (Fig. V-26a), and it is forecast to begin rapidly deepening and achieve a SLP = 974 mb in the next 12 h.

Calculations of 900-mb frontogenesis (Fig. V-27a, using the same method described in Chap. III) at 36 h in the control forecast indicate a weak confluence term contribution to frontogenesis $> 5 \times 10^{-10} \text{ K m}^{-1} \text{ s}^{-1}$ 200 n mi north of the storm that

extends several hundred miles to the east. A vertical south-north cross-section through the center of the storm suggests that this lower-tropospheric confluence produces ascent $> 10 \times 10^{-3} \text{ mb s}^{-1}$ within the tilted potential temperature region 300 n mi north of the storm center at 500 mb (Fig. V-27b).

At 36 h in the Bart-SW simulation (Fig. V-28a), the confluence term is forecast to be frontogenetic in a region adjacent to and poleward of the storm center, with a maximum 10 units greater than that in the control. This lower-tropospheric confluence contributes to an ascent $> 10 \times 10^{-3} \text{ mb s}^{-1}$ at 500 mb above the storm center (Fig. V-28b), with an ascent maximum > 13 units over tilted isentropic surfaces only 120 n mi poleward of the storm center. Notice also that the isentropes are more sharply tilted at and north of the Bart-SW center than those in the control (compare Fig. V-27b versus Fig. V-28b).

Significant PVA and warm advection are predicted at 36 h near the storm in both the control forecast and Bart-SW simulation. However, values of 200-mb divergence above the storm are significantly higher in the Bart-SW simulation than in the control forecast, in which the 200-mb divergence maximum is farther east. Therefore, the Bart-SW cyclone is in a critical region, while the critical region in the control forecast is farther downstream from the storm. Furthermore, the Bart-SW cyclone advanced farther poleward into lower-tropospheric baroclinity so that the cold air to the west advanced farther equatorward, and larger values of lower-tropospheric warm advection and 900-mb frontogenesis are predicted adjacent to the storm. Thus, it is concluded that the phasing of the Bart-SW cyclone, with its more poleward and westward track, produced a more optimal interaction with the lower-tropospheric baroclinity in the mid-latitude circulation

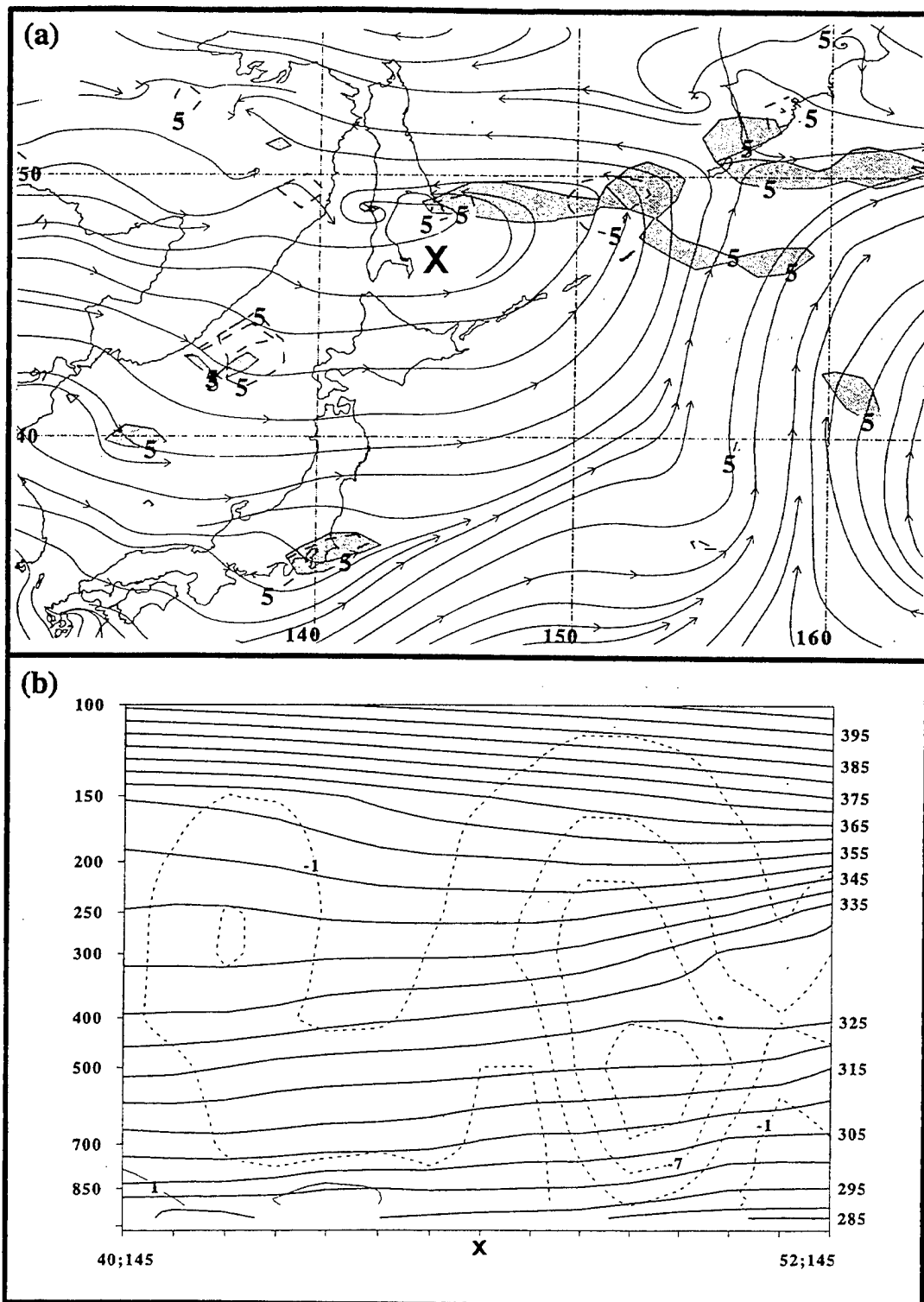


Fig. V-27. (a) Streamlines and frontogenesis (interval $10 \times 10^{-10} \text{ K/(m s)}$ beginning with the $5 \times 10^{-10} \text{ K/(m s)}$ contour) at 900 mb with solid (dashed) contours depicting frontogenetic confluence (shear) term contributions at 36 h in the control forecast of STY Bart initialized at 0000 UTC 24 September 1999, and (b) vertical south-north cross-section of potential temperature (thick solid contours, 5 K interval) and COAMPS analyzed vertical motion with dashed (thin solid) contours depicting ascent (descent) at a $3 (1) \times 10^{-3} \text{ mb/s}$ interval.

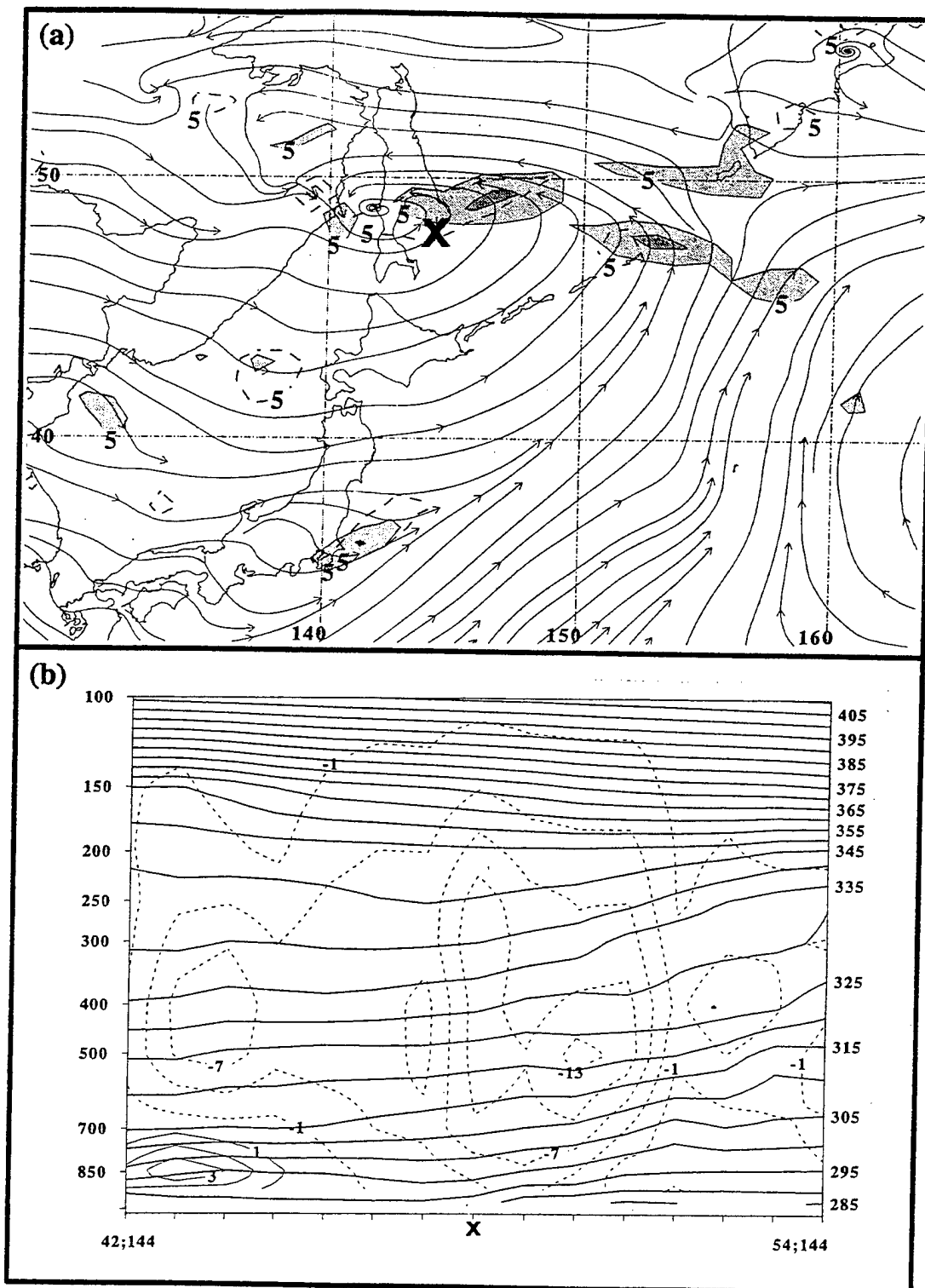


Fig. V-28. (a) Streamlines and frontogenesis (interval $10 \times 10^{-10} \text{ K/(m s)}$) beginning with the $5 \times 10^{-10} \text{ K/(m s)}$ contour) at 900 mb with solid (dashed) contours depicting frontogenetic confluence (shear) term contributions at 36 h in the Bart-SW simulation initialized at 0000 UTC 24 September 1999, and (b) vertical south-north cross-section of potential temperature (thick solid contours, 5 K interval) and COAMPS analyzed vertical motion with dashed (thin solid) contours depicting ascent (descent) at a $3 (1) \times 10^{-3} \text{ mb/s}$ interval.

pattern than in the control. This interaction in the Bart-SW simulation is responsible for the increased frontogenesis and greater ascent over tilted isentropic surfaces. The larger values of ascent at the Bart-SW storm center are also consistent with the highest values of 200-mb divergence being predicted above the storm center. Thus, the displacement of the critical region in the Bart SW simulation results in the cyclone experiencing more intense Petterssen Type-B extratropical cyclogenesis than in the control forecast, and thus achieving a deeper re-intensification.

Even though the initial SLP in the Bart-NE simulation is about 2 mb higher than in the control forecast (Fig. V-25a), the SLP does not increase as much during the transformation stage. Between 6 h and 30 h, the Bart-NE simulation is a nearly constant 4 mb lower than in the control forecast. However, the initial cyclone displacement to the NE results in a distinctly smaller rate of deepening than in the control forecast so that the minimum SLP = 986 mb (982 mb) at 54 h in the Bart-NE (control) forecast. The question is then why did the northeastward displacement to achieve an earlier phasing with the critical region in the control forecast not achieve deeper re-intensification? The displaced Bart-NE cyclone is farther along the control forecast track (Fig. V-25a) from the initial time until 30 h when the cyclone is at 45° N, 145° E, and then has a more zonal track than in the control forecast. At 54 h, the Bart-NE cyclone is at 50° N, 150° E (Fig. V-25b), which is 200 n mi farther east than the control.

At 36 h in the Bart-NE simulation, the storm is near 46° N, 148° E (Fig. V-29a), which is nearly 200 n mi farther downstream than in the control forecast. A broad region of lower-tropospheric $PV > 8 \times 10^{-7} \text{ K m}^2 \text{ s}^{-1} \text{ kg}^{-1}$ is oriented east-west along 49° N and

is south of the upper-level PV maxima > 32 units (Fig. V-29a). The Bart-NE cyclone is much farther from the 500-mb trough to the northwest than in the control (compare the location of the storm to the 5520 m and 5580 m 500-mb contours in Fig. V-29b versus Fig. V-17b). As a result, the Bart-NE cyclone is more than 600 n mi upstream from the 500-mb PVA maxima (Fig. V-29b), whereas the storm in the control is beneath PVA $> 30 \times 10^{-10} \text{ s}^{-2}$ (Fig. V-17b). Furthermore, the 200-mb divergence maximum $> 5 \times 10^{-5} \text{ s}^{-1}$ (Fig. V-29c) west of 160° E is also farther east than in the control, and more than 600 n mi downstream of the Bart-NE cyclone. Notice that the cold air (295 K 925-mb isentrope) has not advanced as far equatorward into the Japan Sea, and at the same time is farther to the east at 146° E than in the control forecast (Fig. V-17d), which is consistent with the weaker lower-tropospheric baroclinity evident in the Bart-NE simulation. Whereas a large area of warm advection with values $> 50 \times 10^{-5} \text{ K s}^{-1}$ (Fig. V-29d) exists downstream of the Bart-NE cyclone in the same location as the 500-mb PVA and the 200-mb divergence, a critical region is present between 151° E and 159° E (Fig. V-29a). As for the control storm, the Bart-NE cyclone is west of the critical region in the 36-h forecast (compare Fig. V-17a to Fig. V-29a), with the critical region (and the actual storm position) farther downstream in the Bart-NE simulation than in the control forecast.

At 36 h in the Bart-NE simulation, large confluence term contributions to frontogenesis are predicted 100 n mi north of the storm center (Fig. V-30a), with the confluence term maximum 600 n mi downstream of the storm center. These values are about 10 units greater than in the control forecast. A vertical south-north cross section through the center of the storm (Fig. V-30b) of potential temperature and vertical motion

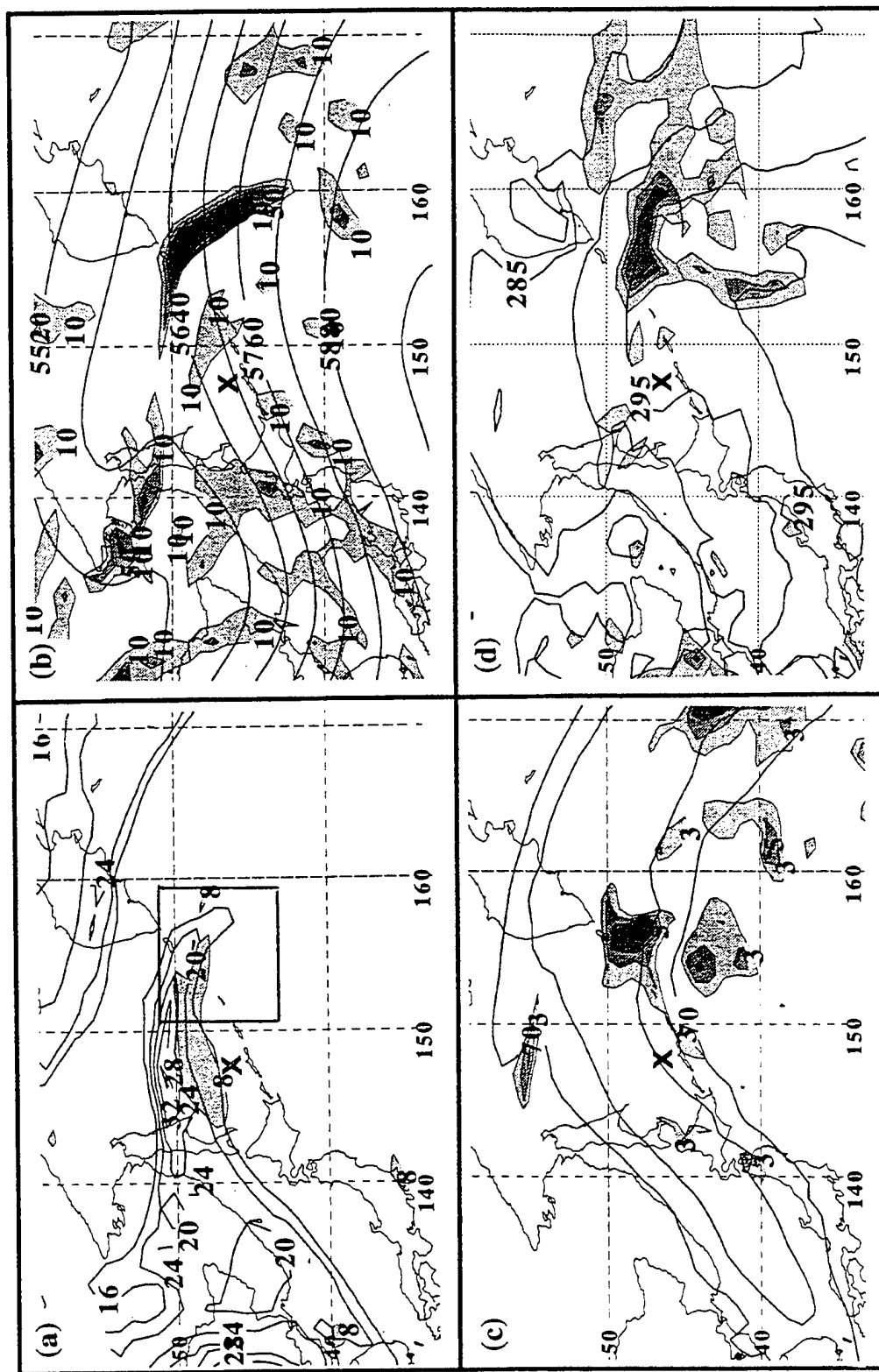


Fig. V-29. (a) Layer-averaged PV between 925 mb and 700 mb (shaded) and 500 mb (solid contours), (b) 500-mb isoheights and PVA, (c) 200-mb isotachs and divergence, and (d) 925-mb warm advection and isentropes of potential temperature as in Fig. V-26, except for Bart-NE simulation.

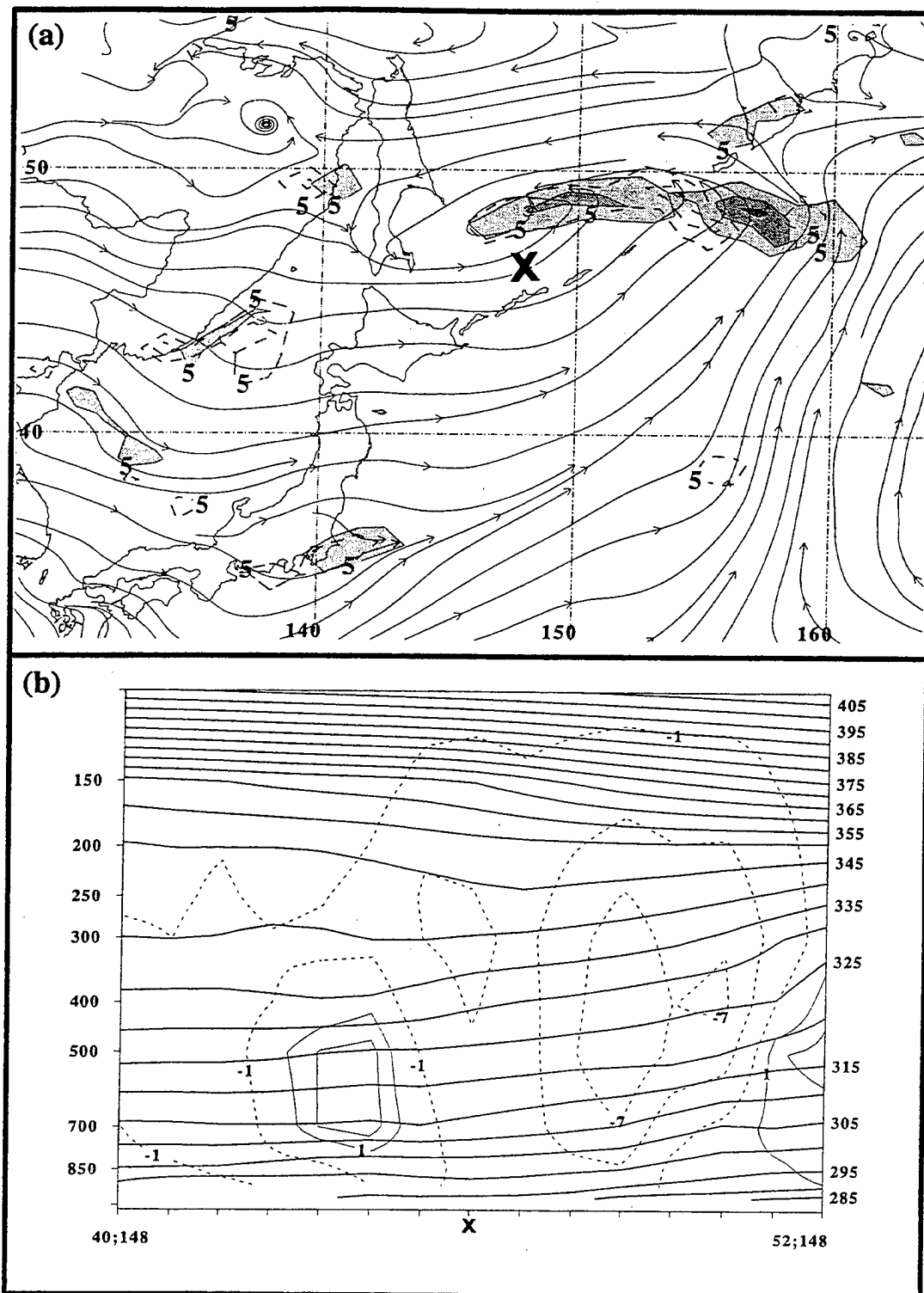


Fig. V-30. (a) Streamlines and frontogenesis (interval $10 \times 10^{-10} \text{ K/(m s)}$ beginning with the $5 \times 10^{-10} \text{ K/(m s)}$ contour) at 900 mb with solid (dashed) contours depicting frontogenetic confluence (shear) term contributions at 36 h in the Bart-NE simulation initialized at 0000 UTC 24 September 1999, and (b) vertical south-north cross-section of potential temperature (thick solid contours, 5 K interval) and COAMPS analyzed vertical motion with dashed (thin solid) contours depicting ascent (descent) at a $3 \times 10^{-3} \text{ mb/s}$ interval.

suggest that this lower-tropospheric confluence produces an ascent maximum $> 7 \times 10^{-3}$ mb s⁻¹ nearly 200 n mi north of the storm center. In the control forecast, the ascent maximum was 3 units larger than in the Bart-NE simulation. As in the case of the control forecast, the best support for extratropical cyclogenesis in the Bart-NE simulation is forecast to be in a critical region that is downstream of the storm location. As the critical region is farther downstream than in the control forecast, and it is forecast to continue to translate ahead of the Bart-NE cyclone (not shown), the cyclone in the Bart-NE simulation never enters it. The control forecast has greater 500-mb PVA (Fig. V-17b) and 900-mb warm advection (Fig. V-17d) than in the case of Bart-NE. It is believed that the increased 500-mb PVA is responsible for the larger ascent predicted in the control forecast, which in turn caused the storm to deepen 11 mb in 12 h to a SLP = 983 mb, whereas the cyclone in the Bart-NE simulation deepened only 4 mb to 989 mb during the same period. Displacing the initial vortex to the northeast resulted in a more zonal track, so that the cyclone in the Bart-NE simulation is farther downstream and thus does not interact as strongly with the mid-latitude short-wave trough and its associated lower-tropospheric baroclinity to the west.

In summary, these simulations of STY Bart demonstrate that rather small displacements of the initial TC vortex will result in a deeper (weaker) re-intensification than the ET in the control forecast if the phasing with the critical region is improved (made worse). According to the hypothesis, since the Bart remnants are upstream of the critical region at 36 h in the control forecast, the Bart-NE (Bart-SW) vortex should have phased more (less) optimally with the critical region and deepened more (less) relative to

the control. Although the intent was to displace the vortex to the northeast (southwest) so that it coupled with (missed) the critical region predicted in the control forecast (Fig. V-17a), the Bart-SW cyclone is forecast to translate into a critical region while the storm in the Bart-NE simulation and control forecast do not. As a result, the Bart-SW cyclone is predicted to achieve a deep re-intensification, and the cyclones in the Bart-NE simulation and control forecast are forecast to re-intensify only moderately.

This result appears to be counter-intuitive, since the cyclone in the Bart-NE (Bart-SW) simulation was displaced poleward (equatorward) at the initial time relative to the control. Thus, the Bart-NE cyclone should have penetrated farther and earlier into the pre-existing baroclinic zone to the northeast. However, the Bart-SW storm translates the farthest poleward by 36 h, is in the tightest gradient of isentropes in the lower-tropospheric baroclinic zone, and has the largest values of lower-tropospheric warm advection and frontogenesis forecast adjacent to the storm center. By contrast, the cyclone in the Bart-NE simulation translates more zonally and is farthest downstream of the lower-tropospheric baroclinicity predicted between 140° E and 145° E, so that smaller lower-tropospheric warm advection is forecast, and the maximum 900-mb frontogenesis is almost 600 n mi east of the storm center. Therefore, the lower troposphere is most (least) favorable for Petterssen Type-B extratropical cyclogenesis in the Bart-SW (Bart-NE) simulation.

Furthermore, the displacement of the storm in the Bart-SW simulation brought it closer to the 500-mb trough northwest of the storm, so that the subsequent translation of the cyclone and its phasing with the 500-mb trough to the southwest better resembled the

northwest synoptic pattern of Harr et al. (2000) described in Chap. I (Fig. I-2a) than the control. The Bart-NE cyclone, which translated away from the 500-mb trough to the northwest, resembled more an ET in the northeast synoptic pattern (Fig. I-2b) at 36 h than the control. Since storms in the northwest pattern interact more optimally with upper-tropospheric PV and lower-tropospheric baroclinity than those in the northeast pattern (Harr et al. 2000), the fact that the cyclone in the Bart-SW (Bart-NE) simulation deepened more (less) than the control could have been anticipated based on these synoptic pattern descriptions.

The location of the critical region at 36 h also varies between the Bart-NE, control, and Bart-SW forecasts. In the case of the Bart-SW simulation, the critical region is farther west (Fig. V-26a) than in the control forecast (Fig. V-17a), which is farther upstream than the critical region in the Bart-NE simulation (Fig. V-29a). The primary reason for this difference is the location of the 200-mb jet streak and the divergence maximum associated with its equatorward entrance region. The 200-mb divergence maximum in the Bart-SW simulation is 6° long. west of that in the control forecast (compare Fig. V-26c to Fig. V-17c), and nearly 11° long. west of the maximum in the Bart-NE simulation (compare Fig. V-26c to V-29c). Thus, the cyclone in the Bart-SW simulation is in the critical region at 36 h, i.e., beneath a 200-mb divergence maximum, 500-mb PVA, and adjacent to lower-tropospheric warm advection. The storm in the control forecast is beneath 500-mb PVA and near lower-tropospheric warm advection, but lacked 200-mb divergence, which is predicted to be a maximum farther downstream. Therefore, the critical region in the control forecast is also farther downstream where, as

in the Bart-NE simulation, additional 500-mb PVA and lower-tropospheric warm advection are predicted.

The conclusion is that the location of the TC and its subsequent track and phasing with the mid-latitude circulation pattern in these three COAMPS forecasts helped determine the location of the critical region, and whether or not the TC coupled with the critical region to achieve an optimum interaction with lower-tropospheric baroclinity and upper-tropospheric support for Petterssen Type-B extratropical cyclogenesis. Based on this first "favorable" mid-latitude case, it is suggested that the location of the critical region is sensitive to the location of the 200-mb divergence maximum, and that the location of this upper-tropospheric divergence maximum is in part determined by the location of the re-intensifying storm. These contributions of the TC to the re-intensification stage of ET will be discussed further in a summary section that follows presentation of additional scenarios in the mid-latitude neutral (STY Ginger) and unfavorable (STY Bing) regimes.

2. STY Ginger, Mid-Latitude "Neutral" Contribution

At 36 h in the control forecast of the ET of STY Ginger, the critical region is predicted to be between 178° E and 172° W (Fig. V-21a). Displacing STY Ginger so that it is farther north and east at the initial time should result in a better phasing between it and the critical region, since the displaced vortex should advance poleward into the mid-latitude circulation pattern faster. Unlike the case of STY Bart, such a displacement actually produces a result that deepens more than the control. As indicated by the Bart-SW case, a vortex displacement to the southwest might interact more optimally with the

500-mb trough to the northwest and its associated lower-tropospheric baroclinity and achieve the deepest re-intensification. Thus, STY Ginger is displaced four gridpoints equatorward and two gridpoints west (about 270 n mi to the southwest; hereafter referred to as Ginger-SW) to determine if it would interact more optimally with a deepening 500-mb short-wave trough to the northwest than in the control forecast (Fig. V-21b). STY Ginger is also displaced two gridpoints poleward and one gridpoint east to determine if it would interact more optimally with the critical region identified in the control forecast.

For the first 18 h of both the control forecast and the Ginger-SW simulation, the storm is forecast to translate northeastward (Fig. V-31b). Whereas the control forecast storm is predicted to continue moving northeastward, the Ginger-SW storm is forecast to turn sharply poleward. The transformation stage of Ginger is predicted to be completed after 12 h in the control forecast (Fig. V-31a) as the storm rapidly fills 12 mb to 990 mb, and then begin the re-intensification stage. Not only is the initial vortex in the Ginger-SW simulation about 6 mb deeper than in the control, the storm does not fill nearly as rapidly. Given the large displacement to the southwest, this storm was over warmer water and farther from the inhibiting baroclinic effects and vertical wind shear. Even when the Ginger-SW storm is at the same latitude as the initial position in the control (Fig. V-31b), the rate of filling is still comparatively slow. The control forecast storm completes ET at 42 h after a deep re-intensification, and achieves a SLP = 979 mb near 47° N, 178° W (Fig. V-31b). The storm in the Ginger-SW simulation is predicted to complete transformation after 24 h with a SLP = 979 mb, and then begin the re-intensification stage. In the case of Ginger-SW, rapid deepening is predicted to begin at 30 h as the storm intensifies 20 mb in

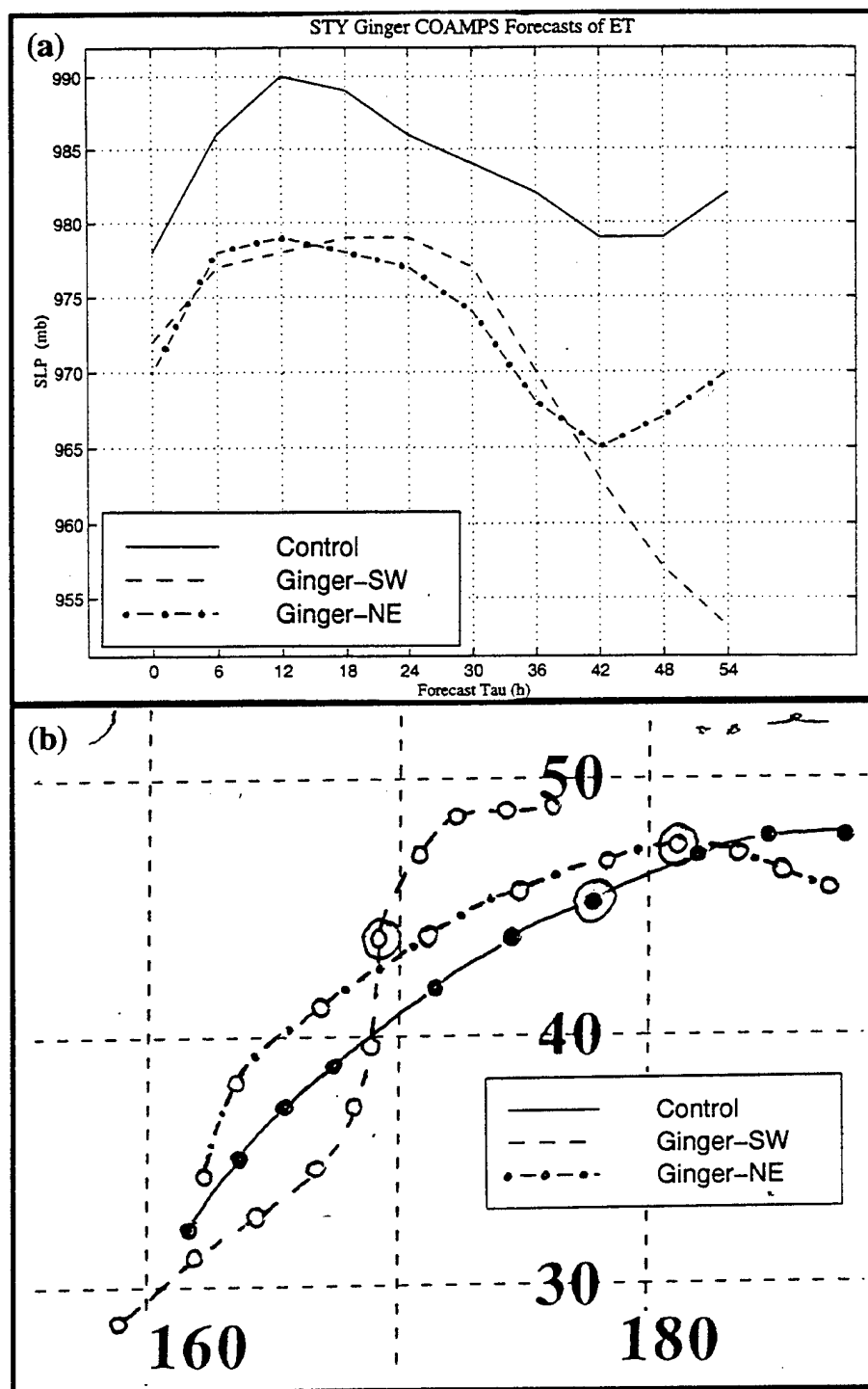
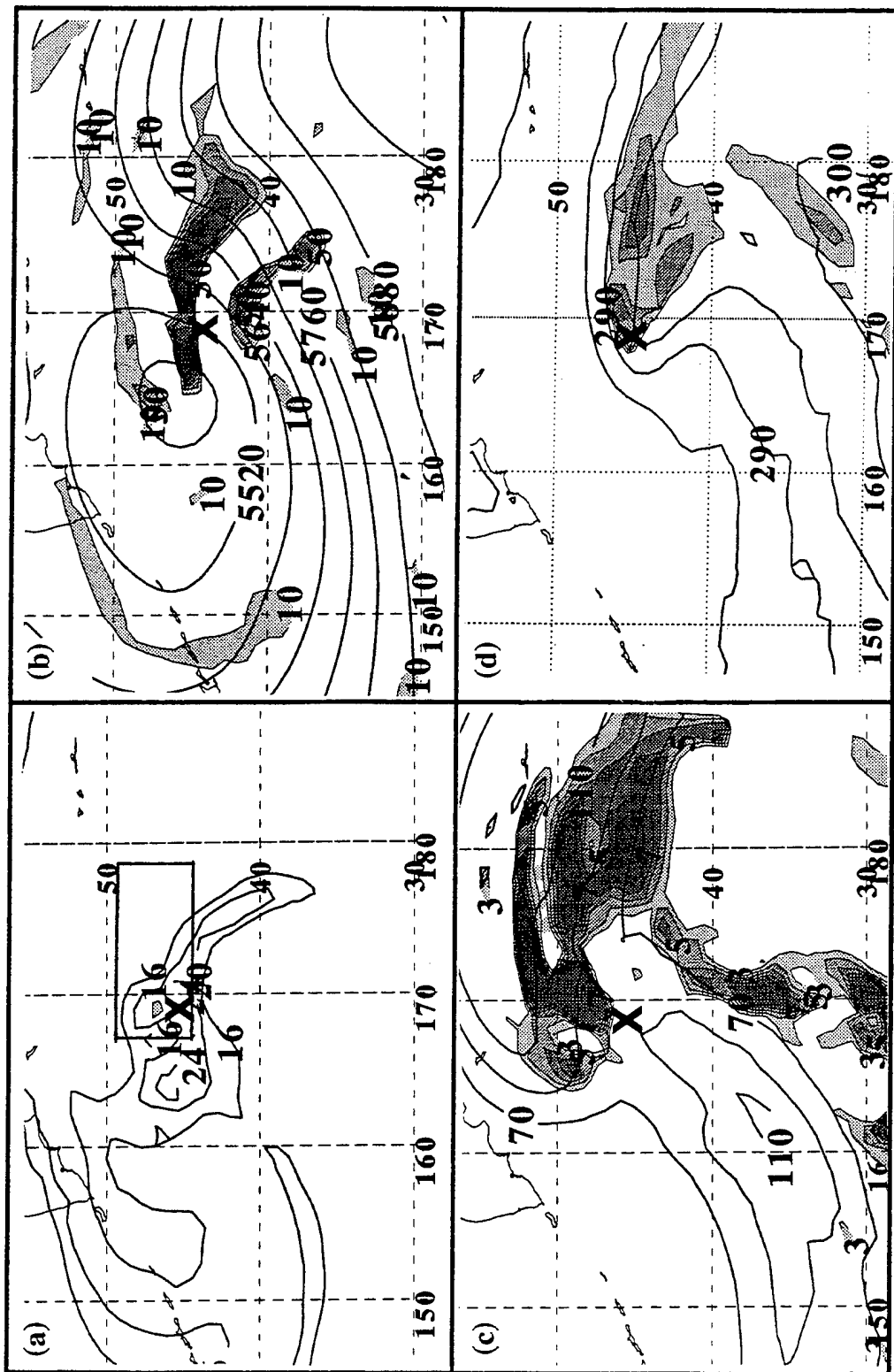


Fig. V-31. As in Fig. V-25, except for the case of STY Ginger initialized at 1200 UTC 29 September 1997, depicting (a) the SLP of the storm in the control forecast, Ginger-SW simulation, and Ginger-NE simulation (interval 6 h), and (b) the storm tracks each 6 h for the control (solid, filled dots), Ginger-SW (dashed, open circles), and Ginger-NE (dashed-dot, open circles). The 36-h positions are circled for later discussion.

18 h, and then completes ET 6 h later with a SLP = 953 mb (Fig. V-31a). Notice that at 54 h the Ginger-SW storm is 700 n mi west-northwest of the storm in the control forecast (Fig. V-31b).

Recall that a critical region is predicted between 178° E and 172° W at 36 h in the control forecast (Fig. V-21a). At 36 h in the Ginger-SW simulation, the storm is forecast to be in the midst of rapid deepening, and a small lower-tropospheric PV maximum $> 8 \times 10^{-7} \text{ K m}^2 \text{ kg}^{-1} \text{ s}^{-1}$ at the storm center (Fig. V-32a) is predicted with upper-level PV maxima > 24 units above and west of the storm. As will be documented in the other three panels, a critical region is forecast between 167° E and 178° W, which is farther west than the critical region in the control forecast. The Ginger-SW cyclone is in the critical region (Fig. V-32a), while the storm in the control had not yet entered the critical region at 36 h (Fig. V-21a).

In the control forecast, the 500-mb trough defined by the 5520 m contour is near 174° E (Fig. V-21b). At 36 h of the Ginger-SW simulation, a cutoff 500-mb low is west-northwest of the storm at 56° N, 164° W (Fig. V-32b) and 700 n mi west of the 500-mb trough in the control forecast. Thus, the Ginger-SW storm is beneath a 500-mb PVA maximum $> 50 \times 10^{-10} \text{ s}^{-2}$, while the strongest PVA was farther downstream of the storm center at 36 h in the control forecast. The Ginger-SW cyclone is also at the edge of a region of 200-mb divergence $> 7 \times 10^{-5} \text{ s}^{-1}$ (Fig. V-32c) associated with the equatorward entrance region of a downstream 200-mb jet streak with > 110 kt winds. A second 200-mb jet streak is southwest of the storm, so that its divergent poleward exit region is predicted to be approaching the storm location. These jet streaks are as much as 20 kt



greater than those in the control forecast (compare Fig. V-32c to Fig. V-21c). Finally, the cyclone in the Ginger-SW simulation is within a tighter gradient of 925-mb isentropes than the storm in the control forecast (compare Fig. V-32d to Fig. V-21d), and the cold air is predicted to penetrate farther equatorward and wrap around to the southeast of the storm (compare the 295 K and 290 K isentropes in Fig. V-32d with Fig. V-21d). Large values of warm advection $> 50 \times 10^{-5} \text{ K s}^{-1}$ (which exceed those at 36 h of the control forecast by 40 units) are found at the storm center (Fig. V-21d), and extend several hundred n mi eastward.

At 36 h in the Ginger control forecast (Fig. V-33a), large shear and confluence contributions to 900-mb frontogenesis $> 25 \times 10^{-10} \text{ K m}^{-1} \text{ s}^{-1}$ are collocated in a swath extending 700 n mi eastward from the storm center, although the maxima for both terms are 300 n mi east of the storm center. A vertical south-north cross section through the center of the storm (Fig. V-33b) of potential temperature and vertical motion suggests that this lower-tropospheric frontogenesis contributes to ascent on tilted isentropic surfaces with a maximum 400 mb value $> 30 \times 10^{-3} \text{ mb s}^{-1}$ 60 n mi north of the storm center.

At 36 h in the Ginger-SW simulation, both the shear and confluence terms are forecast to be frontogenetic (Fig. V-34a) with values $> 45 \times 10^{-10} \text{ K m}^{-1} \text{ s}^{-1}$, which is nearly twice that predicted in the control forecast (Fig. V-33a). Furthermore, these maxima are closer to and northeast the storm center, with a second frontogenesis maximum $> 5 \times 10^{-10} \text{ K m}^{-1} \text{ s}^{-1}$ adjacent to the storm center that extends southeast of the storm. The strong lower-tropospheric frontogenesis is believed to contribute to the ascent maximum between 500 and 400 mb above the storm center (Fig. V-34b) that is $> 50 \times$

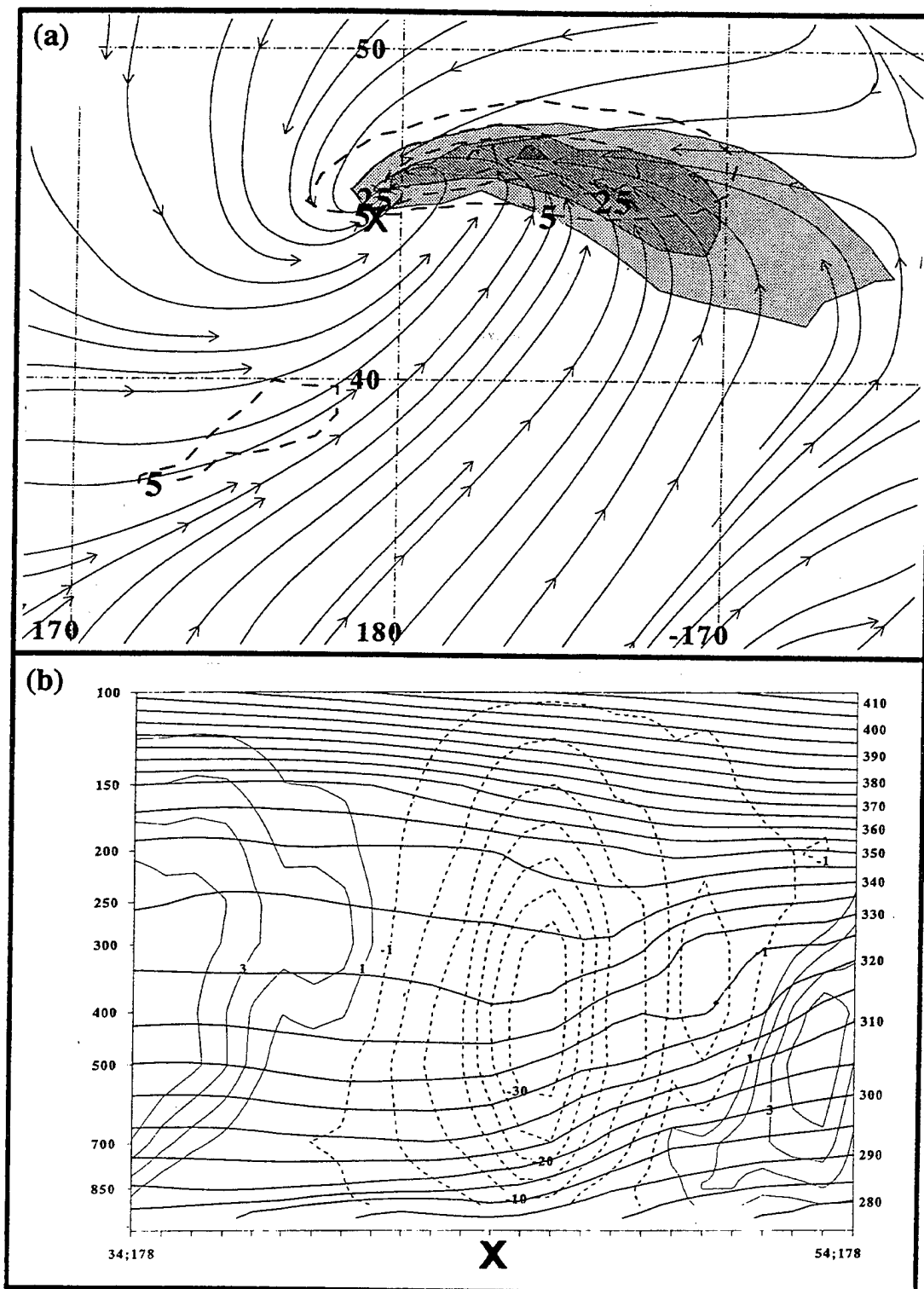


Fig. V-33. (a) Streamlines and frontogenesis (interval $10 \times 10^{-10} \text{ K/ (m s)}$) beginning with the $5 \times 10^{-10} \text{ K/ (m s)}$ contour) at 900 mb with solid (dashed) contours depicting frontogenetic confluence (shear) term contributions at 36 h in the control forecast of STY Ginger initialized at 1200 UTC 29 September 1997, and (b) vertical south-north cross-section of potential temperature (thick solid contours, 5 K interval) and COAMPS analyzed vertical motion with dashed (thin solid) contours depicting ascent (descent) at a $3 (1) \times 10^{-3} \text{ mb/s}$ interval.

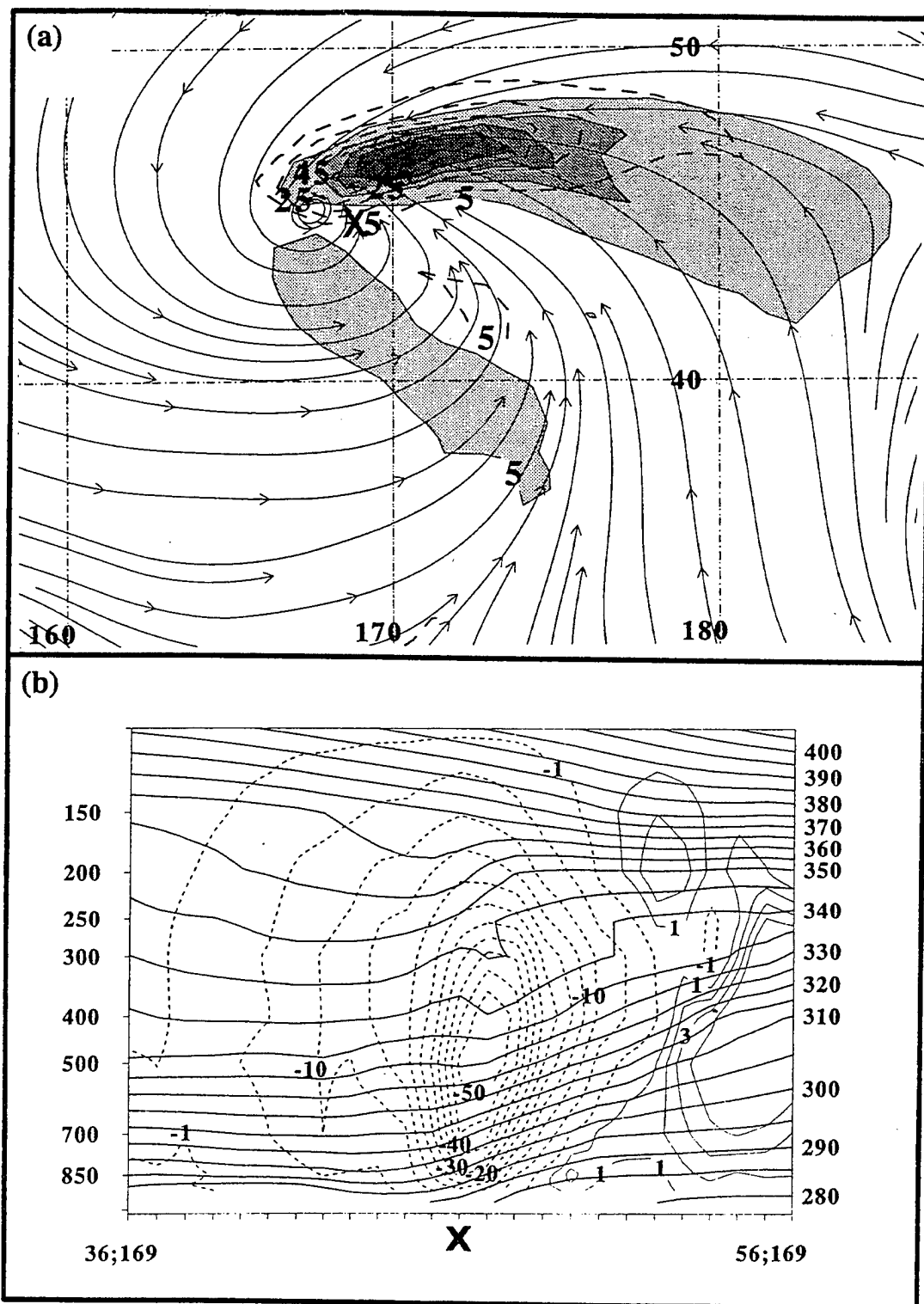


Fig. V-34. (a) Streamlines and frontogenesis (interval $10 \times 10^{-10} \text{ K}/(\text{m s})$ beginning with the $5 \times 10^{-10} \text{ K}/(\text{m s})$ contour) at 900 mb with solid (dashed) contours depicting frontogenetic confluence (shear) term contributions at 36 h in the Ginger-SW simulation initialized at 1200 UTC 29 September 1997, and (b) vertical south-north cross-section of potential temperature (thick solid contours, 5 K interval) and COAMPS analyzed vertical motion with dashed (thin solid) contours depicting ascent (descent) at a $3 (1) \times 10^{-3} \text{ mb/s}$ interval.

$10^{-3} \text{ mb s}^{-1}$, which exceeds the maximum ascent in the control forecast by 20 units. Notice also that a tropopause fold is forecast between 400 and 200 mb above the storm center.

As in the Bart-SW simulation, values of 200-mb divergence above the storm are significantly higher in the Ginger-SW simulation than in the control forecast, in which the 200-mb divergence maximum is farther east. Therefore, the Ginger-SW cyclone is in a critical region that is farther west than the one in the control forecast, while the critical region in the control forecast is farther downstream from the storm. Furthermore, the phasing of the Ginger-SW cyclone, with its more poleward and westward track, produces a more optimal interaction with the lower-tropospheric baroclinity in the mid-latitude circulation pattern than in the control. This interaction is responsible for the larger values of 925-mb lower-tropospheric warm advection and 900-mb frontogenesis and greater ascent over tilted isentropic surfaces. As in the case of the Bart-SW simulation, the phasing of the Ginger-SW cyclone with the displaced critical region, and the subsequent interaction between the Ginger-SW cyclone and lower-tropospheric baroclinity, results in the cyclone experiencing more intense Petterssen Type-B extratropical cyclogenesis than in the control forecast, and achieving a deeper re-intensification.

After the first 6 h, the Ginger-NE cyclone moves northeastward as does the control (Fig. V-31b), although the track of the Ginger-NE cyclone is about 150 n mi farther poleward. At 12 h, the Ginger NE cyclone is about as far downstream as the control storm is at 18 h, and from 18 h to 42 h the location of the Ginger-NE cyclone downstream is similar to that of the control cyclone 6 h later. The initial vortex in the

Ginger-NE simulation is about 8 mb deeper than in the control, and fills somewhat less, although both storms complete the transformation stage at 12 h (Fig. V-31a). After 12 h, the Ginger-NE cyclone re-intensifies at nearly the same rate as the control, and like the control storm completes ET at 42 h with a SLP = 965 mb, which is 14 mb deeper than in the control. Notice that the Ginger-NE cyclone has turned south-southeastward at the end of ET, and is near 47° N, 176° W (Fig. V-31b), so that it is just downstream of the control storm at 42 h. The control storm then moves east-northeastward after 42 h so that it is poleward of the Ginger-NE cyclone through 54 h.

At 36 h in the Ginger-NE simulation, an upper-level PV maximum > 28 units is northwest of the storm, which is 4 units larger than in the control forecast (compare Fig. V-35a to Fig. V-21a). The 500-mb trough is deeper (notice the 5460 m contour and the closed 5400 m contour in Fig. V-35b) as well, although the 500-mb PVA in both cases is $> 50 \times 10^{-10} \text{ s}^{-2}$ above the storm. In the Ginger-NE simulation, the 200-mb divergence associated with the equatorward entrance region of the jet is downstream the storm as in the control forecast (compare Fig. V-35c with Fig. V-21c). However, there is a second maximum $> 5 \times 10^{-5} \text{ s}^{-1}$ south of the Ginger-NE cyclone (Fig. V-35c). The lower-tropospheric warm advection > 30 units is larger than in the control and located adjacent to the Ginger-NE cyclone. Furthermore, the gradient of 925-mb isentropes is also larger than in the control (compare Fig. V-35d to Fig. V-21d). Like the Ginger-NE cyclone which is farther poleward and east than in the control, the critical region at 36 h in the Ginger-NE simulation is somewhat farther downstream than in the control (Fig. V-35a), and the Ginger-NE cyclone is just inside its western edge.

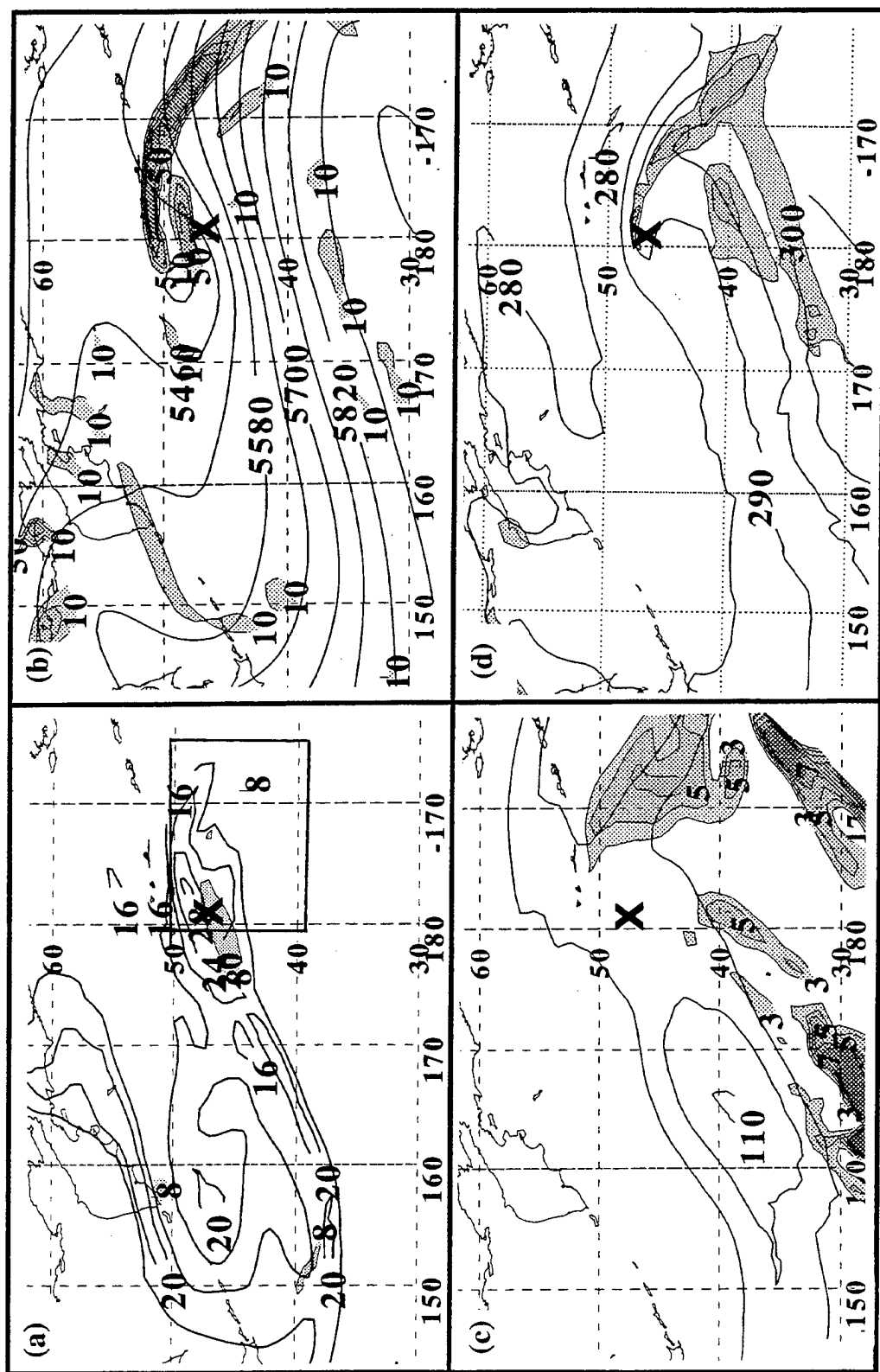


Fig. V-35. (a) Layer-averaged PV between 925 mb and 700 mb (shaded) and 500 mb to 300 mb (solid contours), (b) 500-mb isoheights and PVAs, (c) 200-mb isotachs and divergence, and (d) 925-mb warm advection and isentropes of potential temperature as in Fig. V-32, except for 36-h interval of Ginger-NE simulation.

Although the values of upper-tropospheric divergence and mid-tropospheric are not much different in the Ginger-NE simulation than in the control, the cyclone in the control forecast is adjacent to, not inside, the critical region at 36 h, and the lower-troposphere in the Ginger-NE simulation is more optimal for extratropical cyclogenesis (Fig. V-35d). Both storms have a similar rate of deepening during the re-intensification stage, although the Ginger-NE cyclone is 14 mb deeper than the control by the end of ET at 42 h. Based on the similar SLP trace (Fig. V-31a) and critical region (Fig. V-21 and Fig. V-35) in both cases, it is likely that because the Ginger-NE cyclone is already 8 mb deeper than the control at the initial time and 11 mb deeper when the transformation stage ends at 12 h, it would also be deeper at the end of ET. Nevertheless, a displacement of the initial vortex about 120 n mi to the northeast did result in a more optimal coupling with the critical region and a subsequent deep re-intensification, unlike the Bart-NE simulation.

In summary, the phasing and subsequent interaction between the Ginger-SW cyclone and the mid-latitude circulation is predicted to be more optimal than in the control forecast. As in the case of the Bart-SW simulation, the southwestward displacement of the Ginger vortex is forecast to cause the vortex to be closer to the 500-mb short-wave trough to the northwest and its associated lower-tropospheric baroclinity. The phasing between the Ginger-SW cyclone and this northwest synoptic pattern is predicted to produce a more vigorous critical region that is farther west than in the control. Unlike the control forecast, the storm in the Ginger-SW simulation is forecast at 36 h to already be within a critical region, with higher values of 200-mb divergence and 500-mb PVA superposed above larger values of lower-tropospheric warm advection and frontogenesis

than those in the control, and therefore it is predicted to achieve a deeper re-intensification. A simulation in which STY Ginger is displaced to the northeast results in a more optimal phasing with the critical region and a deeper re-intensification than that in the control forecast.

As in the STY Bart simulations, the location of the critical region appears to depend more sensitively on the maximum 200-mb divergence location, which in turn appears to be influenced by the location of the translating, re-intensifying storm. After 30 h, the Ginger-SW cyclone is farther west than the control cyclone (Fig. V-31b), as is the 200-mb divergence maximum and critical region at 36 h (Fig. V-32a). At 36 h, the Ginger-NE cyclone and critical region (Fig. V-35a) are farther downstream than in the control forecast (Fig. V-31b). Furthermore, since the atmospheric conditions did not appear to be favorable for deep and/or rapid extratropical cyclogenesis in the no-TC simulation (Fig. V-20), the contribution of the Ginger remnants to the re-intensification stage is concluded to be profound, as the control cyclone, Ginger-NE cyclone, and Ginger-SW cyclone (which experienced rapid deepening) are all predicted to achieve deep re-intensification (Fig. V-31a).

3. STY Bing, Mid-Latitude "Unfavorable" Contribution

At 36 h in the control forecast of the ET of STY Bing, the storm is in a critical region between 169° E and 179° W (Fig. V-24a). The upper-level PV maximum is forecast to be slightly north-northwest of the control forecast storm at 36 h (Fig. V-24a) with a 500-mb trough to the northwest (Fig. V-24b). STY Bing is displaced two gridpoints poleward and one gridpoint west (about 120 n mi to the northwest; hereafter

Bing-NW) so that it would interact optimally with the deepening 500-mb short-wave trough in the control forecast.

At the initial time, the TC in the Bing-NW simulation is 4 mb deeper than the control storm, and remains at least 4 mb deeper throughout the entire ET (Fig. V-36a). At 30 h in both the control forecast and Bing-NW simulation, the storm completes the transformation stage, with SLPs = 999 mb and 994 mb, respectively. During the first 36 h of both the control forecast and the Bing-NW simulation, the storm is forecast to translate northeastward (Fig. V-36b) before slightly turning east-northeastward. The storm in the control forecast completed ET at 66 h after achieving moderate re-intensification with a SLP = 982 mb (Fig. V-36a), and a position near 53° N, 170° W (Fig. V-36b). In the Bing-NW case, the storm is predicted to deepen 16 mb in 36 h and achieve a SLP = 978 mb at the end of ET (Fig. V-35a). Notice that at 66 h the Bing-NW storm is about 300 n mi west-northwest of the storm in the control forecast (Fig. V-36b).

At 36 h of the Bing-NW simulation, the storm is forecast to be south-southwest of an upper-level PV maximum (Fig. V-37a). Based on the other panels, the critical region is between 172° E and 177° W, which is in nearly the same location as in the control forecast (Fig. V-24a). In both the control forecast and the Bing-NW simulation, a 500-mb trough is northwest of the storm. Whereas the storm in the control forecast is predicted to be beneath a 500-mb PVA maximum $> 50 \times 10^{-10} \text{ s}^{-2}$, the Bing-NW storm is beneath weaker 500-mb PVA (compare Fig. V-37b to Fig. V-24b). In the Bing-NW simulation, no well-defined jet streak is present, in contrast to the two distinct 110-kt jet streaks predicted in the control (compare Fig. V-37c to Fig. V-24c). Despite this, both cases

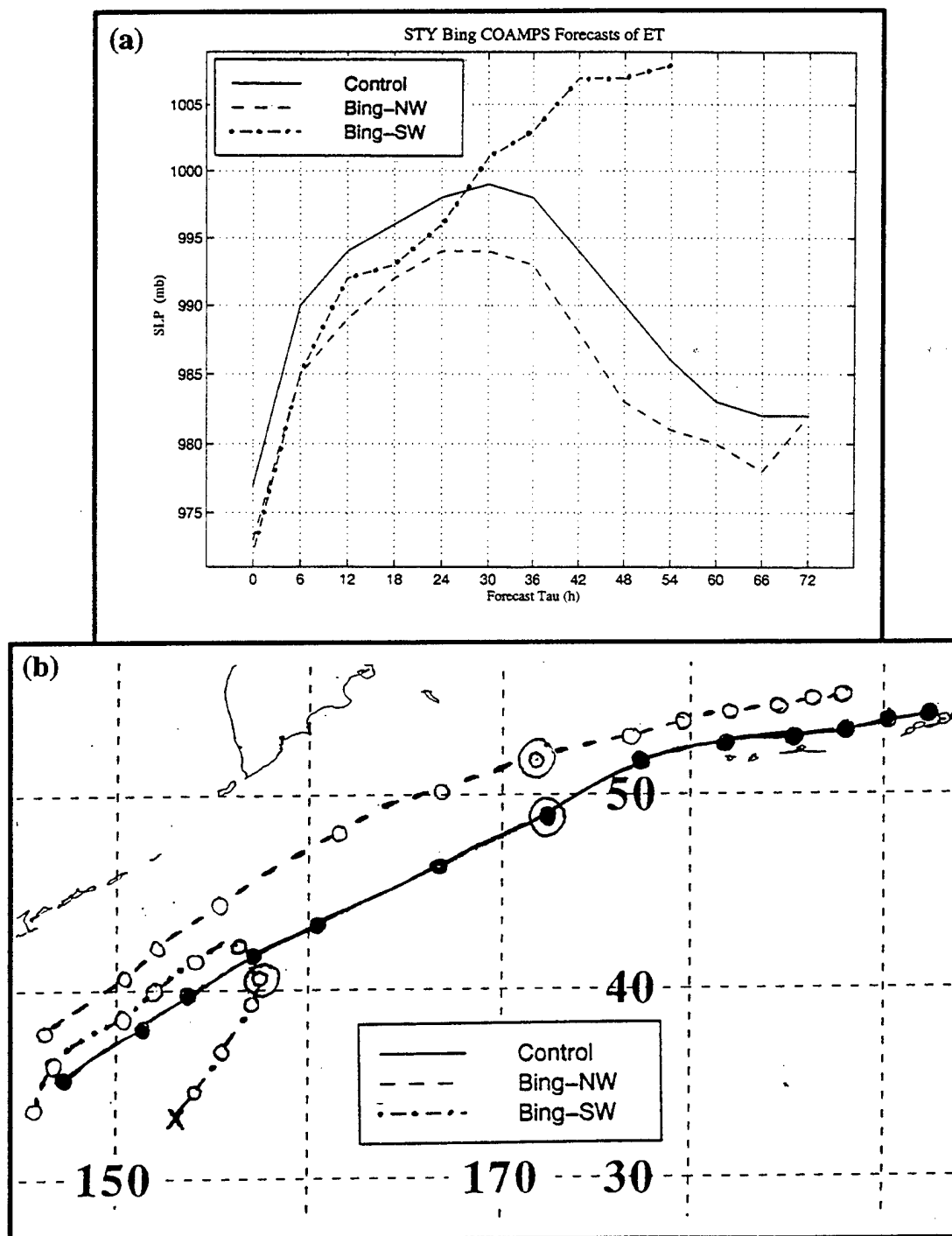


Fig. V-36. The control forecast and displaced-TC simulations in the case of STY Bing initialized at 0000 UTC 4 September 1997, depicting (a) the SLP of the storm in the control forecast, Bing-NW simulation, and Bing-SW simulation (interval 6 h), and (b) the storm tracks each 6 h for the control (solid, filled dots), Bing-NW (dashed, open circles) and Bing-SW (dashed-dot, open circles). The 36-h positions are circled for later discussion.

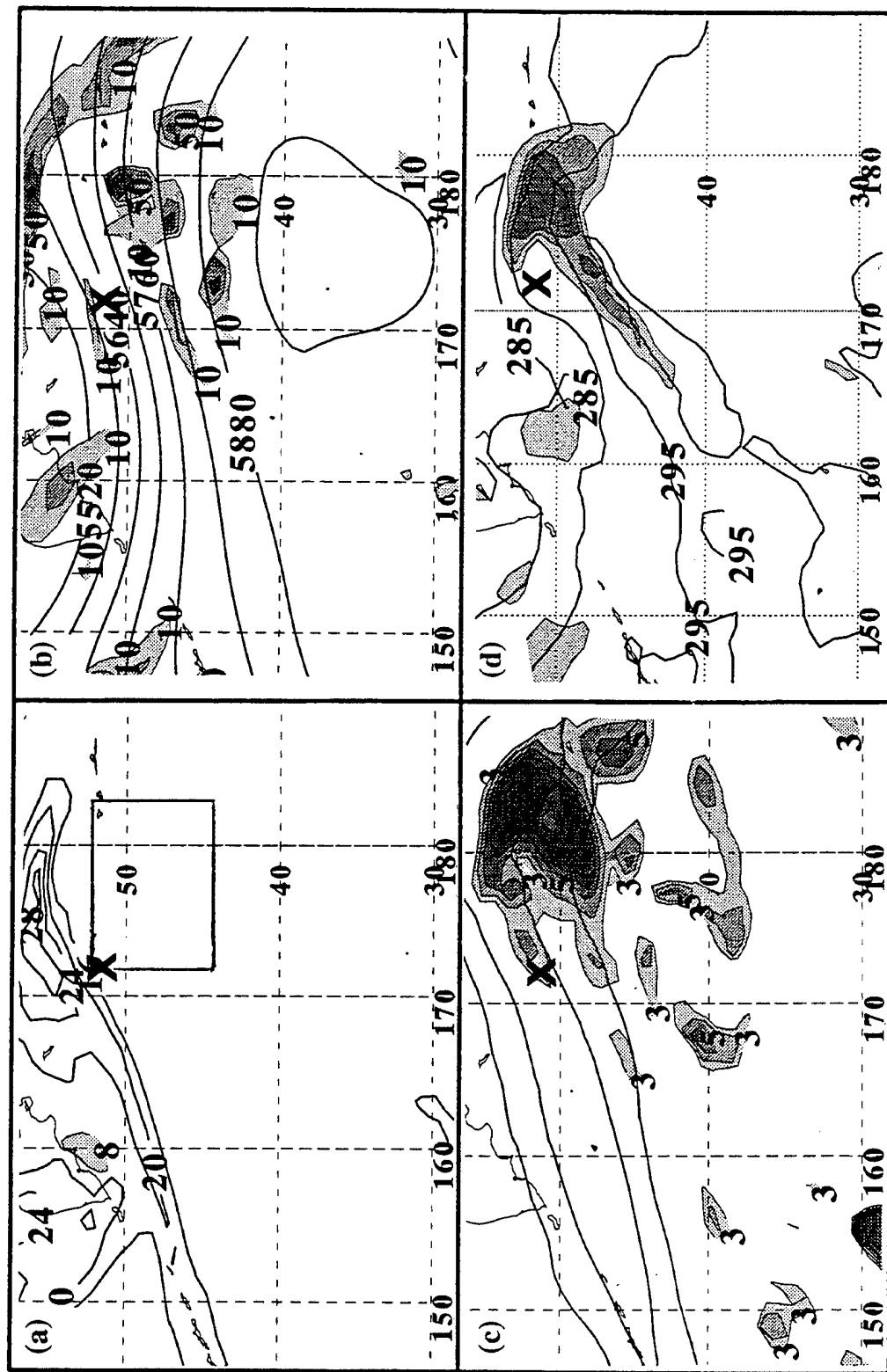


Fig. V-37. (a) Layer-averaged PV between 925 mb and 700 mb (shaded) and 500 mb to 300 mb (solid contours), (b) 500-mb isoheights and PVA, (c) 200-mb isotachs and divergence, and (d) 925-mb warm advection and isentropes of potential temperature as in Fig. V-15, except for 36-h interval of Bing-NW simulation initialized at 0000 UTC 4 September 1997. The critical region is depicted by a solid box in (a), and the storm location is denoted with an "X."

have 200-mb divergence $> 4 \times 10^{-5} \text{ s}^{-1}$ above and adjacent to the storm. The greatest difference between these two cases is a more equatorward intrusion of cold air in the lower troposphere in the Bing-NW case (notice the 285 K isentrope has progressed equatorward to 47° N near 166° E in Fig. V-37d, while that isentrope is not predicted to advance farther equatorward than 49° N in Fig. V-24d). As a result, the horizontal gradient of isentropes is greater near the Bing-NW storm than for the control storm (compare Fig. V-37d to Fig. V-24d along 170° E). Large ($> 50 \times 10^{-5} \text{ K s}^{-1}$) values of warm advection are found in both cases, although the warm advection is nearer to the storm center in the control forecast.

At 36 h in the Bing control forecast (Fig. V-38a), large shear and confluence term contributions to 900-mb frontogenesis $> 25 \times 10^{-10} \text{ K m}^{-1} \text{ s}^{-1}$ are in an east-west oriented swath, with the confluence term maximum about 200 n mi east of the storm center, and the shear term maximum west of and adjacent to the storm center. A vertical south-north cross section through the center of the storm (Fig. V-38b) of potential temperature and vertical motion suggests that this lower-tropospheric frontogenesis contributes to ascent along tilted isentropic surfaces with a maximum 400 mb value $> 25 \times 10^{-3} \text{ mb s}^{-1}$ about 60 n mi north of the storm center.

At 36 h in the Bing-NW simulation, both the shear and confluence terms are forecast to be frontogenetic (Fig. V-39a) and $> 25 \times 10^{-10} \text{ K m}^{-1} \text{ s}^{-1}$ as in the control. A larger shear term contribution is predicted southwest of the Bing-NW storm. This lower-tropospheric frontogenesis is believed to be responsible for the ascent maximum between

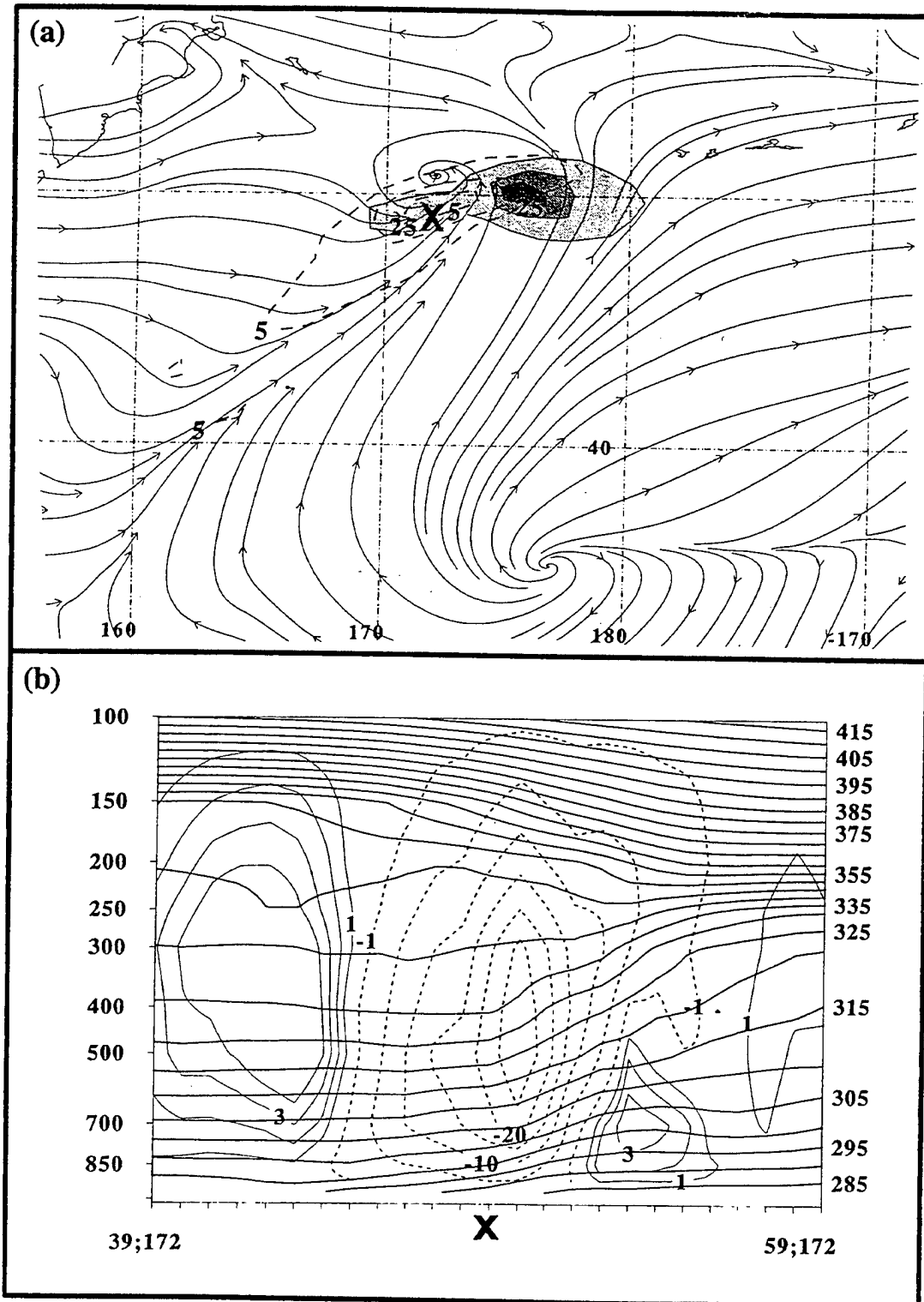


Fig. V-38. (a) Streamlines and frontogenesis (interval $10 \times 10^{-10} \text{ K}/(\text{m s})$ beginning with the $5 \times 10^{-10} \text{ K}/(\text{m s})$ contour) at 900 mb with solid (dashed) contours depicting frontogenetic confluence (shear) term contributions at 36 h in the control forecast of STY Bing initialized at 0000 UTC 4 September 1997, and (b) vertical south-north cross-section of potential temperature (thick solid contours, 5 K interval) and COAMPS analyzed vertical motion with dashed (thin solid) contours depicting ascent (descent) at a $3 (1) \times 10^{-3} \text{ mb/s}$ interval.

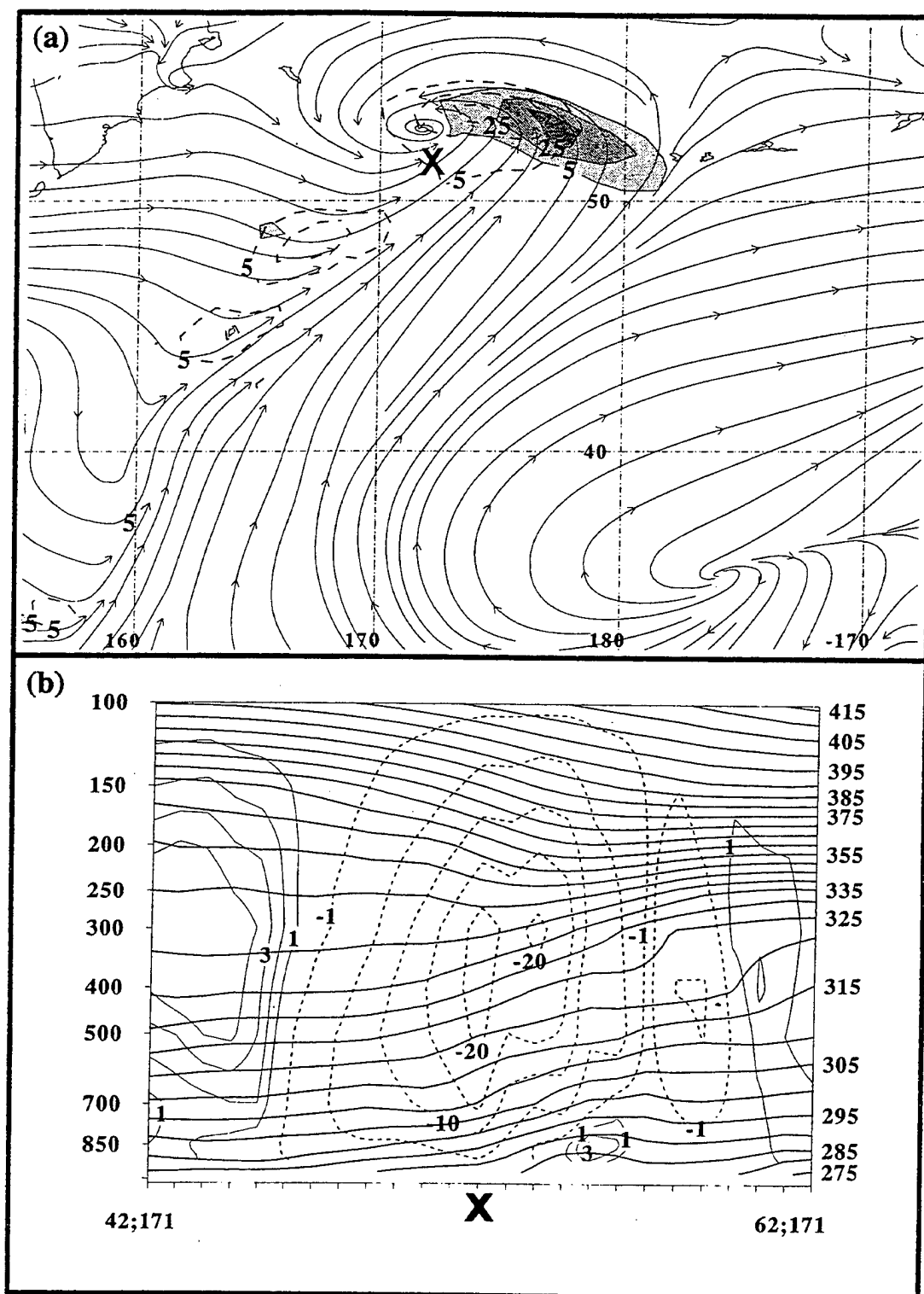


Fig. V-39. (a) Streamlines and frontogenesis (interval 10×10^{-10} K/(m s) beginning with the 5×10^{-10} K/(m s) contour) at 900 mb with solid (dashed) contours depicting frontogenetic confluence (shear) term contributions at 36 h in the Bing-NW simulation initialized at 0000 UTC 4 September 1997, and (b) vertical south-north cross-section of potential temperature (thick solid contours, 5 K interval) and COAMPS analyzed vertical motion with dashed (thin solid) contours depicting ascent (descent) at a $3 (1) \times 10^{-3}$ mb/s interval.

500 and 400 mb above the storm center (Fig. V-39b) that is about 5 units smaller than in the control, but is directly over the storm center.

Although the differences between the control and the Bing-NW simulation are subtle, the lower troposphere appears to be more favorable for Petterssen Type-B extratropical cyclogenesis in the Bing-NW simulation. The cyclone in the Bing-NW simulation translates more poleward and westward compared to the control (Fig. V-36b) and thus was closer to the 500-mb trough to the northwest and its associated lower-tropospheric baroclinity. Thus, the interaction of the Bing-NW cyclone and the mid-latitude circulation is forecast to produce greater values of lower-tropospheric baroclinity. Otherwise, the critical regions in the control and the Bing-NW simulations are nearly the same. The Bing-NW cyclone achieves a deep re-intensification, but is only 4 mb deeper than the control at the end of ET, just as it was at the initial time.

In a third simulation, the initial vortex is displaced two gridpoints equatorward and one gridpoint west (about 120 n mi to the southwest; hereafter referred to as Bing-SW) so that it would not phase with the critical region, which according to the hypothesis should cause the storm to re-intensify less than in the control. The TC in the Bing-SW simulation is again 4 mb deeper than the control at the initial time (Fig. V-36a). However, the Bing-SW storm steadily filled so that after 24 h it is not as deep as the control storm, and it dissipated by 54 h. For the first 30 h, the Bing-SW storm translates east-northeastward as in the control, but it turns sharply equatorward at 30 h (Fig. V-35b) as it begins to dissipate. At 36 h in the Bing-SW simulation, the storm is at 41° N, 159° E. Although a lower-tropospheric PV maximum > 8 units is predicted at the Bing-SW storm center, this

maximum is far upstream of the critical region (Fig. V-40a). The 500-mb PVA value above the storm is less than $10 \times 10^{-10} \text{ s}^{-2}$ (Fig. V-40b). Similarly, only weak 200-mb divergence (Fig. V-40c) is above the Bing-SW cyclone, which thus never couples with the critical region downstream and dissipates 18 h later (not shown).

A second region of lower-tropospheric $PV > 8$ units is predicted at 50° N , 169° E , which is near the location of the storm at 36 h in the control forecast. Thus, a separate extratropical cyclogenesis is forecast to begin at this location at 36 h in the Bing-SW simulation. This incipient cyclone is already in the critical region (Fig. V-40a), where $PVA > 50 \times 10^{-10} \text{ s}^{-2}$ (Fig. V-40b) and 200-mb divergence $> 7 \times 10^{-5} \text{ s}^{-1}$ (Fig. V-40c) is above lower-tropospheric warm advection $> 30 \times 10^{-5} \text{ K s}^{-1}$ (Fig. V-40d). This cyclone deepens 25 mb in 36 h to 982 mb and is at 50° N , 169° W at 72 h (not shown), which is the same intensity as, and is only 1° long. west of, the storm at 72 h in the control forecast.

Recall that in the Bing no-TC simulation (Fig. V-22) anticyclogenesis is predicted at 36 h. In the Bing-SW simulation, the Bing remnants dissipate and thus are not predicted to complete ET. Nevertheless, the Bing-SW remnants interacted with the mid-latitude circulation pattern such that the 200-mb jet streak is more sharply curved (notice at 170° E in Fig. V-40c that the long axis of the jet streak is 4° lat. poleward of that in Fig. V-23c), and is larger in areal extent than in the no-TC simulation. As a result, a 200-mb divergence maximum > 7 units is predicted at 170° E rather than farther east at 176° W . Furthermore, the interaction of the TC with lower-tropospheric baroclinity is forecast to produce warm advection > 30 units as far west as 162° E (compare Fig. V-40d versus Fig. V-23d). Thus, a critical region is predicted (Fig. V-40a) and a separate extratropical

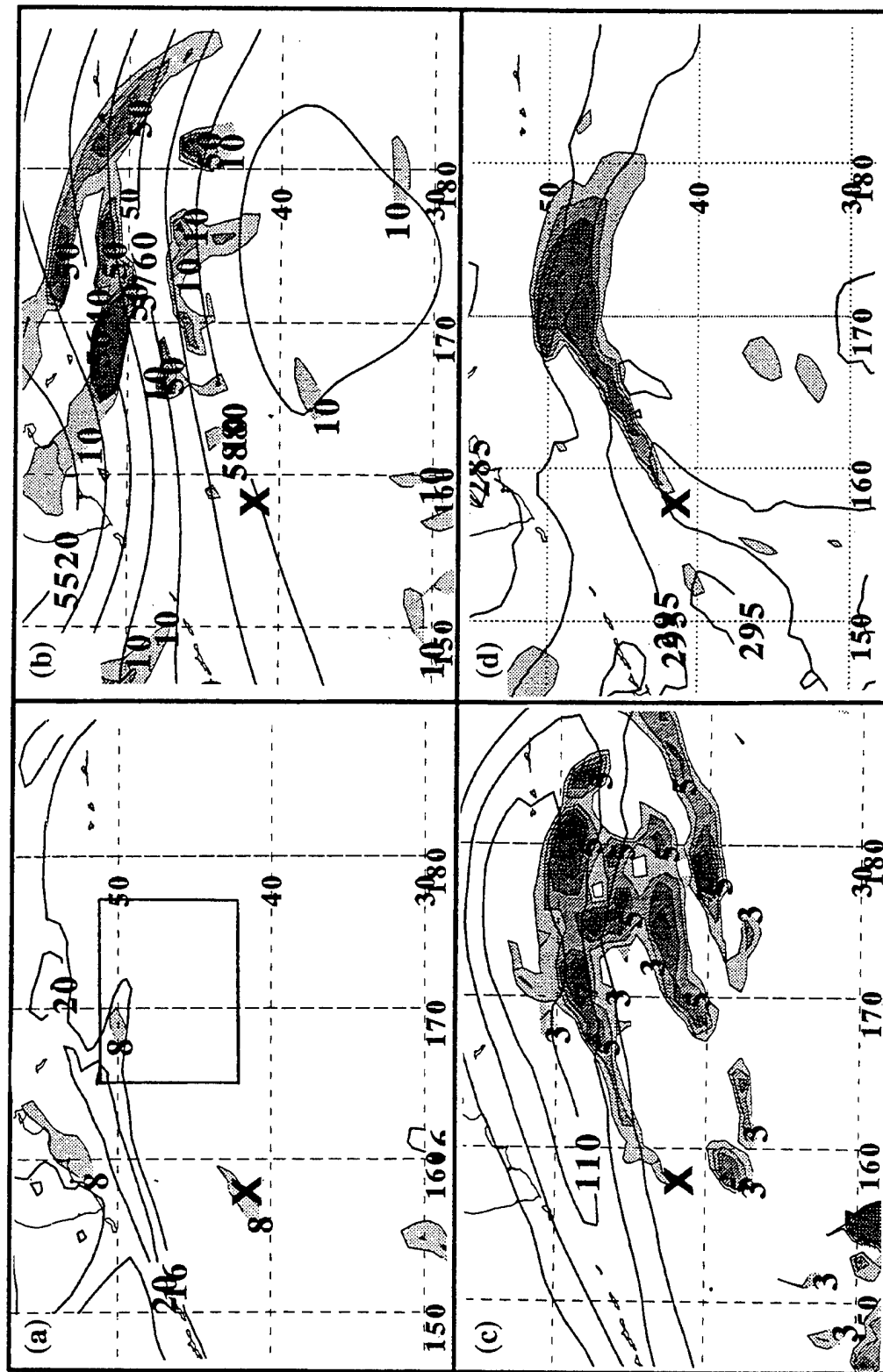


Fig. V-40. (a) Layer-averaged PV between 925 mb and 700 mb (shaded) and 500 mb to 300 mb (solid contours), (b) 500-mb isoheights and PVA, (c) 200-mb isotachs and divergence, and (d) 925-mb warm advection and isentropes of potential temperature as in Fig. V-36, except for Bing-SW simulation.

cyclogenesis is initiated northeast of the Bing-SW remnants that dissipate and fail to complete ET.

In summary, a simulation in which the initial vortex is displaced downstream as in the case of STY Ginger to couple more optimally with the critical region does produce an ET with a deeper SLP than the control storm. As in the cases of STY Bart and STY Ginger, the deepest re-intensification is predicted when the storm is displaced so that it is closer to the 500-mb trough to the northwest so that it interacts optimally with the lower-tropospheric baroclinity associated with that trough. However, the STY Bing cyclone does not couple with the upstream upper-tropospheric PV as do the cyclones in the Bart-SW and Ginger-SW simulations. Rather, the 500-mb height contours in the Bing control forecast and in the Bing-NW and -SW simulations more closely resemble the northeast pattern (Harr et al. 2000; compare Figs. V-24b, V-37b, and V-40b with Fig. I-2b). The Bing control forecast and Bing-NW simulation are predicted to translate quickly downstream and as a result come into phase with a critical region downstream, as discussed earlier in the ET of STY Oscar (Fig. V-6). Thus, the cyclone in the Bing-NW simulation resembled the ET of TY Orson (September 1996), which did re-intensify to 975 mb despite translating into a northeast pattern.

Displacement of the initial Bing vortex to the southwest results in dissipation and a track reversal so that the storm does not couple with the critical region downstream. However, a separate cyclogenesis is initiated at 36 h within that critical region (Fig. V-40). The resulting cyclone actually translates along a similar track as the storm in the control

forecast, although with a slight lag (not shown). At the end of the simulation, the separate cyclone is in nearly the same place, and achieves the same SLP, as the control cyclone.

As in the cases of STY Bart and STY Ginger, the phasing of STY Bing with the mid-latitude circulation pattern determines whether or not the TC enters or interacts optimally with a critical region. As the TC translates into the mid-latitude circulation pattern, its interaction with a 500-mb trough and its associated lower-tropospheric baroclinity also changes the location of the 200-mb divergence maximum and the maximum lower-tropospheric baroclinity, and thus ultimately where the critical region is found.

4. Discussion of Other Displaced-TC Simulations

The results of the control and displaced-TC forecasts that were completed in this study are summarized in Appendix B. Displacements of the initial vortex in the cases of TY David (mid-latitude circulation favorable) and TY Rex (mid-latitude circulation neutral) results in the cyclone re-intensifying more (less) than the control storm if its phasing with the critical region is more (less) optimal. In the case of TY David, displacing the initial vortex two gridpoints poleward and one gridpoint to the east (about 120 n mi northeastward) produces a more optimal coupling with the critical region so that the cyclone completes ET 6 h earlier and with a final SLP 3 mb deeper than the storm in the control forecast. Displacing the initial vortex two gridpoints equatorward and one gridpoint to the west (about 120 n mi southwestward) results in a dissipation, although a separate cyclogenesis occurs northeast of the David remnants. Similarly, displacing the initial TY Rex vortex two gridpoints poleward and one gridpoint to the east (120 n mi

northeastward) and two gridpoints equatorward and one gridpoint to the west (120 n mi southwestward) results in a more optimal phasing with a critical region, so that the cyclone achieves a minimum SLP = 3 mb and 12 mb deeper than the control storm, respectively. By contrast, displacing the initial vortex five gridpoints equatorward and five gridpoints to the west (about 400 n mi southwestward) prevents the cyclone from entering the critical region and results in only a moderate re-intensification with a final SLP 5 mb higher than the control storm.

An extreme test of the mid-latitude circulation superposition hypothesis is also attempted in which an initial TC vortex that dissipated in the control forecast is displaced an unreasonable distance to achieve re-intensification within a remote critical region identified in the control forecast. Based on the definitions presented earlier in this Chapter, the mid-latitude contribution in the case of STY Oliwa is classified as neutral. At the initial time of the control forecast of STY Oliwa, the storm had a SLP of 990 mb (Fig. V-41a). Over the next 24 h, the storm fills steadily as it translates over Japan (Fig. V-41b) and dissipates. During this time, no critical region is predicted in the control forecast (not shown). However, a critical region between 140° E and 150° E is predicted 12 h after Oliwa dissipates (Fig. V-42a). A separate cyclogenesis (marked "X" in Fig. V-42a) is forecast to be initiated adjacent to this critical region, in which the 500-mb PVA > 50 units (Fig. V-42b), the 200-mb divergence > 7 units (Fig. V-42c), and the lower-tropospheric warm advection > 30 units (Fig. V-42d).

STY Oliwa is thus displaced six gridpoints poleward and four gridpoints to the west (a northwestward displacement of 420 n mi) in order to phase with the critical region

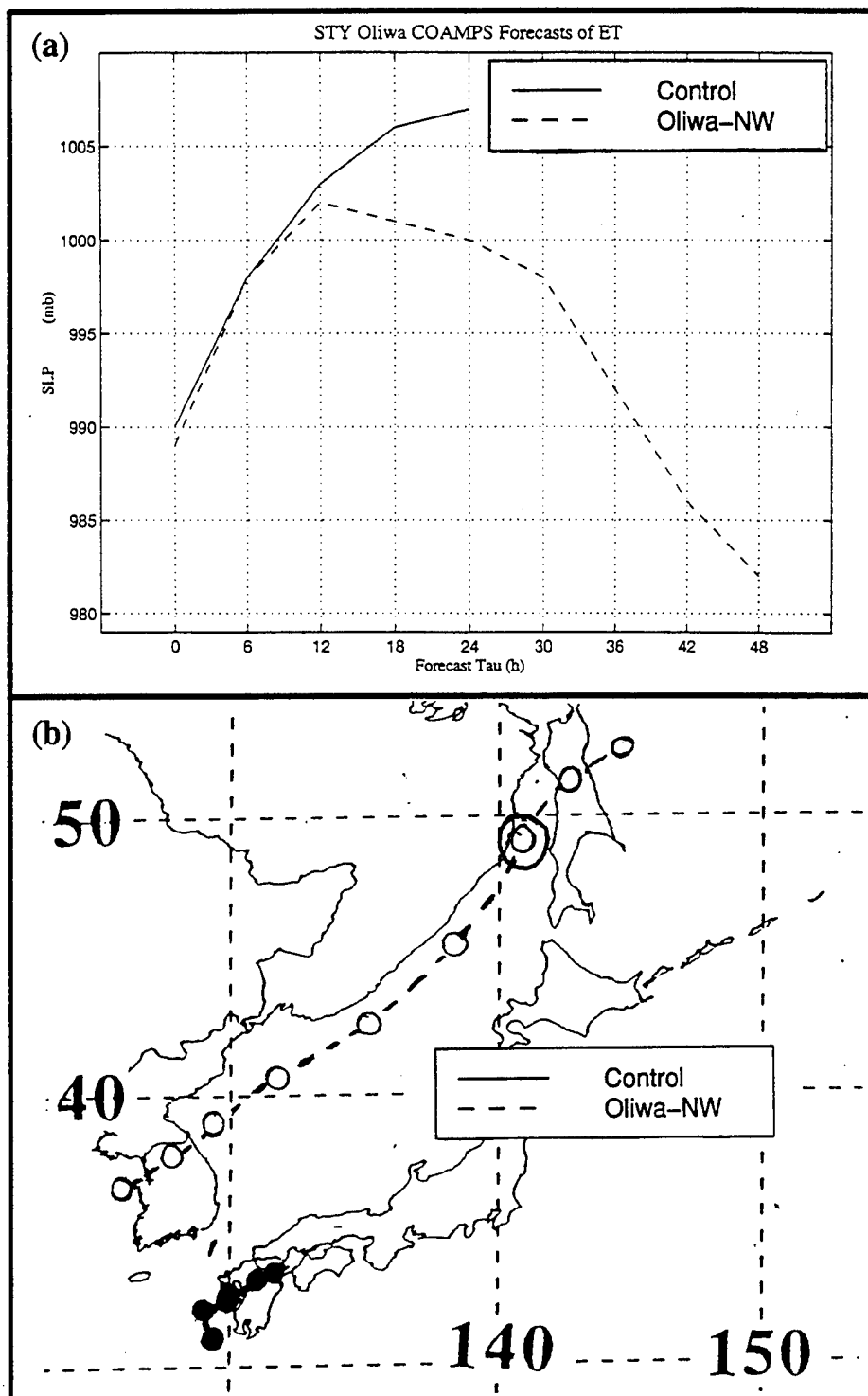


Fig. V-41. As in Fig. V-25, except for the case of STY Oliwa initialized at 0000 UTC 16 September 1997, depicting (a) the SLP of the storm in the control forecast, and Oliwa-NW simulation (interval 6 h), and (b) the storm tracks each 6 h for the control (solid, filled dots) and Oliwa-NW (dashed, open circles). The 36-h position of Oliwa-NW is circled for later discussion.

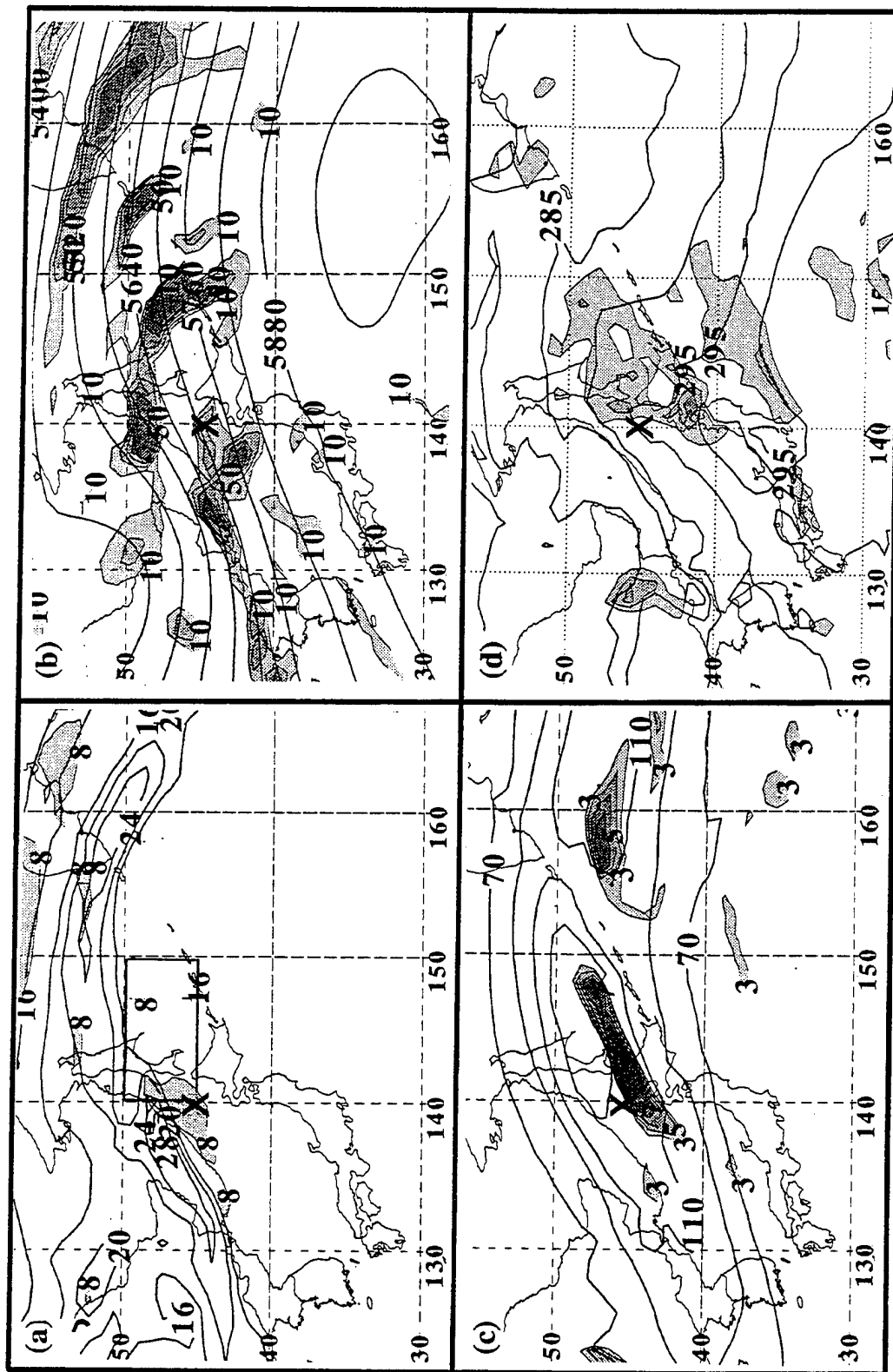


Fig. V-42. (a) Layer-averaged PV between 925 mb and 700 mb (shaded) and 500 mb to 300 mb (solid contours), (b) 500-mb isoheights and PVA, (c) 200-mb isotachs and divergence, and (d) 925-mb warm advection and isentropes of potential temperature as in Fig. V-15, except for 36-h interval of Oliwa control forecast initialized at 0000 UTC 16 September 1997. The critical region is depicted by a solid box in (a), and the location of a separate cyclogenesis is denoted with an "X."

predicted in the control forecast (hereafter referred to as Oliwa-NW). In the Oliwa-NW simulation, the transforming storm at the initial time is at 37° N, 125° E (Fig. V-41b) and is 2 mb deeper than the control storm (Fig. V-41a). The Oliwa-NW storm is forecast to complete the transformation stage 12 h later, during which time it fills at a similar rate as did the control storm. At 12 h, the Oliwa-NW cyclone begins to re-intensify (Fig. V-41a) as it translates northeastward (Fig. V-41b) toward where the critical region is in the control forecast. A period of rapid deepening is forecast between 30 h and 42 h in the Oliwa-NW simulation, and the storm eventually deepens to 982 mb at 48 h, at which time the storm is at 53° N, 144° E (Fig. V-41).

At 36 h in the Oliwa-NW simulation, the storm is predicted to be in a critical region (Fig. V-43a) that is 3° lat. poleward of the one in the control forecast (Fig. V-41a). The other significant differences between the Oliwa-NW simulation and the control forecast include the upper-level PV maximum > 32 units above the cyclone (Fig. V-43a), the polar jet streak and 200-mb divergence are farther poleward (Fig. V-43c), and larger values of lower-tropospheric warm advection (Fig. V-43d) are predicted in the Oliwa-NW simulation. The cyclone in the Oliwa-NW simulation is forecast to remain in the critical region (not shown) and complete ET after a moderate re-intensification to 982 mb (Fig. V-41a).

In the Oliwa-NW simulation, the initial position of the vortex was altered extremely so that the storm would translate in phase with a critical region in the mid-latitude circulation pattern. This simulation is successful in that the storm rapidly deepened to 982 mb instead of dissipating as in the control forecast. In this sense, the initial TC

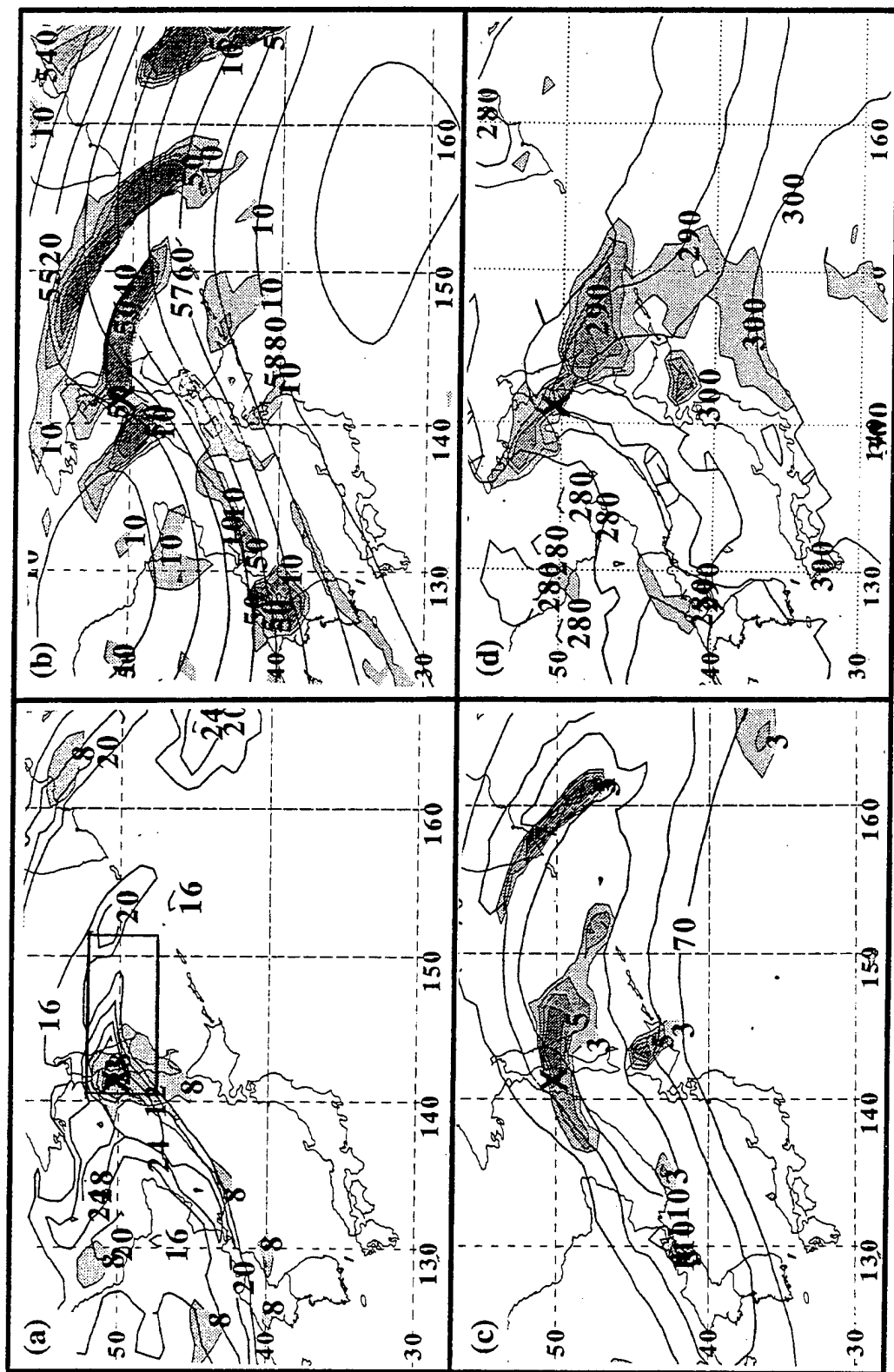


Fig. V-43. (a) Layer-averaged PV between 925 mb and 700 mb (shaded) and 500 mb to 300 mb (solid contours), (b) 500-mb isoheights and PVA, (c) 200-mb isotachs and divergence, and (d) 925-mb warm advection and isentropes of potential temperature as in Fig. V-41, except for 36-h interval of Oliwa-NW simulation initialized at 0000 UTC 16 September 1997. The critical region is depicted by a solid box in (a), and the storm location is denoted with an "X."

vortex can be displaced and deepened consistent with the hypothesis presented in Chap. V-B. Although the critical region at 36 h is farther equatorward in the control forecast, it still provides guidance as to how (the direction) the initial vortex must be displaced to achieve a phasing with the mid-latitude circulation to achieve a re-intensification rather than a dissipation. That is, the vortex displacement in the Oliwa-NW simulation is predicted to result in a phasing and interaction with the northwest pattern. It is of interest that the vortex displacement also shifts the location of the 200-mb divergence maximum and the maximum lower-tropospheric baroclinity, and therefore the critical region, as demonstrated in the forecasts of STY Bart, STY Ginger, and STY Bing.

5. Discussion of TC Contributions to the Re-Intensification Stage of ET

In the previous discussion, it was demonstrated that displacement of the vortex at the initial time of the forecast in the cases of STY Bart, STY Ginger, TY Bing, and STY Oliwa altered the phasing of the translating TC with the evolving mid-latitude circulation pattern so that their interaction later in the forecast was also different. Specifically, the altered phasing determined the location of maximum upper-tropospheric divergence and strongest lower-tropospheric baroclinity, and thus the location of the critical region. In some of these simulations, the TC phased with this critical region and achieved deep re-intensification after the initial displacement (Appendix B). In other simulations with different displacements, the TC failed to phase with the critical region and either achieved moderate or little re-intensification (if there was at least some upper-tropospheric divergence, mid-level PVA and lower-tropospheric baroclinity) or dissipated (Appendix B).

Insight as to *how* the TC displacement might phase with and interact with the mid-latitude circulation pattern so as to shift the location of upper-level divergence and a local maximum of lower-tropospheric baroclinity is offered using the conceptual model of the transformation stage (Fig. III-18) that sets the conditions preceding the re-intensification stage. In particular, comparison of the Ginger-SW simulation and the Ginger no-TC simulation will be used to describe specific TC contributions to the re-intensification stage of ET that arise from optimal phasing of the TC with the critical region in the mid-latitude circulation pattern.

Klein (1997) hypothesized that the interaction of the warm, upper-tropospheric outflow of a TC with a downstream polar jet streak would improve the upper-tropospheric support for Petterssen "Type-B" extratropical cyclogenesis during the re-intensification stage. The warm, upper-tropospheric outflow and TC warm core in a mature TC raise the height of the tropopause (notice the isentropes above 200 mb in Fig. I-3a) as the TC translates poleward. At Step 2 of transformation, the upper-tropospheric TC warm core is dispersed downstream by vertical shear, and by Step 3 only a residual warm core remains in the mid-troposphere (Fig. III-18). If the phasing of the TC and the mid-latitude circulation pattern during ET is optimal, advection of this warm upper troposphere raises the tropopause adjacent to the downstream polar jet maximum, which increases the wind speed in the jet maximum and also results in increased divergence in the equatorward entrance region of the jet.

The Ginger-SW cyclone completes Step 3 of the transformation stage by 24 h, and as in the NOGAPS analysis of TY David (Fig. V-16a), the dispersal of the upper-

tropospheric warm core downstream of the Ginger-SW storm center at 24 h (Fig. V-44a) raises the tropopause northeastward of the storm above 150 mb. Based on the path of a Vis5D trajectory that originates in this warm upper troposphere (marked "O" at about 348 K) and moves northeastward (Fig. V-44b), the remnants of the TC warm core are advected downstream in 12 h to 178° E by the upper-level winds while the storm translates north-northeastward (Fig. V-31b).

Recall that at 36 h in the Ginger no-TC simulation, a divergence maximum $> 3 \times 10^{-5} \text{ s}^{-1}$ is near 39° N, 168° E (Fig. V-20d), and is associated with the equatorward entrance region of a 250-mb jet streak of 60 m/s near 47° N, 178° E (Fig. V-45a). In the Ginger-SW simulation, a divergence maximum $> 8 \times 10^{-5} \text{ s}^{-1}$ is near 48° N, 169° E, and is associated with the equatorward entrance region of a 250-mb jet streak at 80 m s^{-1} near 56° N, 178° E (Fig. V-45b). At 36 h in the Ginger-SW simulation, advection of the upper-tropospheric warm core remnants over the previous 12 h (Fig. V-44b) has warmed the 500 mb - 150 mb layer to the southeast of the jet along 49° N, so that the 345 K, 340 K, and 335 K isentropes are 100 mb, 150 mb, and 100 mb lower, respectively, in the Ginger-SW simulation than in the control (compare Fig. V-45b with Fig. V-45a). As a result, the meridional gradient of the isentropes beneath the jet maximum is greater in the Ginger-SW simulation at 36 h, which according to the thermal wind relationship is consistent with the Ginger-SW jet maximum being 20 m s^{-1} higher than in the control forecast. This increase in the jet maximum is believed to produce the 200-mb divergence maximum in the equatorward entrance region of the jet streak in the Ginger-SW

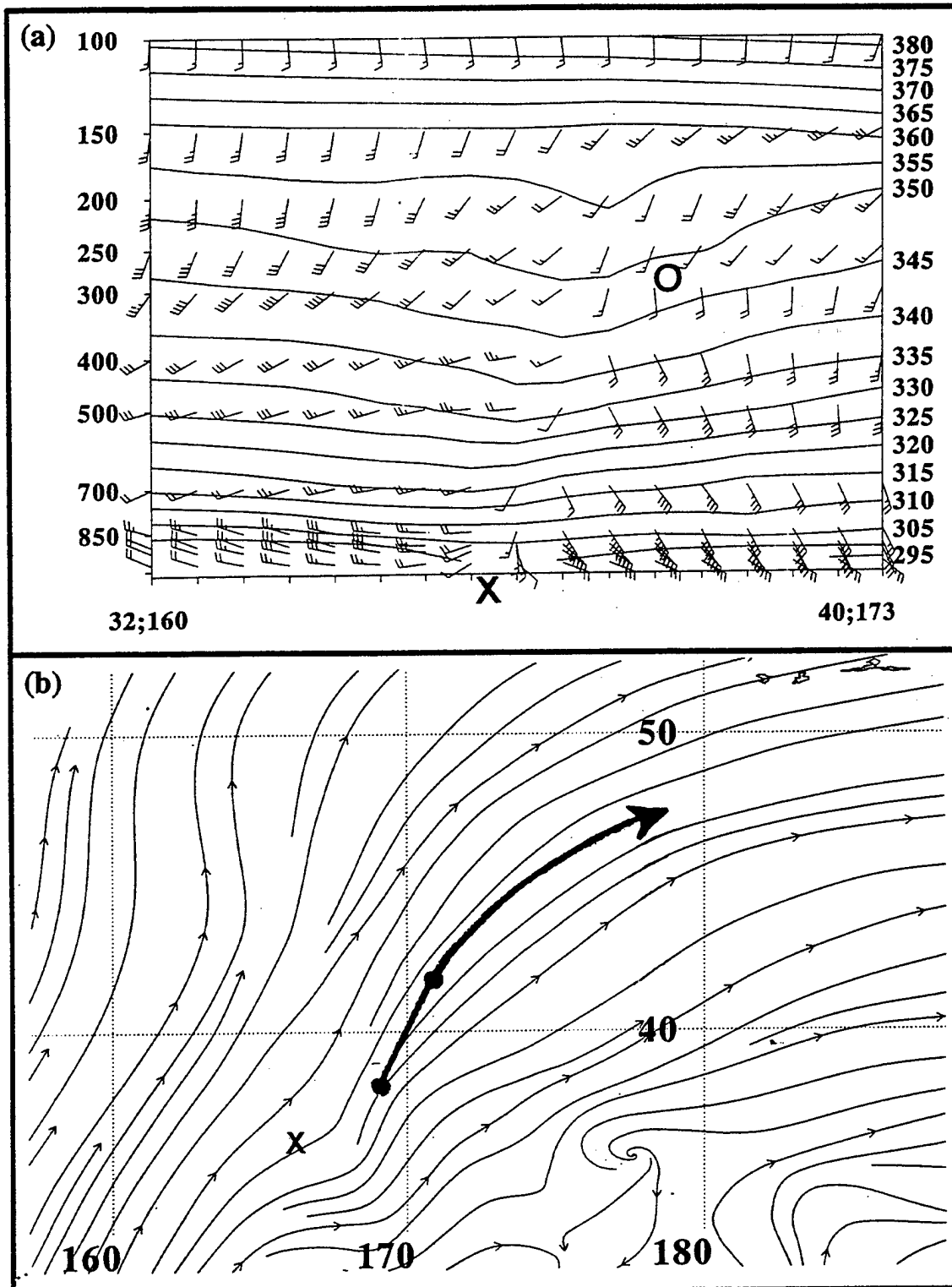


Fig. V-44. (a) Vertical southwest-northeast cross-sections of potential temperature (solid, 5 K interval) and wind (full barb = 10 m/s) and (b) 200-mb streamlines (thin solid) at 24 h in the Ginger-SW simulation initialized at 1200 UTC 29 September 1997. A plan view Vis5D trajectory from 24 h to 36 h (heavy solid line, 6 h intervals) is depicted in (b). The location of the storm center is denoted with an "X," and the starting location of the Vis5D trajectory is marked "O" in (a).

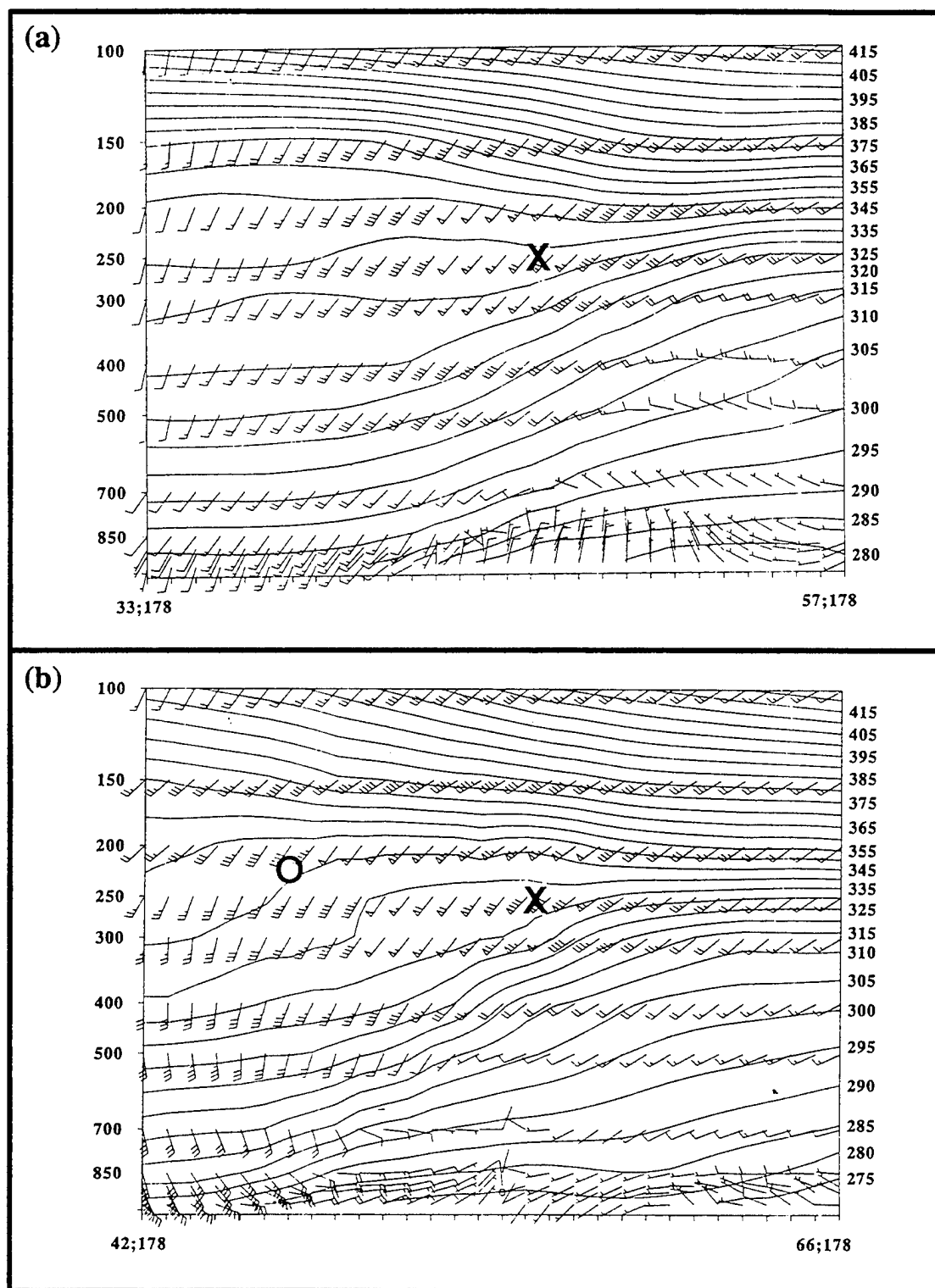


Fig. V-45. Vertical south-north cross-sections of potential temperature (solid, 5 K interval) and wind (full barb = 10 m/s) at 36 h in the (a) STY Ginger control forecast and (b) Ginger-SW simulation initialized at 1200 UTC 29 September 1997. The location of the jet maximum is denoted with an "X" and the endpoint of the Vis5D trajectory in Fig. V-44b is marked "O" in (b).

simulation (Fig. V-31d) that is more than double the value in the Ginger no-TC simulation (Fig. V-20d).

The phasing of the TC with the critical region also determines the type of interaction with the lower-tropospheric baroclinic zone. During the transformation stage (see conceptual model in Fig. III-18 and the discussion of the transformation of TY David in Chap. III), the TC vortex moves poleward into the pre-existing lower-tropospheric baroclinic zone such that cold (warm) advection is initiated west (east) of the storm, and the horizontal gradient of isentropes is increased (Fig. III-14). As the TC progresses farther into this baroclinic zone, this lower-tropospheric temperature advection and horizontal gradient of isentropes are increased further, and the baroclinic zone is rotated cyclonically so that the orientation of the trailing baroclinic zone is more southwest-to-northeast. Therefore, the interaction of the TC and the baroclinic zone during the transformation stage results in a lower troposphere that is already optimal for Petterssen Type-B extratropical cyclogenesis. By contrast, a decayer (STY Ivan) that moves more zonally and produces only a weak dipole of temperature advection, and does not interact with the lower-tropospheric baroclinity so that the horizontal isentropes gradient does not increase, does not have an optimum baroclinic zone orientation for re-intensification. Harr and Elsberry (2000) show that this change in the orientation of the baroclinic zone is due to rotational frontogenesis. Furthermore, this rotational frontogenesis depends on the relative orientation of the horizontal isentropes gradient to the gradient of vertical motion and the relative vorticity pattern. Thus, it is proposed that in the phasing of a TC with the mid-latitude lower-tropospheric baroclinity during ET, a more meridional (zonal) storm

track is more (less) optimal in its interaction with the pre-existing lower-tropospheric baroclinic zone in contributing to the re-intensification.

More favorable conditions in the lower troposphere for extratropical cyclogenesis are predicted in cases where the transforming storm has the most meridional translation. As an example, the Ginger-SW cyclone has a more meridional track after 24 h (Fig. V-31b) than the control storm. As a result of its phasing and interaction with the mid-latitude circulation pattern, the Ginger-SW cyclone produces larger values of 925-mb warm advection, a tighter horizontal gradient of isentropes, and a greater meridional deflection of the baroclinic zone than in the control forecast or Ginger-NE simulation (compare Fig. V-32d versus Fig. V-21d and Fig. V-35d). This is consistent with the interpretation of Harr and Elsberry (2000), who illustrate the relationships between rotational and scalar frontogenesis through the relative orientations of the isentropes gradient, vertical motion gradient, and the deformation.

In agreement with the mid-latitude circulation superposition hypothesis, the primary contribution of the TC to the re-intensification stage of ET is still determined by its phasing with the mid-latitude circulation. Specifically, optimal phasing results in an interaction between the TC and its environment that alters upper-tropospheric divergence and lower-tropospheric baroclinity to create or make more favorable the critical region in which the storm re-intensifies. The key point is that the critical region location is not determined solely by the mid-latitude circulation evolution, but that the TC outflow interacting with the jet streak, and the lower-tropospheric baroclinic zone modification by superposing the TC circulation, alters the critical zone location. This characterization of

the TC contribution is the basis for comparison of the control forecast to the no-TC and displaced-TC simulations so that the TC contribution in every case can be assigned in a matrix similar to Fig. V-8 as defined in Chap. V-B-2.

6. Summary of Displaced-TC Simulations and Characterization of the TC Contribution in Each

In Fig. V-8, a matrix is presented of possible outcomes resulting from a combination of mid-latitude and TC contributions to the re-intensification stage of ET. Recall that mid-latitude contributions are determined based on the no-TC simulations as discussed in Chap. V-D. The primary TC contribution is already described as the phasing of the TC with a critical region present in the mid-latitude circulation pattern. Therefore, in these nine cases, the TC contribution is determined first by whether the TC phased with a critical region in the control forecast. In displaced-TC simulations in which the phasing of the TC and the critical region are different from in the control forecast, the location of the critical region is sensitive to the upper-tropospheric divergence maximum that results from the juxtaposition with the polar jet of the warm, upper-tropospheric outflow and dispersed TC warm core that is advected downstream (Chap. V-E-5). The interaction of the transforming TC with a pre-existing mid-latitude baroclinic zone is also sensitive to the translation of the TC, so that a more (less) meridional track results in a more (less) optimal lower troposphere for Petterssen Type-B extratropical cyclogenesis. Thus, the TC contribution to the re-intensification stage is further evaluated based on these specific interactions of the TC in the control forecast with the polar jet and lower-tropospheric baroclinity in the mid-latitude circulation pattern.

MID-LATITUDE CONTRIBUTIONS				
RE-INT STAGE OF ET	TC CONTRIBUTIONS	UNFAVORABLE	NEUTRAL	FAVORABLE
		↑ STY BING (NE) ----- ↓ STY BING (NE)	↑ TY REX (NW) ----- ↓ TY REX (NW)	↑ STY DAVID (NW) ----- ↓ STY BART (NW)
		↑ STY BING (NE)	↑ STY GINGER (NW) ----- ↓ STY OLIVA (NW)	↑ STY BART (NW)
		↑ TY TINA (NE)	↑ TY VICKI (NE)	↑ TY DAVID (NW) ----- ↓ TY STELLA (NE)

Fig. V-46. Characterizations of the mid-latitude circulation pattern and TC contributions to the re-intensification stage as in Fig. V-8, except for the COAMPS control forecasts and displaced-TC simulations of ET. An upward, solid (downward, dashed) arrow depicts a simulation in which the initial vortex in the control forecast is displaced so that it phases more (less) optimally with a critical region and deepens more (less) than the control storm. Cases are designated parenthetically as northwest (northeast) based on the definitions of Harr et al. (2000).

In Appendix B, the results of nine control forecasts and subsequent displaced-TC simulations are summarized. These nine cases are also categorized in the matrix in Fig. V-46 based on the mid-latitude and TC contributions in each during the re-intensification stage⁹. The case of TY David is categorized in Chap. V-D as a favorable mid-latitude contribution to re-intensification. In the TY David control forecast, the cyclone phases optimally with a critical region in the northwest mid-latitude circulation pattern (Chap. V-E-4 and Appendix B). As a result, its interaction with the polar jet is optimal and the cyclone couples with 200-mb divergence in the equatorward entrance region of the polar jet. Furthermore, TY David moves meridionally into the pre-existing baroclinic zone in the mid-latitude circulation during its transformation so that it interacts with the lower troposphere to help generate optimal conditions for Petterssen Type-B extratropical cyclogenesis. The TY David control cyclone achieves deep re-intensification, including a period of rapid deepening from 30 h to 48 h (Appendix B).

Displacement of TY David 120 n mi to the NE also results in a deep re-intensification, as the storm phases with a critical region in the northwest mid-latitude circulation pattern (Chap. V-E-4 and Appendix B). This interaction is more optimal than in the control because the storm advances farther poleward than in the control, so that in its interaction with the lower-tropospheric baroclinic zone and polar jet, somewhat larger values of warm advection and 200-mb divergence are predicted. This ET is also completed 6 h earlier (Appendix B) because the downstream displacement of the storm enables it to advance and phase with the critical region earlier than the control cyclone.

⁹ The meaning of the arrows depicted in Fig. V-46 will be discussed after the assignment of the TC contribution in each of the nine control forecasts studied.

These even more favorable mid-latitude and significant TC contributions for the David-NE case are represented in Fig. V-46 by an upward arrow that signifies more deepening of the central pressure.

Displacement of TY David 120 n mi to the southwest results in the dissipation of David, although with an initiation of a separate cyclogenesis to the northeast (Chap. V-E-4 and Appendix B) in the same location and forecast interval as in the David no-TC simulation. Moving the initial vortex to the southwest prevents it from interacting with the northwest mid-latitude circulation pattern so that it does not arrive in phase with 200-mb divergence and 500-mb PVA, and thus does not enter a critical region. Displacement of TY David farther equatorward in two more simulations (Appendix B) prevents the vortex from interacting with lower-tropospheric baroclinity so that no dipole of temperature advection is developed, and the storm dissipates without entering a critical region. In each case, a separate extratropical cyclogenesis is initiated to the northeast (Appendix B) in the same location and forecast interval as in the David no-TC simulation. These equatorward shifts of TY David are depicted in Fig. V-46 as a downward arrow, which represents that the mid-latitude circulation is favorable, but the TCs beginning in these equatorward positions no longer have a significant TC contribution to re-intensification. Specifically, the equatorward displacements of TY David to the southwest change the TC contribution to "none" since the TC fails to phase with the critical region, and a separate extratropical cyclogenesis occurs at the same location and interval as in the no-TC simulation. Thus, unlike the control forecast cyclone that achieves deep re-intensification, these cases do not re-intensify at all and decay.

Based on these results, the TC contribution to the re-intensification stage in the TY David control forecast is designated as *significant* (Fig. V-46). Even though the mid-latitude contribution is favorable and supports extratropical cyclogenesis in the absence of a TC (Chap. V-D), the location of the critical region and magnitudes of lower-tropospheric warm advection and 200-mb divergence in the critical region are modified by the interaction of the storm and its environment in the control forecast. That is, the cyclone in the control forecast couples in an optimal manner with the critical region and achieves deep re-intensification. Furthermore, the locations of the critical regions in the control forecast and displaced-TC simulations vary since maxima of lower-tropospheric warm advection and 200-mb divergence are sensitive to the location of the TC and move upstream (downstream) as the TC is displaced upstream (downstream). In the David-NE case, the displacement results in an even more optimum coupling, and a deeper re-intensification of the storm, than in the control forecast.

The results of the STY Bart control forecast and displaced-TC simulations are discussed in detail in Chap. V-E-1. Unlike the case of TY David, the cyclone in the STY Bart control forecast never enters a critical region in the mid-latitude circulation pattern (Fig. V-17). Thus, the Bart contribution to re-intensification is characterized in Fig. V-46 as being *minor*. However, the interaction between STY Bart and lower-tropospheric baroclinity and the polar jet is made more optimal by displacing STY Bart to the southwest (Fig. V-26, Appendix B), and less optimal by displacing it to the northeast (Fig. V-29, Appendix B).

In the Bart-SW simulation, the cyclone interacts optimally with the northwest mid-latitude circulation pattern, which alters the critical region location as well as the magnitude of 925-mb warm advection and 200-mb divergence. With this more optimum phasing with the critical region, the Bart-SW cyclone rapidly deepens to achieve deep re-intensification (Appendix B). Thus, an upward solid arrow in Fig. V-46 represents that the Bart-SW cyclone may be moved into the "significant" TC contribution category. The cyclone in the Bart-NE simulation does not change the assignment of a TC contribution of "minor," since the cyclone fails to phase with the critical region. Nevertheless, the location of the critical region in the Bart-NE simulation has been affected by the interaction of the storm with its environment (Fig. V-30).

In the case of TY Stella, the cyclones in the control forecast and displaced-TC simulations never couple with a critical region (Appendix B). In all of these forecasts of northeast ET cases, a separate extratropical cyclogenesis is initiated to the northeast in the same place at 36 h as in the no-TC simulation. Whereas the Stella control cyclone re-intensifies slightly, all of the displaced-TC cyclones dissipate (Appendix B). Other than the presence of the TC circulation, little difference is found in the outcome of the control forecast and the no-TC simulation. Therefore, the TC contribution to the re-intensification in the case of TY Stella is designated as *none* (Fig. V-46) for the control forecast and all displaced-TC simulations. Hypothetically, a displaced-TC that would have a proper phasing with the critical region in the control forecast would have more of a contribution to re-intensification (upward arrow in Fig. V-46). For the limited number of

displaced-vortex simulations attempted for the Stella case, this hypothesized displacement was not validated.

As in the case of TY David, the TY Rex control forecast cyclone is a northwest ET case that couples with the critical region to complete a deep re-intensification (Appendix B). Displacement of the initial vortex 120 n mi to the northeast produces a northwest ET case with an earlier and more optimal phasing with the critical region identified in the control forecast. As in the Bart-SW simulation, displacement of TY Rex 120 n mi or 240 n mi to the southwest results in northwest ET cases and the most optimal interactions with the lower-tropospheric baroclinic zone associated with a 500-mb short wave trough to the west and with the polar jet-induced divergence. In these southwest displacement simulations, the larger values of warm advection and 200-mb divergence are predicted, so that these cases achieve deeper re-intensifications, than either the Rex control forecast or the simulation in which the TY Rex initial vortex is displaced to the northeast. The upward arrow in Fig. V-46 represents that the already significant TC contribution in the control forecast can be made even more effective by these two southwestward displacements. If the TY Rex initial vortex is displaced even farther equatorward (Appendix B), the storm does not interact so optimally with the northwest mid-latitude circulation pattern because its phasing with the baroclinic zone and the polar jet is altered so that no warm advection > 10 units is predicted, and the storm does not couple with 200-mb divergence. Thus, the larger southwestward-displaced cyclone completes only a moderate re-intensification, which is represented in Fig. V-46 by a downward arrow that shifts the TC contribution from significant to minor.

Although the interaction of TY Rex and the mid-latitude circulation may be made more and less optimal than in the control forecast (as in the case of STY Bart), the cyclone in the control forecast did couple with a critical region and achieve deep re-intensification (as did TY David). Furthermore, only weak cyclogenesis is predicted in the no-TC simulation. As in the case of TY David, the location of the critical region in the control forecast and displaced-TC simulations is different from that in the no-TC simulation, since the maxima of lower-tropospheric warm advection and 200-mb divergence are sensitive to the location of the TC and move upstream (downstream) as the TC is displaced upstream (downstream). Thus, the TC contribution to the re-intensification stage is not a simple translation and superposition of a static critical region. Rather, this interaction between the TC remnants and the mid-latitude circulation is a dynamic process.

The results of the STY Ginger control forecast and displaced-TC simulations are discussed in detail in Chap. V-E-2, Chap. V-E-5, and summarized in Appendix B. As in the case of TY Rex, the cyclone in the STY Ginger control forecast is a northwest case that couples with a critical region and achieves deep re-intensification, while only weak cyclogenesis is predicted by the end of the no-TC simulation. Thus, the TC contribution to the re-intensification stage in the STY Ginger control forecast is designated as *significant* (Fig. V-46). All equatorward displacements of STY Ginger attempted (Appendix B) are also northwest cases that result in a more optimal interaction with the lower-tropospheric baroclinity associated with the 500-mb short-wave trough to the northwest and the polar jet. Therefore, the values of 925-mb warm advection and 200-mb

divergence exceed those predicted in the control forecast, and contribute to a deeper re-intensification. Since the equatorward displacements of STY Ginger result in a deeper re-intensification than in the already strong re-intensification in the control forecast, they are represented in Fig. V-46 as an upward arrow. As in the cases of TY Rex and TY David, displacement of STY Ginger to the northeast (Chap. V-E-2) results in a northwest case with more optimal phasing and a deeper re-intensification than in the control forecast, and this is also represented in Fig. V-46 by the upward arrow.

As in the cases of TY David and TY Rex, the location of the critical region in the control forecast and displaced-TC simulations is different from in the no-TC simulation. Maxima of lower-tropospheric warm advection and 200-mb divergence that define the critical region are again sensitive to the location of the TC and move upstream (downstream) as the TC is displaced upstream (downstream).

In the case of TY Vicki, the storm in the control forecast and each displaced-TC simulation is a northeast ET case that interacts weakly with the environment in a less than optimal phasing. That is, the storm does not couple with significant 200-mb divergence and undergoes only little re-intensification outside of the critical region (Appendix B). However, these re-intensifications are deeper than the weak extratropical cyclogenesis that is predicted in the Vicki no-TC simulation. Therefore, the TC contribution to the re-intensification stage of ET in the case of TY Vicki is designated as *minor* (Fig. V-46) for the control forecast and all displaced-TC simulations. Neither upward or downward arrows are included as the displacements attempted did not markedly change the re-intensification predicted in the control forecast.

In the case of STY Oliwa (Chap. V-E-4, Fig. V-42, and Appendix B), the storm in the control forecast is a northeast ET case that dissipates, and no critical region exists despite the interaction of the TC with the environment. Therefore, the TC contribution to the re-intensification stage of ET in the case of STY Oliwa is designated as *none* (Fig. V-46). However, a critical region is predicted after the storm dissipates (Fig. V-42a). In a hypothetical experiment with an extremely large displacement of the initial vortex to the northwest, the Oliwa-NW cyclone phases with the critical region (Fig. V-43) and rapidly deepens to achieve a moderate re-intensification (Appendix B) as a northwest ET case. Furthermore, the critical region is altered by its interaction with the Oliwa-NW cyclone (as described in Chap. V-E-4). Based on this extreme displacement simulation, the TC contribution of the Oliwa-NW simulation may be considered to be shifted from "none" to "significant" (upward arrow in Fig. V-46).

The STY Bing control forecast and displaced-TC simulations are northeast cases of ET that are discussed in detail in Chap. V-E-3. In the STY Bing control forecast (Fig. V-24), the cyclone phases with a critical region. Whereas the cyclone in the control forecast achieves only moderate re-intensification within that critical region, anticyclogenesis is actually forecast in the region of the (expected TC) position in the no-TC simulation (Fig. V-22). While no critical region is forecast in the no-TC simulation, the interaction of STY Bing with the environment is predicted to result in a critical region in the displaced-TC simulations. Therefore, the TC contribution to the re-intensification stage in the STY Bing control forecast is designated as *significant* (Fig. V-46). In the Bing-NW simulation, a deeper re-intensification is predicted, which is represented in Fig.

V-46 by an upward arrow. In the Bing-SW simulation, the storm dissipates. Nevertheless, the interaction of the Bing-SW cyclone with the environment produces a critical region in which a separate extratropical cyclogenesis is initiated. Since no critical region is predicted in the no-TC simulation, the contribution of the Bing-SW cyclone is considered to be "minor" (downward arrow in Fig. V-46) even though it dissipated. This characterization of the Bing-SW cyclone is consistent with the matrix in Fig. V-8, in which the combination of an unfavorable mid-latitude and minor TC contribution results in decay of the TC.

As in the case of STY Oliwa, the storm in the control forecast of TY Tina is a northeast ET case that dissipated, and no critical region exists despite the interaction of the TC with the environment. Therefore, the TC contribution to the re-intensification stage of ET in the case of TY Tina is designated as *none* (Fig. V-46).

In summary, notice that in nearly all of these displaced-TC simulations the shift in the initial TC vortex is only a small distance along its track. Only in selected cases are extreme displacements > 300 n mi imposed (Appendix B). In the cases of TY David, STY Bart, TY Rex, and STY Bing, the initial vortex displacements may change the phasing with the mid-latitude circulation pattern so as to produce either a stronger or a weaker re-intensification than predicted in the control forecast. The re-intensification responses to the altered phasing between the TC and the mid-latitude circulation pattern that results from these displacements can be quite dramatic despite the small distances involved. In the case of TY David, displacement separated by only 240 n mi in initial positions result in one cyclone that completes deep re-intensification in 48 h to a SLP = 974 mb, and another

cyclone that dissipates. In the case of STY Bart, initial positions separated by only 300 n mi result in one cyclone that rapidly deepens to 974 mb, and another that completes moderate re-intensification with a SLP = 986 mb. Displacing STY Ginger 240 n mi to the southwest results in a storm that is predicted to rapidly deepen and be 26 mb deeper than the control. The crucial point is that whether or not the TC couples with a critical region and interacts favorably with the mid-latitude circulation pattern is sensitive to that initial displacement, which determines the phasing of the TC with the critical region, the magnitudes of maximum lower-tropospheric warm advection and upper-tropospheric divergence, and the position of the critical region.

Only two of the 16 simulations in which the TC remnants phased with a critical region did the cyclone fail to achieve deep re-intensification (Appendix B). However, both the STY Bing control forecast and Oliwa-NW simulation had a SLP = 982 at the end of ET, which is acceptably close to the 980 mb threshold defined here. The average final SLP of these 16 simulations is 971 mb (standard deviation 11 mb). No storm that failed to enter a critical region achieved a deep re-intensification, which implies that deep re-intensification is restricted to ET cases that phase with a critical region in the mid-latitude circulation. In 15 of these 16 cases in which the TC fails to phase with the critical region, it is because the TC did not couple with 200-mb divergence $> 3 \times 10^{-5} \text{ m s}^{-1}$ (Appendix B). In eight (three) of these 16 cases, another missing element needed to define a critical region is a too small 500-mb PVA (925-mb warm advection). This distribution emphasizes the sensitivity of the definition of the critical region to the upper-divergence

maximum, and thus the importance of the interaction between the TC and the polar jet as discussed in Chap. V-E-5.

In Chap. V-B-3, the final SLP achieved at the end of ET is hypothesized to depend on the combination of the mid-latitude and TC contributions to the re-intensification stage (Fig. V-8). Based on the results presented in Chap. V-E and Appendix B, only the moderate re-intensification predicted in the control forecast of STY Bart (mid-latitude "favorable," TC "minor") did not fit well in the matrix in Fig. V-8. However, the STY Bart control cyclone did deepen to 982 mb, so it is still believed possible that the combination of mid-latitude "favorable" and TC "minor" contributions can produce deep re-intensification (980 mb as defined here). Consequently, the ability to characterize almost all cases in Fig. V-46 in the framework of Fig. V-8 is considered to be a validation of the mid-latitude circulation phasing hypothesis. These simulations also demonstrate clearly that the phasing of the TC remnants with the mid-latitude circulation critical region is not a static process, but a dynamic process in which both the TC and mid-latitude circulations have a contribution.

VI. SUMMARY AND CONCLUSIONS

A. SUMMARY OF THE STAGES OF ET

The threat posed to coastal and maritime interests by storms completing ET has been discussed in Chap. I. Differences between TCs and the extratropical, baroclinic low they evolve into during ET were highlighted (Table 1 and Fig. I-3), particularly the location of the radius of maximum winds (Table 1). It is emphasized that the symmetric cloud, wind, and precipitation patterns associated with TCs become quite asymmetric during ET (Figs. I-4 through I-6), and are distributed very differently. Therefore, issuing advisories and warnings on storms completing ET as if they were still TCs is inadequate to guarantee safe navigation and guide appropriate precautions before these storms strike.

Following Klein (1997) and based on review of 30 ET cases in the western North Pacific, ET is described in terms of a transformation stage during which the TC is transformed into a baroclinic low, and a re-intensification stage, in which that transformed storm then deepens as a baroclinic low. Transformation has been defined here to begin (Step 1 in Fig. III-18) when the outer circulation of the TC begins interacting with a pre-existing, mid-latitude baroclinic zone or front, while simultaneously exhibiting an asymmetric appearance of clouds and precipitation that include a widespread decrease of deep convection in the western quadrant of the TC outer circulation. Transformation is defined to end when the storm has become embedded in a pre-existing, mid-latitude baroclinic zone, such that the surface center is in cold, descending air that has undercut

over-running ascent above and east of the storm center (Step 3 of the conceptual model in Fig. III-18). Re-intensification begins when the transformed storm deepens after achieving its highest central SLP at or after the completion of transformation. Re-intensification concludes when the transformed storm has achieved the deepest SLP before either filling or holding steady in the next analysis. Storms that fail to complete both stages of ET and therefore simply dissipate over cooler SSTs and in an environment of vertical shear are classified as decayers.

The primary objective of this study has been to address three specific aspects of ET that have not been completely explained by previous research: (i) practical descriptions of when a TC commences and completes the transformation stage of ET, and understanding the physical processes that are important in that transformation; (ii) describing the physical processes that trigger extratropical cyclogenesis during the re-intensification stage, and the relative contributions of the TC remnants and the mid-latitude circulation pattern to that re-intensification; and (iii) determining if the outcome of the re-intensification stage could be anticipated and predicted so that the ET cases that re-intensify only moderately can be distinguished from those that become the most intense.

The first step in this research has been to review the 30 ET cases that occurred in the western North Pacific from 1 June through 31 October 1994-98 using NOGAPS analyses, and IR, visible, water vapor, and microwave imagery, and improve the descriptions of the transformation stage of ET presented in Klein (1997). As indicated above, new definitions of the beginning and end of the transformation and re-intensification stages of ET have been developed (see the examples in Chap. II-B).

A three-dimensional conceptual model of the three-step transformation stage of ET introduced in Fig. III-18 describes and explains how nearly all cases of ET in the western North Pacific evolve from a TC to a baroclinic low. As in the conceptual model of Matano and Sekioka (1971), and as described in the case of Hurricane Agnes (DiMego and Bosart 1982), this model highlights the importance of an interaction between the TC and pre-existing, mid-latitude baroclinity in the lower troposphere. In each of the three steps of the transformation stage, four important physical processes are examined: (i) environmental inflow of colder, drier (warm, moist) air in the western (eastern) quadrant that initiates an asymmetric distribution of clouds and precipitation, and a dipole of lower-tropospheric temperature advection; (ii) the interaction of the TC and a pre-existing, mid-latitude baroclinic zone to produce ascent over tilted isentropic surfaces; (iii) systematic decay, tilt, and dispersal downstream of the warm core aloft in response to vertical wind shear; and (iv) evolution of the TC outer circulation into a pattern in which lower-tropospheric frontogenesis has commenced. Empirical thresholds for evaluating temperature advection and vertical motion dipoles, vertical shear, and lower-tropospheric frontogenesis and using them to identify the second and third steps of the transformation stage in which they are occurring have been developed (Tables 3 and 4). Together, these tools have addressed the first of the three aspects of ET described earlier, and offer operational forecasters information that would help them anticipate, diagnose, and understand the sequential steps that occur during the transformation stage.

A short-term climatology in Chap. IV has been developed that describes the physical characteristics and tracks of the storms that complete ET (Tables 5 through 8 and

Figs. IV-1 and IV-2). Eleven cases of deep re-intensification (below 980 mb) are statistically deeper at a 99% confidence level than cases of moderate re-intensification (between 980 mb and 1000 mb). This categorization of the re-intensification stage was used to differentiate between the most powerful storms and weaker ET cases, and demonstrated that more than 30% of ETs result in a potentially dangerous extratropical cyclone. Four cases where a transforming TC eventually "merged" with a pre-existing, mid-latitude baroclinic cyclone are found to transform according to the same, three-step conceptual model (Fig. III-18) of the transformation stage described earlier like the other 26 cases of ET studied in the western North Pacific.

The primary hypothesis examined in Chap. V is that the final SLP at the end of the re-intensification stage depends on the phasing of a poleward-moving TC with a critical region in the mid-latitude circulation that supports deep and/or rapid Petterssen Type-B extratropical cyclogenesis, and specifically that deep (moderate or weak) re-intensification will result in cases in which a more (less) favorable phasing occurs (Fig. V-7). It was further hypothesized that the final storm intensity (in SLP) may be characterized by the dynamic interaction between this mid-latitude contribution of the critical region, and a TC contribution to the phasing, first through its position and motion, and secondarily through its modification of the critical region location and parameter magnitudes (Fig. V-8).

Validation of this mid-latitude circulation superposition hypothesis used COAMPS simulations of nine cases of ET. The Kurihara et al. (1995) technique to remove a TC vortex from a NOGAPS initial analysis field has been modified to facilitate displacement of the initial position of the TC vortex, as described in Chap. V-B. In the no-TC simulations

in which a critical region was (not) predicted, significant extratropical cyclogenesis (weak cyclogenesis or even anticyclogenesis) was forecast. The mid-latitude circulation pattern contribution to the re-intensification stage has been characterized in Fig. V-8 as being favorable if a cyclogenesis and critical region are predicted in the nine no-TC simulations. If no critical region and only a weak cyclogenesis (anticyclogenesis) is predicted without the presence of a TC, the mid-latitude contribution to the re-intensification stage is defined to be neutral (unfavorable).

The results of the nine control forecasts have been used as a first step toward validation of the mid-latitude circulation superposition hypothesis. In these control forecasts, deep (moderate or no) re-intensification occurred only if the poleward-moving TC remnants arrived in phase with a critical region (failed to phase with a critical region). Next, the results of the control forecasts are used as the basis for validating whether or not small displacements of the TC vortex initial position altered the outcome of the re-intensification stage and achieved more (less) deepening relative to the control when the displaced TC produced more (less) optimal phasing between the TC and the critical region. These displaced simulations have demonstrated that a more optimal (less optimal) phasing of the TC remnants with the mid-latitude circulation pattern does indeed result in a deeper (weaker) re-intensification than predicted in the control forecast (Chap. V-E-6). Even in the case of a control forecast that predicted decay of STY Oliwa, it was demonstrated that an extreme vortex displacement such that the TC remnants phased with a remote critical region would also achieve rapid re-intensification.

A shift in the location and parameter amplitude of the critical region in some of these displaced-vortex simulations occurred as the TC remnants phased with the mid-latitude circulation. A greater deepening during the re-intensification seemed to be most sensitive to the displacement downstream (upstream) of upper-tropospheric divergence when the initial TC vortex was shifted downstream (upstream). The interpretation from these simulations is the TC outflow and/or advection of the warm core downstream such that an interaction with the polar jet may account for a shift in the location of the upper-tropospheric divergence maximum, and therefore the critical region. Based on these results, the TC contribution to the re-intensification stage has been defined as significant, minor, or none in Chap. V-E-5 by evaluating these interactions of the TC with the upper troposphere and lower-tropospheric baroclinity after phasing with the mid-latitude critical region.

Finally, the control forecasts and displaced-TC simulations of the re-intensification stage of ET have been summarized in Appendix B, and the strength of the re-intensification has been characterized in the matrix presented in Fig. V-46 based on the combination of the mid-latitude and the TC contributions. The phasing of the translating TC remnants with the critical region in the evolving mid-latitude circulation has been demonstrated to be a dynamic process rather than a static one of an unchanging mid-latitude critical region simply translating to a superposition with the TC remnants.

B. CONCLUSIONS

This research has provided advances in three areas: (i) understanding the transformation of a TC into a baroclinic low during ET in the western North Pacific; (ii)

provision of a climatology of ET in the western North Pacific; and (iii) understanding the dynamics of the extratropical re-intensification of these transformed TCs during ET.

1. The Transformation Stage of ET: New Findings

A conceptual model is proposed (Fig. III-18) that describes the three-step transformation stage of nearly every ET case that occurs in the western North Pacific. What is new here is that this conceptual model recognizes the similar appearance of the evolution of 30 TCs into a baroclinic cyclone, and explains this evolution as the result of four key physical processes acting together to change the structure of every transforming TC that was studied. *Thus, it is concluded that this conceptual model is representative of virtually every transformation in the western North Pacific.* This conceptual model is the first to describe the transformation stage as a three-dimensional process in which the upper troposphere plays a significant role, and is based on new terminology and definitions presented herein that will serve as the foundation for recognizing and studying ET in the future.

2. Climatology of ET in the Western North Pacific

Until this study, no knowledge base existed that described the physical characteristics of storms that completed ET. The duration of the stages of ET, and the size, intensity and translation direction and speed characteristics exhibited by storms as they are undergoing ET, are all critical pieces of information that forecasters require in order to better understand and forecast ET. It is concluded that the statistics presented in Chap. IV can be used to warn forecasters of the quick duration of ET, and give

forecasters intensity and time parameters that can be related to each step of the conceptual model of the transformation stage, thus making the model more useful.

3. The Re-intensification Stage of ET: New Findings

Previous research has showed that the extratropical cyclogenesis observed during ET is the result of Petterssen Type-B extratropical cyclogenesis. Two paradigms shape this view. One paradigm is that an upper-level PV maximum in the mid-latitude circulation pattern triggers extratropical re-intensification of TC remnants if they become coupled. Those who accept this hypothesis would suggest that extratropical cyclogenesis would occur anyway in the absence of the TC. The other paradigm is that the TC contributes significantly to its own extratropical re-intensification through processes such as downstream ridging (Bosart and Lackmann 1995) described in the introduction, in which warm advection and latent heat release associated with the TC builds the ridge to the east so that mid-tropospheric PVA is increased above the storm through self-amplification. This paradigm would suggest that if there are no TC remnants to interact with the environment and serve as the seedling for extratropical cyclogenesis, none would occur. In this study, it is demonstrated in the no-TC simulations that the mid-latitude circulation pattern may be so favorable for Petterssen Type-B extratropical cyclogenesis that significant cyclogenesis will be forecast in the absence of the TC (e.g., TY David, STY Bart, and TY Stella). If no critical region is predicted in the absence of the TC, weak cyclogenesis (e.g., STY Ginger, TY Rex, TY Vicki, and STY Oliwa), or even the building of a ridge (e.g., STY Bing, TY Tina), will be forecast.

What is new here is this superposition hypothesis recognizes that *both the mid-latitude circulation pattern and the TC contribute to the re-intensification stage of ET, and that the combination of those contributions (Fig. V-8 and Fig. V-46) determines the outcome of the re-intensification stage of ET.* Although the significant role of the mid-latitude circulation pattern is acknowledged and demonstrated, it is concluded that an optimal phasing of the TC and the critical region allows the TC to interact with the mid-latitude circulation in such a way as to modify the location and characteristics of the critical region.

Previous to the completion of this study, it has been largely presumed that: (i) a bigger TC circulation would generate larger values of warm advection via interaction with a pre-existing mid-latitude baroclinic zone; and (ii) a more intense TC would result in larger values of absolute vorticity in the mid-troposphere, and more latent heat release in areas of concentrated convective rainfall. In both cases, these TC contributions would presumably contribute to enhanced ascent and more intense extratropical cyclogenesis. In this study, no statistical correlation was found between intensity at the completion of ET and the initial size and intensity of TCs. Furthermore, the procedure used to displace the initial vortex almost always made the initial vortex somewhat larger and more intense (based on the diameter of the outermost closed SLP contour and central SLP, respectively). In spite of this, those storms that did not phase with the critical region dissipated, or at most achieved moderate re-intensification, even though they were larger and more intense.

In one COAMPS simulation of TY Stella, the maximum wind speeds at every level between 1000 mb and 500 mb in the initial vortex are doubled without changing the location of the transforming storm. As in the other TY Stella displaced-TC simulations (Appendix B), this "doubled-Stella" simulation resulted in the dissipation of the TC, albeit with a separate extratropical cyclogenesis to the northeast at the same interval and nearly the same location as in the control forecast (not shown). This result is consistent with the statistical analysis in Chap. IV and the displaced-TC simulations discussed in Chap. V and Appendix B, which suggest that size and intensity are not correlated with the outcome of ET.

C. RECOMMENDATIONS

1. Guidance to Operational Forecasters

A forecaster using the conceptual model of the transformation stage of ET in the western North Pacific (Fig. III-18) would require 1° lat./long. resolution NWP analyses and forecasts in addition to hourly geostationary satellite imagery (including visible, IR, and water vapor channels), and microwave imagery. In addition, radar data would be helpful when the storm either passes over or close to land. Specifically, guidance products should be available so the forecaster can easily examine streamlines, isentropes of θ_e , temperature advection, and frontogenesis in the lower troposphere, 500-mb winds and isoheights, 200-mb winds and isoheights, and vertical cross-sections of winds, θ_e , PV, and vertical motion. With these tools, the forecaster should be able to anticipate, and then recognize each of the three steps of the transformation stage of ET. Understanding the structure and evolution of the transformation will better prepare the forecaster for the

subsequent re-intensification stage. Such knowledge will enable the forecaster to disseminate improved warnings to coastal and maritime interests, since the forecaster will expect the location of gale- and storm-force winds, high seas, and heavy precipitation in transformed TCs to change drastically from when the storm was a mature TC. It is further suggested that this model may be useful in other ocean basins in which recurving TCs may also interact with pre-existing lower-tropospheric baroclinity and vertical wind shear. However, the model may have to be adapted to the characteristics (baroclinic zone orientation, jet stream structures, coastline, currents, climatological TC storm tracks, etc.) unique to these other ocean basins.

An important goal of this research was to determine if the outcome of the re-intensification stage could be anticipated and predicted so that forecasters could differentiate decayers and storms completing moderate re-intensification from those that become the most intense. As demonstrated in this study, the superposition hypothesis describing the phasing of the TC remnants with the mid-latitude circulation pattern is the key to the re-intensification stage. Furthermore, the description of the outcome of the re-intensification stage of ET as a combination of both mid-latitude and TC contributions can be used to better understand why some cases of ET are forecast to achieve deep re-intensification, while others are predicted to decay, or at best deepen only moderately. To forecast properly the final intensity of storms completing ET, the forecaster must correctly interpret the NWP model guidance regarding the evolution of the mid-latitude circulation pattern, and especially the existence of critical regions. Of course, the track of the TC

must also be correctly forecast, so that the interaction of the TC and the mid-latitude circulation pattern commences at the proper time. This is a critical aspect as the sensitivity of the outcome of the forecast of ET to small displacements of the initial vortex has been well demonstrated in this study. If these small shifts in the location of the initial vortex are the result of NWP error instead of intentional displacements, the resulting forecast would be sensitive to those errors in the initial conditions, and be responsible for erroneous predictions of the cyclone intensity at the end of ET.

A forecaster could use this information as early as Step 1 of the transformation stage to determine whether or not the NWP model is predicting a critical region in the mid-latitude circulation pattern, or if one is indicated in the analyses at the initial time. If no mid-latitude critical region is predicted in the NWP forecasts, a forecaster could consult verifying analyses to determine if one should have existed. As the transformation stage continues, the forecaster could then decide whether or not the model is skillfully predicting the location of the TC and its track, and ascertain whether or not the model is forecasting a displacement of the transforming storm into the critical region. Unfortunately, ET with a deep re-intensification can be completed as quickly as 60 h (Table 4), which does not give the forecaster a great deal of time to determine if the model is correctly depicting the critical region in the mid-latitude circulation, as well as the track of the transforming TC. Furthermore, by the time a forecaster is able to determine if the phasing of the TC with the critical region has been properly forecast by the model, it will be too late to issue timely warnings and advisories because the re-intensification will have already begun.

2. Future Research

Several areas of future research are suggested as a result of this study. A kinetic energy budget could be prepared for the COAMPS control forecast, no-TC simulation, and displaced-TC simulations of selected ET cases to determine how the phasing of the TC with the critical region affects the amount of the baroclinic conversion in the lower troposphere, as well as the TC interaction with the polar jet. The mid-latitude and TC contributions described herein could be further examined within the context of the northwest and northeast synoptic patterns of Harr et al. (2000) to determine if certain combinations of these contributions should be expected in one pattern or the other.

A comprehensive study of NWP model forecast errors during ET in the western North Pacific should be made using the conceptual model of the transformation stage (Fig. III-18) and the mid-latitude circulation superposition hypothesis as the framework for understanding how the atmosphere evolves during ET. This effort should closely examine the impact of synthetic TC observations on the location and intensity of the TC vortex during the transformation stage of ET to determine if these mature TC-type observations adversely affect the prediction of vortex during the transformation stage, and/or the phasing of the translating storm with the critical region in the mid-latitude circulation pattern.

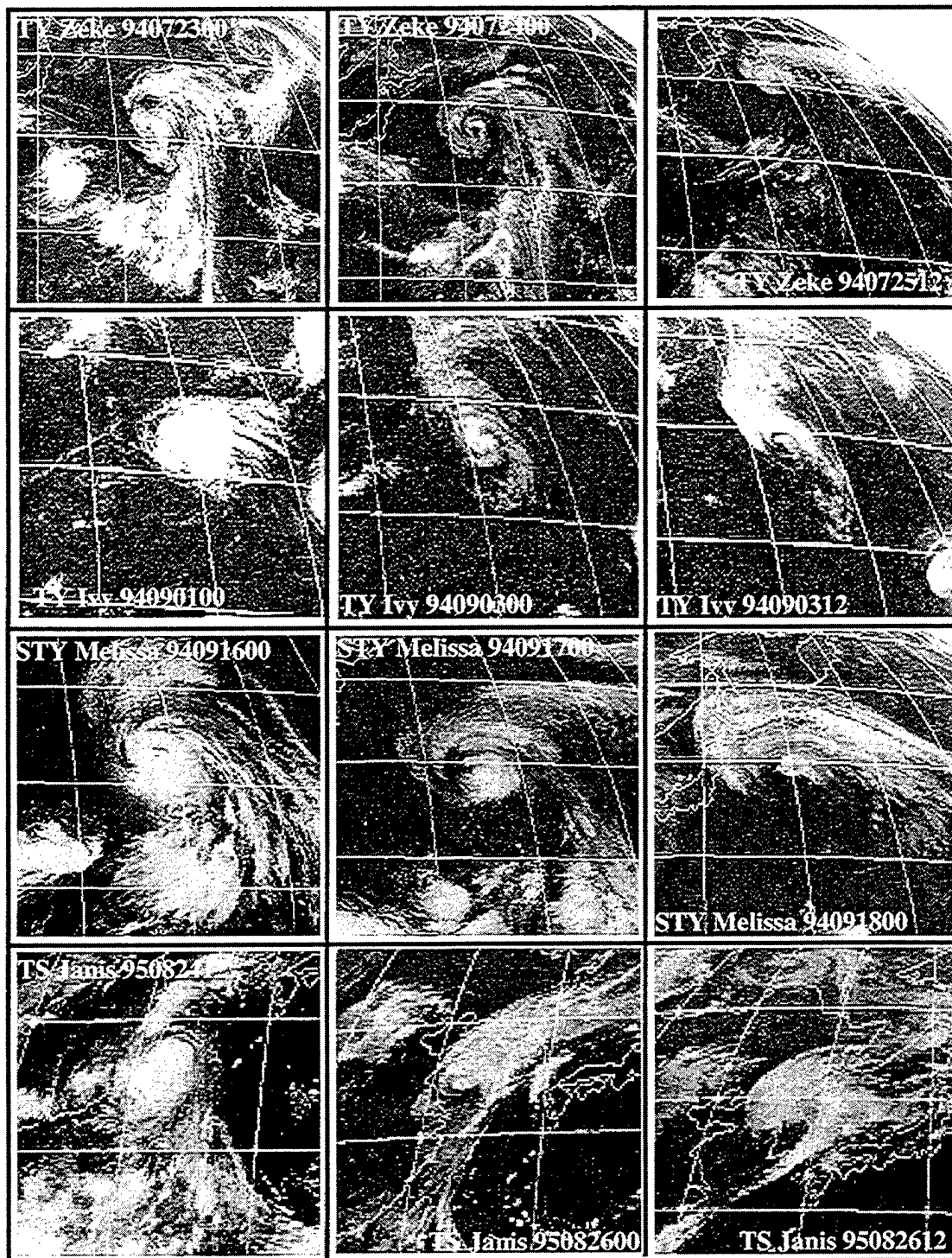
Finally, a field experiment could verify the detailed structure changes in the conceptual model of the transformation stage of ET. Sequences of observations of the transforming TC inner core would be valuable for comparison with the synthetic TC observations imposed in the NWP model. In addition, the structure of the baroclinic

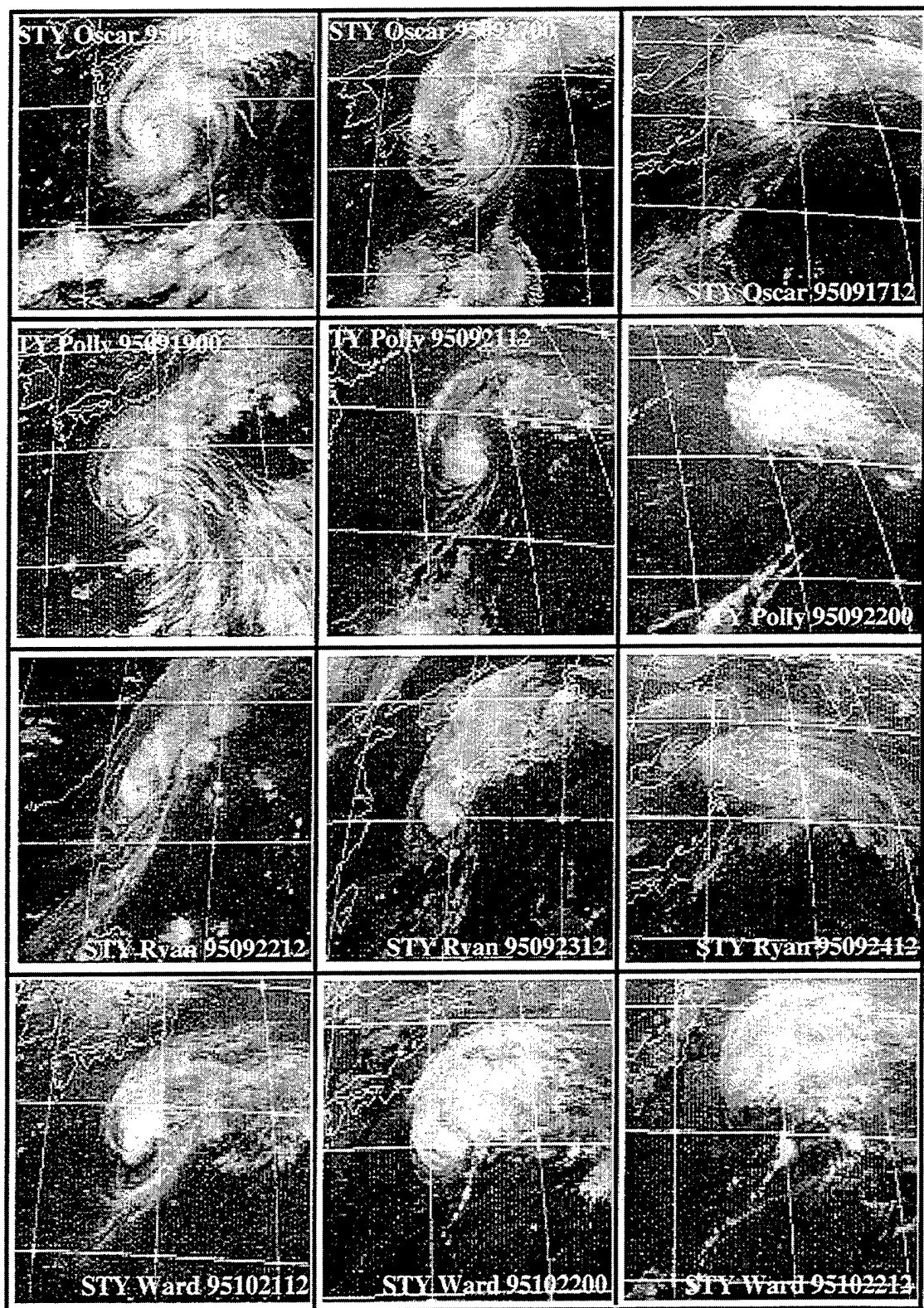
cyclone at the beginning of the re-intensification stage may help one better understand the mid-latitude circulation superposition hypothesis. These observations of the atmosphere in the lower troposphere where the TC is interacting with a pre-existing baroclinic zone, and in the upper troposphere where it is proposed that the dispersed TC warm core interacts with the polar jet, are important aspects of the superposition hypothesis. An adaptive observation targeting strategy might be used to test whether or not such observations improve NWP forecasts of ET.

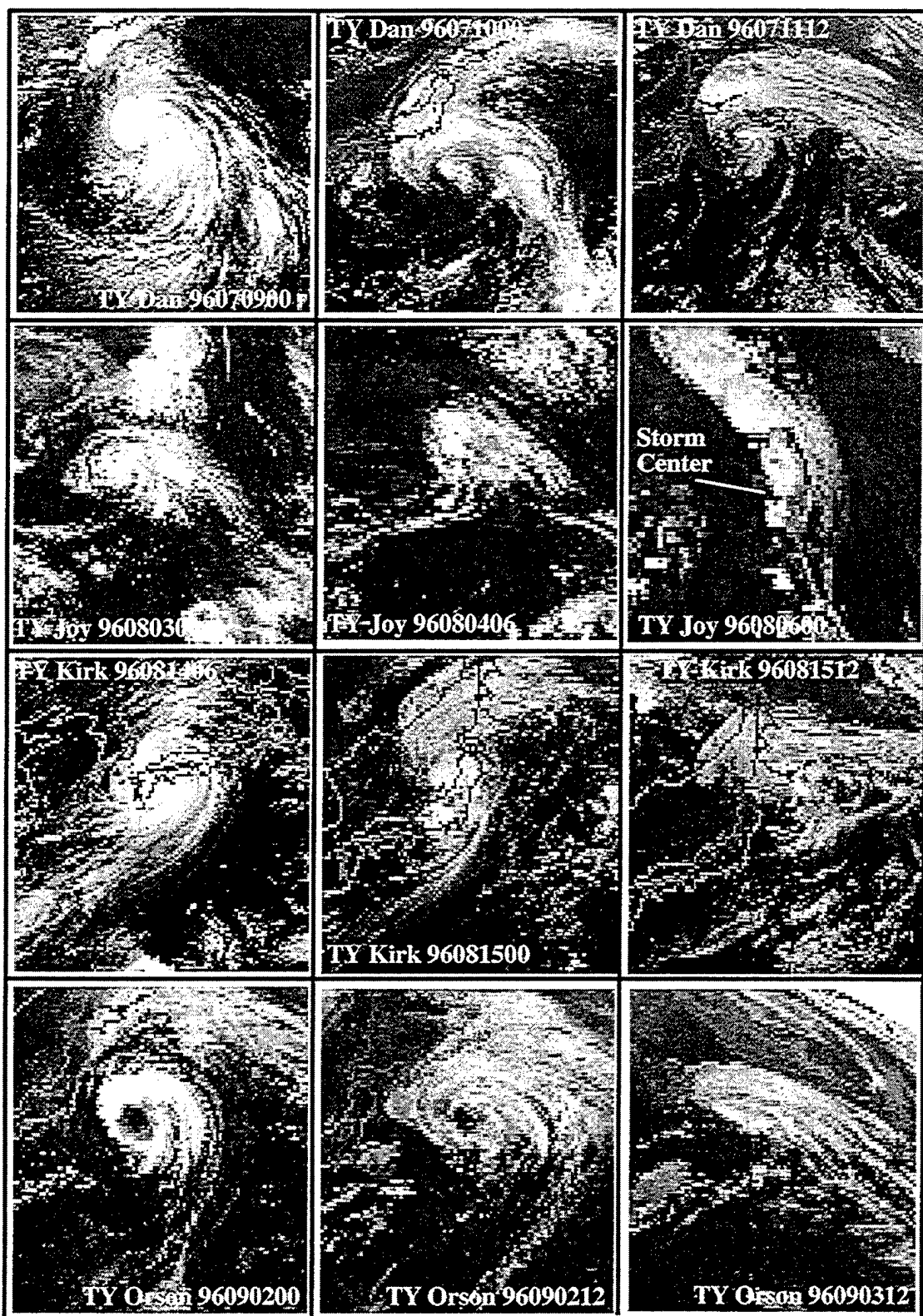
Although this study has contributed to a better understanding of western North Pacific ET, it is clear that in situ observations are required to confirm many of these conclusions based on remotely sensed data and relatively coarse (compared to TC inner core) NWP analyses and predictions. Furthermore, detailed budget calculations of vorticity, thermodynamics, moisture, and energetics will be required to confirm some of the inferences regarding physical processes. As better understanding and appropriate guidance products are provided the forecasters, better warnings should be available to the U. S. Navy and other maritime activities affected by these dangerous storms.

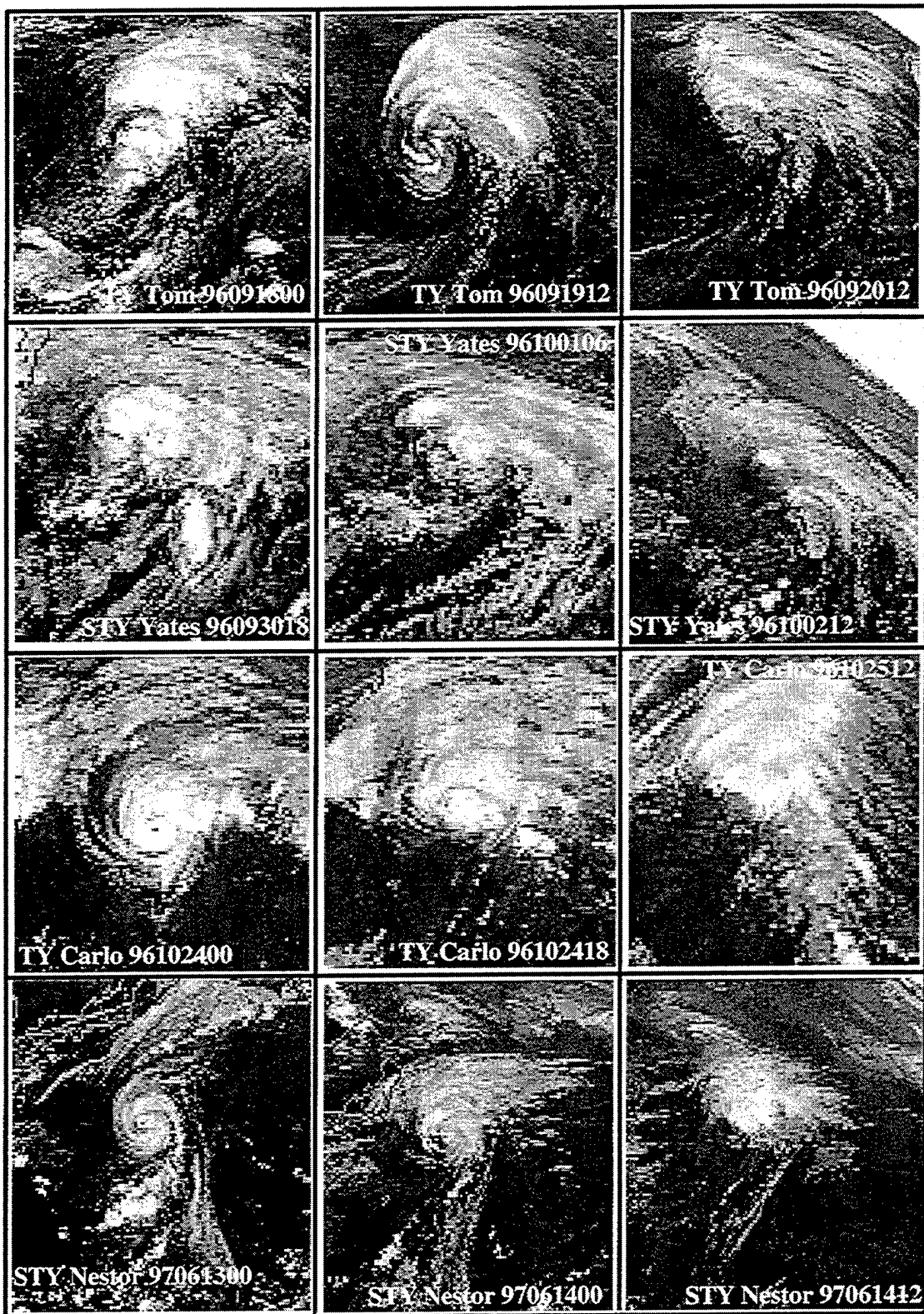
APPENDIX A

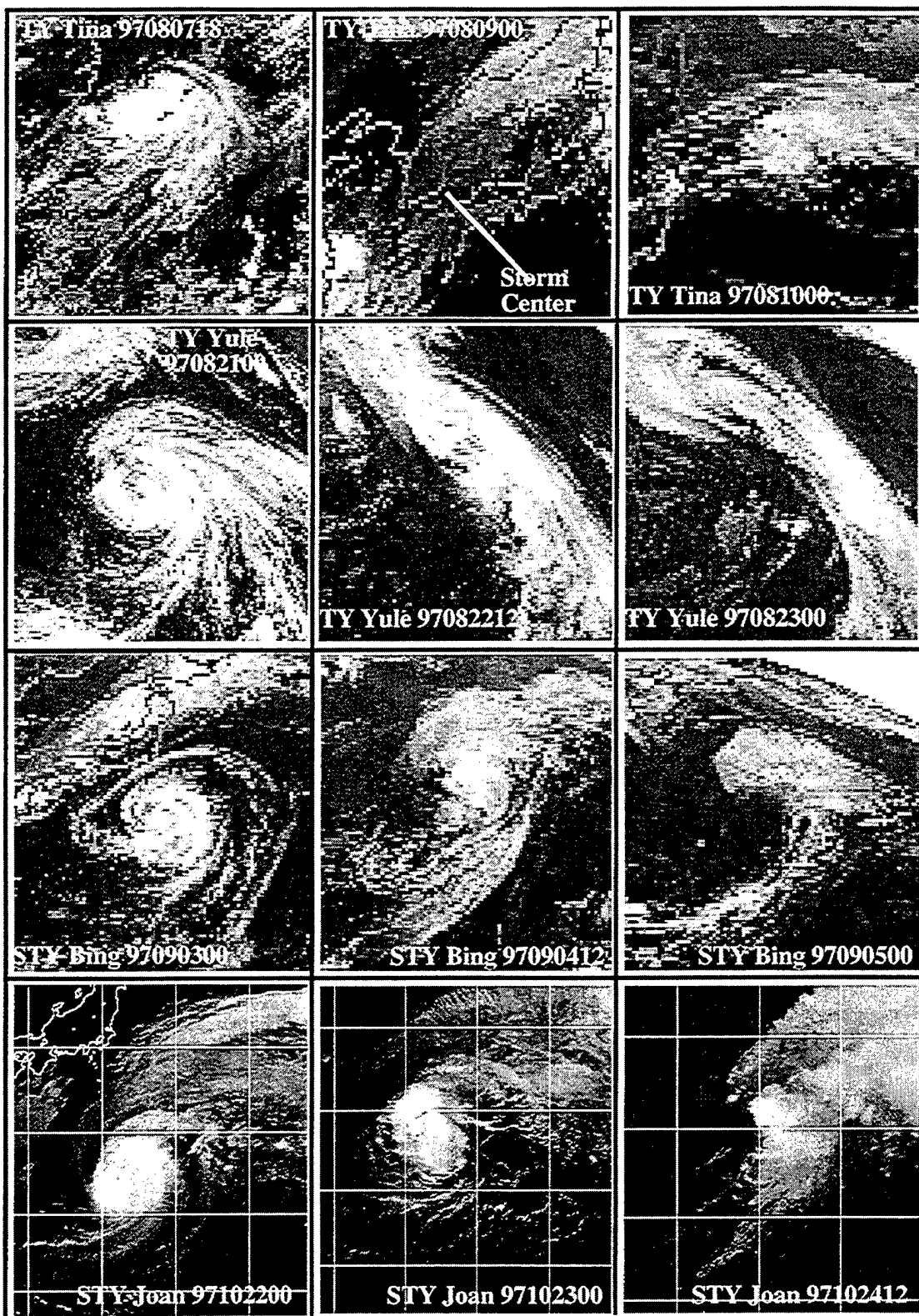
The IR imagery sequence of the transformation stage of ET is depicted for the 23 ET cases not shown in Chap III. On each image, the name of the storm, date, and time (yymmddhh) depicted are listed. In all cases, Step 1 is presented in the column to the left, Step 2 in the middle column, and Step 3 in the column to the right.

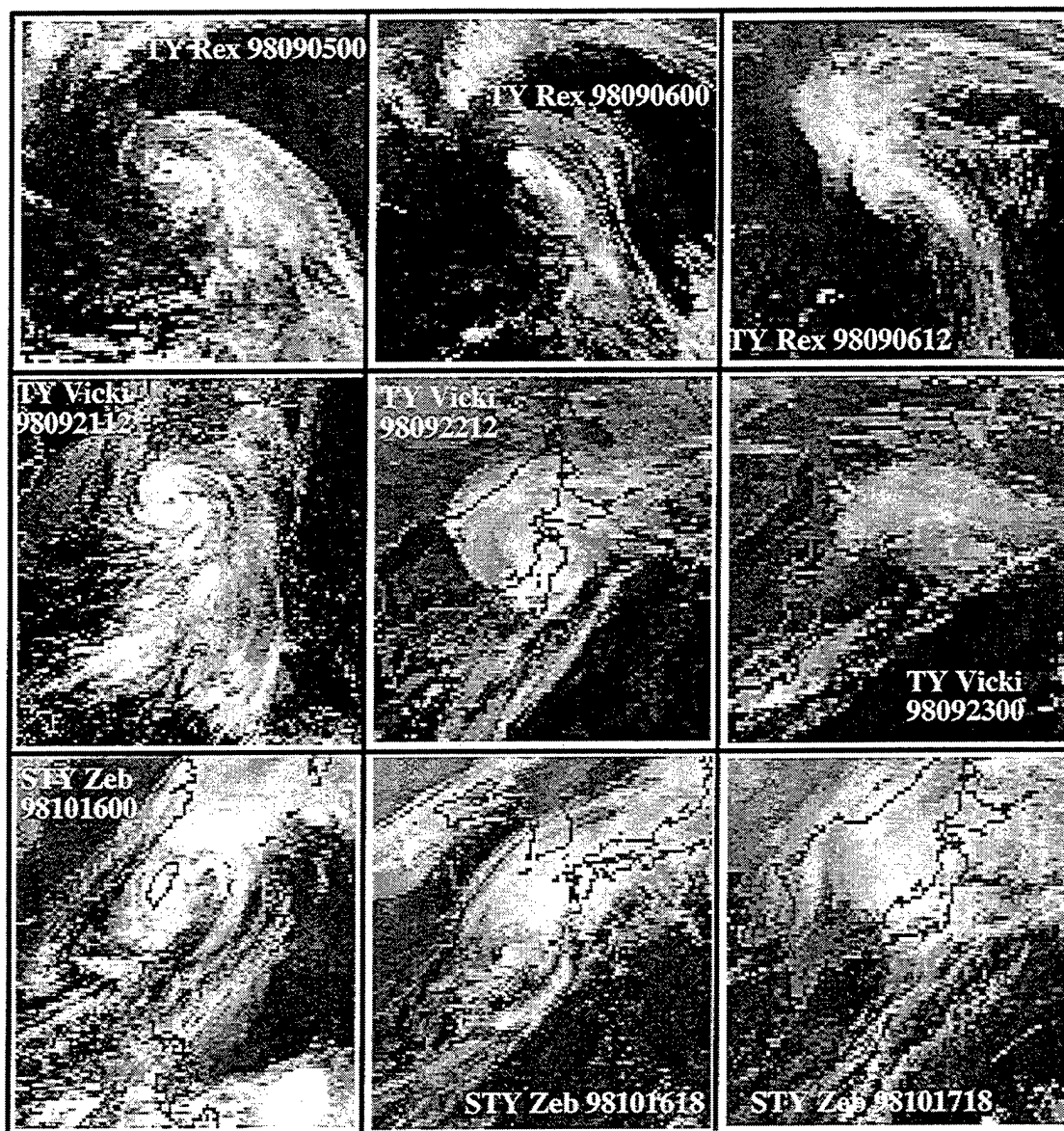












APPENDIX B

Using the definition of a critical region presented in Chap. V, the control forecasts and displaced-TC simulations are summarized in the following table. If at any point in the control forecast or displaced-TC simulation the storm is within a volume of the atmosphere where upper-tropospheric divergence $> 3 \times 10^{-5} \text{ s}^{-1}$, 500-mb PVA $> 50 \times 10^{-10} \text{ s}^{-2}$, and a dipole of 925-mb temperature advection $> \pm 10 \times 10^3 \text{ K s}^{-1}$, then the storm has phased with a critical region in the mid-latitude circulation pattern. Comments describing 900-mb frontogenesis and the type of re-intensification the storm achieved are also included.

Case Description (Initial Time in yymmddhh)		Physical Process Description					Comments on TC Interaction with the mid-latitude circulation pattern
TV David, Mid-latitude Favorable, initialized 97091900		Lower Tropospheric Warm/Cold Advection Dipole > +/- 10 units?	500-mb PVA with a maximum > 50 units?	200-mb Divergence > 3 units?	Lower- Tropospheric Frontogenesis		
1. David Control		Y	Y	Y, storm phased with equatorward entrance region	Warm frontogenesis forecast at 900 mb	Phases with critical region, rapid deepening predicted from 30 h to 48 h, completed deep re-intensification at 48 h with final SLP = 977 mb at completion of ET.	
2. David displaced 2 gridpoints poleward, 1 gridpoint east		Y	Y	Y, storm phased with equatorward entrance region	Warm frontogenesis forecast at 900 mb	Phases with critical region, completed deep re-intensification at 42 h with final SLP = 974 mb at completion of ET.	
3. David displaced 2 gridpoints equatorward, 1 gridpoint west		Y	N	N	Warm frontogenesis forecast at 900 mb	Does not phase with critical region, and dissipates, although a separate cyclogenesis northeast of David is initiated within critical region at 30 h.	
4. David displaced 6 gridpoints poleward, 3 gridpoints east		N	N	N	N	Does not phase with critical region, and dissipates, although a separate cyclogenesis northeast of David is initiated within critical region at 30 h.	
5. David displaced 6 gridpoints equatorward, 3 gridpoints west		N	N	N	N	Does not phase with critical region, and dissipates, although a separate cyclogenesis northeast of David is initiated within critical region at 30 h.	

STY Bart, Mid-latitude Favorable, Initialized 99092400	Lower Tropospheric Warm/Cold Advection Dipole > +/- 10 units?	500-mb PVA with a maximum > 50 units?	200-mb Divergence > 3 units?	Lower-Tropospheric Frontogenesis	Comments on TC interaction with the mid-latitude circulation pattern
1. Bart control	Y	Y	N, divergence maximum associated with equatorward entrance region remains downstream of the storm.	Warm frontogenesis forecast at 900 mb	Does not couple with critical region, although storm completed moderate re-intensification at 54 h with final SLP = 982 mb at completion of ET. A separate cyclogenesis is initiated downstream at 60 h beneath the critical region.
2. Bart displaced 2 gridpoints equatorward, 2 gridpoint west	Y	Y	Y, storm phased with equatorward entrance region	Warm frontogenesis forecast at 900 mb	Phases with critical region, rapid deepening predicted from 30 h to 42 h, completed deep re-intensification at 48 h with final SLP = 977 mb at completion of ET.
3. Bart displaced 2 gridpoints poleward, 2 gridpoint east	Y	Y	N, divergence maximum associated with equatorward entrance region remains downstream of the storm	Warm frontogenesis forecast at 900 mb	Does not couple with critical region, although storm completed moderate re-intensification at 54 h with final SLP = 986 mb at completion of ET. A separate cyclogenesis is initiated downstream at 48 h beneath the critical region.
TY Stella, Mid-latitude Favorable, Initialized 98091600	Lower Tropospheric Warm/Cold Advection Dipole > +/- 10 units?	500-mb PVA with a maximum > 50 units?	200-mb Divergence > 3 units?	Lower-Tropospheric Frontogenesis	Comments on TC interaction with the mid-latitude circulation pattern
1. Stella control	Y	Y	N	Warm frontogenesis forecast at 900 mb	Does not phase with critical region, and achieved little re-intensification, although a separate cyclogenesis east of Stella is initiated within the critical region downstream at 36 h, which rapidly deepened and achieved a SLP = 978 mb at 72 h.
2. Stella displaced 2 gridpoints poleward, 1 gridpoint east	Y	Y	N, divergence maximum associated with equatorward entrance region remains downstream of the storm	Warm frontogenesis forecast at 900 mb	Does not phase with critical region, and dissipates, although a separate cyclogenesis to the northeast is initiated within critical region at 36 h at same location as in the control.

3. Stella displaced 2 gridpoints equatorward, 1 gridpoint west	Y	N	Y	Warm frontogenesis forecast at 900 mb	Does not phase with critical region, and dissipates, although a separate cyclogenesis to the northeast is initiated within critical region at 36 h at same location as in the control.
4. Stella displaced 2 gridpoints equatorward, 2 gridpoint east	Y	N	N	Warm frontogenesis forecast at 900 mb	Does not phase with critical region, and dissipates, although a separate cyclogenesis to the northeast is initiated within critical region at 36 h at same location as in the control.
TY Rex, Mid-latitude Neutral, Initialized 98090600	Lower Tropospheric Warm/Cold Advection Dipole > +/- 10 units?	500-mb PVA with a maximum > 50 units?	200-mb Divergence > 3 units?	Lower-Tropospheric Frontogenesis	Comments on TC interaction with the mid-latitude circulation pattern
1. Rex control	Y	Y	Y, storm phased with equatorward entrance region	Warm frontogenesis forecast at 900 mb	Phases with critical region, completed deep re-intensification at 48 h with final SLP = 977 mb at completion of ET.
2. Rex displaced 2 gridpoints poleward, 1 gridpoint east	Y	Y	Y, storm phased with equatorward entrance region	Warm and cold frontogenesis forecast at 900 mb	Phases with critical region, completed deep re-intensification at 42 h with final SLP = 974 mb at completion of ET.
3. Rex displaced 2 gridpoints equatorward, 1 gridpoint west	Y	Y	Y, storm phased with equatorward entrance region of downstream jet streak, poleward exit region of upstream jet streak	Warm and cold frontogenesis forecast at 900 mb	Phases with critical region, completed deep re-intensification at 48 h with final SLP = 965 mb at completion of ET.
4. Rex displaced 4 gridpoints equatorward, 2 gridpoint west	Y	Y	Y, storm phased with equatorward entrance region	Warm and cold frontogenesis forecast at 900 mb	Phases with critical region, completed deep re-intensification at 54 h with final SLP = 973 mb at completion of ET.
5. Rex displaced 5 gridpoints equatorward, 5 gridpoint west	N	Y	N, divergence maximum associated with equatorward entrance region remains downstream of the storm	Warm frontogenesis forecast at 900 mb	Does not couple with critical region, although storm completed moderate re-intensification at 48 h with final SLP = 982 mb at completion of ET.

STY Ginger, Mid-latitude Neutral, Initialized 97092912	Lower Tropospheric Warm/Cold Advection Dipole > +/- 10 units?	500-mb PVA with a maximum > 50 units?	200-mb Divergence > 3 units?	Lower-Tropospheric Frontogenesis	Comments on TC interaction with the mid-latitude circulation pattern
1. Ginger control	Y	Y	Y, storm phased with equatorward entrance region	Warm frontogenesis forecast at 900 mb	Phases with critical region, completed deep re-intensification at 42 h with final SLP = 979 mb at completion of ET.
2. Ginger displaced 2 gridpoints poleward, 1 gridpoint east	Y	Y	Y, storm phased with equatorward entrance region	Warm frontogenesis forecast at 900 mb	Phases with critical region, completed deep re-intensification at 42 h with final SLP = 965 mb at completion of ET.
3. Ginger displaced 4 gridpoints equatorward, 2 gridpoint west	Y	Y	Y, storm phased with equatorward entrance region of downstream jet streak, poleward exit region of upstream jet streak	Warm frontogenesis forecast at 900 mb	Phases with critical region, rapidly deepened from 30 h to 42 h, and completed deep re-intensification at 54 h with final SLP = 953 mb.
4. Ginger displaced 6 gridpoints equatorward, 3 gridpoint west	Y	Y	Y, storm phased with equatorward entrance region of downstream jet streak, poleward exit region of upstream jet streak	Warm and cold frontogenesis forecast at 900 mb	Phases with critical region, rapidly deepened from 48 h to 60 h, completed deep re-intensification at 60 h with final SLP = 946 mb at completion of ET.
5. Ginger displaced 6 gridpoints equatorward, 3 gridpoint east	Y	Y	Y, storm phased with equatorward entrance region of downstream jet streak, poleward exit region of upstream jet streak	Warm and cold frontogenesis forecast at 900 mb	Phases with critical region, rapidly deepened from 48 h to 60 h, completed deep re-intensification at 60 h with final SLP = 954 mb at completion of ET.
TY Vicki, Mid-latitude Neutral, Initialized 98092200	Lower Tropospheric Warm/Cold Advection Dipole > +/- 10 units?	500-mb PVA with a maximum > 50 units?	200-mb Divergence > 3 units?	Lower-Tropospheric Frontogenesis	Comments on TC interaction with the mid-latitude circulation pattern
1. Vicki control	Y	Y	N, storm northeast of equatorward entrance region	Warm frontogenesis forecast at 900 mb	Does not phase with critical region, but completes little re-intensification to 1003 mb.
2. Vicki displaced 2 gridpoints poleward, 1 gridpoint east	Y	Y	N, storm northeast of equatorward entrance region	Warm frontogenesis forecast at 900 mb	Does not phase with critical region, but completes little re-intensification to 1007 mb.
3. Vicki displaced 2 gridpoints equatorward, 1 gridpoint west	Y	Y	N, storm northeast of equatorward entrance region	Warm frontogenesis forecast at 900 mb	Does not phase with critical region, but completes little re-intensification to 1013 mb.

STY Oliwa, Mid-latitude Neutral, initialized 97091600	Lower Tropospheric Warm/Cold Advection Dipole > +/- 10 units?	500-mb PVA with a maximum > 50 units?	200-mb Divergence > 3 units?	Lower-Tropospheric Frontogenesis	Comments on TC interaction with the mid-latitude circulation pattern
1. Oliwa control	Y	N	N	N	Oliwa dissipates by 24 h, before a critical region appears at 36 h.
2. Oliwa displaced displaced 6 gridpoints poleward, 4 gridpoint west	Y	Y	Y	Warm frontogenesis forecast at 900 mb	Phases with critical region, rapid deepening predicted from 30 h to 42 h, completed moderate re-intensification at 48 h with final SLP = 982 after deepening a total of 20 mb.
STY Bing, Mid-latitude Unfavorable, initialized 97090400	Lower Tropospheric Warm/Cold Advection Dipole > +/- 10 units?	500-mb PVA with a maximum > 50 units?	200-mb Divergence > 3 units?	Lower-Tropospheric Frontogenesis	Comments on TC interaction with the mid-latitude circulation pattern
1. Bing control	Y	Y	Y, storm phased with equatorward entrance region	Warm frontogenesis forecast at 900 mb	Phases with critical region, completed moderate re-intensification at 66 h with final SLP = 982 mb at completion of ET.
2. Bing displaced 2 gridpoints poleward, 1 gridpoint east	Y	Y	Y, storm phased with equatorward entrance region	Warm and cold frontogenesis forecast at 900 mb	Phases with critical region, completed deep re-intensification at 60 h with final SLP = 979 mb at completion of ET.
3. Bing displaced 2 gridpoints poleward, 1 gridpoint west	Y	Y	Y, storm phased with equatorward entrance region of downstream jet streak, poleward exit region of upstream jet streak	Warm and cold frontogenesis forecast at 900 mb	Phases with critical region, completed deep re-intensification at 66 h with final SLP = 978 mb at completion of ET.
4. Bing displaced 2 gridpoints equatorward, 2 gridpoint west	Y	N	N, divergence maximum associated with equatorward entrance region remains downstream of the storm	Warm frontogenesis forecast at 900 mb	Does not phase with critical region, and dissipates, although a separate cyclogenesis northeast of Bing is initiated within critical region at 36 h
TY Tina, Mid-latitude Unfavorable, initialized 97080900	Lower Tropospheric Warm/Cold Advection Dipole > +/- 10 units?	500-mb PVA with a maximum > 50 units?	200-mb Divergence > 3 units?	Lower-Tropospheric Frontogenesis	Comments on TC interaction with the mid-latitude circulation pattern
1. Tina control	Y	N	N	Warm frontogenesis forecast at 900 mb	Does not phase with critical region, and dissipates by 60 h.

THIS PAGE LEFT INTENTIONALLY BLANK

LIST OF REFERENCES

- Bader, M. J., G. S. Forbes, J. D. Grant, R. B. E. Lilley, and A. J. Waters, 1995: *Images in Weather Forecasting: A Practical Guide for Interpreting Satellite and Radar Imagery*. Cambridge University Press, Cambridge, U. K. CB2-1RP, 499 pp.
- Bosart, L. F., and G. M. Lackmann, 1995: Post landfall tropical cyclone reintensification in a weakly baroclinic environment: A case study of Hurricane David (September 1979). *Mon. Wea. Rev.*, **123**, 3268-3291.
- Bowyer, P. J., 2000: Phenomenal waves with a transitioning tropical cyclone (Luis, the queen, and the buoys). *Preprints, 24th Conference on Hurricanes and Tropical Meteorology*, Ft. Lauderdale, FL, Amer. Meteor. Soc., Boston, MA 02108, 294-295.
- Brand, S., and C. P. Guard, 1978: Extratropical storm evolution from tropical cyclones in the western North Pacific Ocean. Tech. Rep. TR 78 02, Naval Environmental Prediction Research Facility (Now NRL-Monterey), 20 pp.
- Browning, K. A., G. Vaughan, and P. Panagi, 1998: Analysis of an extratropical cyclone after its reintensification as a warm core extratropical cyclone. *Quart. J. Roy. Meteor. Soc.*, **124**, 2329-2356.
- Carr, L. E. III., and R. L. Elsberry, 1994: Systematic approach to tropical cyclone track forecasting. Part I: Approach overview and description of meteorological basis. Tech. Rep. NPS-MR-94-002, Naval Postgraduate School, Monterey, CA 93943, 96 pp.
- Carr, L. E. III., and R. L. Elsberry, 1999: Systematic and integrated approach to tropical cyclone track forecasting. Part III: Traits knowledge base for JTWC track forecast models in the western North Pacific. Tech. Rep. NPS-MR-99-002, Naval Postgraduate School, Monterey, CA 93943, 227 pp.
- Carlson, T. N., 1991: *Mid-latitude Weather Systems*. Harper Collins Academic, New York, NY, 507 pp.
- DeMaria, M., and M. Huber, 1998: The effect of vertical shear on tropical cyclone intensity change: An historical perspective. *Preprints, Symposium on Tropical Cyclone Intensity Change*, Phoenix, AZ, Amer. Meteor. Soc., Boston, MA 02108, 22-29.
- DiMego, G. J., and L. F. Bosart, 1982: The transformation of tropical storm Agnes into an extratropical cyclone. Part I: The observed fields and vertical motion computations. *Mon. Wea. Rev.*, **110**, 385-411.

- Foley, G. R., and B. N. Hanstrum, 1994: The capture of tropical cyclones by cold fronts off of the west coast of Australia. *Wea. Forecasting*, **9**, 577-592.
- Frank, W. M., and E. A. Ritchie, 1999: Effects of environmental flow upon tropical cyclone structure. *Mon. Wea. Rev.*, **127**, 2044-2061.
- Harr, P. A., and R. L. Elsberry, 2000: Extratropical transition of tropical cyclones over the western North Pacific. Part I: Evolution of structural characteristics during the transition process. *Mon. Wea. Rev.*, **128**, 2613-2633.
- _____, _____, and T. F. Hogan, 2000: Extratropical transition of tropical cyclones over the western North Pacific. Part II: The impact of midlatitude circulation characteristics. *Mon. Wea. Rev.*, **128**, 2634-2653.
- Hodur, R. M., 1997: The Naval Research Laboratory's coupled ocean/atmosphere mesoscale prediction system (COAMPS). *Mon. Wea. Rev.*, **125**, 1414-1430.
- JTWC, 1997: Annual Tropical Cyclone Report, Joint Typhoon Warning Center, 425 Luapele Road, Pearl Harbor, HI 96860. [Available on-line from http://www.npmoc.navy.mil/products/jtwc/1997_atcr]
- Klein, P. M., 1997: Extratropical transition of western North Pacific tropical cyclones. M. S. thesis, Dept. of Meteorology, Naval Postgraduate School, Monterey, CA 93943-5114, 101 pp. [NTIS ADA-341-420.]
- _____, P. A. Harr, and R. L. Elsberry, 1999: Tropical cyclone and mid-latitude characteristics and physical mechanisms contributing to extratropical transition in the western North Pacific. *Preprints, 23rd Conference on Hurricanes and Tropical Meteorology*, Dallas, TX, Amer. Meteor. Soc., Boston, MA 02108, 799-802.
- _____, P. A. Harr, and R. L. Elsberry, 2000a: Extratropical transition of western North Pacific tropical cyclones: An overview and conceptual model of the transformation stage. *Wea. Forecasting*, **15**, 373-395.
- _____, P. A. Harr, and R. L. Elsberry, 2000b: Extratropical transition in the western North Pacific: Demonstration of the importance of phasing with the mid-latitude circulation pattern during the re-intensification stage. *Preprints, 24th Conference on Hurricanes and Tropical Meteorology*, Ft. Lauderdale, FL, Amer. Meteor. Soc., Boston, MA 02108, 316-317.
- Kurihara, Y., M. A. Bender, R. E. Tuleya, and R. J. Ross, 1995: Improvements in the GFDL hurricane prediction system. *Mon. Wea. Rev.*, **123**, 2791-2802.
- Matano, H., and M. Sekioka, 1971: Some aspects of the extratropical transformation of a tropical cyclone. *J. Meteor. Soc. Japan*, **49**, 736-743.

- Miller, D. W., and M. A. Lander, 1997: Intensity estimation of tropical cyclones during extratropical transition. Tech. Memo. to Joint Typhoon Warning Center, Pearl Harbor, HI, 11pp. [Available from Joint Typhoon Warning Center, 425 Luapele Road, Pearl Harbor, HI 96860]
- Petterssen, S., and S. J. Smebye, 1971: On the development of extratropical storms. *Quart. J. Roy. Meteor. Soc.*, **97**, 457-482.
- Riehl, H., 1972: Intensity of recurved typhoons. *J. Appl. Meteor.*, **11**, 613-615
- Ritchie, E. A., and G. J. Holland, 1993: On the interaction of tropical cyclone scale vortices. Part II: Interacting vortex patches. *Quart. J. Roy. Meteor. Soc.*, **119**, 1363-1379.
- _____, and R. L. Elsberry, 1999: Mechanisms contributing to extratropical transition of tropical cyclones in the western North Pacific: An idealized study. *Preprints, 23rd Conference on Hurricanes and Tropical Meteorology*, Dallas, TX, Amer. Meteor. Soc., Boston, MA 02108, 811-814.
- Schultz, D. M., D. Keyser, and L. F. Bosart, 1998: The effect of large-scale flow on low-level frontal structure and evolution in midlatitude cyclones. *Mon. Wea. Rev.*, **126**, 1767-1791.
- Shimazu, Y., 1998: Classification of precipitation systems in mature and early weakening stages of typhoons around Japan. *J. Meteor. Soc. Japan*, **76**, 437-445.
- Sinclair, M. R., 1993: Synoptic-scale diagnosis of the extratropical transition of a southwest Pacific tropical cyclone. *Mon. Wea. Rev.*, **121**, 941-960.
- Warrenfeltz, L. L., and R. L. Elsberry, 1988: Superposition effects in rapid cyclogenesis--linear model studies. *J. Atmos. Sci.*, **46**, 789-802.

THIS PAGE INTENTIONALLY LEFT BLANK

INITIAL DISTRIBUTION LIST

	No. Copies
1. Defense Technical Information Center, 8725 John J. Kingman Rd., STE 0944 Ft. Belvoir, VA 22060-6218	2
2. Dudley Knox Library Naval Postgraduate School 411 Dyer Rd. Monterey, CA 93943-5101	2
3. Chairman Meteorology Department (Code MR/Wx) Naval Postgraduate School Monterey, CA 93943	1
4. Chairman Oceanography Department (Code OC/Gd) Naval Postgraduate School Monterey, CA 93943	1
5. Professor Russell Elsberry, (Code MR/Es). Meteorology Department Naval Postgraduate School Monterey, CA 93943	1
5. Professor Terry Williams, (Code MR/Wu). Meteorology Department Naval Postgraduate School Monterey, CA 93943	1
6. Professor Pat Harr, (Code MR/Hp). Meteorology Department Naval Postgraduate School Monterey, CA 93943	1
7. Dr. R. F. Abbey, Jr Office of Naval Research Code 322 800 N. Quincy Street Arlington, VA 22217	1

8. Commander 1
Naval Meteorology and Oceanography Command
1020 Balch Boulevard
Stennis Space Center, MS 39529-5005
9. Commanding Officer 1
Fleet Numerical Meteorology and Oceanography Center
7 Grace Hopper Avenue Stop 4
Monterey, CA 93943-5501
10. Director, Joint Typhoon Warning Center 1
Naval Pacific Meteorology and Oceanography Center, Pearl Harbor
425 Luapele Road
Pearl Harbor, HI 96860-3103
11. Commanding Officer 1
Naval Pacific Meteorology and Oceanography Center
Yokosuka, Japan PSC 473 Box 68
FPO AP 96349-2902
13. LCDR Peter M. Klein 1
USS KEARSARGE (LHD 3)
FPO AE 09534-1662